

**EXPERIMENTAL AND COMPUTATIONAL
INVESTIGATION OF H₂-F₂ REACTION IN A TUBULAR
REACTOR**

By

ANIL KUMAR TIWARI

(Registration No: ENGG01200704011)

Chemical Technology Division, Bhabha Atomic Research Centre, Trombay, Mumbai.

A Thesis submitted to the
Board of Studies in Engineering Sciences
In partial fulfilment of requirements
For the Degree of

DOCTOR OF PHILOSOPHY

of

HOMI BHABHA NATIONAL INSTITUTE



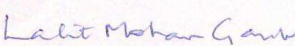
August, 2013

Homi Bhabha National Institute
Recommendations of the Viva Voce Board

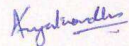
As members of the Viva Voce Board, we certify that we have read the dissertation prepared by **Shri Anil Kumar Tiwari** entitled "**Experimental and Computational Investigation of H₂-F₂ Reaction in a Tubular Reactor**" and recommend that it may be accepted as fulfilling the dissertation requirement for the Degree of Doctor of Philosophy.


Chairman: **Prof. P.K. Tewari**

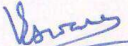
Date: 26.8.2014


Guide/Convener: **Prof. L.M. Gantayet**

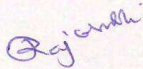
Date: 26.8.2014


Co-Guide: **Prof. A. W. Patwardhan**

Date: 26.8.2014


Member 1: **Prof. Vinayak Eswaran**
IIT Hyderabad, INDIA
(External Examiner)

Date: 26/8/14


Member 2: **Prof. R. C. Hubli**

Date: 26/8/14


Member 3: **Prof. Dinesh Srivastava**

Date: 26.8.2014


Member 3: **Prof. S. Mukhopadhyay**

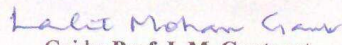
Date: 26/8/2014

Final approval and acceptance of this dissertation is contingent upon the candidate's submission of the final copies of the dissertation to HBNI.

I hereby certify that I have read this dissertation prepared under my direction and recommend that it may be accepted as fulfilling the dissertation requirement.

Date: 26.8.2014

Place: Mumbai


Guide: **Prof. L.M. Gantayet**

STATEMENT BY AUTHOR

This dissertation has been submitted in partial fulfillment of requirements for an advanced degree at Homi Bhabha National Institute (HBNI) and is deposited in the Library to be made available to borrowers under rules of the HBNI.

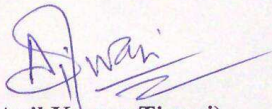
Brief quotations from this dissertation are allowable without special permission, provided that accurate acknowledgement of source is made. Requests for permission for extended quotation from or reproduction of this manuscript in whole, or in part, may be granted by the Competent Authority of HBNI, when in his or her judgment, the proposed use of the material is in the interests of scholarship. In all other instances, however, permission must be obtained from the author.



(Anil Kumar Tiwari)

DECLARATION

I, hereby declare that the investigations presented in the thesis have been carried out by me. The work is original and has not been submitted earlier as a whole or in part for a degree / diploma at this or any other Institution / University.


(Anil Kumar Tiwari)

DEDICATIONS

I dedicate this thesis to my Parents

Shri R.M.Tiwari and Smt. Devwati Tiwari

and, In-laws

Shri R.K.Dubey and Smt. Premlata Dubey

ACKNOWLEDGEMENTS

A PhD thesis is a great learning experience; academic, intellectual as well as personal. My first and foremost thanks goes to my mentor and guru *Dr. L.M. Gantayet*, a Distinguished Scientist and Director, Beam Technology Development Group, BARC, who bestowed on me, an attitude towards attending a problem with meticulous planning and an extremely focused approach. He is a brilliant teacher and believes in shaping his student to be able to guide others in course of pursuance of research work of a supreme quality. He has not only nurtured me to adopt a scientific approach and work on a set target scrupulously but also taught how to present one's ideas in a logically correct, simple and effective manner. It was nothing less than a priceless privilege to work under his guidance all these years. It is indeed a matter of great honour to be called a disciple of Dr. Gantayet.

I would like to express my honest gratitude towards Shri C. S. R. Prasad, former Head, ChTD, BARC for constantly encouraging me to believe oneself, think deeper and harder on attempting a tough problem. I am sure the concepts and fundamentals imbibed during countless meetings with him will stand me in good stead for the rest of my life. I would like to thank Dr A. W. Patwardhan for his unwavering support and guidance especially during the simulation work. I owe a lot to him for his scientific advice and positive outlook under all circumstances. I also like to place on record my sincere thanks to the erstwhile doctoral committee chaired by Dr. D. Sathiyamoorthi for their constant advice and helpful comments in all the progress meetings. I am grateful to the present doctoral committee headed by Dr. P.K. Tewari for helping me conclude and present my work in an effective and convincing manner.

Shri T.K.Bera, Director, Chemical Technology Group, BARC deserves special thanks for enabling me to work on a project of imminent importance and also guiding me

appropriately during the PhD programme. I am extremely grateful to Shri A. Sanyal, Head, ChTD, BARC and Shri A. K. Kalburgi, Head, PTS, ChTD, BARC for always being with me in the moment of need and sharing my workload selflessly to provide me ample time to conclude my research work. Colleagues at ChTD find a special mention in my work for their untiring efforts and a very professional outlook towards the conduct of a very large number of potentially dangerous scientific experiments followed by compilation of the experimental data. Useful discussions had with them in the control room helped in further improving the quality of my research work. I am obliged to Dr. V.C. Patkar and Shri C. Yadav for helping me during simulations.

Thanks are due to all those researchers and scientists who directly or indirectly enlightened me with their results and observations which was helpful en-route to accomplish my envisaged objectives. The deliberations and the interpretations provided in their articles were extremely useful in planning the targeted research work. I also accord my humble gratitude to all those whom I might have missed at this juncture.

Without the blessings of my respected parents and parent-in-laws, I would not have been able to get to this point. They always showered unconditional love and extended a token of appreciation for however small success I would achieve, just to keep me on track and ensure that I work with more zeal. I also extend by gratefulness to my kith and kin for always keeping me in a very secured and caring framework so that I could further concentrate on my goal.

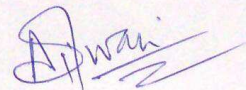
My thanks giving gesture would be grossly incomplete without mentioning the cute Anika, my doting daughter, who was only two years old when I started my work. She has been an incessant source of energy for me. She grew up with me always entertaining with her extremely loving gestures and innocent actions. Though a toddler, she would want to sit with

me at home and turn over the pages of a voluminous book pretending to be a budding junior scientist, seriously in the making. She, at times, would caress my head and give me a soothing massage as if she knew that it would alleviate fatigue generated from my hectic schedule. I also wish to place on record my heartfelt thanks to the new entrant (currently, serenely dwelling in her/his mother's womb) into our family whose mere news of arrival has instilled joyous moments in our life and helped creating an upbeat atmosphere congenial to pursue a research work. Needless to say, without the support of my better half, Mrs. Archana Tiwari, I would not have been able to complete my assignment with so ease and comfort. She conscientiously used her management skills learnt during her MBA days and steered her 'sweet home' seamlessly keeping me at abeyance from the house hold chores. She, as a true companion always stood by me and was always there to handle my successes and failures unequivocally during the course of this journey.

I have no words to thank the almighty for keeping me in good state of health all these years. He has also been kind to ponder his love and blessings on those who matter the most to me so that I remained unperturbed during the work.

Last but not the least, I would like to thank all my friends and well wishers for wanting me to earn 'Dr.' as a prefix to my name.

Finally, I owe my doctorate to all the above and hope to get the same kind of love affection, blessings, concern and words of encouragement in all my ventures in future.



(Anil Kumar Tiwari)

CONTENTS

<u>Topic</u>	<u>Page No.</u>
LIST OF FIGURES	i
LIST OF TABLES	viii
ABBREVIATIONS AND NOMENCLATURE	x
CHAPTER 1: INTRODUCTION	1
1.1 Importance of H ₂ -F ₂ flame reactor	2
1.2 Current status and trends	3
1.3 Motivation	4
1.4 Objectives	5
1.5 Organization of the thesis	6
CHAPTER 2: LITERATURE SURVEY ON REACTION MECHANISMS	8
OF H₂-F₂ AND SIMILAR FUEL-OXIDIZER SYSTEMS	
2.1 Introduction	9
2.2 H ₂ -O ₂ reaction system	12
2.2.1 H ₂ -O ₂ reaction mechanisms	12
2.2.2 Effect of steam on H ₂ -O ₂ reaction	15
2.2.3 Effect of O ₂ diluent on H ₂ -O ₂ reaction	16
2.2.4 Effect of other diluents on H ₂ -O ₂ reaction	16
2.3 H ₂ -F ₂ reaction system	18
2.3.1 Proposed H ₂ -F ₂ reaction steps	19
2.3.2 H ₂ -F ₂ reaction mechanism with diluents	21
2.4 Effect of diluents on other fuel-oxidizer systems	23

2.5 Comparison between H ₂ -O ₂ and H ₂ -F ₂ reaction systems	26
CHAPTER 3: PLAN OF EXPERIMENTS	29
3.1 Introduction	30
3.2 Preliminary experiments to establish feasibility of handling H ₂ -F ₂ reaction	31
3.3 Flow ratios of hydrogen, nitrogen and fluorine in a tubular reactor	33
3.4 Reactor and reactant preheating	35
3.5 Fluorine flow rates	36
3.6 Study of effects of type and quantity of diluents on H ₂ -F ₂ reaction in a flame in a batch reactor	38
3.7 Generation of temperature curve with variation in the fluorine composition	41
3.8 Study on dilution effect in a flowing type H ₂ -F ₂ flame reactor	43
3.9 Conclusions	45
CHAPTER 4: EXPERIMENTAL SET UP AND DESIGN	46
METHODOLOGIES	
4.1 Introduction	47
2.2 The safety issues	47
4.3 Setting up of experimental facilities	48
4.3.1 Details of the experimental facility involving the VCR	48
4.3.2 Details of the experimental facility involving the HCR	55
4.3.3 Selection of instruments	60
4.3.4 Placement of instruments	61
4.3.5 Control and data acquisition system	62
4.3.6 Safety measures	63
4.4 Sequence of operation	64
4.4.1 Operation sequence of facility comprising of the VCR	64

4.4.2	Operation sequence of facility comprising of the VCR	65
CHAPTER 5: CFD MODELING OF THE FLAME REACTOR		67
5.1	Introduction	68
5.2	Identification of the CFD tool	72
5.3	Selection of the turbulence model	73
5.4	Effect of the grid size on computational results	76
5.5	CFD modeling and the governing equations	77
5.5.1	CFD modeling	77
5.5.2	Governing equations	78
5.6	Effect of radiation modeling in temperature predictions	82
5.7	Summary of the modeling	84
5.8	Conclusions	87
CHAPTER 6: EXPERIMENTAL OBSERVATIONS, SIMULATIONS AND DISCUSSIONS		89
6.1	The preliminary experiments to establish feasibility of handling H ₂ -F ₂ reaction	90
6.1.1	Introduction	90
6.1.2	Experimental observations and discussions	90
6.1.3	Discussion of experimental and simulation results	93
6.1.4	Summary of the results of the preliminary experiments to establish the feasibility of handling H ₂ -F ₂ reaction	99
6.2	Influence of excess hydrogen and nitrogen on behaviour of H ₂ -F ₂ flame reactor	100
6.2.1	Introduction	100
6.2.2	Experimental observations and discussions	101

6.2.2.1	Effect of percentage excess of hydrogen	102
6.2.2.2	Effect of nitrogen flow	104
6.2.3	Discussion experimental and simulation results	107
6.2.4	Summary of the results of influence of excess hydrogen and nitrogen in the H ₂ -F ₂ flame reactor	118
6.3	Effect of preheating of the reactant gases and the reactor wall on the reactor temperature distribution	119
6.3.1	Introduction	119
6.3.2	Experimental observations	120
6.3.3	Discussion of experimental and simulation results	125
6.3.4	Summary of the results of the effect of preheating	131
6.4	Behaviour of H ₂ -F ₂ flame reactor at higher fluorine flow rates	131
6.4.1	Introduction	131
6.4.2	Discussion of simulation results	132
6.4.3	Experimental observations	133
6.4.4	Comparison between the simulation and the experimental results	137
6.4.5	Summary of reactor behaviour at higher fluorine flow rates	137
6.5	Study of effects of type and quantity of diluents on H ₂ -F ₂ reaction in a batch reactor	138
6.5.1	Introduction	138
6.5.2	Experimental observations and discussions	138
6.5.2.1	Reactor behaviour with diluents at higher initial pressure (800 mbar)	140
6.5.2.2	Reactor behaviour with diluents at lower initial pressure (100 mbar)	153

6.5.3	Summary of the effects of type and quantity of diluents on H ₂ -F ₂ reaction in a flame	156
6.6	Study of the temperature response with variation in the fluorine composition from lean to rich	157
6.6.1	Introduction	157
6.6.2	Preliminary calculations, experimental observations and discussions	158
6.6.3	Summary of the temperature response with variation in the fluorine composition from lean to rich	162
6.7	Dilution effect in a flowing type H ₂ -F ₂ flame reactor	162
6.7.1	Introduction	162
6.7.2	Experimental observations and discussions	163
6.7.3	Results from simulations, comparison with experiments and discussions	167
6.7.4	Summary of the dilution effect in a flowing type H ₂ -F ₂ flame reactor	176
CHAPTER 7: STUDY OF SCALE-UP OF H₂-F₂ FLAME REACTOR		178
7.1	Introduction	179
7.2	Scale-up criteria	180
7.3	Simulation results and discussions	185
7.4	Conclusions	199
CHAPTER 8: SUMMARY AND CONCLUSIONS		201
8.1	Flame reactor: H ₂ -F ₂ and H ₂ -O ₂ systems	202
8.2	Plan for safe conduct of experiments and range of experimental studies	204
8.3	CFD modeling of the flame reactor	207

8.4 Performance analysis of scale-up designs	209
8.5 Important conclusions	210
8.5.1 Experimental investigations	210
8.5.2 Computational investigations	212
8.6 Major contributions	213
8.7 Future work	214
REFERENCES	216
LIST OF PUBLICATIONS	230

LIST OF FIGURES

- Figure 2.1 : Multiple explosion limits in H₂-O₂ reaction
- Figure 4.1 : Block diagram for H₂-F₂ reaction system (VCR)
- Figure 4.2 : The vertical cylindrical reactor (VCR)
- Figure 4.3 (a) : Thermocouple locations in the reactor (VCR) in the axial direction
- Figure 4.3 (b) : Radial (mm) and angular positions of the thermocouple in the reactor (VCR)
- Figure 4.4 : Block Diagram for the experimental set up of H₂-F₂ reaction studies (HCR)
- Figure 4.5 : The horizontal cylindrical reactor (HCR)
- Figure 4.6 : Schematic of the H₂-F₂ batch reactor (HCR)
- Figure 4.7 : Spread of the un-reacted fluorine jet in the reactor
- Figure 4.8 : Centerline velocity of un-reacted fluorine jet in the reactor
- Figure 5.1 : Sketch of a non-premixed diffusion flame
- Figure 5.2 : Sketch of a premixed flame
- Figure 5.3 : Contour plots of temperature (K) for Case 2 using standard k- ω and k- ϵ model
- Figure 5.4 : Comparison of turbulence model on temperature at different thermocouple locations for Case 2.
- Figure 5.5 : Comparison of grid size on temperature at different thermocouple locations for Case 2.
- Figure 5.6 : Effect of radiative heat transfer on reactor temperatures for case 82
- Figure 6.1 : Experimental temperature values for (a) case 1 (F₂-0.44, H₂-2 slpm), (b) case2 (F₂-0.5, H₂-2 slpm) and (c) case 3 (F₂-0.48, H₂-1 slpm)
- Figure 6.2 : Simulated temperature predictions for (a) case 1 (F₂-0.44, H₂-2 slpm),

- (b) case 2 (F_2 -0.5, H_2 -2 slpm) and (c) case 3 (F_2 -0.48, H_2 -1 slpm)
- Figure 6.3 : Comparison between experimental and predicted reactor temperatures for (a) case 1 (F_2 -0.44, H_2 -2 slpm), (b) case 2 (F_2 -0.5, H_2 -2 slpm) and (c) case 3 (F_2 -0.48, H_2 -1 slpm)
- Figure 6.4 : Contour plots of axial velocity (m/s) for (a) case 1 (F_2 -0.44, H_2 -2 slpm), (b) case 2 (F_2 -0.5, H_2 -2 slpm) and (c) case 3 (F_2 -0.48, H_2 -1 slpm)
- Figure 6.5 : Vector plots of velocity for (a) case 1 (F_2 -0.44, H_2 -2 slpm), (b) case 2 (F_2 -0.5, H_2 -2 slpm) and (c) case 3 (F_2 -0.48, H_2 -1 slpm)
- Figure 6.6 : Contour plots of hydrogen mole fraction for a) case 1 (F_2 -0.44, H_2 -2 slpm), (b) case 2 (F_2 -0.5, H_2 -2 slpm) and (c) case 3 (F_2 -0.48, H_2 -1 slpm)
- Figure 6.7 : Contour plots of fluorine mole fraction for a) case 1 (F_2 -0.44, H_2 -2 slpm), (b) case 2 (F_2 -0.5, H_2 -2 slpm) and (c) case 3 (F_2 -0.48, H_2 -1 slpm)
- Figure 6.8 : Contour plots of hydrogen fluoride (HF) mole fraction for a) case 1 (F_2 -0.44, H_2 -2 slpm), (b) case 2 (F_2 -0.5, H_2 -2 slpm) and (c) case 3 (F_2 -0.48, H_2 -1 slpm)
- Figure 6.9 : Contour plots of nitrogen mole fraction for a) case 1 (F_2 -0.44, H_2 -2 slpm), (b) case 2 (F_2 -0.5, H_2 -2 slpm) and (c) case 3 (F_2 -0.48, H_2 -1 slpm)
- Figure 6.10 : Effect of excess of hydrogen on the reactor temperatures for (a) 0.2 (b) 0.3 and (c) 0.4 slpm of fluorine
- Figure 6.11 : Effect of nitrogen flow rate on the reactor temperatures for (a) 0.2 (b) 0.3 and (c) 0.4 slpm of fluorine with ~325% excess of hydrogen

- Figure 6.12 : Contour plots of temperature (K) for cases 4 to 18
- Figure 6.13 (a) : Comparison between the simulated and the experimental reactor temperatures for cases 4 to 9
- Figure 6.13 (b) : Comparison between the simulated and the experimental reactor temperatures for cases 10 to 15
- Figure 6.13 (c) : Comparison between the simulated and the experimental reactor temperatures for cases 16 to 18
- Figure 6.14 : Contour plots of axial velocity (m/s) for cases 4 to 18
- Figure 6.15 : Contour plots of hydrogen mole fraction for cases 4 to 18
- Figure 6.16 : Contour plots of fluorine mole fraction for cases 4 to 18
- Figure 6.17 : Contour plots of hydrogen fluoride mole fraction for cases 4 to 18
- Figure 6.18 : Contour plots of nitrogen mole fraction for cases 4 to 18
- Figure 6.19 : The reactor temperature profile for (a) case 31 (0.2 slpm F₂), (b) case 32 (0.3 slpm F₂), and (c) case 33 (0.4 slpm F₂)
- Figure 6.20 : The reactor temperature profile for (a) case 34 (0.2 slpm F₂), (b) case 35 (0.3 slpm F₂), and (c) case 36 (0.4 slpm F₂)
- Figure 6.21 : The reactor temperature profile for (a) case 37 (0.2 slpm F₂), (b) case 38 (0.3 slpm F₂), and (c) case 39 (0.4 slpm F₂)
- Figure 6.22 : Temperature contours when reactor preheater is switched off for (a) case 31 (0.2 slpm F₂), (b) case 32 (0.3 slpm F₂), and (c) case 33 (0.4 slpm F₂)
- Figure 6.23 : Comparison between the experimental and the predicted temperature values when the reactor preheater is switched off for (a) case 31 (0.2 slpm F₂), (b) case 32 (0.3 slpm F₂), and (c) case 33 (0.4 slpm F₂)
- Figure 6.24 : Velocity contours when reactor preheater is switched off for (a) case 31 (0.2 slpm F₂), (b) case 32 (0.3 slpm F₂), and (c) case 33 (0.4 slpm

- F_2)
- Figure 6.25 : Contours of hydrogen mole fraction when reactor preheater is switched off for (a) case 31(0.2 slpm F_2), (b) case 32 (0.3 slpm F_2), and (c) case 33 (0.4 slpm F_2)
- Figure 6.26 : Contours of fluorine mole fraction when reactor preheater is switched off for (a) case 31(0.2 slpm F_2), (b) case 32 (0.3 slpm F_2), and (c) case 33 (0.4 slpm F_2)
- Figure 6.27 : Contours of hydrogen fluoride mole fraction when reactor preheater is switched off for (a) case 31(0.2 slpm F_2), (b) case 32 (0.3 slpm F_2), and (c) case 33 (0.4 slpm F_2)
- Figure 6.28 : Contours of nitrogen mole fraction when reactor preheater is switched off for (a) case 31(0.2 slpm F_2), (b) case 32 (0.3 slpm F_2), and (c) case 33 (0.4 slpm F_2)
- Figure 6.29 : Contours of reactor temperature with higher fluorine flow rates for (a) case 40 (0.4 slpm F_2), (b) case 41 (0.5 slpm F_2) and, (c) case 42 (0.8 slpm F_2)
- Figure 6.30 : Change in the reactor temperatures with higher fluorine flow rates at (a) near the nozzle region, (b) 120 mm from the nozzle exit and (c) far nozzle region
- Figure 6.31 : Comparison between the recorded and the simulated reactor temperatures with higher fluorine flow rates for (a) case 40 (0.4 slpm F_2), (b) case 41 (0.5 slpm F_2) and, (c) case 42 (0.8 slpm F_2)
- Figure 6.32 : Temporal changes in the reactor temperature (T21)
- Figure 6.33 : Maximum temperature recorded during H_2 - F_2 reaction experiment in the HCR at higher pressure

- Figure 6.34 : Comparison of the responses of thermocouples (a) T17, (b) T20 and (c) T21
- Figure 6.35 : Temporal change in the reactor pressure with change in helium concentration
- Figure 6.36 : Maximum pressure recorded during H₂-F₂ reaction
- Figure 6.37 : Comparison between modeling and experimental reactor temperature for (a) helium (b) nitrogen and (c) argon as diluent
- Figure 6.38 : (a) Maximum temperature and (b) peak pressure recorded during H₂-F₂ reaction experiment at initial pressure of 100 mbar
- Figure 6.39 : Equilibrium conversion of H₂+F₂⇌2HF reaction with temperature
- Figure 6.40 : Variation in the maximum reactor temperature recorded with change in the fluorine mole fraction
- Figure 6.41 : Pressure surge ratio recorded with change in fluorine mole fraction
- Figure 6.42 : Effect of diluent content in fluorine on reactor temperatures in flowing condition: (a) Change in near nozzle temperature, T1 and (b) Change in temperature, 120 mm away from nozzle (T7). T1₀ and T7₀ are T1 and T7 temperatures at zero diluent concentration in fluorine. (c) Change in temperature, 450 mm away from nozzle (T8) and (d) Change in temperature, 620 mm away from nozzle (T9). T8₀ and T9₀ are T8 and T9 temperatures at zero diluent concentration in fluorine
- Figure 6.43 : Temperature contours of different cases
- Figure 6.44 : Comparison between the experimental and the simulated data
- Figure 6.45 : Radial temperature distribution in presence of diluents as predicted at various longitudinal distances. 'r' is any radial distance whereas 'R' is the reactor radius

- Figure 6.46 : Radial distribution of HF mole fraction in presence of diluents as predicted at various longitudinal distances. 'r' is any radial distance whereas 'R' is the reactor radius
- Figure 6.47 : Velocity vectors near the nozzles as obtained from simulations
- Figure 6.48 : Radial variation in the velocity in presence of the diluents as predicted at various longitudinal distances. 'r' is any radial distance whereas 'R' is the reactor radius
- Figure 7.1 : Sketch of scale-up reactor (multiple feed nozzles)
- Figure 7.2 : Sketch of the scale-up geometry, (a) based on same Reynolds number at the nozzle exits and (b) based on the same velocity at the nozzle exits
- Figure 7.3 : Temperature contours of the multiple nozzle scale-up reactor (a) section at $z=0$ on x-y plane and (b) section at $x=0$ on y-z plane
- Figure 7.4 : Vector plot of the multiple nozzle scale-up reactor (a) section at $z=0$ on x-y plane and (b) section at $x=0$ on y-z plane
- Figure 7.5 : (a) Temperature and (b) velocity plots for the multiple nozzle scale-up reactor (section at $z=0$ on x-y plane)
- Figure 7.6 : (a) Temperature and (b) velocity plots for the multiple nozzle scale-up reactor (section at $x=0$ on y-z plane)
- Figure 7.7 : (a) Temperature contour and (b) Temperature plot for the scale-up reactor based on similar Reynolds no. at the nozzle exits
- Figure 7.8 : (a) Velocity contour and (b) Velocity plot for the scale-up reactor based on similar Reynolds no. at the nozzle exits
- Figure 7.9 : (a) Temperature contour and (b) Temperature plot for the scale-up reactor based on similar velocity at the nozzle exits

- Figure 7.10 : (a) Velocity contour and (b) velocity plots for the scale-up reactor based on similar velocity at the nozzle exit
- Figure 7.11 : (a) Temperature contour and (b) Temperature plots for the scale-up reactor based on fluorine mixed with nitrogen as the diluent
- Figure 7.12 : (a) Velocity contour and (b) Velocity plots for the scale-up reactor based on fluorine mixed with nitrogen as the diluent
- Figure 7.13 : Vector plots for (a) Reynolds no. based, (b) Velocity based and (c) fluorine mixed with nitrogen as diluent based scale-up designs

LIST OF TABLES

- Table 2.1 : Change in the equilibrium constants of the $\text{H}_2\text{-O}_2$ and the $\text{H}_2\text{-F}_2$ reactions with temperature
- Table 3.1 : Theoretical flame temperature by Wilson et al.(1951)
- Table 3.2 : Gaseous flow rates and adiabatic flame temperature
- Table 3.3 : Gaseous flow rates and adiabatic flame temperature
- Table 3.4 : Gaseous flow rates and adiabatic flame temperature
- Table 3.5 : Higher flow rates of gaseous in the tubular reactor
- Table 3.6 : Quantity of diluents in the batch reactor operating at higher pressure
- Table 3.7 : Quantity of diluents in the batch reactor operating at lower pressure
- Table 3.8 : Mole fractions of F_2 in $\text{H}_2\text{-F}_2$ reaction and corresponding adiabatic temperature
- Table 3.9 : Flow rates of gases for dilution study in the flow reactor
- Table 4.1 : Location of thermocouples in cylindrical coordinates
- Table 4.2 : Radial distance of 'B' type thermocouples from the centre of the F_2 nozzle tip
- Table 5.1 : Details of type and size of mesh
- Table 6.1 : Energy balance with increasing fluorine flow rate
- Table 6.2 : Lennard-Jones (L-J) Potential parameters for gases
- Table 6.3 : Thermal and transport properties of gases
- Table 6.4 : Maximum temperature and pressure during reaction at higher pressure (800 mbar)
- Table 6.5 : Maximum temperature and pressure during reaction at lower pressure (100 mbar)
- Table 6.6 : Mole fractions of F_2 and corresponding peak temperature in the $\text{H}_2\text{-F}_2$

batch reactor (HCR)

Table 6.7 : The experimental and the predicted temperature values of T7 when 66.66% diluent is added with the fluorine stream

Table 8.1 : Summary of experimental investigations

Table 8.2 : Details of CFD modeling

ABBREVIATIONS AND NOMENCLATURE

ABBREVIATIONS USED

CFD	Computational fluid dynamics
EDM	Eddy dissipation model
EDC	Eddy dissipation concept
GUI	Graphics user interface
HCR	Horizontal cylindrical reactor
LES	Large eddy simulation
PID	Proportional-Integrative-Derivative
RANS	Reynolds-averaged Navier Stokes
RSM	Reynolds stress model
SCADA	Supervisory control and data acquisition system
SIMPLE	Semi implicit method for pressure linked equations
slpm	Standard litres per minute [standard conditions: 1 bar (abs) pressure and 273.18 K temperature (IUPAC practice)]
SS	Stainless steel
VCR	Vertical cylindrical reactor

NOMENCLATURE

A	Empirical constant equal to 4.0
A_f	Heat transfer area of the flame (m^2)
A_r	Heat transfer area of reactor (m^2)
A_w	Inner surface area of reactor (m^2)
B	Thickness of thermowell pipe (m)
B'	Empirical constant equal to 0.5

C_p	Specific heat (J/kg-K)
C_{pg}	Specific heat of the chamber gas (J/kg-K)
C_{pw}	Specific heat of the reactor wall (J/kg-K)
C	Concentration (mols/m ³ -s)
$C_\mu, C_{\epsilon 1}, C_{\epsilon 2}$	Equation constants
d_f	Diameter of the flame (m)
d_o	Fluorine nozzle diameter (m)
E	Total energy per unit mass (J/kg)
\vec{F}_b	Body force per unit mass (m/s ²)
Gr	Grashoff no.
ΔG°_R	Gibbs free energy (J/gmol)
h_c	Convective heat transfer coefficient in the chamber gas (W/m ² -K)
h_r	Radiative heat coefficient from the flame (W/m ² -K)
J_m	Mass flux of m th species (kg/m ² -s)
k	Turbulent kinetic energy per unit mass (m ² /s ²)
k'	Thermal conductivity (W/m-K)
\dot{k}	Reaction rate constant (s ⁻¹)
k_r	Equivalent radiative conductivity (W/m-K)
k_b	Boltzman constant
k_{eff}	Effective thermal conductivity (W/m-K)
k_g	Thermal conductivity of the chamber gas (W/m-K)
k_r	Radiative thermal conductivity (W/m-K)
k_{th}	Thermal conductivity of the thermowell material (W/m-K)
k_{tw}	Thermal conductivity of the thermowell (W/m-K)
kJ	Kilo Joule

l	Length of the thermowell (m)
l_f	Length of the flame (m)
m	Any species m
m_g	Mass of the chamber gas (kg)
m_w	Mass of reactor wall (kg)
M	Any inert molecule or even a solid wall
MJ	Mega Joule
mJ	Milli Joule
ms	Milli Second
$M_{w,m}$	Molecular weight of species m
N	Total no of species in the system
n	Number of active species/radicals per unit reactor volume (mols/m ³)
nm	Nano meter
p	Pressure in Pascal
P	Product
Pr	Prandtl no.
Pr_t	Turbulent Prandtl no.
Q	Reactant
Q_0	Total heat energy released from chemical reaction (J)
Q_d	Heat energy available to be dissipated (J)
q_d	Heat transfer by diffusion (J/m ²)
Q_r	Radiative heat transfer from the flame (W)
r	Reactor radius (m)
R	Rate of reaction (mols/m ³ -s)
R_m	Reaction rate for m^{th} species (mols/m ³ -s)

S_u	Burning velocity (m/s)
T	Reactor temperature (K)
T_f	Temperature of the flame (K)
T_g	Temperature of the chamber gas (K)
T_r	Temperature as a result of reaction (K)
T_{tw}	Temperature of the thermowell (K)
T_w	Temperature of the reactor wall (K)
ΔT_g	Difference in chamber gas temperature (K)
ΔT_w	Difference in reactor wall temperature (K)
$\overline{u_i u_j^i}$	Averaged value of fluctuating components of velocity (m^2/s^2)
U_i	Ensemble-averaged velocity component in the x_i direction (m/s)
U_j	Ensemble-averaged component in the x_j direction (m/s)
V_c	Centre line fluid velocity (m/s)
V_0	The fluid velocity at nozzle exit (m/s)
V_r	Volume of reactor (m^3)
x	Linear distance in the reaction chamber (m)
$x_i x_j$	Distance variable in i and j direction (m)
Y_p	Mass fraction of any product species, P
Y_Q	Mass fraction of any reactant species, Q

Greek symbols

α	Thermal diffusivity (m^2/s)
β	Thermal expansion coefficient (K^{-1})
δ	Distance between the cold and hot surfaces (m)
ε	Turbulence energy dissipation rate (m^2/s^3)

ε_f	Effective emissivity of the flame
$(\varepsilon/k_b)_{L-J}$	Lennard-Jones energy parameter (K)
μ	Viscosity of fluid (kg/m-s)
μ_t	Turbulent kinematic viscosity of fluid (m ² /s)
ν	Kinematic viscosity of fluid (m ² /s)
$\nu'_{m,r}$	Stoichiometric coefficient of m in the reactants of reaction 'r'
$\nu''_{m,r}$	Stoichiometric coefficient of m in the products of reaction 'r'
ρ	Density of gases (kg/m ³)
ρ_0	Constant density of the flow (kg/m ³)
σ	Stefan Boltzmann constant (5.67*10 ⁸ W/m ² -K ⁴)
σ_ε	Turbulent Dissipation Energy Prandtl Number
σ_k	Turbulent Kinetic Energy Prandtl Number
σ_{L-J}	Lennard-Jones size parameter (m)
θ	Time (s)
ω	Specific dissipation rate, ε/k (s ⁻¹)

CHAPTER 1

INTRODUCTION

1.1 Importance of H₂-F₂ flame reactor

Many chemical processes of industrial importance require higher temperatures and the requirement of heat energy to provide higher temperatures may be provided externally by means of resistance/induction heating, steam/thermic fluid heating or, internally, by carrying out highly exothermic chemical reactions in the region of interest. The equipments based on the principle of external heating are called hot-wall reactors, while those following the latter principle are categorized as cold-wall reactors. Due to higher metal temperature in a hot wall reactor, the formation of slag on the reactor wall leads to corrosion problems, gradual deterioration of the heat transfer and contamination of the final product. Therefore, the wall needs to be scraped frequently resulting in an increase in the maintenance period and decrease in the reactor throughput. In order to avoid such situations, while keeping the region of interest in the reactor at higher temperatures, a lower wall temperature is maintained in a cold wall reactor. For a cold wall reactor, inter alia, the required energy can also be provided by in-situ generation of heat through an exothermic chemical reaction, for example, in a flame reactor. Flame reactors are compact, possess high energy density and can be highly energy efficient. Some of the promising examples of the source of chemical heat include the reaction between H₂ and O₂ and between H₂ and F₂. The use of hydrogen as a fuel is common for attaining high temperatures because of its high mass-related energy density. Since both the H₂-O₂ and H₂-F₂ reactions are fast and chain type, they can lead to explosion under specific conditions. Between the two, the hydrogen-fluorine reaction is more advantageous as a heat source for those chemical processes where temperature requirement is higher and the oxide contamination of the final product is not acceptable. Basov et al. (1969) and Sullivan et al. (1975) consider that the reaction between H₂ and F₂ is very fast and involves a branched chain mechanism where the free radicals help in propagation of the reaction steps. A large amount of energy (~540 kJ/g-mol) is released whenever hydrogen and fluorine react raising

the temperature and the pressure. A flame, which results from a complex interaction of flow, heat transfer, diffusion and chemical reaction, is produced consequent to the chemical reaction. This flame becomes a source of heat for many chemical reactions and material processing.

1.2 Current status and trends

Majority of the published work deal with H_2-F_2 reaction in the context of HF lasers [Chen et al. (1975), Kapralova et al. (1976), Kim and Cho (1994)]. The energy release in the H_2-F_2 reaction is used to generate HF molecules at higher energy levels. Very little work has been reported on the utilization of chemical energy for material processing in chemical/nuclear industries. The flame reactors offer a wide range of applications from nanoparticle synthesis to nuclear processing. Degussa [<http://www.azonano.com>], who has investigated several processes in flame reactors, hot wall reactors, plasma reactors and laser evaporation reactors reports that, although each process delivers unique capabilities, the flame process is the preferred option because of its scalability, versatility and cost-efficient production. Nanomaterials, which broadly consist of powders with particle diameters below 100 nm are receiving an increased interest in the industry and academia. They open door to the development of novel materials with applications, for instance, in ceramics, catalysis, fuel cells, electronics, chemical–mechanical polishing, data storage, coatings [Rittner (2002)] etc. In nuclear industry, flame reactors are deployed in variety of applications, namely, reduction of Uranium Hexafluoride [Galkin and Sudarikov (1964)], fluorination of uranium tetrafluoride [IAEA-Tecdoc-1115 (1999)], pyrohydrolysis of uranium hexafluoride [Galkin et al. (1961)] etc. The conversion of uranium oxide to uranium hexafluoride is achieved by a dry fluoride volatility process in a flame reactor in the USA [www.world-nuclear.org]. Also, there are reports on the preparation of nuclear-pure uranium hexafluoride from uranium ore

concentrates and rich uranium ores by the method of direct fluorination in a flame reactor [Lavroskii et al. (1959); Smiley and Brater (1959)]. Rakov et al. (2001) have studied the possibility of using a computer program to perform calculations on the adiabatic temperature of combustion, chemical equilibrium and kinetics using the available thermodynamic database and characteristics of uranium compounds. They suggest that the flame reactors similar to those used in these activities can also be used for processes where temperatures not less than 1200-1300 K are required. Kobayashi et al. (2005) have carried out several experiments for fluorination test of the mixture of UO_2 and PuO_2 with wide range of production rate and proposed a new reprocessing technology called the FLUOREX process, which is safe, technically matured, cost competitive and reduces waste generation. Kani et al. (2009) too have found that the uranium in the spent fuels can be selectively volatilized by fluorination in the flame reactor and the selectivity can be adjusted by changing the quantity of F_2 supplied to the reactor. In view of the wide range of applicability of the flame reactors, the emphasis in the present work has been to acquire a variety of data which is useful in developing an industrial scale $\text{H}_2\text{-F}_2$ flame reactor.

1.3 Motivation

Sufficient data on the combustion properties of the $\text{H}_2\text{-O}_2$ mixture exist, which includes the ignition temperature, the flame temperature, the burning velocity, the flammability limits, the reaction kinetics, etc. However, scant information is available in the literature on the $\text{H}_2\text{-F}_2$ reaction. Moreover, there is no published data of engineering scale experimental investigations on this system. In a flame reactor, the process can be stable or unstable depending on the operating parameters and the fluctuations in the feeding of the reactants. It is therefore necessary to understand the behaviour of the $\text{H}_2\text{-F}_2$ flame reactor under the influence of various parameters.

Hitherto, researchers have carried out studies on H_2-F_2 reaction at laboratory scale for specific requirements, such as, generation of HF chemical laser etc. No attempts have been made to conduct H_2-F_2 reaction at relatively higher scale (>0.1 slpm) in a continuous type of reactor which will be of industrial importance. The investigations with higher fluorine flow rate in a flow reactor and the safety issues involved in the smooth handling of such type of inherently dangerous reactions is necessary. It is required to know the effect of the parameters such as gas flow rates, flow ratios, reactant preheating and the solid wall preheating on the behaviour of H_2-F_2 flame reactor, which has not yet been reported in the literature. The effect of diluents such as helium, nitrogen and argon on H_2-F_2 reaction mechanisms have been numerically investigated and published. In order to predict the H_2-F_2 reactor behaviour under the influence of diluents, the transient as well as the steady state experiments need to be carried out. A precise criterion for the scale-up of a flame reactor is not available in the literature. The present thesis, while presenting the basis for the scale-up, aims also to discuss the simulation results (using a standard computational fluid dynamics tool) obtained for various designs of a scaled-up H_2-F_2 flame reactor.

1.4 Objectives

One of the goals of this work is to establish a methodology for conducting safe and controlled reaction between hydrogen and fluorine. The objective is also to acquire understanding on the effect of various parameters on the behaviour of the H_2-F_2 flame reactor. Another goal of the work includes the selection of a simulation tool and using it to make a CFD model which can predict the temperature, the velocity and the concentration profile inside the reactor, and subsequently can be used for planned scale-up. The following studies will be covered in the reported work.

- The experimental investigation of H_2-F_2 reaction in a tubular reactor at sub-atmospheric pressure.
- Development of a CFD tool for the computational simulation and validation by the experimental data.
- Influence of excess hydrogen and nitrogen on the temperature distribution of the H_2-F_2 flame reactor.
- Effect of preheating on the thermal behaviour of the H_2-F_2 reactor flame reactor.
- Effect of type and quantity of diluents on H_2-F_2 reaction in a flame.
- Design of H_2-F_2 flame reactor for an envisaged scale-up.

1.5 Organization of the thesis

The literature survey in Chapter-2 helps understand the reaction mechanisms of both the systems, namely, H_2-O_2 and H_2-F_2 , as proposed by various researchers. It also discusses the effect of diluents such as oxygen, helium, argon, nitrogen etc. on the H_2-O_2 and other fuel-oxidizer systems. Unlike H_2-O_2 and other systems, in the H_2-F_2 system, the entire proportion of H_2 and F_2 mixture can be potentially explosive if not handled carefully. Chapter-3 thus discusses about the planning of different experimental trials that would establish the feasibility of a controlled and safe operation of H_2-F_2 reaction. It also discusses about the range of gaseous flow rates, selection of flow ratios, effect of preheating, generation of temperature curve with variation in the fluorine composition and study of effects of dilution with inerts on the behaviour of the H_2-F_2 flame reactor. Two types of reactors, namely, a batch type (a horizontal cylindrical reactor, HCR) and a continuous type (a vertical cylindrical reactor, VCR) are required to fulfill the envisaged objectives. The details of the entire experimental set up comprising of the two types of reactors and the sequence of operation are given in Chapter-4. Chapter-5 discusses the development of a

simulation tool, the selection of CFD models and validation of the simulation by experiments. The observations of the conducted experiments and the corresponding simulation results are discussed in Chapter-6. The validated CFD tool is further utilized to simulate a number of possible scale-up designs and the resultant temperature and the velocity distribution profiles are discussed in Chapter-7. The concluding remarks on the completed work are summarized and the recommendations for future work are given in Chapter-8.

.....

CHAPTER 2

LITERATURE SURVEY ON REACTION **MECHANISMS OF** **H₂-F₂ AND SIMILAR FUEL-OXIDIZER** **SYSTEMS**

This chapter presents a comprehensive review on H₂-O₂ system starting from reaction mechanisms, occurrence of multiple explosion limits and the effect of steam, oxygen and inerts on the H₂-O₂ reaction. It also gives an overview of the possible mechanisms of H₂-F₂ reaction. A comparison has been made between the two systems for a better understanding.

2.1 Introduction

Some of the fuel-oxidizer systems such as H_2-O_2 , H_2-Br_2 , H_2-Cl_2 etc. belong to the chain type reactions, which are initiated either by sunlight or an external ignition source. The free radicals and or active atoms produced by the initiation process become the chain carriers. While more and more active species are produced by these carriers, they also get killed simultaneously by colliding against the reactor wall or inert molecules. A continuous chain propagation with the evolution of heat leads to explosion. The reaction is said to be uncontrolled if a) there is an accumulation of the concentration of active atoms/radicals leading to chain avalanche or, b) there is an accumulation of heat augmenting the reaction kinetics and thereby leading to thermal avalanche. In most of the hydrogen-halogen reactions, both the phenomena take place and, therefore, there is a continuous rise in the temperature and the pressure if the reaction is not controlled. If n_0 be the initial concentration of an atom/radical present in the system, and α and β be the rate of their generation and termination respectively, then the rate of accumulation of these species is given as,

$$\frac{dn}{d\theta} = n_0 + (\alpha - \beta)n \quad (2.1)$$

As is clear from the above expression, when $\alpha > \beta$, it leads to chain avalanche. Similarly, the thermal avalanche occurs when the rate of generation of heat through chemical reaction is more than the dissipation and consequently, there is a continuous accumulation of the heat ($\frac{dq}{d\theta}$) in the system. This is expressed by the equation

$$\frac{dq}{d\theta} = Q_0 V_R R - k_{eff} A_r (T_r - T_w) \quad (2.2)$$

The first term on the right hand side of equation (2.2) is the rate of heat generation by virtue of reaction whereas the second term gives the loss of heat through the diffusive heat transfer from the reactor.

A good amount of data is available in the literature on H₂-O₂ reaction. The hydrogen-oxygen reaction has got varied application such as in rocket engines because of its high energy content of 141790 kJ/kg [<http://www.engineeringtoolbox.com>]. Unless ignited with the ignition energy requirement of hydrogen, 0.017 mJ [<http://www.hysafe.org>], they do not react at ambient conditions without a catalyst. The energy requirement further decreases with increasing temperature, pressure or oxygen content. They require higher temperature than the auto ignition temperature of hydrogen, that is, 809 K [http://en.wikipedia.org/wiki/Autoignition_temperature] for initiation. In the presence of platinum as a catalyst, the hydrogen reacts with oxygen even at ambient conditions. According to Das (1996), if a mixture of hydrogen and oxygen is exposed to light, the oxygen molecule is dissociated into oxygen atoms and, in presence of the sensitizers such as Cl, N₂O and NH₃, a set of secondary reactions take place producing H atoms. These H atoms in turn interact with the oxygen atoms and produce water. The hydrogen combustion in oxygen primarily produces heat and water. The temperature of the hydrogen flame in air is around 2318 K [<http://www1.eere.energy.gov>]. The flammability limits based on the volume percent of hydrogen in air at one atmospheric pressure are between 4 and 75 while the flammability limits based on the volume percent of hydrogen in oxygen at one atmospheric pressure are between 4 and 94. The explosive or detonable limits of hydrogen in air are usually between 18.3 to 59 percent by volume [http://en.wikipedia.org/wiki/Hydrogen_safety]. However, this range was found to be depending on the size of the system. While Tieszen (1986) reported a detonation range of 13-70% of H₂ in a 43 cm tube, in one of the Russian test facilities, a detonability limit of as low as 12.5 volume percent has been observed [<http://www.hysafe.org>]. In pure oxygen, Zabetakis (1967) reported the explosive range of hydrogen between 15 and 90 volume percent. Schroeder and Holtappels (2005) have studied the effect of the initial temperature and pressure on the explosion limits of hydrogen-air and

hydrogen-oxygen mixtures. At atmospheric pressure, the range of the explosion limits of hydrogen gets widened at both low and high ends with higher initial temperature, whereas at room temperature, it gets squeezed if the initial mixture pressure is more.

The reaction between H_2 and F_2 is another attractive option for providing heat energy. Hydrogen is an efficient fuel and fluorine is a strong oxidizer. The literature data on H_2 - F_2 reaction, however, indicate possibilities of self ignition on mixing of the two gases. Eyring and Kassel (1933) reported ignition and explosion free mixing of the two gases in the whole range from ~100% H_2 to ~100% F_2 at room temperature. Occasional explosions occurred, which they believed were initiated either by cosmic ray bursts, local radioactivity or catalytic material. Grosse and Kirshenbaum (1955) have discussed that the self ignition takes place whenever fluorine gas issues into the hydrogen atmosphere, even at room temperature. However, they were able to premix H_2 and F_2 , at atmospheric pressure, in the whole range of ~100% H_2 to ~100% F_2 by (1) eliminating impurities such as HF in the gases, (2) avoiding the presence of all transition metals and their compounds (particularly Cu, Fe, Ni) in the mixing chamber, and (3) precooling both the gases to 90 K. The gases could be warmed up to 195 K in Pyrex glass apparatus without ignition. According to them, the presence of oxygen in fluorine could be one of the reasons for the results observed by Eyring and Kassel (1933). The effect of the hypergolic reaction between H_2 and F_2 on the shear layer have been investigated by Mungal and Dimotakis (1984) and Hermanson and Dimotakis (1989). The volumetric compositions of hydrogen and fluorine were between 0 and 24% and 0 and 6% respectively. The resultant adiabatic temperature rise was up to 900 K. Nitric oxide was added to the hydrogen stream to generate radicals on contact with fluorine and initiate the hydrogen-fluorine reaction. Dimotakis and Hall (1987) proposed a simple thermodynamic model to assess the effect of Damkohler number on the H_2 /NO/ F_2 and H_2 /Air chemical systems. Egolpoulos et al. (1996) reported a numerical investigation on the dynamics and

the structure of non-premixed and premixed, H₂/NO/F₂ flames and concluded that the major fraction of the product formation in turbulent, mixing layers must take place in a mode in which the reactants are in premixed, rather than in non-premixed diffusion flames. Bergthorson et al. (2009) further studied the flow field response to the changing levels of mass injection in a rearward-facing geometry.

The maximum theoretical temperature of hydrogen-fluorine flame as reported by Wilson et al. (1951) is 4300 K. While the effect of H₂ to O₂ ratio on its reaction flame temperature is well established, no such data on H₂-F₂ system is available in the literature. Further, sizeable number of publications is available on effect of dilution with inerts such as He, N₂, O₂, H₂ and Ar on several fuel-oxidizer systems including H₂-O₂ system, but their effect on H₂-F₂ reaction is scarcely studied. Possible reaction mechanisms and kinetics data on H₂-O₂ and H₂-F₂ reactions, as investigated by various researchers are summarized and discussed in the following sections. This discussion is also useful while interpreting different experimental observations in this work.

2.2 H₂-O₂ reaction system

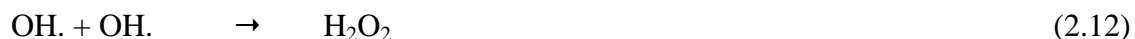
2.2.1 H₂-O₂ reaction mechanisms

The reaction mechanism of H₂-O₂ reaction has been widely studied. A comparative study with H₂-F₂ reaction is of interest to this work. At elevated temperature, the reaction between hydrogen and oxygen takes place through chain branching and breaking mechanisms. There is some ignition lag in H₂-O₂ reaction. The plausible reaction steps involved in this reaction are as follows: [Streblow (1984), Koroll and Mulpuru (1986)]





Reaction (2.4) is endothermic and occurs very slowly until a sufficiently high temperature is reached. Reactions (2.5) and (2.6) have high activation energy and hence, are more temperature sensitive. The above steps produce active atoms and radicals such as H., O. and OH. in the reactive system. Unless these species are used up simultaneously as they are produced, the reaction rate goes on increasing exponentially with time and results in an explosion. Such a situation however, can be avoided if the terminating processes are rapid. Presence of wall and inert molecules plays a significant role in deciding the course of H₂-O₂ reaction. Survival of radicals such as H., O. and OH. depends on the reactor diameter and type of the wall surface (reflecting or non-reflecting type). They are destroyed if they reach the reactor wall. Examples of wall reactions involving recombination are given by:



The chain carriers can also be destroyed in the gas phase by termination reactions (2.8) and (2.9). HO₂ is a stable compound and normally does not take part in chemical reaction. As mentioned, H₂-O₂ reaction does not explode at all pressure and temperature combinations. For every pressure, there exists a minimum temperature above which the mixture is always explosive. However, at a given temperature, the mixture may or may not lead to explosion depending on the pressure. The explosion limits arise because of competition between (a) the reactions occurring in gas phase and at the wall and, (b) the reactions promoting formation of

chain carriers and, those deactivating them. Occurrence of multiple explosion limits in H₂-O₂ reaction is shown in Figure 2.1 [B. Lewis and G.Von Elbe, (1961)]. Since the wall effect dominates at lower pressure, either pressure or temperature has to be higher at the first explosion limit. At the second explosion limit, the chain branching and chain terminating steps [reactions (2.6) and (2.9)] are competitive and hence, temperature required to sustain the explosion increases with pressure. At the third explosion limit however, stable HO₂ molecules outnumber the radicals leading to ‘no explosion’ scenario. At still higher pressures, the HO₂ too becomes reactive and yields more active species by reacting with H₂ according to equation,

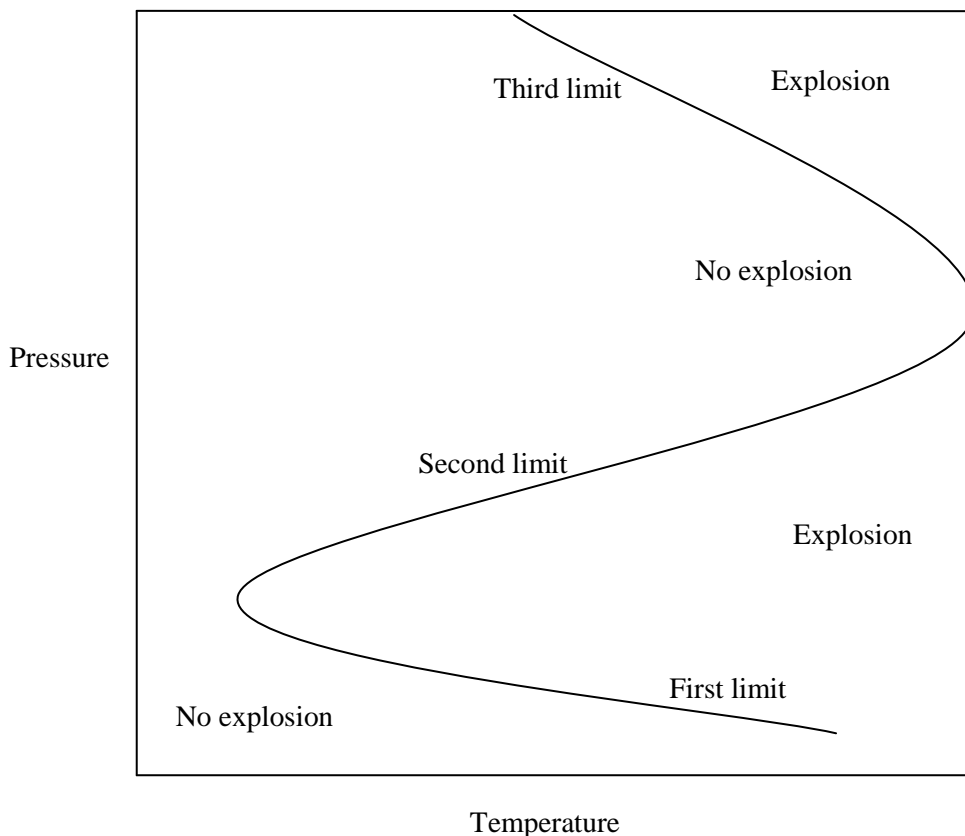
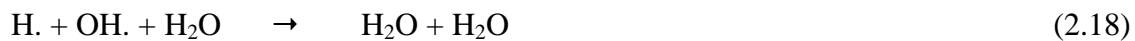


Figure 2.1: Multiple explosion limits in H₂-O₂ reaction [Lewis and Elbe, (1961)]

2.2.2 Effect of steam on H₂-O₂ reaction

Steam is usually considered to behave as a simple diluent in combustion acting as a heat sink. But, David and Mann (1942) observed moist flame temperature to be higher than dry flame temperature for open H₂-air flames. Kuehl (1962) too observed an increase in burning velocity upon replacing N₂ with H₂O vapour in low pressure H₂-air flame and postulated that steam accelerates burning by increasing the radiative heat transport from the hot combustion product to the water vapour in the unburnt gas. Muller-Dethlets and Schlader (1976) reported similar effect of steam on propane and ethylene flames. Following reactions are conceived in the H₂-O₂-steam system.



These reactions were studied numerically. Reaction (2.16) is an exothermic reaction with an enthalpy of 196 kJ/mol. Reactions (2.16) to (2.18) are chain breaking reactions where steam acts as a third body. Though HO₂ molecule formed from reaction (2.16) is stable, the large amount of heat released increases the temperature in the reaction zone by several hundred degrees. At higher temperatures, addition of steam produces more active radicals as per reactions (2.14) and (2.15). The increase in burning velocity caused by this mechanism counteracts the physical effect of steam of reducing flame temperature. However, beyond 60% steam, flame cooling mechanism dominates and hence the burning velocity decreases. The rate of reactions (2.14) and (2.15) slows down when more steam is added. This is because of reduced flame temperature at higher steam fraction. The effect of steam on recombination via reactions (2.17) and (2.18) was found to be almost negligible.

Interestingly, with H₂-Air mixture (instead of H₂-O₂), steam had only physical effect on flame temperature suggesting that the presence of other inerts such as nitrogen reduces the third body efficiency of steam.

2.2.3 Effect of O₂ diluent on H₂-O₂ reaction

The induction time (Induction time is defined as the time at which there is sudden change in the values of pressure and heat flux during reaction between a fuel and a oxidizer in a batch reactor) for 2H₂ + O₂ → 2H₂O reaction as proposed by Cheng and Oppenheim (1984) is given by,

$$\tau_{H_2} (\mu s) = 0.000154 [H_2]^{0.145} [O_2]^{-0.56} e^{\frac{17.20(kcal/mole)}{RT}} \quad (2.19)$$

The equation 2.19 is similar to Arrhenius rate expression where the concentrations of H₂ and O₂ (expressed in large brackets) are in mol/cm³ and the value of the constant is 0.000154 (cm³/mol)^(0.145-0.56)μs. The induction time reduces with increase in oxygen concentration. Though N₂ and O₂ have similar specific heat and thermal diffusivities, Koroll and Mulpuru (1986) observed increase in the burning velocity by virtue of reactions (2.4) and (2.6) (where the order of the reaction is one with respect to oxygen) when 25% nitrogen in the stoichiometric mixture of H₂-O₂ was replaced by additional 25% oxygen.

2.2.4 Effect of other diluents on H₂-O₂ reaction

Willbourn and Hinshelwood (1946) have examined the influence of hydrogen-oxygen proportions and addition of nitrogen on the third explosion limit of H₂-O₂ reaction and qualitatively showed that the third limit does depend upon the branching of reaction chains caused by the presence of inerts like nitrogen. Diluents affect burning velocity by changing transport properties and adiabatic flame temperatures. They also affect chemical kinetics.

Except for steam and O₂, the effect of the diluents on the burning velocity conform to the correlation given by I. Glassman (1986) as,

$$Su = (\alpha \dot{k})^{\frac{1}{2}} \quad (2.20)$$

where, α is the thermal diffusivity, \dot{k} is the reaction rate constant and Su is the burning velocity. Replacement of one chemically inert diluent by another alters the transport term in equation (2.20). In reaction (2.9), N₂ is more effective than Ar and He in reducing the flame temperature by facilitating formation of more HO₂ molecules. The rate constants given for this reaction as suggested by Sullivan et al. (1975) are,

$$\begin{aligned} k_{(2.9)} &= 1.5 \times 10^{15} e^{990/RT} \text{ for Ar, He} \\ &= 5.1 \times 10^{15} e^{990/RT} \text{ for N}_2. \end{aligned}$$

During another study of H₂-O₂ system on the influence of the diluents such as N₂, Ar and He, Koroll and Mulpuru (1986) observed decline in the burning velocity of the mixture to be in the order, N₂ > Ar > He. Based on this observation, they proposed the following modified expression for prediction of the burning velocity:

$$Su \left(\frac{\alpha_0}{\alpha} \right)^{\frac{1}{2}} = Su_0 (1 - x/x_L) \quad (2.21)$$

where, Su_0 and Su are the burning velocities without and with diluent respectively, x is any diluent fraction and x_L is the diluent fraction at which the burning velocity becomes zero. Equation (2.21) was found to be accurate for lean and rich flames containing He, Ar or N₂. Helium and Argon have identical molar heat capacities and therefore the same adiabatic flame temperature. But, they differ in their effect on burning velocity due to different thermal diffusivities. N₂ and Ar have nearly identical thermal diffusivities. Therefore, the difference in their effect on burning velocity can be interpreted in terms of different flame temperatures arising from their not having the same heat capacities. Any behaviour deviating from equation (2.21) would suggest that the diluents also contribute to mechanisms other than

flame cooling and heat transport. The effect of diluents on the flammability limits of H₂-Air mixture was studied by Drell et al. (1957). With addition of diluents, the rich limit sharply decreased whereas the lean limit was hardly affected. The quantity of N₂ required to prevent the flame propagation was more than that for CO₂ mainly because of lower C_p value of the former gas. Water vapour, although a combustion product, behaved similar to CO₂. Shebeko et al. (1994) experimentally studied the reaction between hydrogen-oxygen and the retardant (He, N₂, Ar, CO₂) mixtures at temperature up to 250 °C and pressure up to 20 bar. The retardants with higher heat capacity than the oxidizer were found to be more efficient in extending the lower flammability limit with concentration. However, they observed an anomalous effect of helium on the lower flammability limit of the mixture. The flammability limits for the H₂-O₂-N₂ and H₂-O₂-He mixtures narrowed down at higher pressures due to a drop in the relative concentration of the active species resulting from termolecular recombination reactions. Mellish and Linnet (1953) found the effect of diluents on reducing the flammable range for hydrogen in air as CO₂<N₂<He<Ar in wide tubes and He<CO₂<N₂<Ar in small tubes suggesting at the influence of the reactor dimension on the characteristics of the H₂-air system.

2.3 H₂-F₂ reaction system

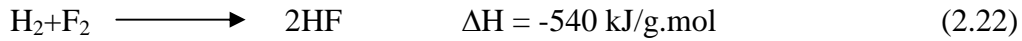
Many researchers have performed fundamental studies to understand the nature of H₂-F₂ reaction at lab scale. The reaction of fluorine with hydrogen, once initiated, proceeds over a wide range of gas compositions as a branched chain reaction [Foon, (1975)]. According to Suchand et al. (1973), H₂ reacts with F₂ spontaneously and often explodes without ignition under some conditions. Levy and Copland (1968) reported that the chain reaction of H₂ and F₂ could be stabilized by O₂ gas in their experiments. Chen et al. (1975) and Frank K Truby (1978) have performed numerous experiments to explain the explosion phenomenon by

controlling the mixing ratio of initial reactants and gas additives. They have also demonstrated the existence of explosion boundaries through gas kinetics studies. To investigate the pre-explosive reaction of an H_2-F_2 mixture, researchers such as Seeger et al. (1981) have used a tubular reactor of 1-2 mm diameter with separated gas inlets for fluorine and hydrogen, and molecular beam analysis to measure the product concentrations. The use of such small diameters is necessary to produce a molecular beam of high intensity. Depending on the initial temperatures, they found that, the reaction is either slow with practically no heat production or fast and autothermal. A few investigations carried out to explore the mechanism of hydrogen-fluorine mechanism are discussed as follows:

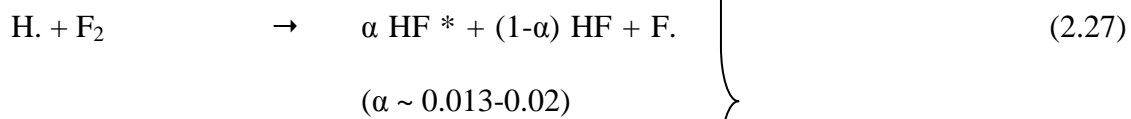
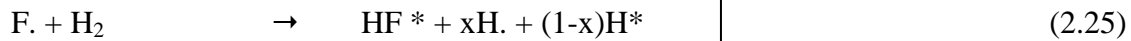
2.3.1 Proposed H_2-F_2 reaction steps

The H_2-F_2 reaction takes place even at room temperature and produces a flame whose temperature is much more than the H_2-O_2 flame. Chen et al. (1975) have discussed the mechanisms of H_2-F_2 reaction. They involve 1) diffusion of active centers like F., H., HF^* and H_2^* which initiate the chain reaction; 2) heat transport or diffusion of translational hot molecules or atoms which heat up the gas; and 3) propagation of pressure waves from the locally heated gases with supersonic speed. Here, HF^* represents HF molecules excited to the fourth vibrational level and above [Brokaw (1965_a)], and, H_2^* is the hydrogen molecule excited to first vibrational level [Kapralova et al. (1976)]. Mechanisms 2) and 3) perturb the stationary reaction kinetics so much so that at constant volume, they can vary the pressure and temperature of the reactants drastically and lead to explosion reactions, which should be avoided at all costs in a chemical reactor. Some of the selected reaction steps in H_2-F_2 reaction as proposed by Brokaw (1965_a) and Sullivan (1975) are summarized here for further discussions.

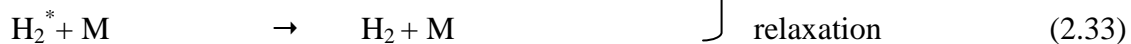
Overall reaction:



[Bond Energies of HF, H₂ and F₂ are 566, 435 and 158 kJ/gmol respectively, (<http://www.nist.gov/data/nsrds>)].



(Albeit, rate of reaction (2.30) being slow, probability of formation of H₂^{*} is less.)



(M can be any inert particle. The excess reactant also acts as an inert.)

The fluorine atoms required to initiate the reaction are formed either by dissociation at higher temperature or by collision of fluorine molecule with another high velocity molecule (reaction 2.23). The reactions (2.24) and (2.27) are exothermic with the heats of reaction being 126 and 410 kJ/gmol, respectively. The HF* molecules are energetic enough to dissociate fluorine by reaction (2.29). Rabideau et al. (1972) found the specific rate constants for reactions (2.24) and (2.26) to be $4 \pm 1 \times 10^{12} \text{ cm}^3/\text{mole}\cdot\text{sec}$ and $2.5 \pm 0.2 \times 10^{12}$

$\text{cm}^3/\text{mole}\cdot\text{sec}$ respectively at 300K; this indicates an almost instantaneous reaction. This was further consolidated by Zebib et al. (1975) who have given the composition profile of a stable, non-premixed burner flame, considering only the straight chain process and neglecting the initiation and termination steps. The scheme of reaction adopted by them included $\text{F}+\text{H}_2 \rightarrow \text{HF}+\text{H}$ and $\text{H}+\text{F}_2 \rightarrow \text{HF}+\text{F}$ only. The concentration profile presented by them showed that H_2 and F_2 never co-existed as the reaction is instantaneous.

2.3.2 $\text{H}_2\text{-F}_2$ reaction mechanism with diluents

Levy and Copeland (1963) have carried out hydrogen fluorine reaction in a flow reactor made of magnesium at 110 °C in which hydrogen was mixed with a stream of nitrogen containing 1-5% fluorine. They proposed the rate of reaction to be first order in fluorine and zero order in hydrogen. The fact that hydrogen does not appear in the kinetics suggests very strongly that it may act as an inhibitor. They further carried out studies on the kinetics of the hydrogen-fluorine reaction [Levy and Copeland (1965)] in a static reactor, where the reaction was found to be inhibited by oxygen in the temperature range of 122 to 162 °C in such a way, that for a given hydrogen and fluorine pressure, the rate reached a limiting value at some oxygen pressure and did not decrease with further oxygen addition. The reactions were carried out at atmospheric pressure, with oxygen varying from 85 to 500 mm and hydrogen and fluorine (in stoichiometric ratio) in the range of 20 to 80 mm water column. The rest was made up by nitrogen and helium. Brokaw (1965_b) and Kim and Cho (1994) also have investigated the inhibition of the hydrogen-fluorine reaction by additive oxygen. According to them, oxygen reacts with H and F atoms to bring down the rate of reaction. Sullivan (1975) and Sullivan et al. (1975) described the vibrational relaxation reaction $\text{HF}^* + \text{M} \rightarrow \text{HF} + \text{M}$, M being a diluent, to be a very fast reaction and suggested that the lighter molecules such as hydrogen and helium are more effective in de-exciting HF

molecules. Millikan and White's (1963) correlation predicts that hydrogen is nearly thirty times more effective than nitrogen in relaxing HF from the first vibrational level. Moreover, the fundamental vibrational frequencies of HF and H₂ differ by only about 6%, so that there is the possibility of de-excitation by transfer of vibrational energy from HF to H₂.

Further, Sullivan et al. (1975) have carried out some numerical simulations to provide data on the influence of the diluents on the H₂-F₂ reaction as follows:



$$k(M = \text{N}_2) = 2.38 \times 10^9 \frac{\text{cm}^3}{\text{mol} \cdot \text{s}}$$

$$k(M = \text{He}) = 7 \times 10^8 \frac{\text{cm}^3}{\text{mol} \cdot \text{s}}$$

$$k(M = \text{Ar}) = 4.6 \times 10^8 \frac{\text{cm}^3}{\text{mol} \cdot \text{s}}$$

Thus, N₂ is more effective in de-exciting HF* followed by He and Ar.



$$k \left(\frac{\text{cm}^3}{\text{mol} \cdot \text{s}} \right) = 8.4 \times 10^9 \text{ T exp} (-82.64/\text{T}^{1/3}) \text{ for He}$$

$$= 5.4 \times 10^9 \text{ T exp} (-87.34/\text{T}^{1/3}) \text{ for Ar}$$

$$= 5.4 \times 10^9 \text{ T exp} (-87.34/\text{T}^{1/3}) \text{ for N}_2$$

Thus, He is more effective in de-exciting H₂* molecules.

The product HF may also restrain the propagation of the reaction by relaxing the excited HF molecules by HF*+HF→2HF. This effect is more prominent when the reaction proceeds to a larger extent producing more HF. Addition of any gas other than hydrogen and fluorine in a F₂-H₂ chemical laser initiated by a relativistic electron beam has a significant effect on the energy and the duration of the laser pulse. Three ways by which a gas additive affects the laser energy are, i) change in specific heat, ii) acceleration of the rotational relaxation of HF

molecules and iii) generation of 'F' atom. Spencer et al. (1972) have used nitrogen and helium to produce F atoms from SF₆ in a continuous HF laser. The laser performance in terms of lasing length and specific power yield improved when nitrogen was replaced by helium because, helium promoted formation of more F atoms. Similarly, Nedoseev et al. (1989) observed that, when initial mixture of F₂, H₂ and O₂ was diluted with helium in the range of 1-2 times of fluorine concentration, the output energy increased by 2-2.5 times and, the duration of the laser increased from 105 to 140 ns. This dependence was attributed to an accelerated rotational relaxation of the HF* molecules. Any further rise in the quantity of helium did not alter the output energy. The rate of chemical reaction slowed down due to increase in specific heat capacity of the mixture. L D Hess (1972) observed the enhancement effect of MoF₆ on the HF chain reaction chemical laser without causing a significant deactivation of vibrationally excited hydrogen fluoride. Addition of small amounts of MoF₆ to the H₂-F₂ chain reaction system resulted in significant increase in the HF laser output power with a reduction in the pulse duration. Equilibrium calculations done by Cummings et al. (1977) indicated negligible possibility of the formation of either NF₃ or NH₃ at higher temperatures, when nitrogen was added as a diluent.

2.4 Effect of diluents on other fuel-oxidizer systems

Wheatly and Linnett (1952) and Clingman, Brokaw and Pease (1953) studied the effect of the diluents on the flame velocity for the acetylene-oxygen and the methane-oxygen system respectively. Rabinowitch (1937) found the order of effectiveness of the inert molecules in causing recombination of hydrogen and bromine atoms to be N₂>H₂>Ar>He. Huffstutler et al. (1955) have discussed the effect of the diluents such as nitrogen, argon and helium on the burning velocity of the hydrogen-bromine flame. In their experiments, helium and nitrogen had a non-repeatable effect on the burning velocity with the change in the

bromine to He/N₂ ratio. Nitrogen caused the highest reduction in the burning velocity because it was more effective in causing recombination of H and Br atoms. Potter et al. (1956) studied the effect of helium, argon and nitrogen on the propane-air mixture. The lower flammability limit of propane in air is 2.38%. When nitrogen in air was replaced by equal amount of helium and argon, the limit reduced to 1.92 and 1.79% respectively. Sandry R. (1956) studied the effect of helium, nitrogen and argon on the methane combustion system. The flame velocity was found to be maximum for helium followed by argon and nitrogen. Tressaud et al. (2007) have studied the effect of diluents such as He, N₂ and Ar on the fluorination of polymers. Compounds of nitrogen such as amines and NO acted as radical quenchers and caused an increase in the termination of the peroxy and the fluoro radicals formed in the fluorinated layer. Okada and Makuuchi (1969) found helium and nitrogen useful in the fluorination of polyethylene powder to improve its physical properties. Both the gases prevented a fiery and intense fluorination reaction in the process. Langan et al. (1996) have studied the role of the diluents (Ar, He, N₂, O₂ and N₂O) in the NF₃ plasma processing to reduce SiO₂ to SiN. They proposed a dominating role of the diluents to control the electronegativity of the plasma discharge. The electrical measurements taken by them revealed that the diluents have a profound effect on the plasma impedance and the actual power dissipated in the discharge. The NF₃ plasma diluted with argon exhibited the lowest impedance and the highest power dissipation while the N₂O diluted plasma had the highest impedance and the lowest power dissipation rates. The premixed oxygen-acetylene flame is utilized in the chemical vapor deposition of diamond. Hahn et al. (1997) found a strong effect of the flame temperature, the stoichiometry and the diluent addition on the diamond film quality. Hanser et al. (2007) have analyzed the influence of diluent gases on the metal-organic vapor phase epitaxy of GaN thin films. The GaN growth rates were found to be ~30% higher when H₂ was used as the diluent. The measured differences in the growth rates

of the GaN films in H₂ and N₂ were attributed to the different transport properties of these mixtures. Sakurai (1974) has reported the rate of BrF₃-UO₂ reaction decreased by nearly a half when the carrier gas for BrF₃ was changed from helium to argon. This was attributed to the decrease in diffusion rate of BrF₃ in the relatively stagnant gas film between the solid phase (UO₂) and the main gas stream. Fackler et al. (2011) described an experimental and numerical study of the dilution effect on the emission of nitrogen oxides (NO_x) from CH₄ combustion. Their results showed that the N₂ dilution increases the NO_x production more effectively than the equivalent CO₂ because of the ability of CO₂ to deplete the radicals taking part in the NO_x formation chemistry. Shrestha and Karim (2001) have analytically explained the effect of nitrogen and CO₂ present in methane on the engine performance and shown the inhibiting characteristics of CO₂ to be much greater than nitrogen. Similar effect was also observed by Liu and Most (2009). The effects of a number of flame retardants such as CF₃I, CF₃Br, and CF₃H, on methane-air system, were studied by Babushok et al. (1996) in a plug flow reactor. As concluded by them, the ignition delay was either increased or decreased by the initial retardant decomposition kinetics, which released the active species into the system. These species could either terminate or initiate the reaction chains. On the other hand, the presence of the retardants always caused increase in the reaction time by reducing the concentration of active radicals such as H., OH. and O., which were formed during the combustion process. Park et al. (2002) have numerically analyzed the effect of the dilution of the air stream on the flame structure in the methane-air combustion. The dilution effect in decreasing the flame temperature varied as CO₂>H₂O>N₂, although the thermal heat capacity of H₂O was the highest. This was because of the different breakdown behaviour shown by CO₂ and H₂O in the high temperature region. The breakdown of H₂O leads to the formation of radicals such as H., O. and OH. so that, the chain reaction step $H+O_2 \rightarrow O+OH$ is

augmented considerably. On the other hand, the breakdown of CO_2 inhibits the chain branching mechanisms.

2.5 Comparison between the $\text{H}_2\text{-O}_2$ and $\text{H}_2\text{-F}_2$ systems

There are some obvious differences between the two systems. At ambient conditions, $\text{H}_2\text{-O}_2$ reaction needs external stimulus (ignition) to start, whereas hydrogen will react readily with fluorine. The calculated adiabatic flame temperatures of $\text{H}_2\text{-O}_2$ and $\text{H}_2\text{-F}_2$ mixtures, at their stoichiometric ratio, are 3473 K [http://en.wikipedia.org/wiki/Adiabatic_flame_temperature] and 4300 K respectively. The nature of reaction products from the two reactions is also different. The combustion product of hydrogen-oxygen system is water vapour. It burns in a non-luminous, almost invisible pale blue, hot flame liberating the chemically bound energy as heat. The thermal energy radiated from the hydrogen flame is very low due to a strong absorption by the ambient water vapour which eventually acts as a flame quencher. Therefore, despite its high flame temperature, the burning hazard is comparatively small in the $\text{H}_2\text{-O}_2$ mixture. The reaction product HF from the $\text{H}_2\text{-F}_2$ reaction on the other hand promotes chain propagation (reactions 2.29 to 2.31). The energy released during de-excitation of the energetic HF molecules has been used in producing HF chemical laser. Unlike hydrogen-oxygen, due to very high equilibrium constant, the hydrogen-fluorine reaction is almost irreversible even up to a temperature as high as 5000 K. A comparison between the thermodynamic data of the two reactions is given in Table 2.1. Further, the influence of diluents such as oxygen is found to be different in both the reaction schemes. Though increase in oxygen content enhances the rate of $\text{H}_2\text{-O}_2$ reaction, Kim and Cho (1994), who worked on the HF chemical laser, found that the rate of formation of HF was reduced by addition of O_2 . The pulse power and the temperature of the system came down with increase in concentration of O_2 in the reaction mixture. Presence of oxygen in $\text{H}_2\text{-F}_2$ reaction leads to termination of chain reaction by forming stable radicals such as

HO₂ and FO₂. Levy and Copeland (1965, 1968) and Brokaw (1965_b) also reported that oxygen inhibits H₂-F₂ reaction by reacting with active H and F atoms and bringing down the reaction rate. One apparent advantage of addition of oxygen however, is that it makes the system easily controllable, so that, the composition of H₂ and F₂ can be kept high at a given pressure. With this arrangement, it is possible to obtain higher output energy than oxygen free environment.

Table 2.1: Change in the equilibrium constants of the H₂-O₂ and the H₂-F₂ reactions with temperature

H ₂ -O ₂ reaction ($\Delta G^{\circ}_R = 228600 \text{ J/gmol}$) [Harrison (1960)]		H ₂ -F ₂ reaction ($\Delta G^{\circ}_R = 542200 \text{ J/gmol}$)	
		Temperature in K	K _{eq}
298	1.0029E+40	298	1.09024E+95
500	7.5225E+22	500	4.38899E+56
1000	1.7564E+10	1000	2.09499E+28
1500	1081560.53	1500	7.59955E+18
2000	8487.15436	2000	1.44741E+14
2500	463.008392	2500	2.13046E+11
3000	66.5998683	3000	2756728701
3500	16.6710251	3500	123528255.9
4000	5.89968746	4000	12030828.08
4500	2.62995035	4500	1966056.61
5000	1.37797833	5000	461568.7702

Besides above discussions on the informations available with respect to H_2-F_2 reaction, there are many areas (such as effect of various parameters namely, flow ratio, presence of diluents, preheating etc. on the behaviour of the reactor handling H_2-F_2 reaction) which need to be addressed by proper planning and systematic investigations.

.....

CHAPTER 3

PLAN OF EXPERIMENTS

The present part of the thesis discusses about the experimental planning to carry out the investigations on the effect of various parameters on the behaviour of H₂-F₂ flame reactor aimed at acquiring useful data for further research and development. Selection of parameters, their range and the sequence of conducting experiments is also presented in this chapter.

3.1 Introduction

The reaction between hydrogen and fluorine is being attempted at this scale with very little literature information in the background, except that it is a chain reaction and could be devastating if the excess heat is not removed from the reactor system. Though the release of heat of reaction for any fuel-oxidizer system is proportional to the concentration of the limiting component, the temperature is the maximum at the stoichiometric ratio. Table 3.1 gives the calculated flame temperature for the pure Hydrogen-Fluorine reaction mixed in different proportions at atmospheric pressure and room temperature [Wilson et al. (1951)].

Table 3.1

Theoretical flame temperature by Wilson et al.(1951)

Mole% F ₂	Mole% H ₂	Theoretical Flame Temperature at 1 atm (K)
10	90	1920
33.3	66.7	3550
50	50	4300
66.7	33.3	3800

Taking safety into cognizance, it is better to deal with reactive mixtures rich in hydrogen so that, not only the temperatures are lower but also the quantum of toxic and hazardous fluorine gas handling will be minimal. Therefore, to be on the conservative side, the experiments are started with a huge excess of hydrogen reacting with fluorine in the flow reactor. The idea is to first establish confidence in handling such kind of reaction in a smooth and sustained manner, and then go about various designs of experiments to study the effect of different parameters on the chemical reaction. Work of this nature demands highly reliable process

instruments, an all inclusive data acquisition system and adequate training in handling. Because of the safety issues, the experiments require careful planning, so that the number of experiments is minimized but yield meaningful results. In the following sections the selection of parameters, their range and also the sequence of experiments are discussed. The design of the experimental set up depends on the plan of experiments. In order to carry out the planned studies on H_2-F_2 reaction, two types of experimental set ups are required to be designed and built. One is a flowing type tubular reactor where the investigations will be performed as described in the sections 3.2, 3.3, 3.4, 3.5 and 3.8, while the other one is a batch reactor which will be used to carry out experiments as mentioned in the sections 3.6 and 3.7. The design, fabrication, assembly and testing of the experimental facility should address the safety. This aspect will be further discussed in Chapter-4 on 'Experimental Set-up and Design Methodologies'.

3.2 Preliminary experiments to establish feasibility of handling H_2-F_2 reaction

The initial few experiments with arbitrarily chosen gas flow rates are planned to test the adequacy of control and the safety system of the experimental set up, and also have some idea about the reaction flame and the temperature distribution inside the reactor resulting from the reaction between hydrogen and fluorine. Another objective is to generate process data primarily in the form of reactor temperatures, which will be used for the validation of the computational model being developed for this purpose. The test run starts with a very high excess of hydrogen (>400%) over F_2 because lean mixtures of F_2 do not have high flame temperatures. The quantity of hydrogen is then reduced stepwise and slowly. The three cases with varying flow rates of F_2 and H_2 are listed in Table 3.2. The content of nitrogen in the fluorine stream is the same in all the cases. The adiabatic flame temperature for these cases varies from ~2500 to 3500 K. It is practically impossible to measure this high temperature,

that too in a highly corrosive atmosphere. Therefore, the temperature sensors are placed in such a way that they do not lie in the flow path of fluorine stream where very high

Table 3.2

Gaseous flow rates and adiabatic flame temperature

Case no	Flow Rate, F ₂ (slpm)	Flow Rate, H ₂ (slpm)	H ₂ /F ₂ ratio	Adiabatic flame temp in K
1	0.44	2	4.54	2488
2	0.5	2	4	2691
3	0.48	1	2.08	3546

(Note: The uncertainty in measurement of the flow rate is within +- 1% of the value)

temperatures are expected. Furthermore, there is a need to provide flexibility in locating the thermocouples near the feeding nozzles so that the sensor position can be adjusted in order to get a clearer picture of the reaction flame. It is important to measure and control the individual gas flow rate with the best possible accuracy. Therefore, the orifice flow meters are calibrated frequently and the flow set points are increased gradually. For example, to reach a value of 0.4 slpm for fluorine, the set points are increased in the sequence of 0.1, 0.2, 0.3 and 0.4 slpm respectively. The set point is changed only when the reactor temperatures are stabilized. These initial experiments are very important, as the range of the parametric investigations and the flame reactor design will be dependent on their results.

In most of the applications, it is desirable to have a flat temperature profile in the reaction zone to maximize the conversion in a chemical process. There can be many parameters such as reactant feed rates, feed ratios, initial temperatures and presence of an

inert etc., which affect flame temperatures as well as the reactor temperatures. It is planned to take up these parametric investigations, one by one, varying a single parameter at a time while holding others constant.

3.3 Flow ratios of hydrogen, nitrogen and fluorine in a tubular reactor

Besides hydrogen and fluorine in the feed, nitrogen is always present in the fluorine stream in small quantities. Due to operational requirements, fluorine is mixed with nitrogen when it is produced from electrolysis of HF. A few experimental studies are planned to see the influence of excess hydrogen, H_2 to F_2 ratio and varying nitrogen flow rates on the reactor temperatures and compare the observations with predictions from the computational model. If there is a good match between the two, then the computational tool can be used to simulate cases involving higher fluorine flow rates and species other than hydrogen and fluorine, which will be required in the design of a flame reactor. The chosen flow rates of gases are as per Table 3.3. Albeit, the composition of hydrogen is varied systematically, the quantity of nitrogen is chosen arbitrarily just to study the role of nitrogen in thermal dissipation inside

Table 3.3

Gaseous flow rates and adiabatic flame temperature

Case no	Flow Rate, F_2 (slpm)	Flow Rate, H_2 (slpm)	Flow Rate, N_2 (slpm)	Parameter	Adiabatic flame temp in K
4	0.2	0.63	0.4		2682
5	0.2	0.85	0.4		2367
6	0.2	1.27	0.4		1954
7	0.3	0.95	0.45		2830

8	0.3	1.27	0.45	Excess Hydrogen	2487
9	0.3	1.91	0.45		2025
10	0.4	1.27	0.5		2911
11	0.4	1.7	0.5		2545
12	0.4	2.54	0.5		2067
13	0.2	0.85	0.9		Additional Nitrogen
14	0.2	0.85	3.4	1090	
15	0.3	1.27	1.95	1715	
16	0.3	1.27	3.45	1333	
17	0.4	1.7	1.5	2043	
18	0.4	1.7	3.5	1500	
19	0.2	0.74	0.4	Excess Hydrogen	2513
20	0.2	1.06	0.4		2137
21	0.3	1.11	0.45		2646
22	0.3	1.6	0.45		2221
23	0.4	1.48	0.5		2718
24	0.4	2.12	0.5		2277
25	0.2	0.85	1.4	Additional Nitrogen	1647
26	0.2	0.85	1.9		1446
27	0.2	0.85	2.4		1296
28	0.3	1.27	2.45		1560
29	0.4	1.7	2		1867
30	0.4	1.7	2.5		1722

(Note: The uncertainty in measurement of the flow rate is within +/- 1% of the value)

the reactor. In the designed set of experiments, hydrogen percentage is varied from 215% (v/v) excess to 535% (v/v) excess for three base flow rates of fluorine, namely, 0.2, 0.3 and 0.4 slpm, respectively. The flow rate of fluorine premixed with nitrogen is held constant while that of hydrogen is varied. Nitrogen, between 0.4 and 3.4 slpm is premixed with the F₂ stream (for all the base flow rates of fluorine) to study its effect on reactor temperatures. In every case involving additional nitrogen, fluorine is made to react with ~325 % excess of hydrogen. The reactor is operated at 1000 mbar (abs) pressure in all the cases.

3.4 Reactor and reactant preheating

The equilibrium constant of dissociation of a gas molecule into its constituent atoms increases with temperature. Initial concentration of active atoms is an important feature of a propagative type reactive gaseous system. In any chain reaction, the promulgation of the chain depends on the rate of active species/radicals created or destroyed. These species may be generated either by thermal dissociation due to thermal avalanche or by colliding with another high energy molecule due to chain avalanche. At the same time, they may lose their energy or recombine either by collision with an inert molecule or hitting against a solid wall. In addition to initial temperatures of the reacting gases, the solid boundary wall temperatures can play a decisive role in dictating the profile of temperature, velocity and species concentration inside the reactor. Hence, it is decided to conduct a few experiments to investigate the effect of reactant preheating and reactor wall preheating on the reactor temperature distribution. With the equipment safety in mind, the upper limit of wall temperature is restricted to 423 K. The base flow rates of fluorine and hydrogen are maintained similar to those discussed in previous section 3.3. The feeding lines and the process reactor are preheated by resistance based nichrome wire heaters. The desired skin

temperature is achieved by using an on/off controller. A total of nine cases, as shown in Table 3.4, are considered for this study.

Table 3.4
Gaseous flow rates and adiabatic flame temperature

Case no	Flow Rate, F ₂ (slpm)	Flow Rate, H ₂ (slpm)	Flow Rate, N ₂ (slpm)	Parameter
31	0.2	0.85	0.4	Only reactor preheating off
32	0.3	1.27	0.45	
33	0.4	1.7	0.5	
34	0.2	0.85	0.4	Only feed line preheating off
35	0.3	1.27	0.45	
36	0.4	1.7	0.5	
37	0.2	0.85	0.4	Both feed line and reactor preheating off
38	0.3	1.27	0.45	
39	0.4	1.7	0.5	

(Note: The uncertainty in measurement of the flow rate is within +- 1% of the value)

3.5 Fluorine flow rates

When reactions between hydrogen and fluorine are carried out, the reactor wall temperature is controlled by regulating the flow of either air or water in the cooling circuits attached to the reactor. With increase in the energy released per unit volume, the choice of the cooling fluid depends on its heat transfer characteristics and the quantity of heat deposited on the reactor walls. The quantity of heat deposited on the walls in turn depends upon the nature

of flame produced in the chemical reaction. Though adiabatic flame temperature remains the same as long as the feed ratio is maintained, the flame dimensions can vary according to the flow rates and the dynamic conditions prevalent inside the reactor. While air is adequate as a cooling medium for lower flow rates of fluorine (up to 0.4 slpm), requirement of water is foreseen as the means of reaction heat removal for higher fluorine flow rates (>0.4 slpm). The maximum envisaged flow rate of fluorine is 0.8 slpm with an energy release of ~320 watts. The advantage one would derive from higher flow rates of fluorine is that it will result in higher reactor temperatures which can be used to drive the chemical reactions needing high activation energies. The augmented capacity of the reactor to process more feed should not be seen only with respect to higher reaction temperatures but also on the basis of energy efficiency. Therefore, the limit on increasing the fluorine flow rate can be applied both from the safety concerns and on the basis of energy utilization efficiency. The results from this exercise offer useful information about the optimized capacity of a given reactor system. In the present consideration, the tubular reactor behaviour has been studied while increasing the fluorine feeding rate from 0.4 to 0.8 slpm for a fixed ratio of hydrogen to fluorine. The planned flow rates of gases in this investigation are given in Table 3.5.

Table 3.5

Higher flow rates of gaseous in the tubular reactor

Case no	Flow Rate, F ₂ (slpm)	Flow Rate, H ₂ (slpm)	Flow Rate, N ₂ (slpm)
40	0.4	1.6	0.22
41	0.5	2	0.27
42	0.8	3.2	0.45

(Note: The uncertainty in measurement of the flow rate is within +- 1% of the value)

3.6 Study of effects of type and quantity of diluents on H₂-F₂ reaction in a flame in a batch reactor

The choice of diluent gases in flame reactors must be made with care, as the temperature distribution can depend strongly on the type of the diluent gas used. The presence of a diluent can bring about significant changes in the combustion characteristics of fuels. It may reduce or improve the effective utilization of fuel in the conventional combustion devices. In a chain type reaction, such as, reaction between hydrogen and fluorine, the diluent gases can propagate chain formation by generating more active species due to enhanced collision. They can also inhibit some of the intermediate reaction steps either by relaxing the excited species, facilitating recombination of active atoms or forming a stable compound which possibly may help in termination of the chain reaction. The enhancing or the inhibiting effect of the diluents is dependent on several factors, such as, the type of inerts, their concentration, the reactor geometry, the mixing pattern etc. In addition to the information that the species other than the participating reagents influence considerably the momentum and energy dissipation, it is important to explore the impact of other diluent species on H₂-F₂ reaction at a relatively more fundamental level. There is a need to understand, as which attributes (thermal, physical and chemical) of an external species affect the kinetics and the course of highly reactive and exothermic reaction between hydrogen and fluorine. The choice of additives or inerts is based on their ease of availability and economic viability. Thus, helium, nitrogen and argon are finalized to be used as diluents in the H₂-F₂ system. It is planned to conduct transient experiments in a batch reactor without compromising on the safety related issues. The philosophy of operation, control and safety for the batch reactor is similar to the flow reactor used previously, except that the frequency of data logging is increased so that, more data is available for analysis. Provision is made for charging and neutralizing the toxic gases. A dedicated evacuation system is installed to

ensure that no trace of product or un-reacted gas is left in the reaction chamber before a fresh trial is taken. Adequate instrumentation in the form of thermocouples and pressure transmitter is integrated to the system for data acquisition. Several sets of unsteady state experiments as listed in Table 3.6 are conducted in the batch reactor, which is designed as a horizontal cylindrical vessel. The main objectives of the experiments are to study the behaviour of the Hydrogen-Fluorine flame reactor with respect to change in temperature and pressure with time, when three types of diluents namely helium, nitrogen and argon are introduced into the system. It is necessary to maintain a high pressure in fluorine surge tank to evade any possibility of back flow of gaseous mixture from the reactor to the tank. The pressure difference between the fluorine surge tank and the reaction chamber, diameter of the fluorine feeding tube and the size of the reactor are so chosen that the jet issuing from the F₂ nozzle

Table 3.6

Quantity of diluents in the batch reactor operating at higher pressure

Case no	Type of diluent	Diluent % (mole basis) wrt H ₂
43	None (base reaction)	0
44	Helium	11.11
45	Helium	33.33
46	Helium	42.86
47	Nitrogen	11.11
48	Nitrogen	33.33
49	Nitrogen	42.86
50	Argon	11.11
51	Argon	33.33
52	Argon	42.86

forms a round, turbulent free jet. Upper limit on the diluent concentration (~43%) is based on the preliminary calculations on permissible pressure rise resulting from the addition of extra molecules and temperature increase. To ensure safety, it is necessary to study the jet behaviour to see if the expanding flame touches the reactor walls soon after the fluorine is introduced into the system. The empirical correlations are available for free expansion of jets discharging into the fluid of equal density, when no buoyancy force is acting on them. Fluorine stream being denser than the mixture of hydrogen and the diluent in the reactor, the actual jet spread will be less rapid than the neutrally-buoyant jet modeled through the available equations. Detailed examination on this issue is further discussed in the Chapter-4.

In combustion, equivalence ratio is defined as the molar ratio of fuel to oxidizer as compared to its stoichiometric ratio. There is a dominant effect of initial pressure on the combustion behaviour at higher and lower equivalence ratios, as there is less dissociation. The mixing effects can be more significant at lower pressure levels. Further, the possibility of chain propagation is less if the reactor is operated at lower pressure. Therefore, while dealing with higher equivalence ratio (~2) in the experiments with the diluents, it is worthwhile to extend the above study of dilution effect to a lower initial chamber pressure. Consequently, a few more experimental trials as detailed out in Table 3.7 are planned wherein, the sequence of operation is similar to the one discussed above. The only distinction between the two sets of experiments is the initial pressure up to which hydrogen is filled in the chamber. Quantities of both hydrogen and fluorine are brought down so as to maintain more or less the same equivalence ratio in the two types of investigations. Since, the operations are carried out at reduced pressure, the pressure surges, as a consequence of the energy release during the reactions will not lead to a rise in pressure that is unsafe for the reactor. Therefore, the content of the diluents in the mixture can be increased from 43% to 83%.

Table 3.7

Quantity of diluents in the batch reactor operating at lower pressure

Case no	Type of diluent	Diluent % (mole basis) wrt H ₂
53	None (base reaction)	0
54	Helium	11.11
55	Helium	33.33
56	Helium	50
57	Helium	66.67
58	Helium	83.33
59	Nitrogen	11.11
60	Nitrogen	33.33
61	Nitrogen	50
62	Nitrogen	66.67
63	Nitrogen	83.33
64	Argon	11.11
65	Argon	33.33
66	Argon	50
67	Argon	66.67
68	Argon	83.33

3.7 Generation of temperature curve with variation in the fluorine composition

Subsequent to transient studies on hydrogen fluorine reaction, experiments are planned to reproduce the reaction temperature curve when the content of fluorine is raised from lean to rich. To avoid increase in the reactor temperatures when the hydrogen-fluorine

composition approaches the stoichiometric ratio, which in turn may cause reactor pressure to reach an unsafe level, the quantities of hydrogen and fluorine to be used for these experiments are reduced by choosing a lower initial reactor chamber pressure. Although the adiabatic flame temperature depends on the fuel to oxidizer ratio rather than their individual quantities, low pressure operations will ensure that the reactor temperatures do not escalate to an alarming value because more margin is provided for hot product gases to expand and cool down subsequently. Thus, keeping the moles of hydrogen constant in the reactor, the fluorine

Table 3.8

Mole fractions of F_2 in H_2 - F_2 reaction and corresponding adiabatic temperature

Case no	Mole fraction of fluorine	Adiabatic flame temperature in K
69	0.166667	2489
70	0.333333	3820
71	0.375	4083
72	0.473684	4626
73	0.545455	4548
74	0.565217	4476
75	0.583333	4415
76	0.6	4365
77	0.62963	4284
78	0.6875	4155
79	0.791667	3986
80	0.846154	3917
81	0.891304	3868

mole fraction is varied from 16 to 90%. Further details along with calculated adiabatic flame temperatures are given in Table 3.8. The components of the experimental set up, the instrumentation and control scheme, the data acquisition system and the operation sequence etc. will be similar to the earlier studies mentioned in the section 3.6. The results from this study will provide new data for Hydrogen-Fluorine system.

3.8 Study on dilution effect in a flowing type H₂-F₂ flame reactor

The research in the area of the hydrogen–fluorine reaction hitherto, mainly concentrated on the reaction thermodynamics, the effect of the reaction on fluid flow, and the probable reaction mechanisms through small scale experiments. Though investigators particularly from the field of HF chemical laser have studied H₂-F₂ reaction with diluents, the experimental investigations on the influence of these diluents on the H₂-F₂ reaction in engineering scale have not been reported. The experiments handling hydrogen and fluorine on fairly large scales have been planned in the earlier section (section 3.2). Study on the influence of excess hydrogen and additional nitrogen on the performance of flame reactor is described in the section 3.3. Furthermore, the transient study on H₂-F₂ reaction induced thermal effects affected by presence of the diluents such as helium, nitrogen and argon in a static, cylindrical, horizontal reactor has been discussed in the section 3.6. The effect of dilution is expected to be different when there is change in the gas feeding configuration and the type of reactor (static/flow). This can be because of the change in the mixing pattern inside the reactor. It is planned to conduct a few experiments with the diluents (He, N₂ and Ar) in the flowing type tubular reactor where the feeding nozzles, their position and the resultant mixing effects are different from that of the batch reactor. The experimental set up, the operation and the control schemes will be similar to the ones discussed under sections 3.2 to 3.5. Fluorine @ 0.5 slpm and hydrogen @ 2 slpm are the selected flow rates for this study.

Thermal effects are studied in the reactor. Hydrogen and the diluents are supplied from commercially available high purity (>99.9%) gas cylinders whereas fluorine is produced by electrolysis of HF. Regulated flow of diluents through a control valve is premixed with the fluorine stream before feeding into the reactor. They are added in the quantities such that the percentage of diluents admixture with fluorine is between 0 and 85. However, the mole fraction of the diluents in the product gaseous mixture (assuming entire fluorine is reacted) varies from 0 to 0.545. The details on the gas flow rates, diluent concentration and the nozzle exit velocities are given in Table 3.9.

Table 3.9

Flow rates of gases for dilution study in the flow reactor

Case no	F ₂ (slpm)	H ₂ (slpm)	He mixed with F ₂ (slpm)	N ₂ mixed with F ₂ (slpm)	Ar mixed with F ₂ (slpm)	Diluent % (mol basis) wrt F ₂ +diluent	Mole fraction of diluent in the product mixture (ass. 100% F ₂ consumption)	Velocity at F ₂ nozzle exit, m/s	Velocity at H ₂ nozzle exit, m/s
82	0.5	2	0	0	0	0	0	5.781	1.6978
83	0.5	2	0.3	0	0	37.5	0.12	8.033	1.6978
84	0.5	2	0.5	0	0	50	0.17	9.534	1.6978
85	0.5	2	1	0	0	66.66	0.286	13.29	1.6978
86	0.5	2	2	0	0	80	0.44	20.8	1.6978
87	0.5	2	3	0	0	85.7	0.545	28.3	1.6978
88	0.5	2	0	0.3	0	37.5	0.12	8.033	1.6978
89	0.5	2	0	0.5	0	50	0.17	9.534	1.6978

90	0.5	2	0	1	0	66.66	0.286	13.29	1.6978
91	0.5	2	0	2	0	80	0.44	20.8	1.6978
92	0.5	2	0	3	0	85.7	0.545	28.3	1.6978
93	0.5	2	0	0	0.3	37.5	0.12	8.033	1.6978
94	0.5	2	0	0	0.5	50	0.17	9.534	1.6978
95	0.5	2	0	0	1	66.66	0.286	13.29	1.6978
96	0.5	2	0	0	2	80	0.44	20.8	1.6978
97	0.5	2	0	0	3	85.7	0.545	28.3	1.6978

(Note: The uncertainty in measurement of the flow rate is within +- 1% of the value)

3.9 Conclusions

Several parametric investigations are planned not only to gain experience in conducting experiments but also to acquire a wide spectrum of process data related to the characteristics of the hydrogen-fluorine reaction. The types of data that can be extracted from the experiments are in the form of reactor temperature and pressure. Details of reactor fabrication, placement of instruments and the operational methodology for this purpose is provided in the Chapter-4.



CHAPTER 4

EXPERIMENTAL SET UP AND DESIGN

METHODOLOGIES

The two types of experimental facilities where the experiments have been conducted are described in this chapter. The objective of using the first type of facility has been to initially establish the feasibility of carrying out H_2-F_2 reaction in a flowing type reactor to study the effect of parameters such as flow ratios, preheating and addition of diluents with the reacting stream and generate data which can later be used to validate a CFD model. The main focus of the experiments carried out in the second facility has been to generate the H_2-F_2 reactor temperature data with fluorine component increasing from lean to rich and study the transient response of the H_2-F_2 flame reactor at different pressure levels when the composition of the inerts is varied. The basis of selection of instruments, the safety measures and the sequence of operation have also been discussed.

4.1 Introduction

An experimental facility is set up where information related to the hydrogen-fluorine reaction can be collected by designing simple and safe experiments. Two types of experimental facilities are created to accomplish the objectives as envisaged under ‘plan of experiments’ in the Chapter-3. Since reaction between hydrogen and fluorine can lead to an explosion at any composition, it is necessary to have adequate instrumentation, controls and safety measures incorporated in the system, which will not only serve to record the process data but also ensure the personnel and the equipment safety. The following steps have been adopted during the installation of the test facility to address the safety concerns.

4.2 The safety issues

To ensure reliable functioning, the integrity of the set up components such as piping, valves and instruments are checked thoroughly during the installation. Seamless pipe has been chosen for the reactor fabrication so that it can withstand a higher internal pressure. The fabrication is carried out by skilled technicians under strict supervision. All the weld joints, whether in an equipment or in piping, are 100% radiographed to rule out any chances of fabrication defect. The equipments and pipelines are subjected to hydro and pneumatic testing at pressures above the design pressure. The leakage testing of the pipe lines, especially hydrogen feed line, is carried out using helium mass spectrometer leak detector. Engineered safety features such as adequate ventilation and installation of the gas detectors are adopted to ensure personnel safety during operation. To carry out the periodic surveillance for leakage of the toxic gases such as fluorine and hydrogen fluoride, hand held detectors are also made available to the operating staff. The reactor is kept in a larger room with multiple access points, which will be helpful in event of an emergency. Furthermore, to meet an exigency, an emergency door and windows are also provided in the reactor room. All the instruments such

as thermocouples, pressure transmitters, pressure switches and the flow meters used during the trials are procured from reputed sources and are periodically tested and calibrated using standard references. Adequate process interlocks and the safety trips are identified and implemented in the system. Manual intervention during the trials is minimized and the entire operation is designed to be operated from a remotely located control room with a provision for data logging, alarm annunciation and safe shutdown of the entire facility. The above safety precautions and the operation methodologies are implemented in all the intended experimental trials. Further details on the components of the experimental set ups are discussed below.

4.3 Setting up of experimental facilities

The fundamental difference between the two types of facilities is with respect to the type of the process reactor where reaction between the two gases is carried out. The first reactor is a vertical cylindrical reactor (VCR) where flow experiments are conducted, whereas the other reactor is a horizontal cylindrical reactor (HCR) where the transient studies on H_2-F_2 reaction are performed. The VCR is employed in the investigations described under sections 3.2, 3.3, 3.4, 3.5 and 3.8 of the Chapter-3, whereas studies covered under the sections 3.6 and 3.7 of the same chapter have used the experimental facility involving the HCR. Sources for feeding hydrogen and fluorine are the same in both the cases. In either case, the product HF along with other gases, namely, hydrogen and inerts such as nitrogen, helium or argon are sent to the scrubbing system. Various components of the experimental systems are described below.

4.3.1 Details of the experimental facility involving the VCR

Figure 4.1 shows the block diagram for the H₂-F₂ reaction system with the VCR. The experimental set up consists of a process reactor (Figure 4.2), feeding system and the scrubbing system. The VCR is made from 2" NB, Sch-40 seamless Monel-400 pipe with flanges at either end. Hydrogen and fluorine nozzles are fixed by welding to the top cover flange. They are slightly inclined towards each other and also with respect to the longitudinal axis of the reactor. Hydrogen nozzle is shorter than the fluorine nozzle inside the reactor. The fluorine gas is fed from a 2 mm diffuser type nozzle, whereas hydrogen is discharged into the reactor through a 12.5 mm diameter distributor having multiple pores of 1 mm size. The pores provided in the hydrogen nozzle help distribute the hydrogen gas evenly in the reaction chamber so that a uniform hydrogen cover is formed. The diluent gases are premixed with the fluorine stream before entering the reactor. Hydrogen gas and the diluents (as applicable) are supplied from the respective gas cylinders, while fluorine is generated by electrolysis of hydrogen fluoride in an electrolytic cell using KF.2HF as the electrolyte. Since, the anode chamber of the electrolytic cell where fluorine is produced is always purged with small quantity of N₂, the fluorine stream carries a small fraction of nitrogen along with pure fluorine. The fluorine produced from electrolysis of HF is passed through a chemical trap to remove entrained HF so as to minimize the unwanted effect on the reaction rate between hydrogen and fluorine. Flow rates of the gaseous streams namely hydrogen, fluorine and the diluent are regulated through the respective flow control valves with PID controller. Calibrated orifice meters are employed for the flow measurements. The pressure downstream of the control valves is recorded through the pressure transmitters installed in the line. The gases pass through a preheating section where they are heated to the desired temperature. The reactor wall too is heated to the desired temperature using an on-off temperature controller. The flow resistance between the control valve and the reaction chamber being negligible, the

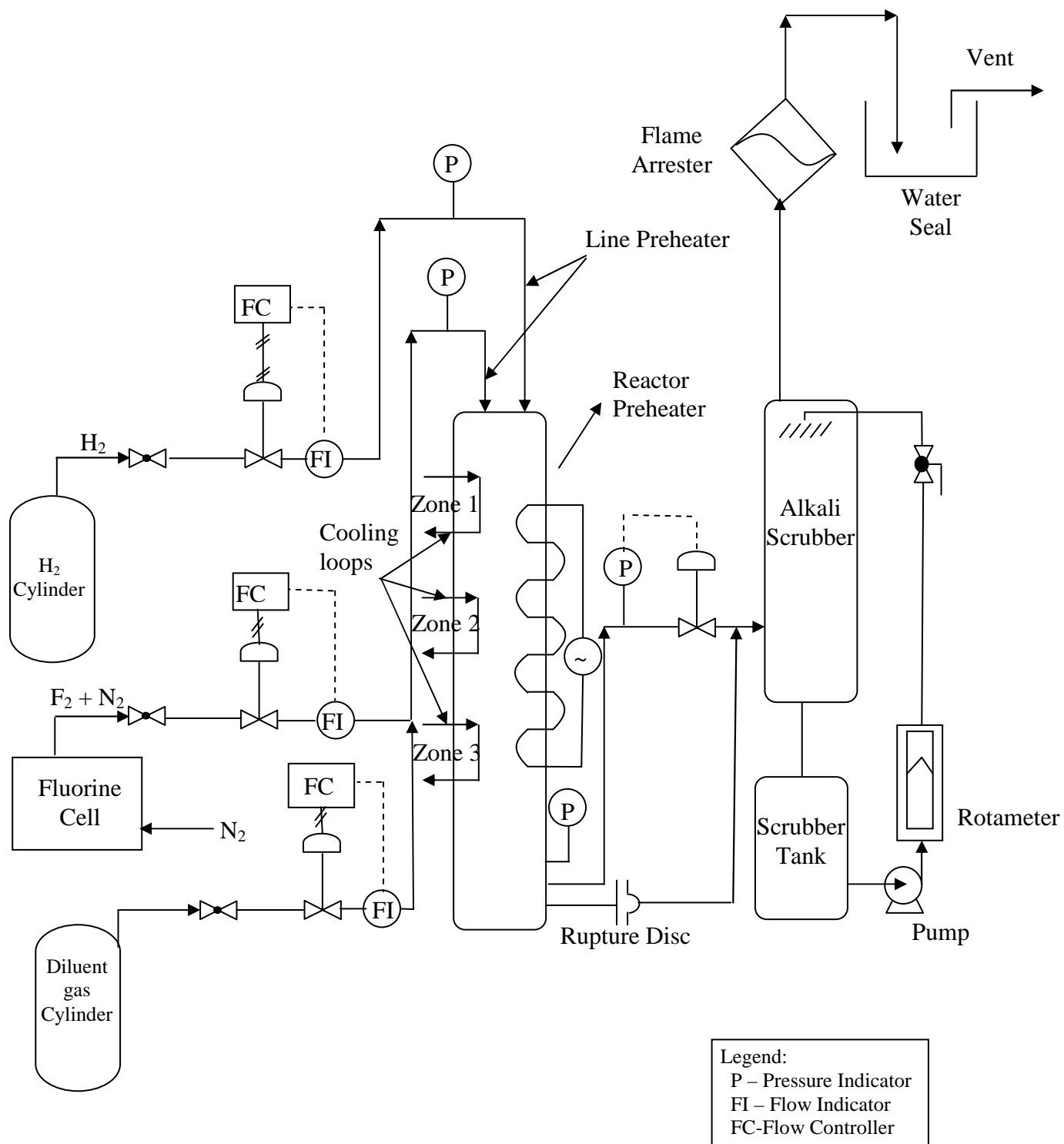


Figure 4.1: Block diagram for H₂-F₂ reaction system (VCR)

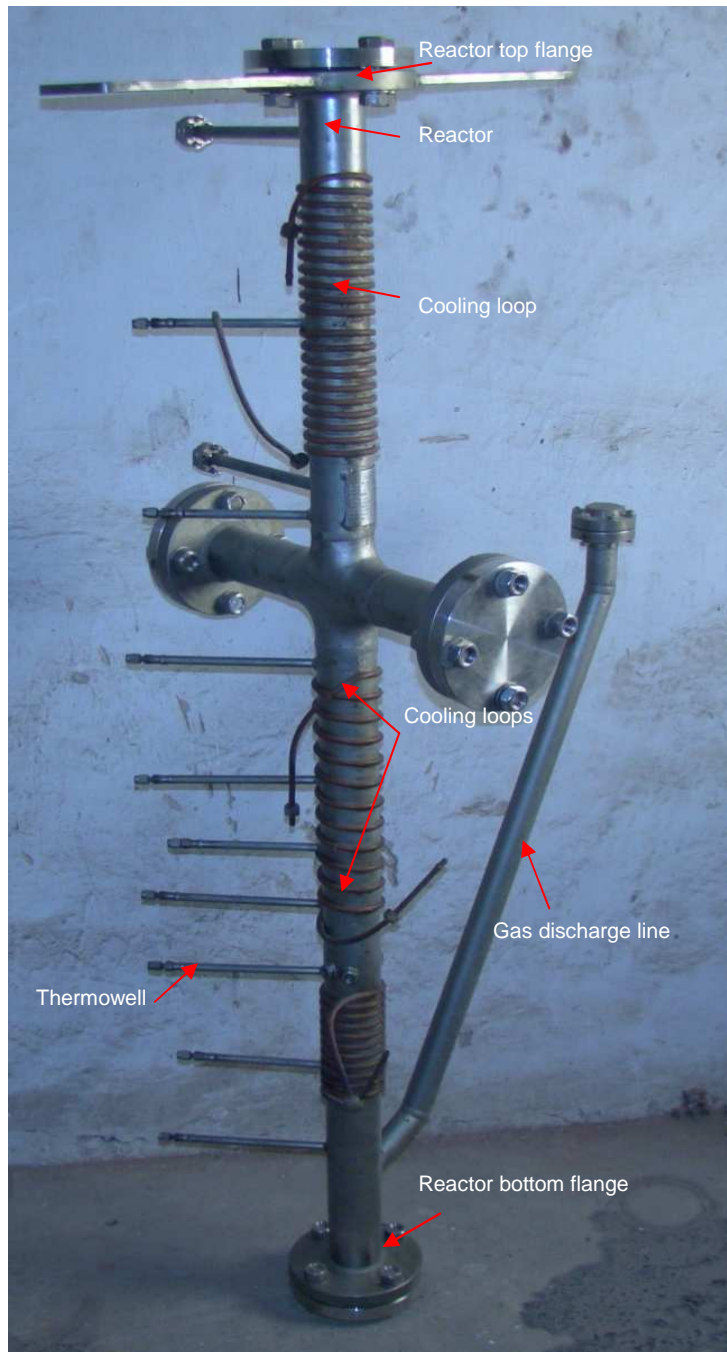


Figure 4.2: The vertical cylindrical reactor (VCR)

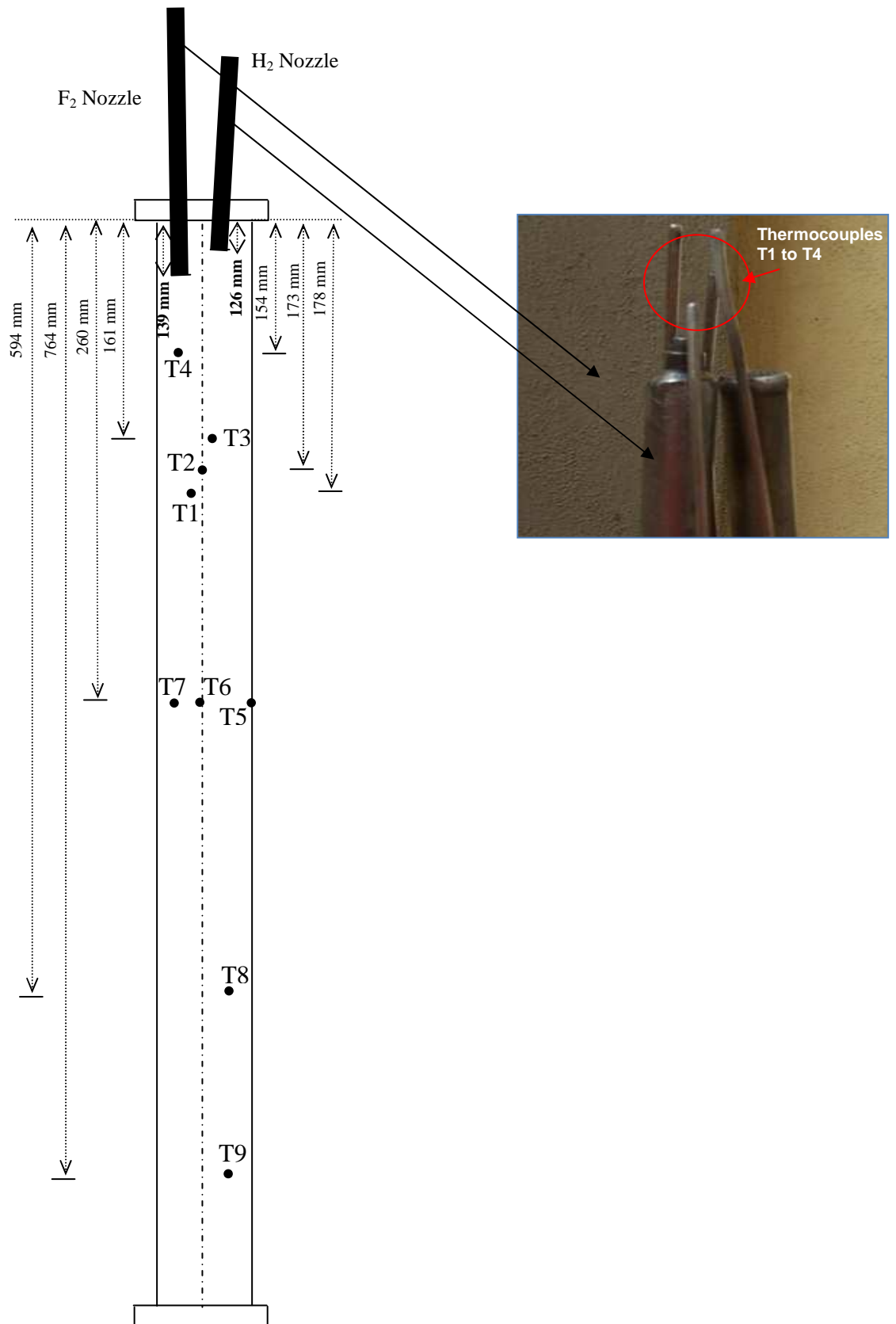


Figure 4.3(a): Thermocouple locations in the reactor (VCR) in the axial direction

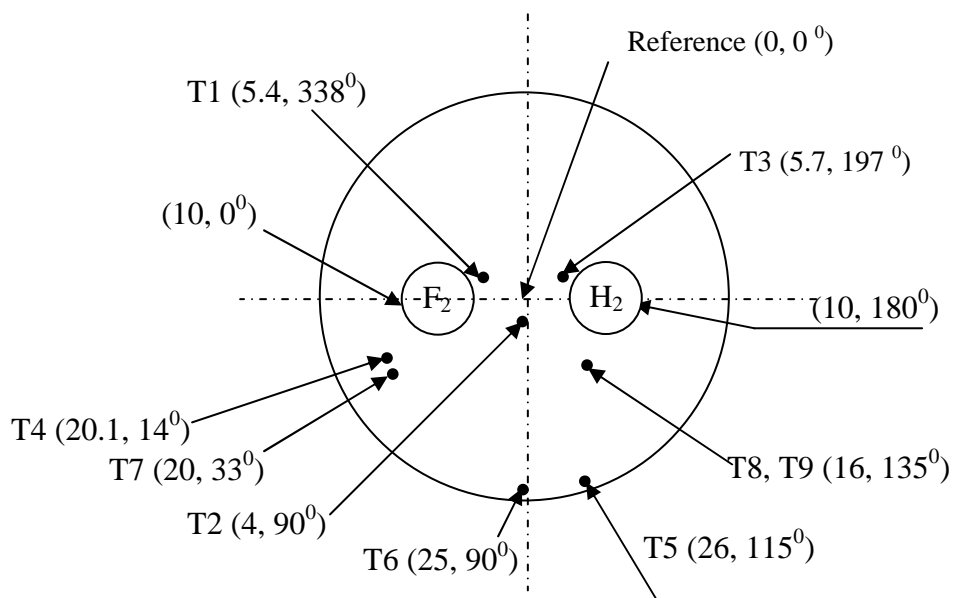


Figure 4.3(b): Radial (mm) and angular positions of the thermocouple in the reactor (VCR)

gases are at similar pressure at the feed point. The effluent from the reactor is connected to a scrubber system, which induces slightly negative pressure in the reactor. The reactions in the reactor are carried out at ~ 1000 mbar (abs) pressure, which is controlled through a control valve installed downstream of the reactor. Further, the reactor is instrumented with several

Table 4.1: Location of thermocouples in cylindrical coordinates

Thermocouple	Angle in anti-clock wise direction	Radius in mm	Distance in mm from Top of the reactor flange
T1	338	5.4	178
T2	90	4	173
T3	197	5.7	161
T4	14	20.1	154
T5	115	26	260

T6	90	25	260
T7	33	20	260
T8	135	16	594
T9	135	16	764

thermocouples placed at different locations to record and monitor reactor temperatures during the course of the reaction. Figures 4.3 (a), 4.3(b) and Table 4.1 show the details of the thermocouple locations in the reactor. All the measurements in the axial direction are taken from the top of the upper flange of the reactor. The radial measurement is taken from the centerline of the reactor while the angle is measured in the anticlockwise direction. Four B-type thermocouples tagged with T1, T2, T3 and T4 have been used near the feed nozzles, where the reaction flame is formed and the temperatures are likely to be higher. These thermocouples can record temperatures up to 2000 K even in the fluoride atmosphere. They are inserted through a guide tube open at one end so that, depending on the requirements, the insertion lengths of the thermocouples can be altered. At other locations away from the feed nozzles, where lower temperatures are expected, five K-type thermocouples tagged T5 to T9 are placed. These thermocouples are inserted through the thermowells to protect them from corrosion. The entire reactor is conceptually divided into three zones, namely, the mixing (zone-1), the reaction (zone-2) and the quenching (zone-3) zone. During the reaction, the reactor wall temperature is controlled by removing the excess heat deposited on the walls by air/water cooling in all the three sections. The flow of air/water in these sections in turn is controlled by individual PID controllers. One pressure transmitter and two pressure switches are installed in the reactor to measure the pressure and also safeguard the reactor against any possible pressure rise resulting from an uncontrolled reaction between hydrogen and fluorine. Adequate process interlocks and safety trips are implemented to protect the reactor from high

temperature and high pressure surges and also prevent the release of toxic fluoride gases. To provide further safety, a rupture disc of 5000 mbar (g) rating is attached to the reactor; the rupture disc is vented through the alkali scrubber. The product gas HF along with the excess hydrogen and the diluent is routed to the scrubber, where it gets neutralized with KOH solution. The excess hydrogen is released to the atmosphere through a flame arrester and finally a water seal. The reaction is carried out from a remotely located control console equipped with Programmable Logic Control (PLC) and the data are recorded through Supervisory Control And Data Acquisition system (SCADA).

4.3.2 Details of the experimental facility involving the HCR

The experiments with the HCR are designed to study the transient behaviour of the hydrogen-fluorine flame reactor in respect of change in temperature and pressure when a) the fluorine composition in the H₂-F₂ mixture varies from lean to rich, and b) various types of diluents in varying concentration levels are mixed with hydrogen before the start of the reaction with fluorine. Thus, several sets of unsteady state experiments with and without diluents such as helium, nitrogen and argon could be planned and conducted in a controlled way in the batch reactor. The block diagram for the experimental set up involving the batch reactor (HCR) is given in Figure 4.4. This facility includes the feed system and the scrubbing system in addition to the reactor (Figure 4.5) system. The evacuation system is also provided to evacuate the reactor before taking up a fresh trial. The reactor is a small horizontal stainless steel (SS) cylindrical vessel flanged at both ends and insulated with ceramic wool. The hydrogen and the diluents are supplied from high purity gas cylinders. The F₂ produced from the electrolysis of HF is compressed and stored in a discharge surge tank whose pressure is maintained using the pressure regulating valve in the fluorine compressor. It is connected to the reactor through a fine control needle valve. Flow meters are not required in

this set up as the quantities of gases in the reactor are controlled by regulating their partial pressures. There is a vacuum pump to evacuate the reactor in the beginning of a batch and discharge into the scrubber. The gases are fed through SS tubes. The fluorine feeding tube, kept at a distance from the reactor wall, is inserted deep into the vessel to avoid the release of intense reaction heat near the reactor walls, leading to a possible burnout situation. Five ‘K’ type thermocouples (T17 to T21) in the metallic thermowells and one absolute pressure transmitter are fitted in the reactor to record temperature and pressure during the course of the

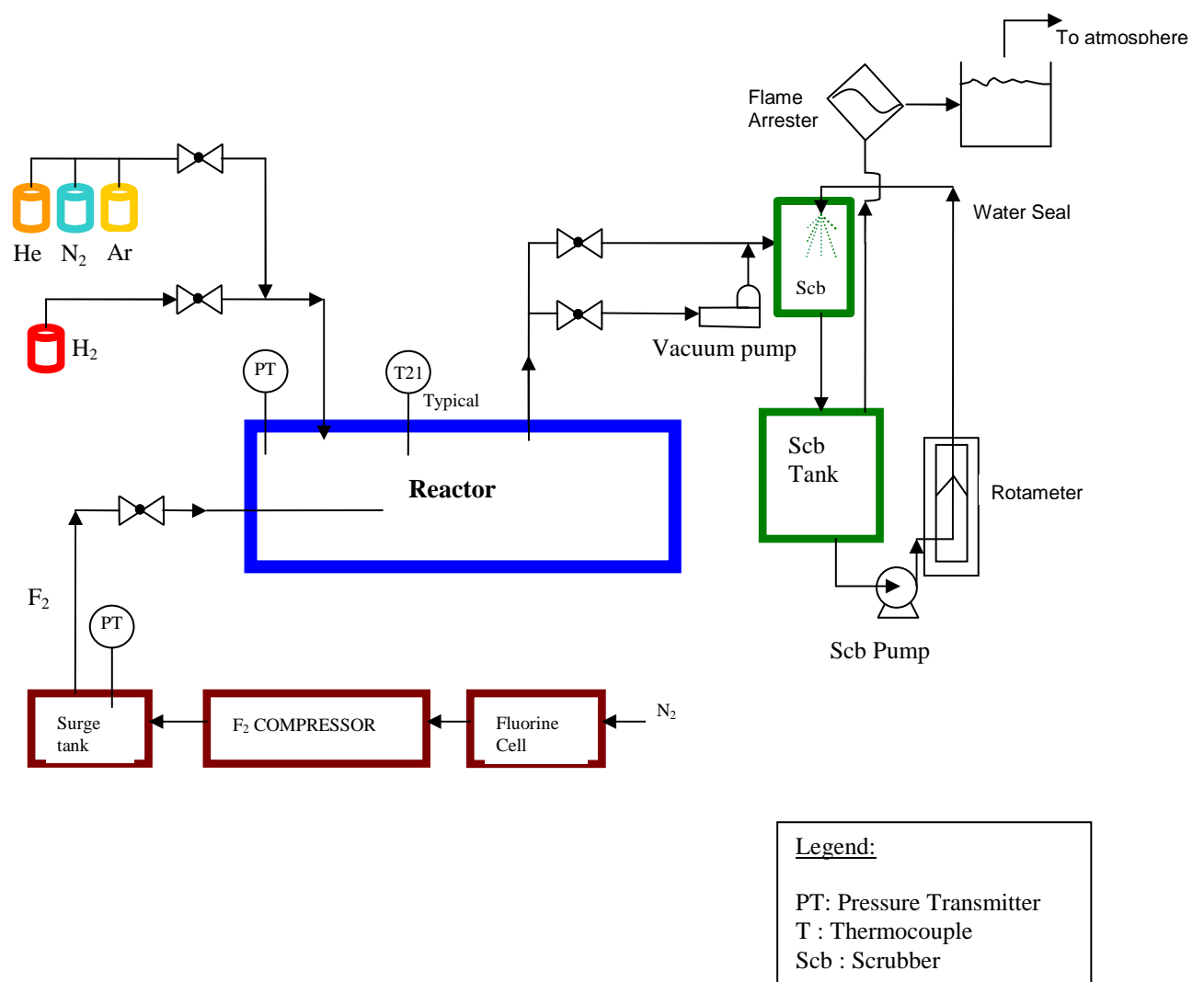


Figure 4.4: Block Diagram for the experimental set up of H₂-F₂ reaction studies (HCR)

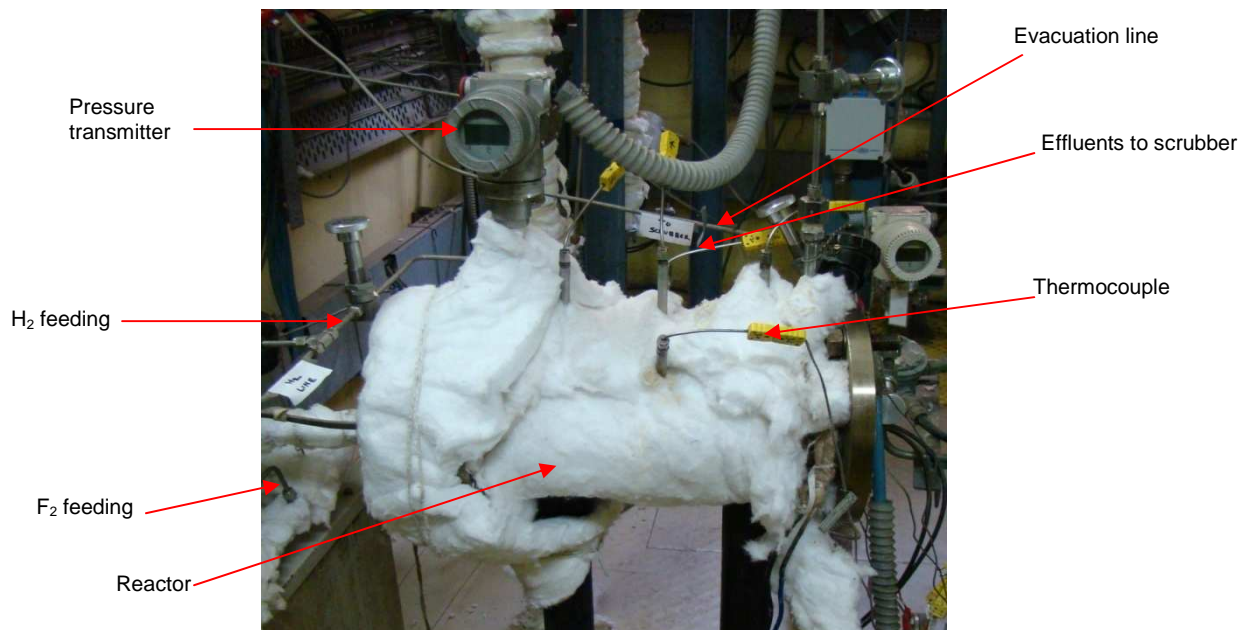
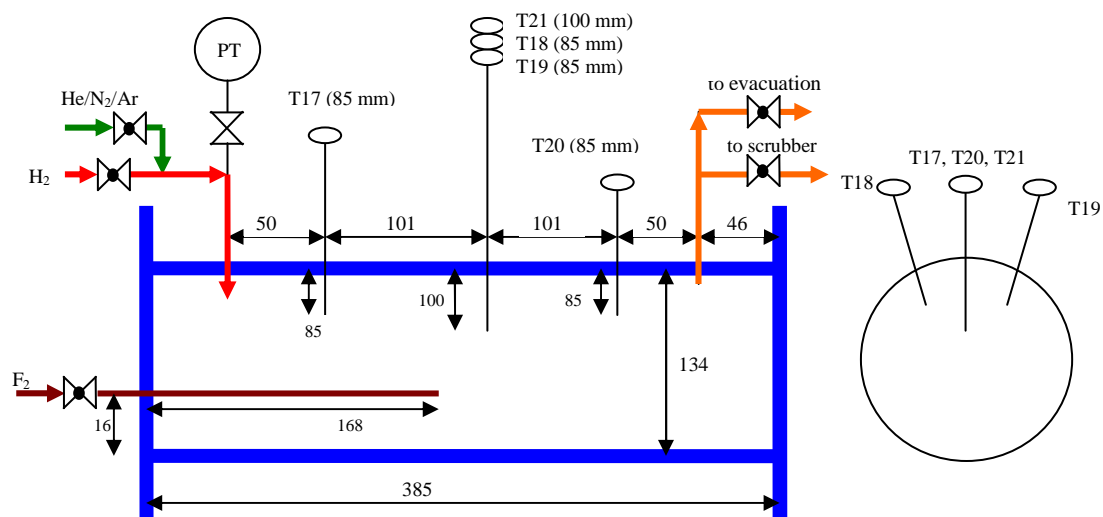


Figure 4.5: The horizontal cylindrical reactor (HCR)



- NOTES:
- (1) All dimensions are in mm.
 - (2) Dimensions shown in the bracket are the insertion lengths of the thermocouples from inside wall of the reactor.
 - (3) T- Temperature indicator (K type thermocouple)
 - (4) PT- Pressure Transmitter

Figure 4.6: Schematic of the H₂-F₂ batch reactor (HCR)

reaction. Figure 4.6 shows the schematic of the instrumented reactor. T18, T19, T20 and T21 are located in the forward direction to study the spread of the jet and the extent of reaction, while T17 is placed in the rear direction to check that even at lower velocities of jet dispersion, free jet conditions are maintained. Fluorine issuing from the nozzle forms a circular free jet in the turbulent regime as, a) Reynolds no. is very high (Jet Reynolds no. at the exit is around 2.7×10^5) and b) the cross sectional area of the chamber is more than five times that of the jet. For a turbulent free jet, when both the jet fluid and the entrained fluid are air, the jet angle α is $\sim 20^\circ$ for $x/d_0 < 100$ (Perry's hand book (7th edition), Table-6-6), where x is the longitudinal distance from the nozzle exit. Thus, the spread of the un-reacted fluorine jet inside the reactor is as shown in Figure 4.7. This profile of the jet is true when the fluorine jet is discharged into fluorine only, so that there is no density difference between the jet and the stagnant gas. Actually, fluorine stream being denser than the mixture of hydrogen and the diluent, actual jet spread in the reactor will be less rapid with distance ($\alpha < 20^\circ$) than the neutrally buoyant jet of fluorine in fluorine. In other words, the jet spread depicted through this figure is wider than the actual jet profile. Therefore, it can be concluded that the jet does not touch the reactor walls. Further, the expansion of the fluorine jet in the axial direction is

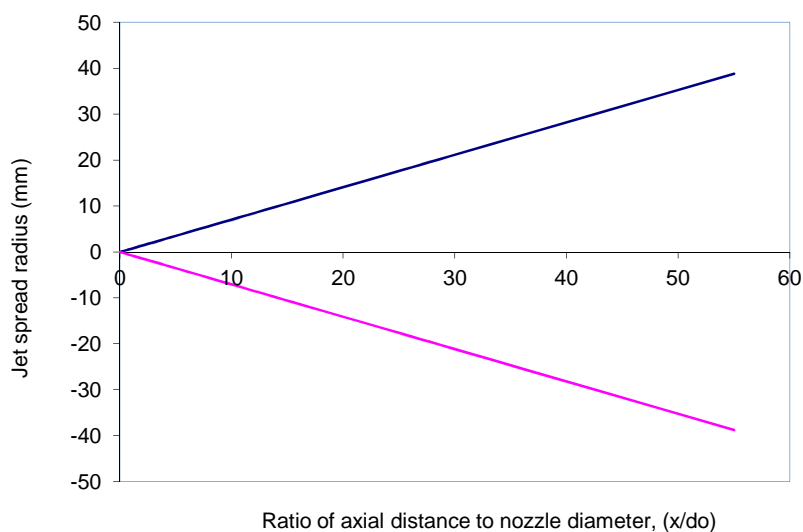


Figure 4.7: Spread of the un-reacted fluorine jet in the reactor

such that it does not touch any of the thermowells installed in line, thus, they are protected from being exposed to the region of high temperature. Since pressure ratio between the source for fluorine (fluorine storage tank) and the reactor where it is discharged, is more than 2; fluorine enters the reactor at sonic velocity of ~320 m/s. Tuve (1953) found that the longitudinal variation in the velocity along the centre line of the jet can be given as,

$$\frac{V_c}{V_0} = 6.2 \frac{d_0}{x} \text{ for } \frac{x}{d_0} < 100 \quad (4.1)$$

Using the above correlation, the reduction in the fluorine jet velocity in the axial direction is as shown in Figure 4.8. With calculated average velocity of ~ 73 m/s, the time taken by the jet to reach the facing wall of the reactor is ~ 3 ms. The observation that the temperature reading of T20 (which is closer to the upstream reactor wall facing the nozzle tip) is always on the lower side, confirms that fluorine does not reach the other end of the reactor.

To study the effect of varying composition of F₂, the reactor is evacuated by vacuum pump, filled with hydrogen and then short duration fluorine pulse is admitted into it. The quantity of fluorine sent to the reactor is controlled by regulating the pressure drop in the fluorine surge tank. As the reaction takes place, the change in the reactor temperatures and pressure is recorded. This exercise has been conducted for fluorine fraction ranging from ~16 mol % to ~90 mol %. Every successive trial is preceded by purging, evacuation followed by fresh filling of hydrogen, so that no residuals of product HF and unused reactants fluorine or/and hydrogen are left in the reactor. For the study on effect of diluents, the chamber is evacuated as earlier and filled with hydrogen. Before fluorine is fed into the reactor, helium, nitrogen or argon is mixed with hydrogen in varying compositions. The initial chamber pressure with hydrogen is deliberately kept a little higher so that, the error involved in achieving the planned diluent concentration is minimized. In all the experiments involving the diluents, the quantities of hydrogen and fluorine have been the same. The H₂-F₂ composition in all the trials has fewer moles of fluorine as compared to hydrogen so as to

maintain the reaction temperatures under control. After each experiment discussed above, the effluents containing excess hydrogen, the diluents and the product HF are sent to the alkali scrubber operating at a slightly sub-atmospheric pressure. H₂ is discharged to the atmosphere through a flame arrester followed by a water seal. The rise in the reactor temperatures and pressure during the reaction are recorded every second. The entire operation and data logging is carried out remotely from control room through SCADA. A few more similar experiments are carried out in the same facility with a slight change in the operating conditions, to study the effect of initial pressure on the H₂-F₂ reaction in the presence of diluents. The sequence of the operation, control and regulation philosophy is the same as discussed above.

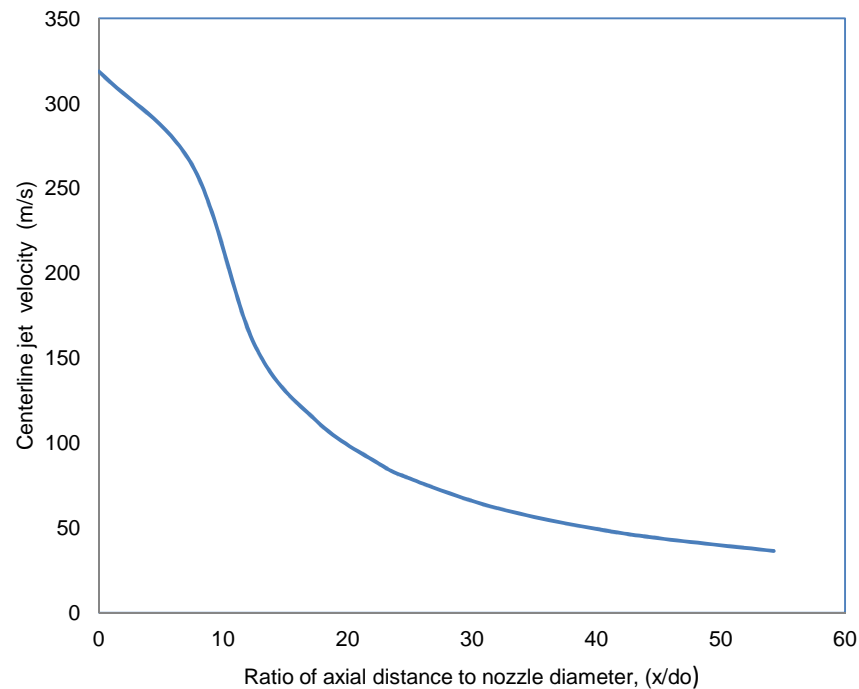


Figure 4.8: Centerline velocity of un-reacted fluorine jet in the reactor

4.3.3 Selection of instruments

The types of instruments which are used in the experimental facilities include thermocouples, pressure transmitters, pressure switches and flow meters. ‘B’ type

thermocouples, whose hot junction and the cold junction are made from platinum-rhodium alloys of different compositions, are selected for measuring near-nozzle temperatures which will be exposed to the corrosive fluoride atmosphere at the open end of the guide tube. They can be used for temperature measurement up to 2000 K. At the other places in the reactor, comparatively cheaper and more easily available ‘K’ type (chromel-alumel) thermocouples are deployed through the thermowells. The response time for the thermocouples varies between 2 and 3 seconds. A response time of 3 seconds has been considered for the purpose of interpretations. Capacitive type, highly sensitive pressure transmitters with wetted parts made from Inconel-600 are chosen as they offer better accuracy and compatibility with the gases being handled. Quick responding, diaphragm type pressure switches are installed to provide redundancy to the reactor protection philosophy. Orifice meters because of their simplicity, ease of installation and the cost efficacy are used to measure the gaseous flow rates and provide input to the respective flow controllers. In order to reduce the error in the flow measurement, they are calibrated every time before being put to use for a given set of planned experiments.

4.3.4 Placement of instruments

The information available in the literature mentions about the high temperature flames resulting from H_2-F_2 reaction. The temperatures reported are so high that it is not possible to measure them with commercially available thermocouples. Furthermore, high temperature measurement techniques such as pyrometry can also not be used because of very low emissivity values of the flames and the optical opacity of the system. Therefore, a more pragmatic approach is to measure temperatures a little away from the flame position where the reactor temperatures are lower. Accordingly, the ‘B’ type thermocouples are placed in a manner that they do not lie in the flow axis of the fluorine nozzle. Further, with respect to the

fluorine nozzle exit point, they are placed in different directions so that, a broad picture of the reaction flame can be inferred during the experiments. Table 4.2 gives detailed information on the placement of ‘B’ type thermocouples in the VCR. Placement of other ‘K’ type thermocouples is planned so as to give an overall temperature profile of the reactor across its length and radius. The pressure transmitter and pressure switches are installed closer to the feeding points in order to capture pressure surges during the course of the chemical reaction.

Table 4.2: Radial distance of ‘B’ type thermocouples from the centre of the F₂ nozzle tip

Thermocouple	Radial distance from the centre of the F ₂ Nozzle (mm)
T1	5.39
T2	10.86
T3	15.67
T4	10.67

4.3.5 Control and data acquisition system

The process control is implemented to get the desired value of process parameters such as flow, temperature and pressure. Safety interlocks and trips are also provided. For example, while on one hand the cooling fluid flow is controlled to maintain the reactor wall temperature at desired value, on the other hand, in case of uncontrolled rise in the wall temperature, the safety is imposed through alarms, interlocks and ultimately trips to avoid occurrence of any unwanted phenomenon and cause damage to man and machinery. Since the reaction between the two gases is very fast and potentially dangerous, operation/control through manual systems has been completely ruled out and the programmable logic based control is incorporated in the system. This not only ensures a smooth and swift operation of

the experimental facility, but also supports personnel safety. The system is equipped with easily retrievable data storage facility along with flexibility to choose the time interval for data storage frequency. Depending upon the length of the planned experiment, the time factor is selected judiciously so as to collect sufficient data for subsequent analysis and simultaneously not putting too much load on the memory device. As a redundant measure, to help and alert the operator, the indications of valve position, process values and alarms are provided both in the control panel as well as on the SCADA screen.

4.3.6 Safety measures

As described earlier, redundancy in the safety approach has been adopted in the system. For example, to protect the reactor from incessant rise in pressure resulting from an uncontrolled reaction between hydrogen and fluorine, a pressure transmitter is backed up by two pressure switches with equally fast response. Provision of alarm annunciation before tripping is kept to minimize the interruptions during an experimental trial. Alarm indications offer the operator some time to take corrective action before the system is forced to shut down automatically. Gas sensors are installed to detect the leakage of hydrogen and other toxic gases such as fluorine and HF from the equipments and the pipelines. Provision of transmission of data from these sensors to the control room along with the alarm annunciation at a given set point enables taking recourse to protective steps before the onset of an emergency situation. Portable gas sensors are kept in the control room for detection of gas release and exactly pinpoint the location of the leakage during periodic surveillance. Further, chemicals such as ammonia vapour and KI solution are also made available to be used to detect the release of HF and F₂ respectively, from the leaking joints. The safety report, the operating manual and the emergency preparedness plan report are made available at a convenient location for reference and guidance to foster corrective action as deemed

necessary during an emergency. No personnel entry into the reactor room is allowed during the progress of an experiment so as to discount any possibility of injury/accident to the operating staff. The integrity of the experimental set up is maintained by following meticulously the laid down operation and maintenance procedures.

4.4 Sequence of operation

Taking the hazardous and dangerous nature of chemicals being handled in the experimental facility into cognizance, it is necessary to follow a well planned operation sequence, which not only offers systematic approach to conduct the experiments but also is operator friendly. The adopted sequences of operation in both the reactors are as follows:

4.4.1 Operation sequence of facility comprising of the VCR

- i. Operating console and data acquisition system are switched on.
- ii. Scrubber system is made operational. Reactor and feed lines are connected to the scrubber system.
- iii. Flow of nitrogen equivalent to desired flow rates of reactant gases is established in both hydrogen and fluorine feed lines.
- iv. The feed line and the reactor are heated with the help of a resistance based heater and the reactor wall temperature is maintained.
- v. Regulated flow of hydrogen is introduced into the reactor replacing nitrogen.
- vi. Similarly, nitrogen in the fluorine feed line is replaced by fluorine in required quantity.
- vii. The reaction between the two takes place in the reactor and continues with the set flow rates of hydrogen and fluorine till the steady state (no change in reactor temperatures with time) is achieved.

- viii. Fluorine flow is stopped and replaced by nitrogen.
- ix. Hydrogen feeding is cut off and replaced by nitrogen.
- x. Steps (v) to (ix) are repeated for a new set of experimental condition. The feed line and the reactor heaters are switched off wherever not required.
- xi. Finally, the stored process data are extracted, processed and analyzed for drawing conclusions and further investigations.

4.4.2 Operation sequence of facility comprising of the HCR

- i. Operating console and data acquisition system are switched on.
- ii. Scrubber system is made operational. Reactor and feed lines are connected to the scrubber system.
- iii. The reactor is evacuated with the help of a vacuum pump and then isolated from all other sub-systems such as scrubber system etc.
- iv. The reactor is charged with hydrogen to the desired pressure by opening the hydrogen feed manual valve.
- v. Wherever applicable, the total pressure of the reactor is raised to the set level by addition of the chosen diluent.
- vi. All other isolation valves (H_2 feeding, diluent feeding, evacuation line and the scrubber line) being closed, a short pulse of fluorine is introduced into the reactor containing mixture of hydrogen and the diluent. The quantity of fluorine fed is controlled by regulating the pressure drop in the fluorine storage tank through remote operation of an isolation valve installed near the reactor entry.
- vii. The reaction in the horizontal reactor is allowed to continue till no further increase in temperature and pressure with time are observed.

- viii. After the reaction, product HF and other gases are directed to the scrubber for neutralization/venting.
- ix. The reactor is purged with nitrogen.
- x. Steps (iii) to (ix) are repeated again for a new set of designed experimental condition.
- xi. Finally, the stored process data are extracted, processed and analyzed for further studies.

Due to practical constraints, it is difficult to obtain the temperature, pressure and the species concentration distribution across the length and breadth of the reactor. Therefore, the experimental information will be utilized for validating a CFD tool which will predict these profiles in the reactor and enhance the understanding about the system. The CFD tool thus developed can be used to optimize the process parameters for diversified applications without requiring much experimental effort. It will also be effective in simulating the reactor designs for an envisaged scale up. The various aspects of flame reactor modeling are presented in Chapter-5.

CHAPTER 5

CFD MODELING OF THE FLAME

REACTOR

The present chapter describes the salient features of a combustion process and the compexicity involved in its analytical modeling. It emphasizes on the need of the computational modeling and its validation with the experimental data. It also discusses the identification of the CFD tool, determination of the governing physical models and the effect of grid size on the computational results. A summary of the inputs given to the CFD solver is also provided.

5.1 Introduction

A combustion phenomenon involves many physical and chemical processes which exhibit a broad range of the time and the length scales. It transforms the chemical enthalpy into the sensible enthalpy. The combustion processes with high heat of reaction produce a flame. The definition of flame length is not universal. In the literature (<http://fire.nist.gov/bfrlpubs/fire96/PDF/f96102.pdf>), flame lengths are normally defined on the basis of the mean temperature, the chemical composition or the luminosity along the flow axis. The interchangeable use of the different definitions may cause confusion regarding the importance of the different physical processes. For example; the definition based on the luminosity is inconsistent because it strongly depends on the physical properties (such as emissivity) of the product formed. For a hypergolic reaction such as between hydrogen and fluorine, it is more appropriate to define flame length based on the chemical composition, which in turn is directly affected by mixing. Since multiple definitions of the flame length may lead to confusion, the discussions and the conclusions in the subsequent chapters are restricted to mixing/reaction zone.

The chemical kinetics occurring in the flame is very complex and involves typically a large number of chemical reactions and formation of intermediate species, most of them radicals. For a given thermodynamic state of a mixture (composition, temperature, pressure), the flame resulting from the combustion exhibits its own dynamics (speed, heat release, spread of the flame jet) on which there is hardly any control. A mathematical description of the combustion is quite complicated, although some analytical solutions exist for simpler situations of the laminar flames. Such models are usually restricted to analysis in the one-dimensional space. In a simplified form, the combustion can be represented by a single irreversible reaction involving a fuel 'F' and an oxidizer 'O' as,



where, n_F and n_O are the stoichiometric coefficients of the fuel and the oxidizer respectively.

The large difference between the temperatures of the burnt and the fresh gas leads to a sharp self-acceleration of the un-burnt gases which subsequently approach the reaction flame with greater velocity. This velocity is called the burning velocity. Compared to the hydrocarbon fuels, it is higher for hydrogen because of its fast chemical kinetics and high diffusivity. The higher the burning velocity, the greater is the chance for transition from deflagration to detonation. The burning velocity of the stoichiometric mixture of hydrogen in air at ambient conditions is 2.55 m/s, reaching a maximum of 3.2 m/s at the hydrogen concentration of 40.1%, and would even increase to 11.75 m/s in pure oxygen [www.hysafe.org]. Explicably, the corresponding values for the hydrogen-fluorine combination would be even more. In contrast to the burning velocity, the flame speed, which is related to a fixed observer, is much greater than the burning velocity due to the expansion of the combustion products, instabilities, and turbulent deformation of the flame. The detonation velocity in the hydrogen-air system reaches values in the range of 2000 m/s, in pure oxygen it goes up to 3500 m/s. From the simple point of view that a flame is a reaction zone, two aspects are considered: (i) τ_d , the characteristic mixing time or the rate at which the reactants are fed, and, (ii) τ_c , the characteristic chemical time or the strength of the chemistry to consume them. The Damkohler number, Da , compares both these time scales and for that reason, it is one of the most integral non-dimensional groups in the field of combustion. Thus, it is given by,

$$Da = \frac{\tau_d}{\tau_c} \quad (5.2)$$

A large Da means that the chemistry has always the time to fully consume the fresh mixture and turn it into equilibrium. Real flames are usually close to this state. The estimated characteristic reaction time is of the order of the tenth of a milli second [http://www.cfd-online.com/Wiki/Combustion]. When Da is small, the fresh mixture cannot be converted into

products by too slow a chemistry and the flow remains almost stationary. The picture of a deflagration lends itself to the description based on the Damkohler number. A reacting wave progresses towards the fresh mixture through preheating of the closest upstream layer. The increase in the temperature reduces the chemical time such that the mixture characteristics changes from a low-Da region (far upstream) to a high-Da region in the flame (intense reaction to equilibrium).

The combustion problem is complicated because it involves the turbulent flows, a highly non-uniform distribution of pressure and temperature and the presence of multiple species. The combustion chemistry is based on chain reaction comprising of the three major steps: (i) generation (where the radicals are created in the fresh mixture), (ii) branching (where the products and the new radicals appear from interaction of the radicals with the reactants), and, (iii) termination (where the radicals recombine). The branching step tends to accelerate the production of the active radicals similar to an autocatalytic process. The investigations of the issues related to a combustion problem require not only methodically planned experimental work, but also numerical modeling. The assumption of rudimentary chemistry can be effective in the combustion analysis and modeling. Every combustion model however, must be validated with the experiments as each one has its own characteristics. Depending on how the fuel and the oxidizer are brought into contact in a combustion system, traditionally, two combustion regimes have been recognized: the non-premixed regime and the premixed regime. In the non-premixed regime, the fuel and the oxidizer are fed separately to the combustion chamber. Since the burning rate is controlled by the diffusion of the reactants, the flame thus produced is also known as the diffusion flame. This configuration is safer because the fuel and the oxidizer are in contact only in a limited region, and are separated elsewhere. Some of the examples in this category include operation of a lighter, burning of a candle or lighting a gas-powered stove. Figure 5.1 shows the

schematic of a non-premixed diffusion flame. In contrast to the non-premixed regime, the reactants in the premixed regime are well mixed before entering into the combustion chamber. The reaction takes place right at the nozzle mouth, creating a shorter flame. The chemical reaction can occur everywhere and the flame can also propagate backward into the feeding system making it inherently unsafe. The sketch of a typical premixed flame is shown

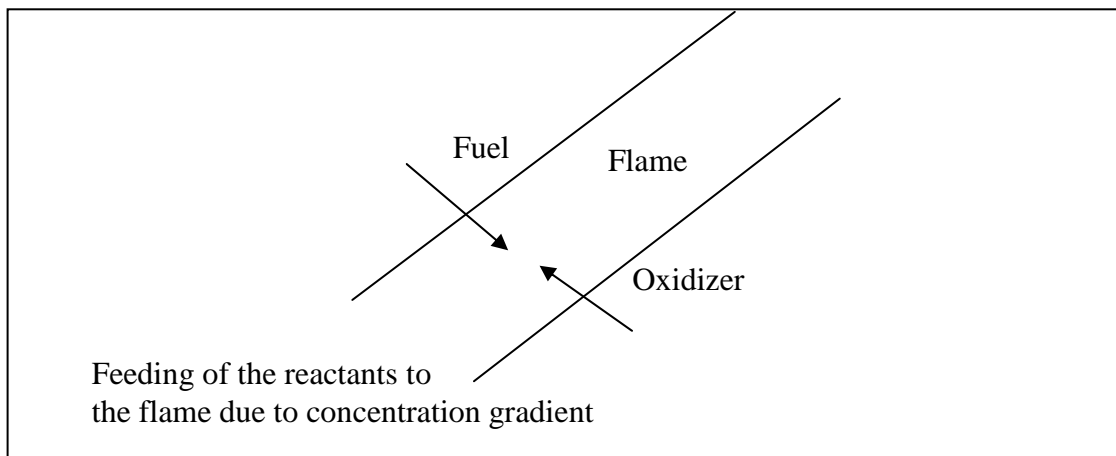


Figure 5.1: Sketch of a non-premixed diffusion flame

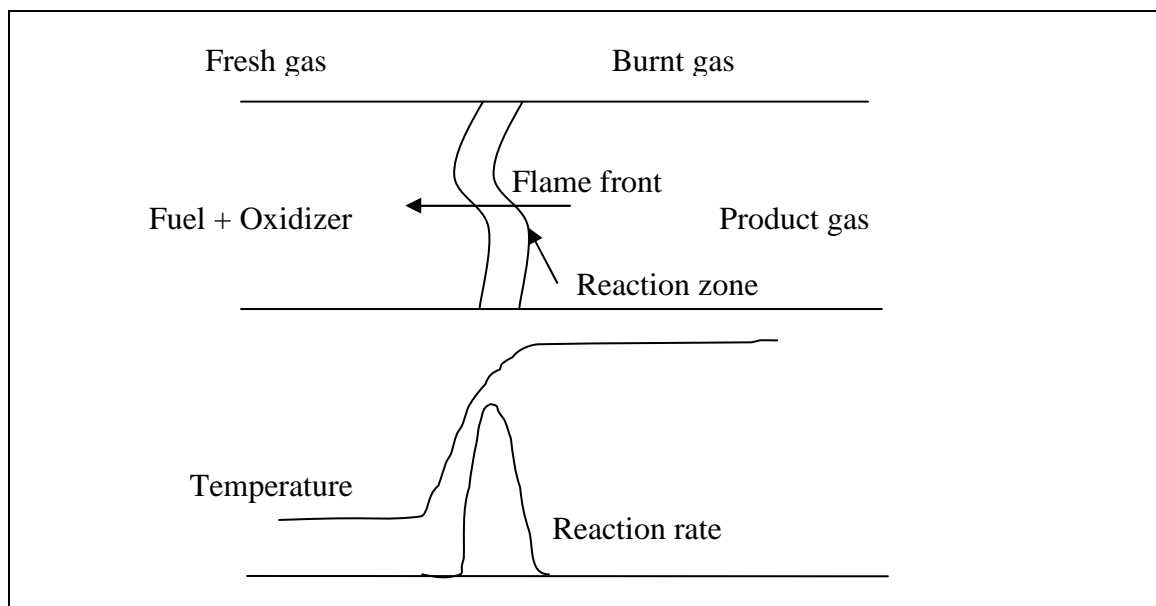


Figure 5.2: Sketch of a premixed flame

in Figure 5.2. As follows from this figure, the fast chemistry is confined within a thin reaction zone stuck to the hot burnt gas at the equilibrium temperature. In this zone, the Damkohler number is high in contrast to the fresh mixture and the reaction rate in this region can be shown by a Gaussian shape with low standard deviation. The hydrogen and fluorine reaction studied in the present work belong to the non-premixed diffusion flame.

The direct measurement of scalars such as temperature and pressure inside a flame reactor or a combustion chamber is difficult as the time scales are very small, temperatures are extremely high and the gaseous atmosphere is often aggressive. Therefore, it is necessary to take help of the computational simulations to conduct a comprehensive investigation on the flame reactors. Before the simulations on the planned problems are carried out, it is important to identify a robust and computationally economic CFD tool and evaluate the suitability of the selected CFD models by devising some simplistic experiments and using the acquired data for validation.

5.2 Identification of the CFD tool

It is known that the chemistry between hydrogen and fluorine is very fast and complex too. It is also clear that the fluid dynamics, the heat transfer and the mass transfer would play a crucial role in dictating the distribution of the velocity, the temperature and the species concentration inside the reactor. Since developing a numerical model from the scratch (where, governing equations of mass, momentum, energy and species conservation have to be solved numerically) will be a very stupendous task by itself, it is decided to use commercially available 'FLUENT' as the CFD tool, which is validated by the experimental data. It solves the problems with unstructured mesh which simplifies the geometry modeling and reduces the time spent on mesh generation for a complex body. The governing equations for the conservation of mass, momentum, energy and other scalars such as turbulence and chemical

species are solved using a control volume based technique. Between the coupled solver and the segregated solver available in FLUENT, the coupled solver was tried for simulation, but it was not possible to see any progress of solution even after one week of computation. However, the pressure based segregated algorithm which has been used for simulating the experimental results is actually a semi coupled algorithm in the sense that, at a given time step, the momentum and the pressure equations are solved first, and then the updated mass flux, pressure and velocity are used to solve the energy, species, turbulence and other scalar equations within the same time step [FLUENT Inc. user guide, chapter 4 (2003)]. The velocity and the scalar fields are time-stepped together. The segregated algorithm arrives at a converged numerical solution through several iterations. Although the lagging causes a small error, it eventually disappears in the steady-state solution. The segregated algorithm is memory efficient and also has been able to simulate the experimental results well. The issues such as definition of modeling goals, the choice of computational model, selection of the physical model and determination of the solution procedures have been fine tuned so that the best possible results are predicted by the CFD simulations.

5.3 Selection of the turbulence model

In the planned investigations, fluorine and hydrogen issuing into the reactor have lower velocities, and the un-mixed flows of these gases are in laminar region. However, when the two gases mix and react together, the temperature goes up to such an extent that the flow becomes turbulent. Therefore, it is important to consider turbulent flow models in the simulation. FLUENT provides many turbulent models such as the Spalart-Allmaras model, the Reynolds Stress Model (RSM), k - ϵ models, k - ω models, v^2 - f model, Large Eddy Simulation (LES) model etc. No single turbulence model is universally accepted as being superior for all classes of problems. The choice of turbulence model depends on

considerations such as the physics included in the flow, the level of accuracy required, the available computational resources, and the amount of time available for the simulation. In the Spalart-Allmaras model, only one additional transport equation (representing turbulent viscosity) is solved. It is effectively a low-Reynolds-number model designed specifically for aerospace applications. The RSM model on the other hand accounts for the effects of streamline curvature, swirl, rotation, and rapid changes in the strain rate in a more rigorous manner than one-equation and two-equation models, and therefore, it has greater potential to give an accurate prediction for the complex flows. However, the reliability of the RSM predictions is limited by the assumptions considered to close the exact transport equations for the Reynolds stresses. It also requires additional computational effort. In the case of the k - ε and k - ω models, two additional transport equations (for the turbulence kinetic energy, k , and either the turbulence dissipation rate, ε , or the specific dissipation rate, ω) are solved, and the turbulent viscosity (μ_t) is computed as a function of k and ε or ω . The standard k - ε model as proposed by Launder and Spalding (1972) is a semi-empirical model, where the derivation of the model equations relies on the phenomenological considerations and empiricism. The standard k - ω model on the other hand is based on the k - ω Wilcox model (1998), which incorporates the modifications for low-Reynolds-number effects, compressibility and shear flow spreading. Because of the robustness and the reasonable accuracy for a wide range of fluid flows, the two models have become the workhorses of the practical engineering flow and the heat transfer simulations. Therefore, they have been considered for the computational investigation of the envisaged H_2 - F_2 reaction system. Simulations for the gaseous flow rates as mentioned in ‘case 2’ (details given in chapter-3) have been carried out using both the models and the temperature contours are presented in Figure 5.3. As follows from this figure, the shape of the flame as predicted by the k - ε model is more stable as compared to the k - ω

model. Further, the predicted temperature values of T1 through T9 are compared with the experimental data in Figure 5.4. It is seen from this figure that the predictions with the k- ϵ

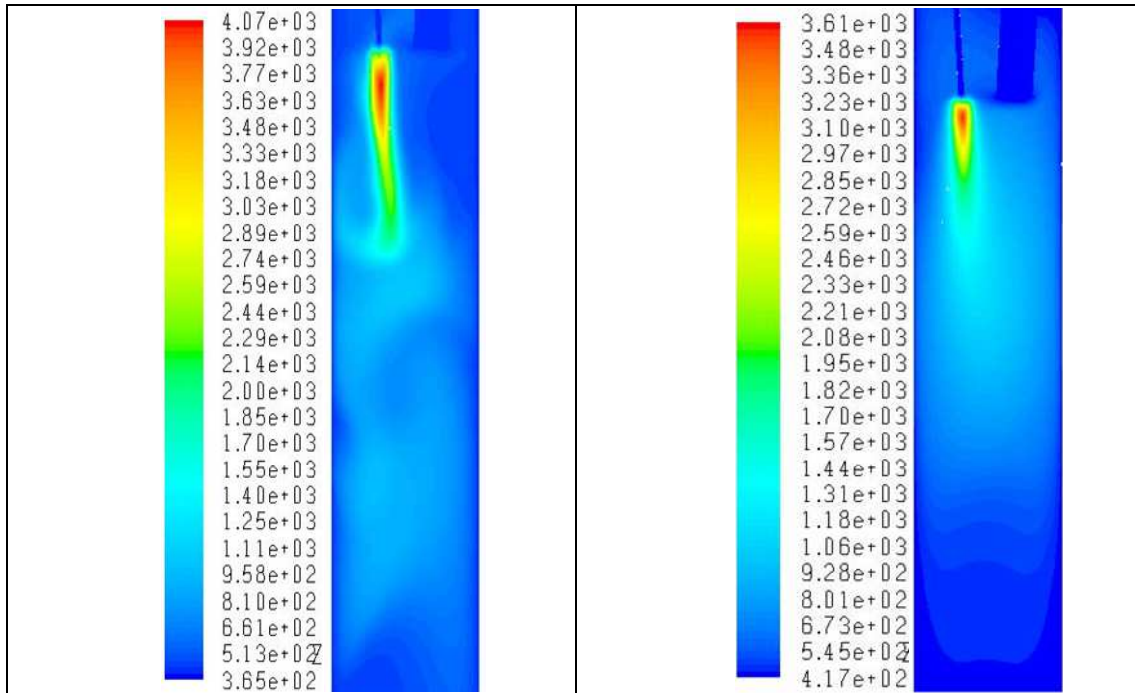


Figure 5.3: Contour plots of temperature (K) for Case 2 using standard k- ω and k- ϵ model

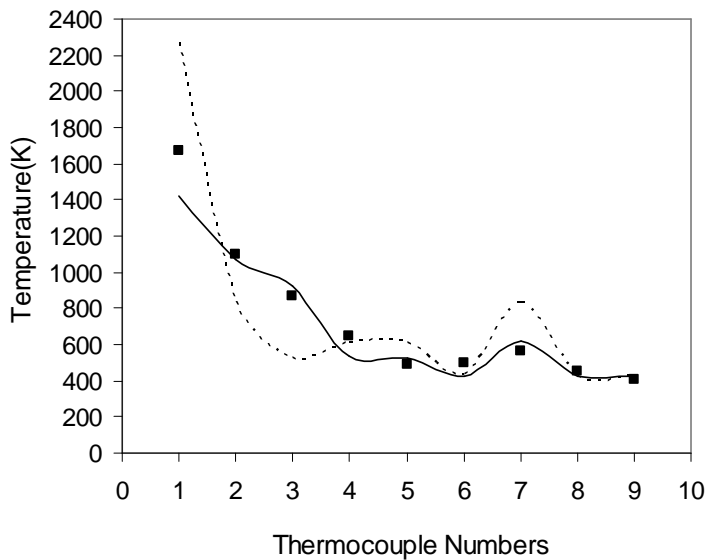


Figure 5.4: Comparison of turbulence model on temperature at different thermocouple locations for Case 2.

—— Std. k- ϵ model, - - - - - Std. k- ω model and ■ Experimental

(Note: In the figure 5.4, the uncertainty in the experimental temperature shown by T1 to T4 is

within $\pm 0.5\%$ of the value whereas the uncertainty in temperature shown by T5 to T9 is within ± 2.2 K. This applies to all the temperature measurements shown by T1 to T9 discussed hereafter.)

model are closer to the experimental data. Therefore, the $k-\epsilon$ model for turbulence is used for simulation of all other cases.

5.4 Effect of the grid size on the computational results

Following the adequacy testing of the turbulence models, further numerical studies are performed on the ‘case 2’ to verify the grid independency. The most plausible effect of the grid size can be in the zone near the feed nozzles. Therefore, simulations are carried out for initial 200 mm (from the fluorine nozzle tip) length of the reactor only. The grid sizes of 0.75 mm and 1 mm have been chosen for the simulations. Figure 5.5 presents the results with the two grid sizes. The difference in temperatures at various locations for both the grid sizes

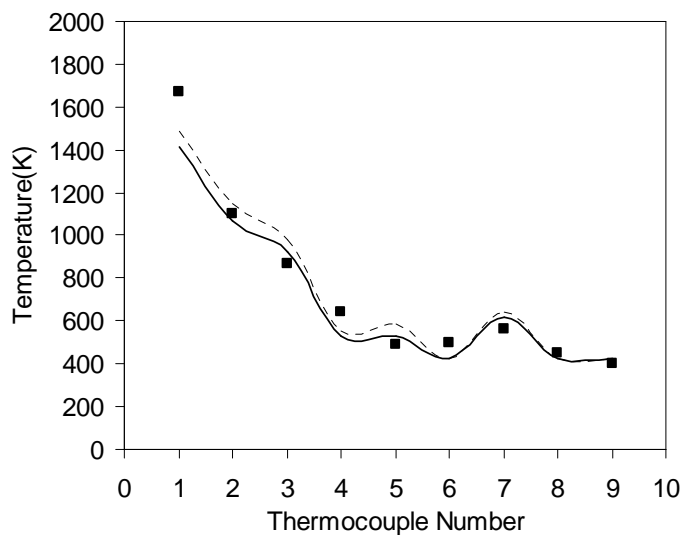


Figure 5.5: Comparison of grid size on temperature at different thermocouple locations for Case 2.

—— With 1 mm grid, With 0.75 mm grid, ■ Experimental

is not significant. However, there is a large difference between the computational time requirements for the two sizes. With 0.75 mm grid (about 4 million grids), more than 2 days are required to obtain a converged solution. The same solution with 1mm grid size (about 1.3 million grids) takes about 20 hours. As a consequence of this, all the subsequent simulations are carried out with 1 mm grid size.

5.5 CFD modeling and the governing equations

5.5.1 CFD modeling

The CFD modeling has been carried out for the vertical cylindrical reactor (VCR) only. A 3-D geometry of the VCR has been prepared using GAMBIT 2.2.30 for the simulations. The reactor length for the computational investigation has been limited to 875 mm, assuming it to be insignificant beyond this length. FLUENT version 6.3 is used as the CFD solver as well as for post processing. The computations are carried out using SGI 64 bit, Xenon QUAD core processor, 16 node machine having 8GB RAM for master and 4GB for each node. The reactor is divided into 3 sections to facilitate the effective meshing. Since the feed nozzles are inclined, the region above the fluorine nozzle tip is meshed with 1 mm Tetra grid. To capture the mixing as well as the reaction phenomena, a fine meshing of 1 mm Hex grid is adopted near the nozzle exit region. In the remaining part of the reactor, 1.5 mm Hex grid mesh has been provided. The details of the length of each section, the type of mesh and the number of cells are reported in Table 5.1. The ideal gas law has been used for the density variation due to the temperature change. First order discretization is used for the momentum, the species, the turbulent kinetic energy and the turbulent dissipation rate. The Boussinesq model [This model treats density as a constant value in all the equations, except for the buoyancy term in the momentum equation, where, $\rho = \rho_0 (1 - \beta \Delta T)$] is not incorporated in the

momentum equation as the temperature variation in the reactor is expected to be very large. SIMPLE (Semi Implicit Method for Pressure Linked Equations) scheme is used for the pressure-velocity coupling. Relaxation factors of 0.3, 0.7, 0.8 and 0.8 have been used for pressure, momentum, turbulent kinetic energy and turbulent dissipation rate respectively. In the first approximation, the radiative heat transfer is not considered in the simulation due to low emissivity values of the flames. Mass flow inlet in kg/s is given as the inlet boundary condition for both the nozzles. ‘Outflow’ is given as the outlet boundary condition. Outflow boundary condition assumes zero diffusion $\left(\frac{\partial \phi}{\partial x} = 0\right)$ flux at the outflow cells, where, ϕ is any flow variable. No-slip boundary condition is assigned at the walls. Unless specified, the inlet temperature for both the hydrogen and the fluorine gas as well as the reactor wall temperature is given as 423 K. The reactor pressure is given as 1000 mbar (abs). The steady state condition is assumed and the solution is iterated until the stipulated convergence criterion of residue $< 10^{-4}$ is achieved.

Table 5.1: Details of type and size of mesh

Zone No.	Length of Reactor from top flange	Type and size of Mesh	No. of Cells
1.	Up to 140 mm	Tetrahedral, 1mm	647790
2.	140-330 mm	Hexahedral, 1mm	870337
3.	330-875 mm	Hexahedral, 1.5 mm	751616
		Total	2269743

5.5.2 Governing equations

Assuming incompressible fluid, the model equations as used in the CFD solver are as

follows:

Continuity equation:

$$\frac{\partial \rho}{\partial \theta} + \frac{\partial(\rho U_i)}{\partial x_i} = 0 \quad (5.3)$$

Momentum equation:

$$\frac{\partial(\rho U_i)}{\partial \theta} + \frac{\partial(\rho U_j U_i)}{\partial x_j} = -\frac{\partial P}{\partial x_i} + \frac{\partial}{\partial x_j} \left[\mu \left(\frac{\partial U_i}{\partial x_j} + \frac{\partial U_j}{\partial x_i} - \frac{2}{3} \delta_{ij} \frac{\partial U_i}{\partial x_j} \right) - \rho \overline{u'_i u'_j} \right] + \rho \overline{F_b} \quad (5.4)$$

The pressure correction takes place using the SIMPLE algorithm such that the continuity equation is satisfied. The equations (5.3) and (5.4) are called the Reynolds-averaged Navier Stokes (RANS) equations. They have the same general form as the instantaneous Navier-Stokes equations, with the velocities now representing ensemble-averaged (or time-averaged) values. Additional terms, the Reynolds stresses, $-\rho \overline{u'_i u'_j}$ represent the effects of turbulence. They are modeled in order to close the equation (5.4). A common method is to employ the Boussinesq hypothesis [Hinze (1975)] to relate the Reynolds stresses to the mean velocity gradients as

$$-\rho \overline{u'_i u'_j} = \mu_t \left(\frac{\partial U_i}{\partial x_j} + \frac{\partial U_j}{\partial x_i} \right) - \frac{2}{3} \left(\rho k + \mu_t \frac{\partial U_i}{\partial x_i} \right) \delta_{ij} \quad (5.5)$$

The turbulent viscosity μ_t is evaluated using the standard k- ϵ model. For this model, the corresponding equations for the turbulent kinetic energy and the turbulent energy dissipation rate are

$$\frac{\partial(\rho k)}{\partial \theta} + \frac{\partial(\rho k U_i)}{\partial x_i} = \frac{\partial}{\partial x_j} \left[\left(\mu + \frac{\mu_t}{\sigma_k} \right) \frac{\partial k}{\partial x_j} \right] + G_k + G_b - \rho \epsilon + S_k \quad (5.6)$$

$$\frac{\partial(\rho \epsilon)}{\partial \theta} + \frac{\partial(\rho \epsilon U_i)}{\partial x_i} = \frac{\partial}{\partial x_j} \left[\left(\mu + \frac{\mu_t}{\sigma_\epsilon} \right) \frac{\partial \epsilon}{\partial x_j} \right] + C_{1\epsilon} \frac{\epsilon}{k} (G_k + C_{3\epsilon} G_b - C_{2\epsilon} \rho \frac{\epsilon^2}{k}) + S_\epsilon \quad (5.7)$$

In the equations (5.6) and (5.7), S_k and S_ε are user-defined source terms. G_k represents the generation of the turbulence kinetic energy due to the mean velocity gradients and is calculated as

$$G_k = -\rho \overline{u_i' u_j'} \frac{\partial U_j}{\partial x_i} \quad (5.8)$$

G_b is the generation of turbulence kinetic energy due to buoyancy and is calculated as

$$G_b = \beta g_i \frac{\mu_t}{Pr_t} \frac{\partial T}{\partial x_i} \quad (5.9)$$

where, Pr_t is the turbulent Prandtl number for energy and g_i is the component of the gravitational vector in the i^{th} direction. The default value of Pr_t is 0.85. The coefficient of the thermal expansion, β , is defined as

$$\beta = -\frac{1}{\rho} \left(\frac{\partial \rho}{\partial T} \right)_P \quad (5.10)$$

The turbulent (or eddy) viscosity, μ_t , is computed by combining k and ε as follows:

$$\mu_t = \rho C_\mu \frac{k^2}{\varepsilon} \quad (5.11)$$

In the equations (5.6), (5.7) and (5.11), $C_{1\varepsilon}$, $C_{2\varepsilon}$, $C_{3\varepsilon}$ and C_μ are the constants. σ_k and σ_ε are the turbulent Prandtl numbers for k and ε respectively. The standard turbulence parameters as reported by Rodi (1993) are taken as $C_\mu = 0.09$, $C_{1\varepsilon} = 1.44$, $C_{2\varepsilon} = 1.92$, $\sigma_k = 1.0$ and $\sigma_\varepsilon = 1.3$.

The degree to which ε is affected by the buoyancy is determined by the constant $C_{3\varepsilon}$, which is calculated according to the following relation [Henkes et al. (1991)]:

$$C_{3\varepsilon} = \tanh \left| \frac{v}{u} \right|, \quad (5.12)$$

where, v is the component of the flow velocity parallel to the gravitational vector and u is the component of the flow velocity perpendicular to the gravitational vector. Thus, $C_{3\varepsilon}$ becomes 1 for the buoyant shear layers in which the main flow direction is aligned with the direction of gravity, and, zero for the buoyant shear layers that are perpendicular to the gravitational vector.

Energy equation:

As regards to the solution for temperature, it is derived from the energy conservation equation under the assumption of a low-Mach number flow (compressibility neglected). The low-Mach number approximation is suitable for the deflagration regime, which is the main focus of the combustion modeling. The governing equation for modeling the turbulent heat transport (excluding viscous dissipation) is given by the following:

$$\frac{\partial(\rho E)}{\partial \theta} + \frac{\partial[U_i (\rho E + p)]}{\partial x_i} = \frac{\partial}{\partial x_j} \left[\left(k' + \frac{C_p \mu_t}{Pr_t} \right) \frac{\partial T}{\partial x_j} \right] + \rho S_h \quad (5.13)$$

where, E is the total energy per unit mass and S_h is the source of energy per unit mass. The source of energy in case of modeling of an exothermic reaction is the enthalpy generated during the course of reaction. Initially, the velocity distribution and the fluid properties affect the heat transfer. Subsequently, through the release of intense heat in a small volume, the combustion influences the flow field and also the species distribution. Thus they all are inter-related.

Species transport equation:

As a consequence of the reaction between hydrogen and fluorine, the reactor under consideration will contain several species such as, the product HF, excess hydrogen, unutilized fluorine (if any) and the inert gases (as used). Therefore, it is necessary to include the species transport modeling with the chemical reaction. The conservation equation for each chemical species is solved by using the convective-diffusive equation as follows:

$$\frac{\partial}{\partial x_j} (\rho U_j Y_m) = - \frac{\partial}{\partial x_j} (J_m) + R_m \quad (5.14)$$

where, Y_m is the mass fraction of m^{th} species, J_m is the mass flux and R_m (equivalent to source term) is the chemical reaction rate at which a particular species is either consumed or produced in one or more reactions. The diffusion term (J_m) is modeled by Fick's law which is usually a good approximation to the rigorous diffusion velocity calculation. The reaction rates that are contained in the source term (R_m), can be computed either from the laminar

finite rate model (Arrhenius model), the eddy dissipation model (EDM) given by Magnussen and Hjertager (1976), or from the eddy dissipation concept (EDC) model [Magnussen (1981)]. The EDM has been selected for the simulations. It is a turbulence-chemistry interaction model where the reaction rates are assumed to be controlled by mixing. The other two models which use the Arrhenius chemical kinetic calculations are avoided as they are computationally expensive. The net rate of production of species m due to reaction r , $R_{m,r}$, is given by the lower of the two values from equations given below.

$$R_{m,r} = v'_{m,r} M_{w,m} A \rho \frac{\varepsilon}{k} \min \left(\frac{Y_Q}{v'_{Q,r} M_{w,Q}} \right), \quad (5.15)$$

$$R_{m,r} = v'_{m,r} M_{w,m} A B' \rho \frac{\varepsilon}{k} \frac{\sum_P Y_P}{\sum_j^N v''_{j,r} M_{w,j}}. \quad (5.16)$$

The model requires products to initiate the reaction; therefore, a default value of product mass fractions equal to 0.01 is considered while initializing the solution. It is usually sufficient to start the reaction.

5.6 Effect of radiation modeling in temperature predictions

The radiation is a prominent mode of heat transport in comparison to the convection and the diffusion when the source temperatures are typically higher than 1000 K. This is due to the fourth-degree dependence of the radiative flux on temperature. But, besides the source and the sink temperatures, the radiative heat transfer also depends on the physical dimensions of the source, relative positions of the source and the sink and the material properties such as emissivity (for emitter) and absorptivity (for receiver). The fact that the temperature of the flame produced from the chemical reaction between hydrogen and fluorine is of the order of 4000 K, the study of the effect of the radiative heat transfer on the near nozzle reactor temperatures becomes evident. Out of the five radiation models available in the FLUENT

solver, the Rosseland model [Siegel and Howell (1992)] has been selected for simulation as it does not solve an extra transport equation for the incident radiation, is faster than others, and requires less memory. To include the radiation flux in the energy equation, besides the conductive heat transfer, an extra term because of the radiative component is added in the equation 5.13, such that the total heat diffusive term becomes,

$$q_d = (k' + k_r) \nabla T \quad (5.17)$$

where, k' is the thermal conductivity and k_r is the equivalent radiative conductivity given as,

$$k_r = 16\sigma \frac{1}{[3(\sigma_s + a) - C \sigma_s]} T^3 \quad (5.18)$$

In the above equation, 'a' is the absorption coefficient, σ_s is the scattering coefficient, and C is the linear-anisotropic phase function coefficient ranging from -1 to 1, which is a property of the fluid. The default value of 'C' in the model is zero. The case no. 82 (details provided in chapter 3) is re-simulated incorporating the selected radiation model. The change in the reactor temperatures thus obtained is as shown in Figure 5.6. All the temperatures except at T8 and T9 locations went up by a small margin. There was no significant variation in the T8 and T9 temperatures. The match with the experimentally recorded temperature is found to be better with the model without the radiation effect. This observation leads to the conclusion that, besides convective diffusion mode, the inclusion of the radiation mode of heat transfer in the energy balance modeling is not crucial and, therefore, can be safely ignored to save computation time. Small dimensions of the flame and its low emissivity values are the most probable reasons for this observation. Having discussed the all above, the composition of the modeling is summarized as described below.

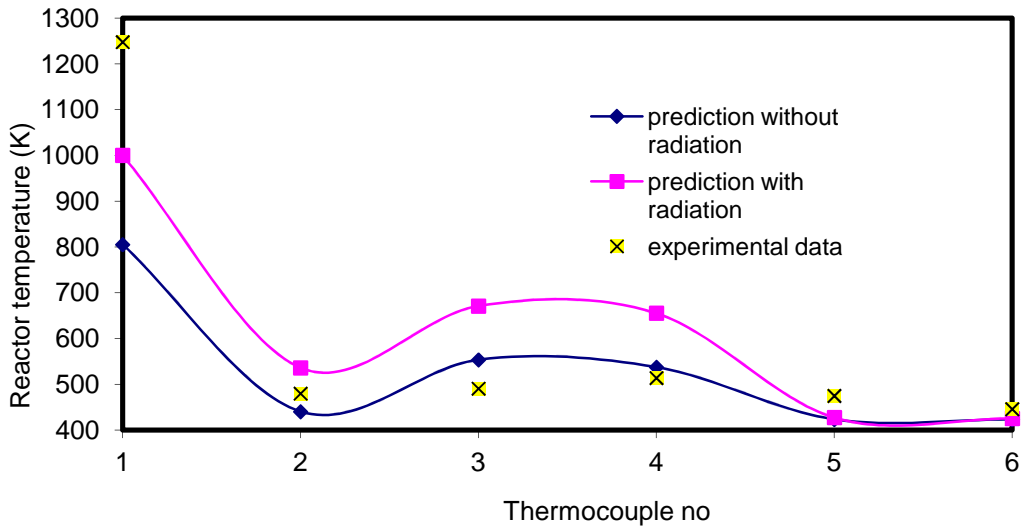


Figure 5.6: Effect of radiative heat transfer on reactor temperatures for case 82

5.7 Summary of the modeling

(Note: The ones not mentioned here are simply checked off in the simulation tool)

- i) Creation of geometry, defining boundary types and unstructured mesh generation using GAMBIT 2.2.30.
- ii) Start of solver for 3D modeling.
- iii) Import of geometry (.msh file) into FLUENT and its adaption
- iv) Types of flows: Steady-state; incompressible and turbulent.
- v) Selection of solver formulation:
 - a. Type of solver: Segregated
 - b. Type of formulation: Implicit, steady, pressure based
 - c. Type of velocity formulation: absolute
 - d. Gradient option: Green-Gauss cell based
- vi) Choosing the basic equations to be solved:
 - a. Flow regime: Turbulent (Viscous model)
 - b. Near wall treatment: Standard wall functions

- c. Type of turbulent model: k- ϵ (standard) model; model constants: by default
- d. No viscous heating and full buoyancy effects
- e. Energy equation: checked
- f. Heat transfer: Convective diffusion, (radiation in only one case, case 82)
- g. Radiation model: Rosseland (Only in case no. 82)
- h. Chemical species and reaction model:
 - i. Model: Species transport
 - ii. No of species: depending on the problem (minimum 4)
 - iii. Reaction: volumetric
 - iv. Turbulent chemistry interaction: Eddy dissipation
- vii) Specifying material properties:
 - a. Individual fluids:
 - i. Density: Incompressible, Ideal gas law (because pressure variations are small and temperature variations are large)
 - ii. Thermal conductivity, viscosity and coefficient of specific heat: Taken from FLUENT database. Since molecular properties play an insignificant role in turbulent cases, they are either treated to be constants or calculated employing piecewise polynomial.
 - iii. Standard enthalpies and entropies: Selected from FLUENT database.
 - iv. Absorption and scattering coefficient: Selected from FLUENT database.
 - v. Kinetic theory parameters: L-J parameters from FLUENT database / user defined.
 - b. Mixture of gases
 - i. Material mixing: mixture template
 - ii. Density: Incompressible - ideal gas

- iii. Specific heat coefficient of the mixture : Ideal gas mixing law
 - iv. Thermal conductivity of the mixture: Ideal gas mixing law
 - v. Viscosity of the mixture: Ideal gas mixing law
 - vi. Mass diffusivity of the mixture: Kinetic theory – Lenard-Jones collision parameters
- c. Reaction: Eddy dissipation
- viii) Defining boundary conditions: Boundary conditions specify the flow and thermal variables on the boundaries of a physical model. They are, therefore, a critical component of CFD simulations and it is important that they are stipulated appropriately. The boundary types input to the solver are as follows:
- a. Inlet boundaries: mass flow inlet at both the feed nozzles and the temperature of the feed gases
 - b. Exit boundaries: Outflow
 - c. Wall boundaries: No slip condition (fluid flow), constant temperature (thermal)
 - d. Internal cell zones: Fluid
 - e. Internal face boundaries: Interior
- ix) Operating Conditions:
- a. Pressure: 101325 Pascal.
(Operating pressure is significant for incompressible ideal gas flows because it directly determines the density)
 - b. Acceleration due to gravity: 9.81 m/s^2
- x) Solution controls:
- a. Under relaxation factors
 - i. Pressure: 0.3

- ii. Density: 1
- iii. Body forces: 1
- iv. Momentum: 0.7
- v. Turbulent kinetic energy: 0.8
- vi. Turbulent dissipation rate: 0.8
- b. Discretization
 - i. Pressure: Standard
 - ii. Pressure-velocity coupling: SIMPLE
 - iii. Momentum: First order upwind
 - iv. Turbulent kinetic energy: First order upwind
 - v. Turbulent dissipation rate: First order upwind
- xi) Finalizing convergence criteria:
 - a. Convergence criteria for continuity equation: 10^{-6}
 - b. Convergence criteria for velocities: 10^{-4}
 - c. Convergence criteria for k: 10^{-5}
 - d. Convergence criteria for ϵ : 10^{-4}
 - e. Convergence criteria for energy: 10^{-6}
 - f. Mass fraction of species: 10^{-4}
- xii) Post processing (Obtaining results in various forms such as contours, vectors, plots etc.)

5.8 Conclusions

FLUENT has been chosen as the commercial CFD tool to simulate the behaviour of the H₂-F₂ flame reactor. The models governing the physics of the problem have been selected based on the closeness of the prediction of the simulations with the experimental data. The

Eddy Dissipation Model as the species transport model and the k- ϵ model as the turbulence model predict reactor temperature values which compare well with the experimental observations. The grid independence test conducted on one of the cases reveals that the results obtained with the finer grid (0.75 mm) are almost similar to that obtained with the grid size of 1 mm. However, there is a huge difference in the respective computation time and therefore, 1 mm grid is chosen for all the simulations. The role of the radiative heat transfer is not found to be significant in the energy dissipation process. The utility of the tuned CFD tool will be further vindicated if it can satisfactorily respond to the changes in the behavioural pattern of the flame reactor with respect to the variation in the operating parameters. In line with this, the experimental observations for a variety of designed experiments and the corresponding simulation results are discussed in the next chapter.

.....

CHAPTER 6

EXPERIMENTAL OBSERVATIONS, SIMULATIONS AND DISCUSSIONS

Several sets of planned experiments beginning with the preliminary studies on H_2-F_2 reaction, the effect of the flow ratio and the preheating on the temperature distribution pattern inside the reactor and, the influence of the diluents on the behavioural change in the H_2-F_2 flame reactor have been carried out. The results are reported in different sections. The main objective of this part of the thesis is to discuss the experimental observations with regards to the scientific interpretation, the simulation results and the mathematical modeling. The simulation predictions are validated by a variety of experimental data to substantiate the usefulness of the CFD tool for future work. Short conclusions are provided at the end of each section.

6.1 THE PRELIMINARY EXPERIMENTS TO ESTABLISH THE FEASIBILITY OF HANDLING H₂-F₂ REACTION

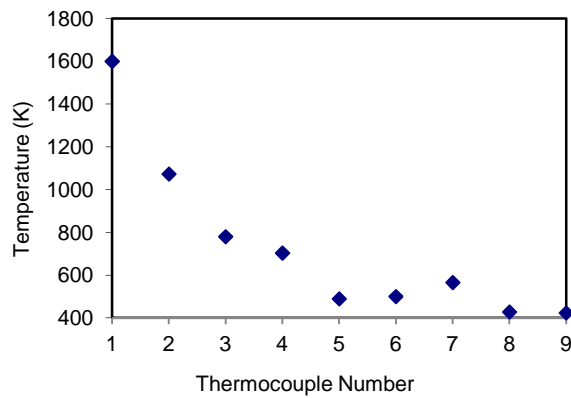
6.1.1 Introduction

The reaction between H₂ and F₂ has been carried out in a long tubular reactor operating at sub-atmospheric pressure. The reaction between H₂ and F₂ is diffusion/mixing controlled. Low pressure operation is beneficial because the reaction zone expands and can be probed more accurately. This also helps in reducing the temperature in the reactor. The design methodologies, the details of the experimental set up, the thermocouple locations and the operation sequence are discussed in the previous chapters (Chapter-3 and Chapter-4). Since all proportions of the H₂ and F₂ mixture are potentially explosive, it was necessary to protect the reactor with a rugged instrumentation and control system. The experimental trials involving hydrogen and fluorine started with high excess of hydrogen over F₂ because lean mixtures of F₂ do not have high flame temperatures. The quantity of hydrogen was reduced stepwise and slowly. The three experimental cases with the flow rates of F₂ and H₂ are listed in Table 3.2 (Chapter-3). The fraction of nitrogen in the fluorine stream was the same in all of them. The three cases were simulated using a commercial computational tool. The experimental data is used to fine-tune and validate the numerical model. This study will be also useful to design many industrially important processes needing high activation energy. The observed experimental findings are as discussed below.

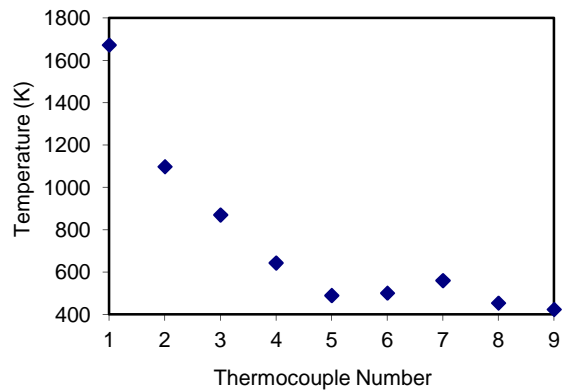
6.1.2 Experimental observations and discussions

The maximum temperature recorded by the thermocouples increased with the increasing F₂ to H₂ ratio. The reactor temperatures responded to the change in the F₂/H₂ ratio within seconds. Thermocouple T1 recorded the highest temperature in all the runs followed

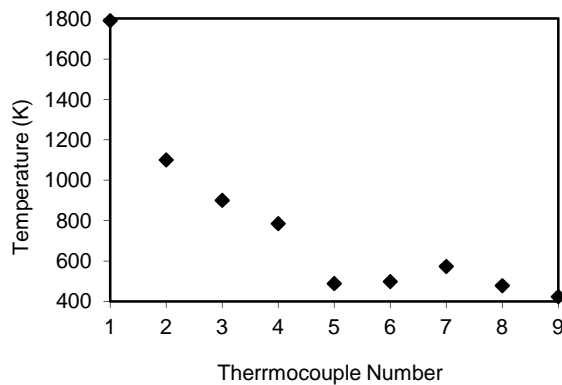
by the thermocouples T2, T3 and T4, respectively. The temperatures as shown by these thermocouples in Figure 6.1 are in the range of 780 to 1790 K. Thermocouple T3, which is radially farther from the F_2 nozzle tip as compared to T4, always recorded higher temperature than the latter. This indicates the expansion of the flame. From the T3 readings, it appears that the flame expands to a radius of ~ 16 mm at a longitudinal distance of 20 mm. T2 and T4 are at the same radial distance, but T2 is 19 mm farther from T4 longitudinally. T2 always measured higher temperature. Assuming symmetry of flame about the fluorine flow axis, the



(a)



(b)



(c)

Figure 6.1: Experimental temperature values for (a) case 1 (F_2 -0.44, H_2 -2 slpm), (b) case2 (F_2 -0.5, H_2 -2 slpm) and (c) case 3 (F_2 -0.48, H_2 -1 slpm)

temperature difference between the two suggests the development of a thermal boundary layer. From the high temperature values of T1, it is obvious that the centre line temperature of the flame is very much higher than 1800 K even at ~40 mm distance from the nozzle. With increasing F_2/H_2 ratio, the difference between T1 and T2 also increased suggesting sharper temperature gradients. Therefore, it is not advisable to operate the reactor at higher F_2/H_2 ratios if uniform reactor temperature profile is a requirement. Thermocouples T5, T6 and T7 which are relatively closer to the reactor wall, recorded temperatures in the range of 490-570 K which are much higher than the wall temperature of 423 K. The temperature profile is flattened down the length of the reactor as the difference between T6 and T7 was 60 – 70 K as compared to 500-700 K, the difference between T1 and T2 placed at the top. Even at a distance of ~450 mm from the nozzle tip, the thermocouple T8 showed temperature in the range of ~430-480 K. However, in all the cases, T9 which is 624 mm away from the tip showed a value close to the wall temperature. Here, the reactor cooling dominates over the reactor heating due to the chemical reaction. It is observed from the above, that the high temperature zone created due to reaction, expands up to a distance of ~450 mm. Quick dissipation of the reaction heat due to high temperature gradients ensures that there are no hot spots.

The temperature values stabilized thirty to forty minutes after the reaction had started. The fact that the preheater, which was used to preheat the reactor wall, remained in the switched off mode almost all the time during the course of the reaction, suggests that always there exists a surplus heat, which needs to be taken away once the reactor wall has been preheated to 423 K. During the experiments, no rise in the reactor pressure was recorded through the pressure transmitter or the pressure switches. Pressure surges, if any, are quickly dissipated into the comparatively larger reactor volume.

6.1.3 Discussion of experimental and simulation results

The CFD model and the solver used for simulation have been described in Chapter-5. The temperature contours are presented in Figure 6.2 for the cases 1, 2 and 3. The theoretical flame temperature as mentioned in Table 3.2 of Chapter-3 varies from ~2500 to 3550 K. However, in the simulation, this varies from ~3300 to 3600 K. From the figures, it can be seen that, the reaction flame does not touch the reactor wall, and its length is around 120 mm in all the cases. Experimentally also, high temperatures were observed at the locations of T5, T6 and T7 at ~120 mm from the nozzle, which further confirms the hypothesis. Figures 6.3 (a) to (c) show the comparison of the simulated and the experimental temperatures as recorded at different locations of the reactor. There is a good match in the temperature readings between the experimental and the numerically predicted data. There is an error to the extent of 18% between these readings. This may be because of the assumptions made in

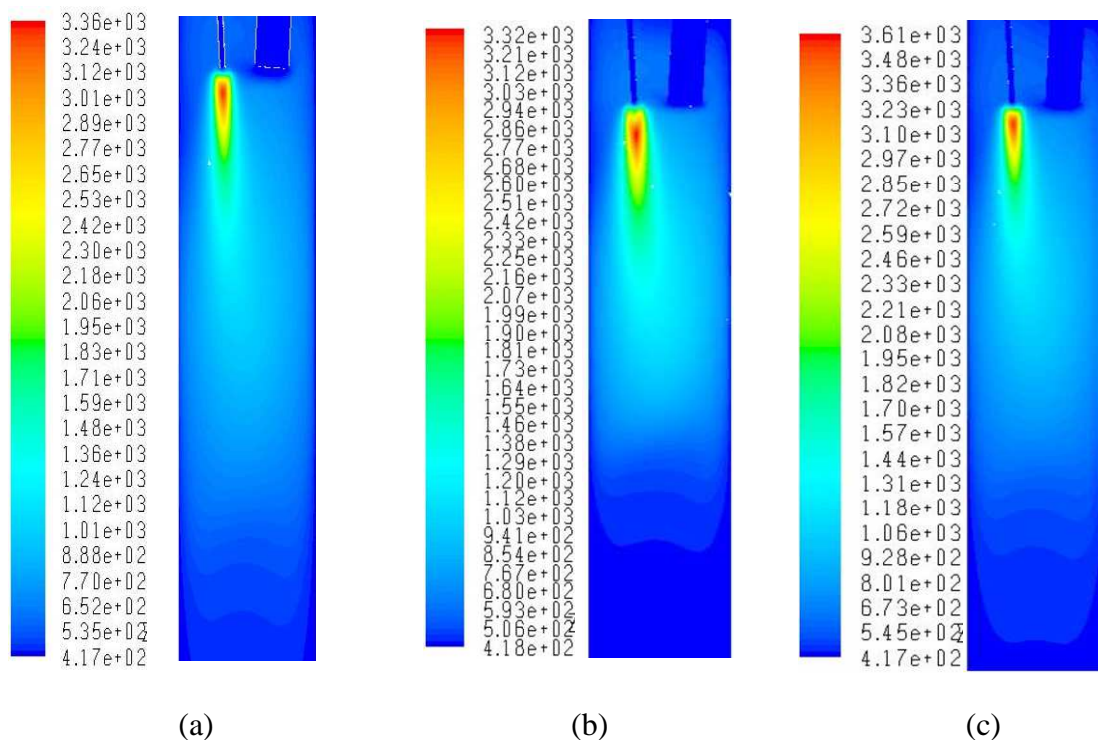


Figure 6.2: Simulated temperature predictions (K) for (a) case 1 (F_2 -0.44, H_2 -2 slpm), (b) case 2 (F_2 -0.5, H_2 -2 slpm) and (c) case 3 (F_2 -0.48, H_2 -1 slpm)

the simulation with respect to the heat generation source, the mode of heat transfer and the wall temperature being fixed. During the experiments, the wall temperature oscillates about a given set point, whereas in the simulation, it is kept constant. A change in the wall temperature can affect the reactor temperature profile.

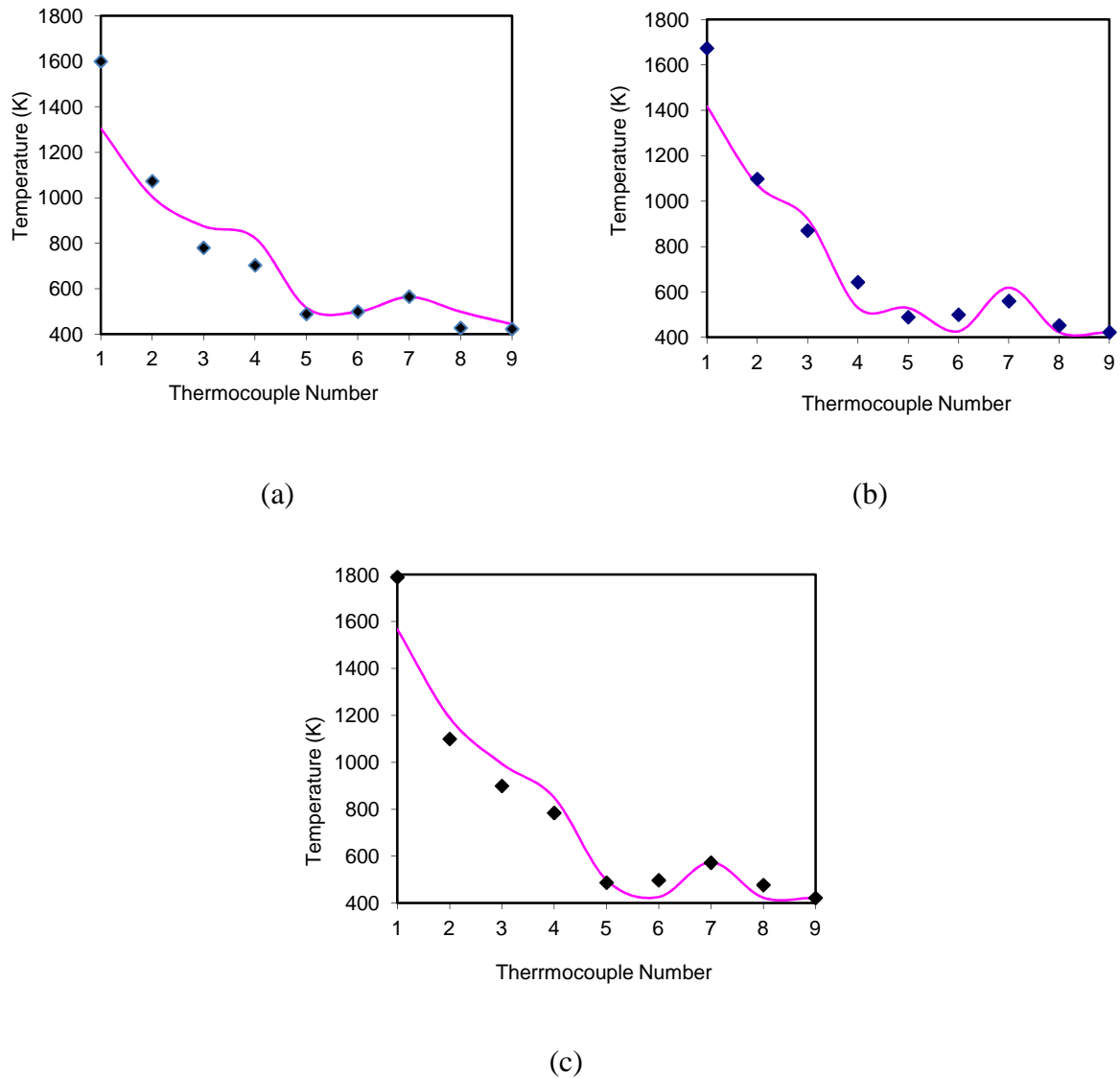


Figure 6.3: Comparison between experimental and predicted reactor temperatures for (a) case 1 (F_2 -0.44, H_2 -2 slpm), (b) case 2 (F_2 -0.5, H_2 -2 slpm) and (c) case 3 (F_2 -0.48, H_2 -1 slpm); dots: experimental data, curve: computed data

The validated numerical model was used to study the velocity and the concentration profiles in the reactor. Figure 6.4 shows the Y velocity (longitudinal) contours for different cases. From this figure, it is seen that there is a difference in the tip velocities of the two gases. Velocity with positive sign shows velocity in the upward direction and that with negative sign shows velocity in the downward direction. Velocity in the downward direction is predominant near the fluorine nozzle. A part of the hydrogen flow has upward motion suggesting some recirculation in the region near the hydrogen feed nozzle. The nozzles were

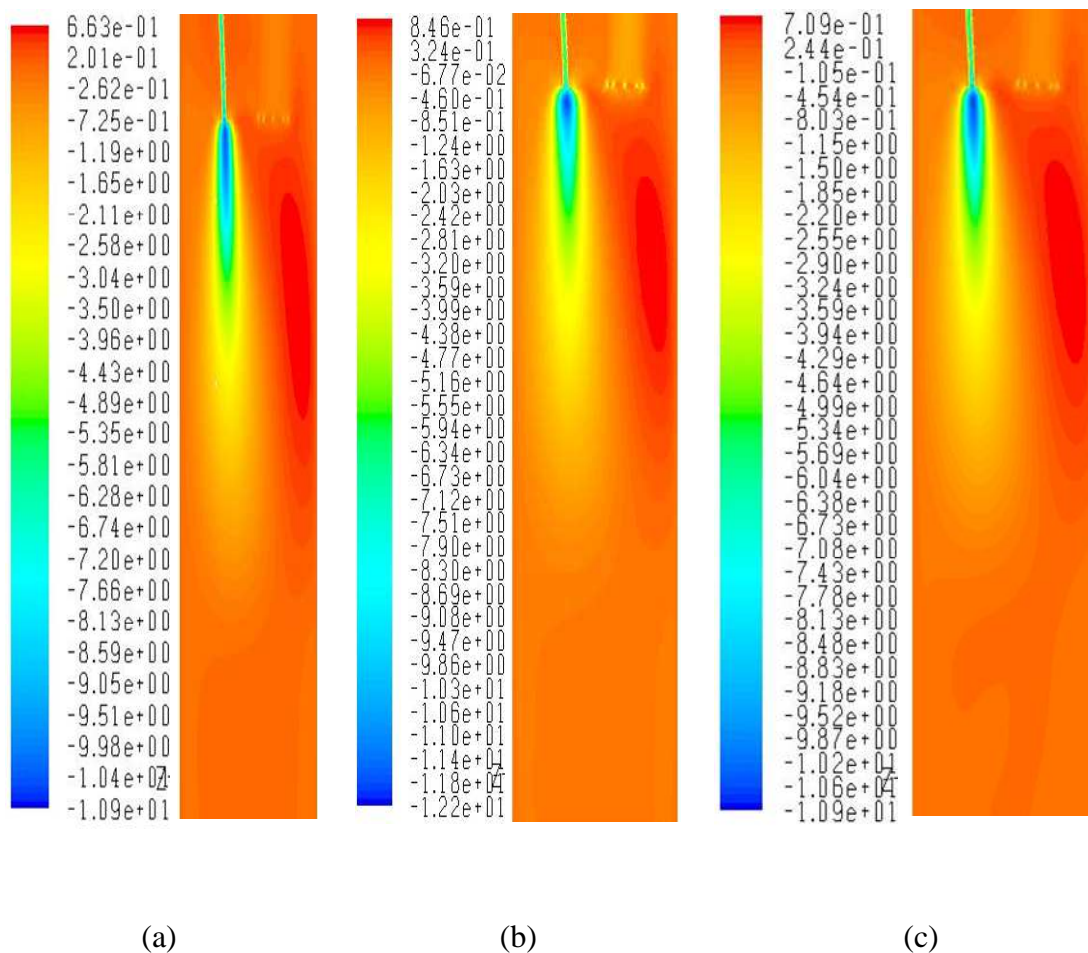


Figure 6.4: Contour plots of axial velocity (m/s) for (a) case 1 (F₂-0.44, H₂-2 slpm), (b) case 2 (F₂-0.5, H₂-2 slpm) and (c) case 3 (F₂-0.48, H₂-1 slpm)

inspected after the reaction had been carried out. Both the nozzles were found to be intact and clean as if they have been passivated with a fluorinating agent. One of the reasons attributed for the clean nozzles could be the distance required for the hydrogen molecules to diffuse and mix with the fluorine molecules and react, due to which the flame is formed away from the

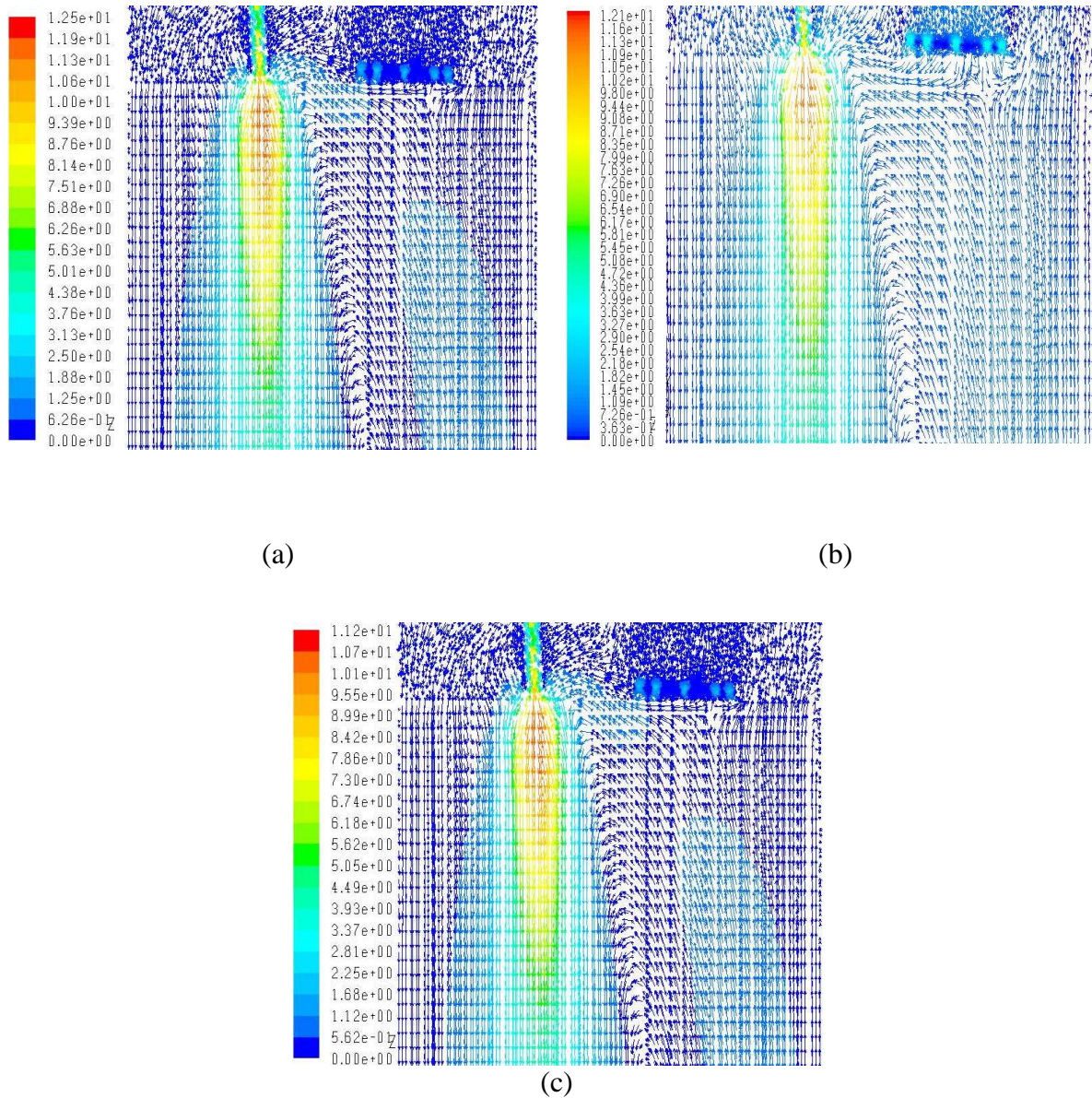


Figure 6.5: Vector plots of velocity for (a) case 1 (F_2 -0.44, H_2 -2 slpm), (b) case 2 (F_2 -0.5, H_2 -2 slpm) and (c) case 3 (F_2 -0.48, H_2 -1 slpm)

fluorine nozzle tip. In other words, lesser number of the H_2 molecules mix with the F_2 molecules near the nozzle tip. This observation is further confirmed by the simulation results shown in Figures 6.5 (a) to (c), which show the velocity vectors near the nozzle outlet for the three cases. Here, the hydrogen streamlines are seen bending towards the fluorine streamlines and intersecting them slightly away from the nozzle tip. Since the velocity of the hydrogen

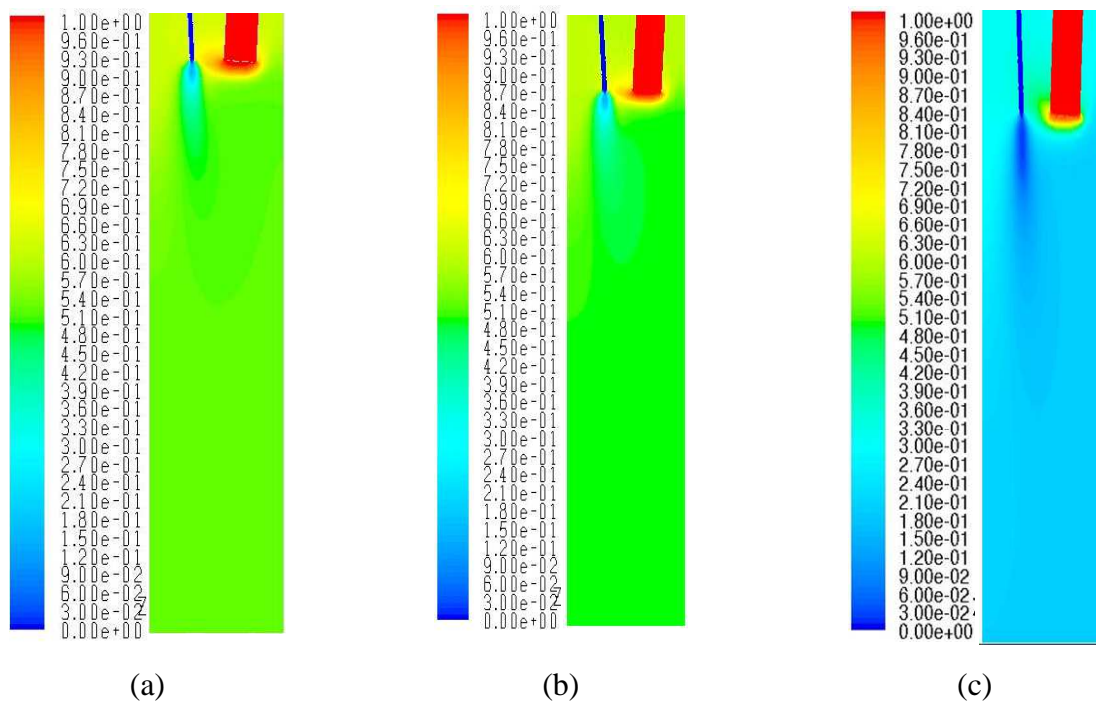


Figure 6.6: Contour plots of hydrogen mole fraction for a) case 1 (F_2 -0.44, H_2 -2 slpm), (b) case 2 (F_2 -0.5, H_2 -2 slpm) and (c) case 3 (F_2 -0.48, H_2 -1 slpm)

stream is lower, it is dragged by the relatively high velocity fluorine stream. Figures 6.6 to 6.9 show the contour plots for the mole fraction of different species present in the reactor. Figure 6.6 shows the contour plot for the unreacted hydrogen in the reactor. Hydrogen, being the lighter gas, moves upward which can be seen in these figures. Figure 6.7 shows the contour plot for the fluorine mole fraction, which is almost zero everywhere except in the small region near the F_2 nozzle. This is the region which has insufficient hydrogen for F_2 to

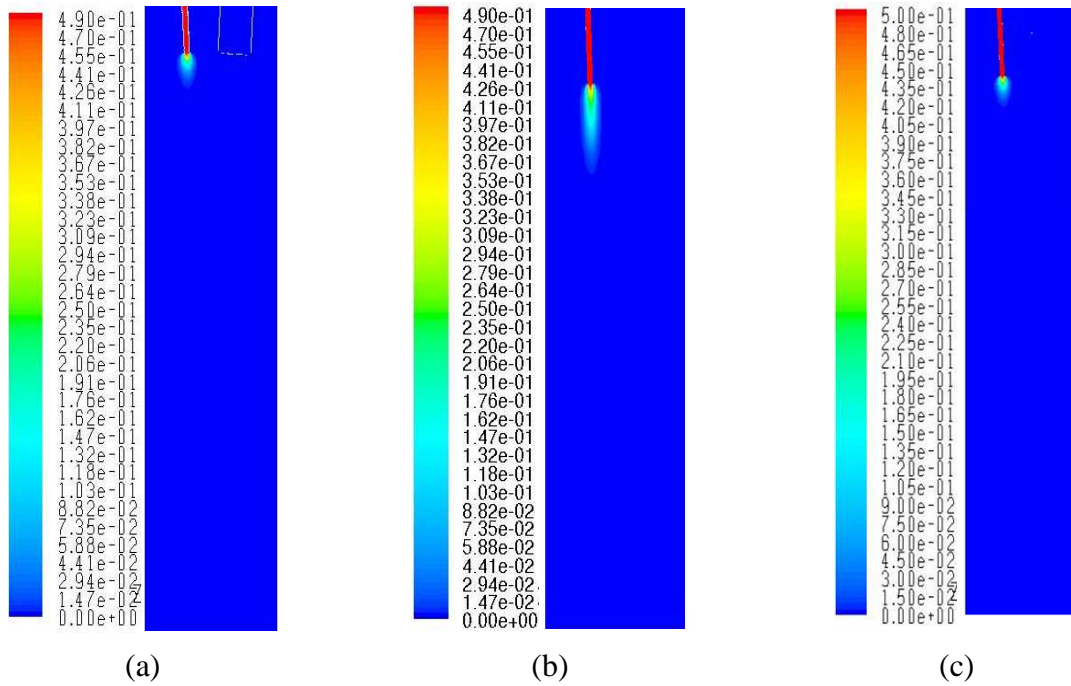


Figure 6.7: Contour plots of fluorine mole fraction for a) case 1 (F_2 -0.44, H_2 -2 slpm), (b) case 2 (F_2 -0.5, H_2 -2 slpm) and (c) case 3 (F_2 -0.48, H_2 -1 slpm)

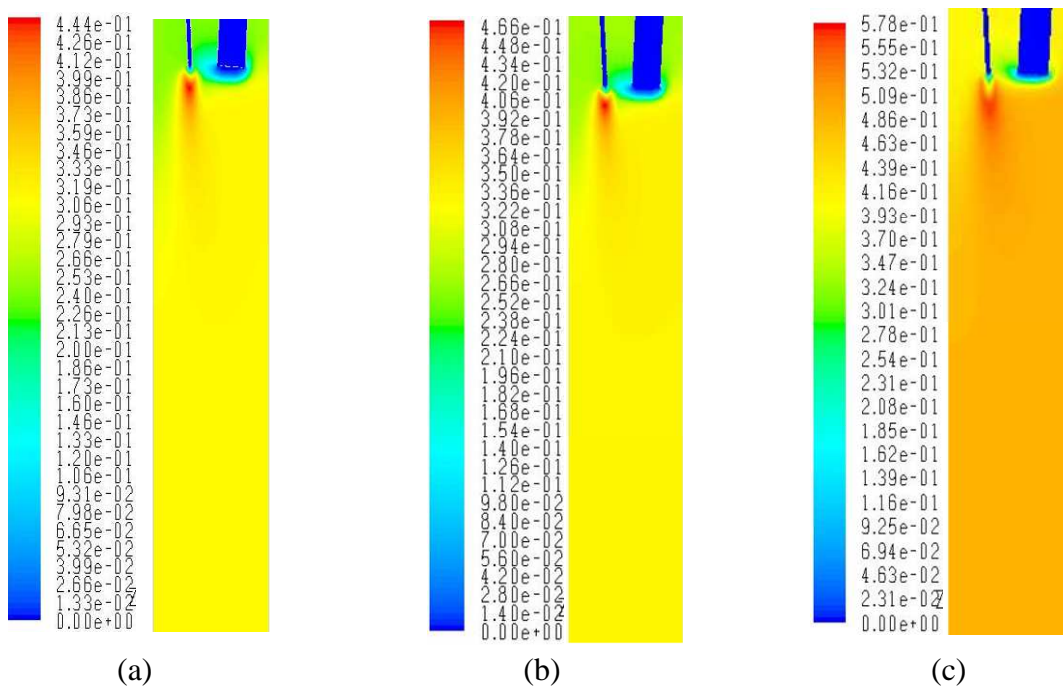


Figure 6.8: Contour plots of hydrogen fluoride (HF) mole fraction for a) case 1 (F_2 -0.44, H_2 -2 slpm), (b) case 2 (F_2 -0.5, H_2 -2 slpm) and (c) case 3 (F_2 -0.48, H_2 -1 slpm)

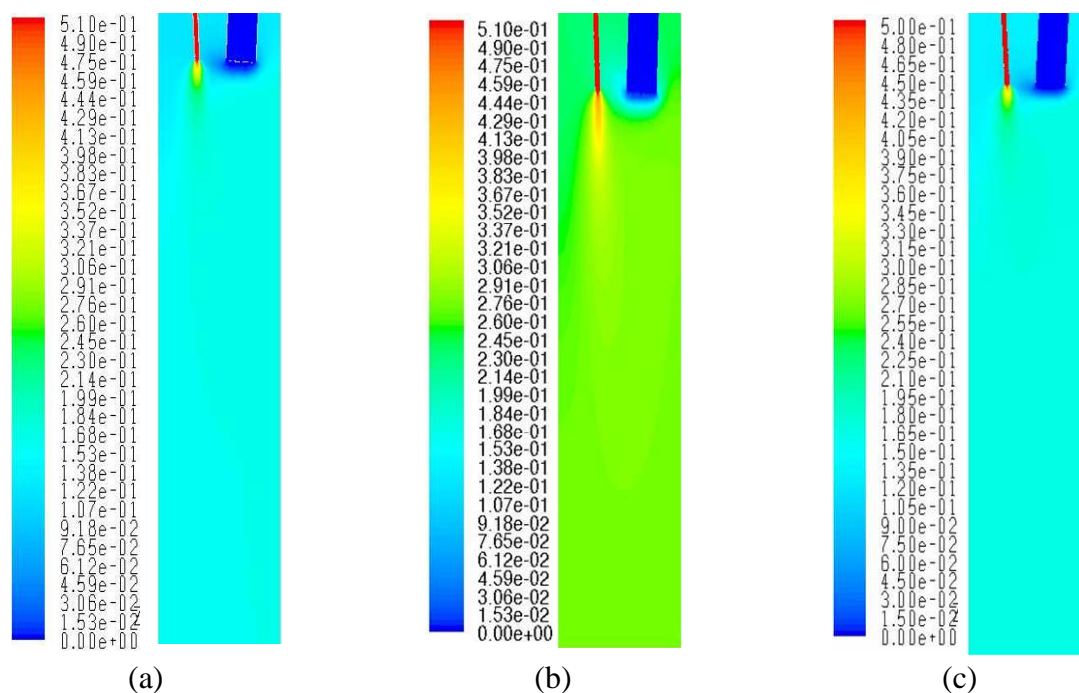


Figure 6.9: Contour plots of nitrogen mole fraction for a) case 1 (F_2 -0.44, H_2 -2 slpm), (b) case 2 (F_2 -0.5, H_2 -2 slpm) and (c) case 3 (F_2 -0.48, H_2 -1 slpm)

react completely. Figure 6.8 shows the contour plot of the hydrogen fluoride mole fraction. Hydrogen fluoride is formed according to the stoichiometry of the reaction. The concentration of HF is more near the fluorine nozzle where the reaction takes place. It gets carried away by other gases like hydrogen and nitrogen to other parts of the reactor. Similarly, Figure 6.9 shows the nitrogen concentration profile in the reactor. At the farther end of the reactor (~300 mm away from the nozzles), the mole fraction values of different species match with the steady state composition of the gaseous mixture obtained after the reaction. This mixture contains excess H_2 , HF and N_2 .

6.1.4 Summary of the results of the preliminary experiments to establish the feasibility of handling H_2 - F_2 reaction

For highly exothermic reactions, turbulence inside the reactor is created due to in-situ release of enormous heat of reaction and convection currents generated due to the wide

difference in temperatures within the reactor. The assumption made for the simulation, that is, the reaction between hydrogen and fluorine is instantaneous and the flow field is turbulent has produced results which match well with the experimental observations. Further, as seen through the experiments, a stable flame is obtained if the flow rates of the reactants are steady and the heat is also steadily removed. This is because the reactor temperatures closer to the feed nozzles remained steady during the course of the experimental trials. The presence of the wall does not affect the flame, as the flame formed is very narrow. The reaction between hydrogen and fluorine takes place along the axis of the fluorine flow jet because the gaseous stream exiting from the fluorine nozzle carries a higher momentum in comparison to the hydrogen stream issuing from the other nozzle. As the flame does not form right at the nozzle tip because of insufficient fuel present locally, the nozzle tip is protected from high reaction temperatures. The present effort, which concentrated on safely carrying out the H_2-F_2 reaction, has provided important data for process design of a reactor. As the flame temperature is affected by several parameters such as the reactor wall temperature, the relative feed rates, excess of hydrogen and the fraction of nitrogen present in fluorine, it is worthwhile to conduct a quantitative investigation of the effect of these parameters on the temperature profile inside the reactor. The results of these studies are discussed below.

6.2 INFLUENCE OF EXCESS HYDROGEN AND NITROGEN ON BEHAVIOUR OF H_2-F_2 FLAME REACTOR

6.2.1 Introduction

In the preliminary experiments described under section 6.1, it is mentioned that the reaction between H_2 and F_2 is almost instantaneous and is mixing controlled. In most of the applications requiring heating of the reactant mixture using the chemical energy, it is

desirable to have a flat temperature profile in the reaction zone to maximize the conversion and the yield. The reactor temperatures are affected by several parameters such as the reactant feed rates and the feed ratios. Nitrogen is always present along with fluorine when it is produced from the electrolysis of HF. Therefore, it is necessary to conduct experimental studies on the effect of the H₂ to F₂ ratios and varying nitrogen flow rates on the reactor temperatures. In the set of experiments of interest, three base flow rates of fluorine at which the studies were performed were 0.2, 0.3 and 0.4 slpm respectively. For every base flow rate of fluorine, the ratio of hydrogen to fluorine was changed by varying the excess of hydrogen from ~215% (v/v) to 535% (v/v). Similarly, nitrogen in the range between 0.4 and 3.4 slpm was premixed with the F₂ stream to observe its effect on the reactor temperatures. The flow rate of nitrogen chosen was arbitrary only to observe the change in the reactor behaviour. While doing so (study in the presence of nitrogen), 325 % excess of hydrogen was used for each flow rate of fluorine mentioned above. The details of the experimental set up used for this study are provided in the Chapter-4. Due to some practical constraints, only two 'B' type thermocouples, namely, T1 and T4 were functional near the feed nozzles where the flame formation took place. Positions of the other thermocouples from T5 to T9 were not altered. The reactor was operated at 1000 mbar (abs) pressure. A total of 27 cases, as detailed in Table 3.3, were experimentally investigated out of which 15 were computationally simulated. The data from these trials were used to validate the computational model.

6.2.2 Experimental observations and discussions

The reactor temperatures responded to the change in parameter within seconds. However, it took around forty minutes for the temperatures to stabilize after the reaction had started. In these experiments too, the pressure transmitter and the pressure switches did not

record any pressure surge. The thermocouple T1 recorded the highest temperature in all the runs. The behaviour of the other experimental parameters are discussed below.

6.2.2.1 Effect of percentage excess of H₂

H₂ plays a dual role of being a reactant as well as a heat carrier. As it was always in surplus with respect to fluorine, the temperatures in the reaction zone were expected to drop with increase in percentage excess of hydrogen. The effect of varying flow rates of hydrogen on the reactor temperatures is shown through Figures 6.10 (a) to (c). In all the cases, values of T1 which is closer to fluorine flow axis, decreases with increase in the hydrogen flow rate. The drop in T1 is in the range of 20-80 K. The net change in T1 decreases at higher fluorine flow rates, suggesting that the effect of excess hydrogen reduces when higher amount of energy is liberated inside the reactor. Figure 6.10 (a) is for a fluorine flow rate of 0.2 slpm. The T4 versus hydrogen flow rate curve here shows an apparent maximum and a minimum. As this behaviour is not noticed at other flow rates of fluorine, the local maxima and minima are considered to be experimental outliers. The temperatures recorded by T8 are invariably higher than T7 for all the flow rates of hydrogen. At higher base flow rates of fluorine (at 0.3 and 0.4 slpm), the trends exhibited by T4, T7 and T8 are different. In the figures 6.10 (b) and 6.10 (c), T4 decreases with increase in the hydrogen flow rate while the values recorded by T7 are always higher than T8. This behaviour is explained in the following manner.

At low fluorine flow rate, the heat evolved is comparatively less and the high temperature zone is confined to a small region. As the hydrogen flow increases, more hydrogen molecules reach near the fluorine nozzle (see Figure 6.15) where the reaction takes place. Since hydrogen has higher thermal diffusivity, the rate of lateral heat dissipation increases, resulting in the increase in the temperature being recorded by T4 which is situated slightly away (radially) from the nozzle. As the fluorine flow rate increases, more heat is

liberated leading to higher temperatures near the nozzles. The high temperature zone also expands due to local turbulence. Therefore, with higher H₂ to F₂ flow ratio, both T1 and T4 values go down while T7 gains temperature. The difference between the values of T4 and T7

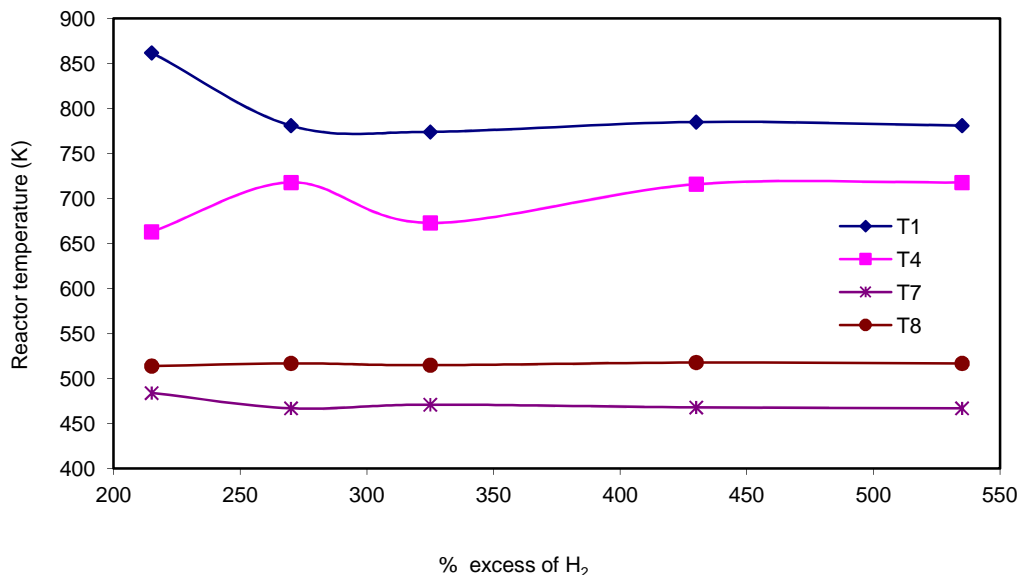


Figure 6.10 (a): Effect of excess of hydrogen on the reactor temperatures for 0.2 slpm of fluorine.

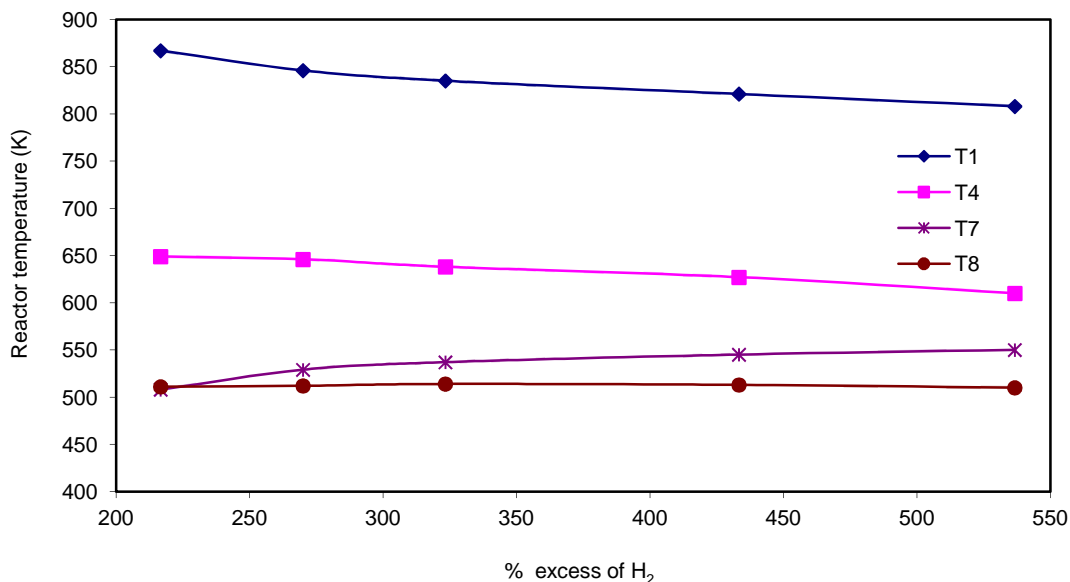
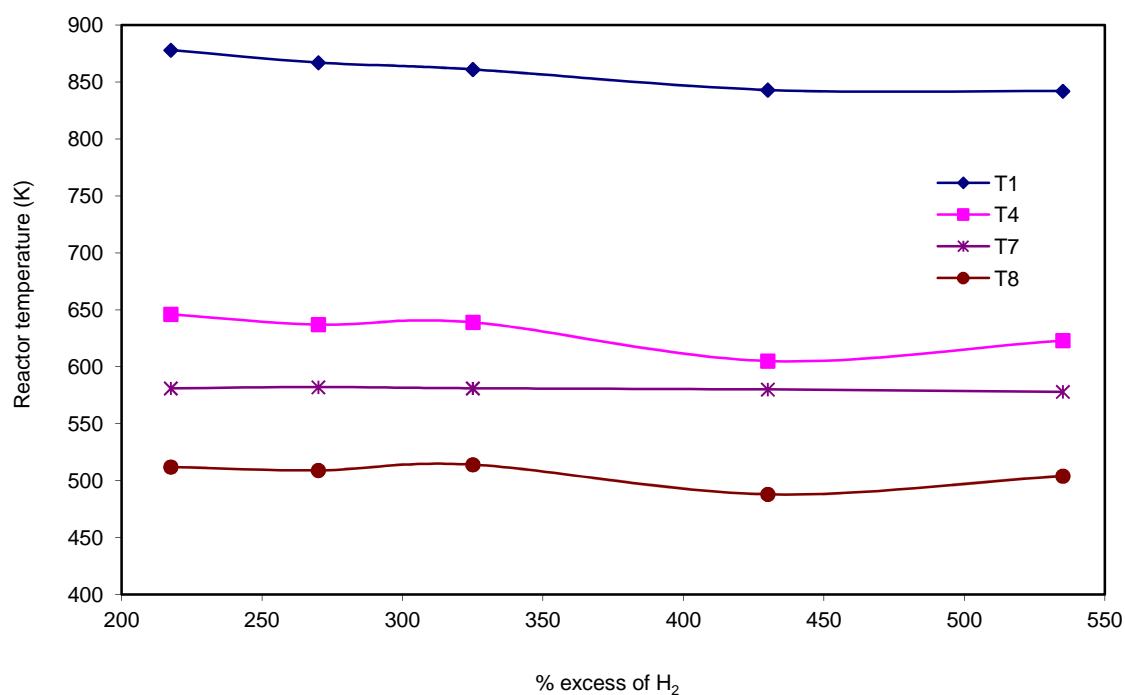


Figure 6.10 (b): Effect of excess of hydrogen on the reactor temperatures for 0.3 slpm of fluorine.



(c)

Figure 6.10 (c): Effect of excess of hydrogen on the reactor temperatures for 0.4 slpm of fluorine.

goes on decreasing with increase in the hydrogen flow rate. There is a slight rise in T7 readings and almost no variation in the values of T8 as the flow of hydrogen increases. This suggests that the effect of excess hydrogen on the reactor temperature is limited to a distance of ~120 mm from the F₂ nozzle tip. Due to practical constraints, the temperature closer to the reaction flame could not be measured but it is evident, that the flame temperature would be affected considerably with increase in the molar ratio of hydrogen with respect to fluorine.

6.2.2.2 Effect of nitrogen flow

Though nitrogen is chemically inert in the reaction, it plays a significant role in the mixing of species and also dissipating the reaction heat. A small quantity of nitrogen is

purged into the electrolytic cell to protect the anode where F_2 is produced. Additional nitrogen was added before the F_2 stream enters the reactor. It is seen in Figures 6.11 (a) to (c), that for all the cases, increase in the flow of nitrogen has significant effect on both T1 and T4. The drop in the temperatures as indicated by T1 and T4 is between 200 and 300 K, when the nitrogen flow is increased from ~ 0.4 slpm to 3.5 slpm. The thermocouples T4 and T7 are located almost at the same radial distance but T7 is ~ 100 mm farther from T4. When the flow of nitrogen is varied for 0.2 slpm of fluorine, initially, at lower nitrogen flow rate (0.4 slpm), the value of T4 is more than T7 [Figure 6.11(a)]. But, as the flow of nitrogen is increased, T7 exceeds T4 by almost 100 K. When the flow rate of nitrogen is increased to 3.4 slpm, the drop in T4 is close to 180 K while the rise in T7 is nearly 100 K. The difference between T1 and T7 reduces with increasing flow of nitrogen. The temperatures as indicated by other thermocouples including T8 were almost unaffected. Similar effects of the nitrogen flow on the reactor temperatures were observed for the other two flow rates of F_2 , that is, 0.3 and 0.4 slpm. The results above indicate the significant change in the temperature profile near the nozzle region. Dip in T1 and T4 values and simultaneous rise in the value of T7 imply expansion of the high temperature jet. The volume of the reaction zone, where comparatively higher temperatures prevail, increases as the energy liberated from the reaction is spread by the expanding jet. More nitrogen flow adds momentum to the fluorine stream leading to increase in the velocity of the latter. This delays the mixing process between H_2 and F_2 . It also results in the spreading of the species and the dissipation of the reaction heat to a larger volume away from the nozzles. However, as observed in the case of excess hydrogen, this effect too appears to be limited to a length of ~ 120 mm as the reactor temperatures beyond this length did not record any notable change.

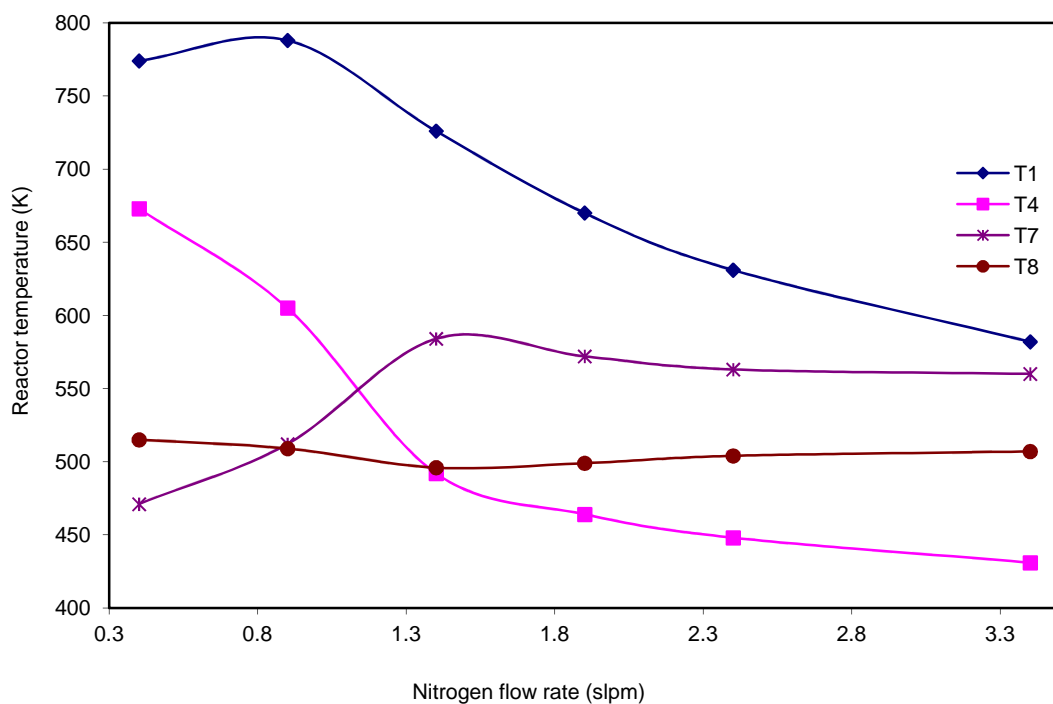


Figure 6.11 (a): Effect of nitrogen flow rate on the reactor temperatures for 0.2 slpm of fluorine with ~325% excess of hydrogen.

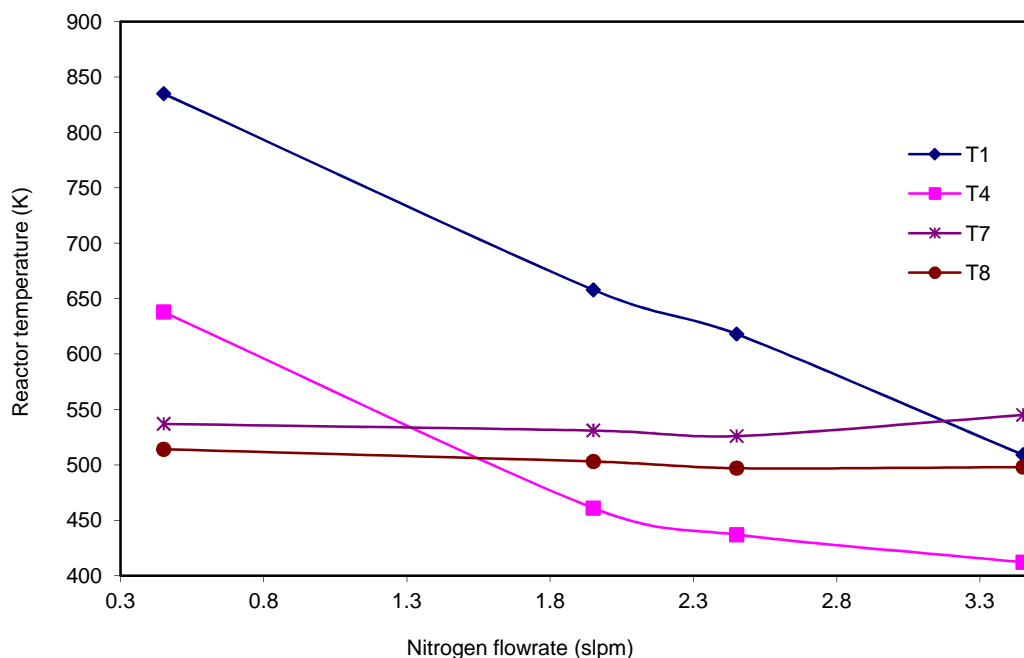
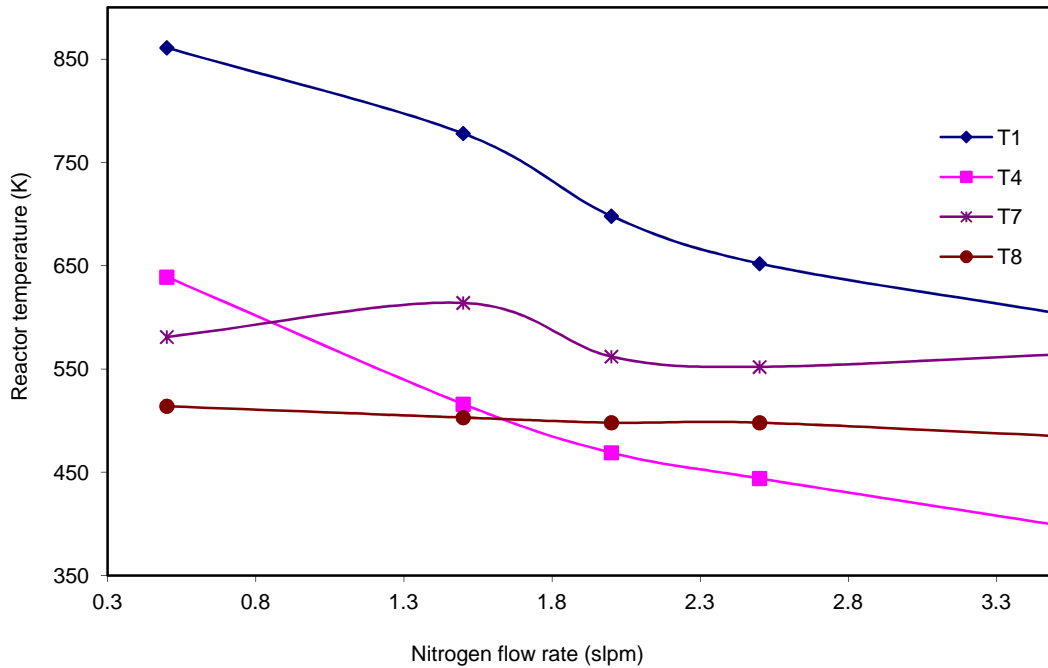


Figure 6.11 (b): Effect of nitrogen flow rate on the reactor temperatures for 0.3 slpm of fluorine with ~325% excess of hydrogen.



(c)

Figure 6.11 (c): Effect of nitrogen flow rate on the reactor temperatures for 0.4 slpm of fluorine with ~325% excess of hydrogen.

6.2.3 Discussion of experimental and simulation results

Out of the total 27 cases, fifteen cases (case 4 to case 18) were simulated. The cases were so chosen that they covered the effect of both the parameters planned during this study. Figure 6.12 shows the temperature contours for the simulated cases. Theoretical calculations were carried out to predict the adiabatic flame temperature for all the cases, which are presented in Table 3.3. It varies from 1090 to 2911 K. The maximum temperature predicted from the simulation for these cases is in the range of 850-3050 K, and it drops immediately with increase in the hydrogen or nitrogen flow rates. The change in the hydrogen or nitrogen flow rate mainly affects the temperature at the T1 and T4 positions. The flame does not touch the reactor wall in any of the simulated cases. No damage was seen on the nozzles after the

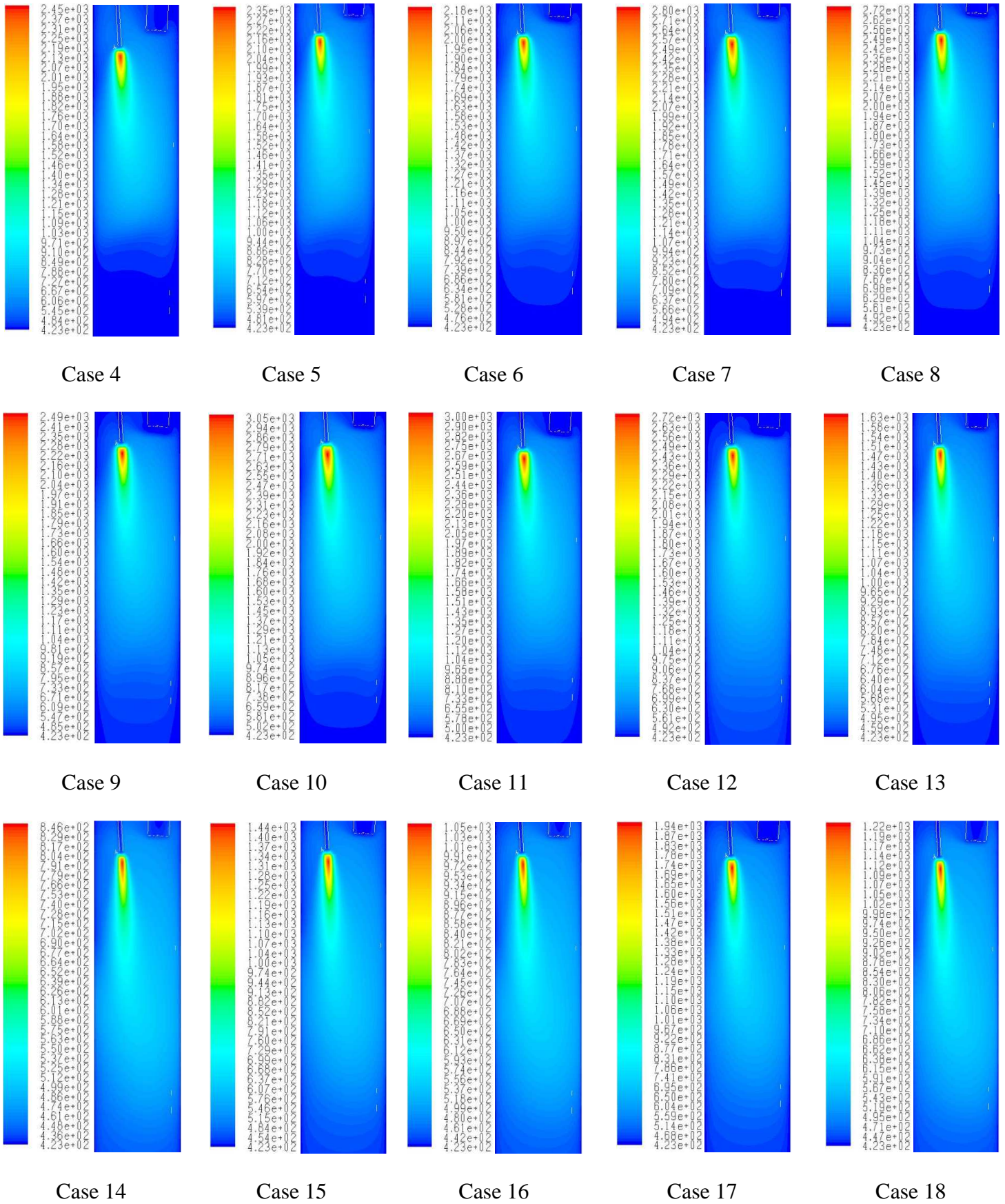
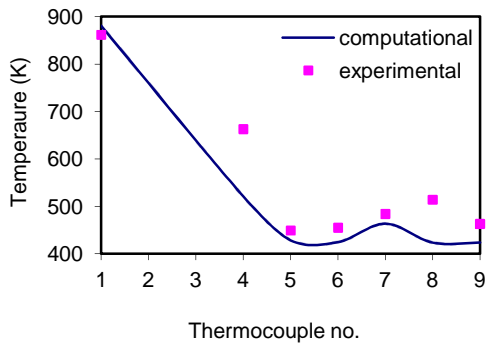
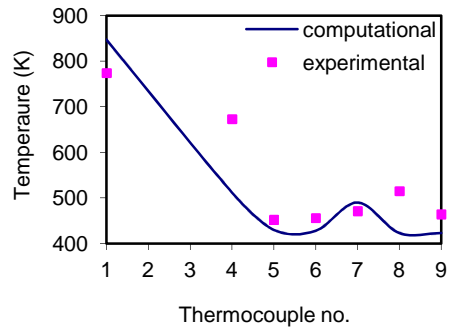


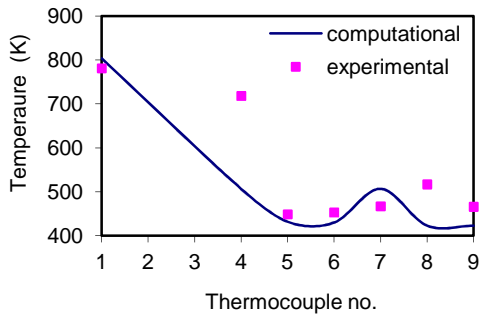
Figure 6.12: Contour plots of temperature (K) for cases 4 to 18



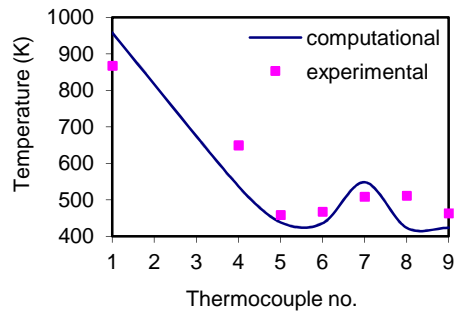
Case 4



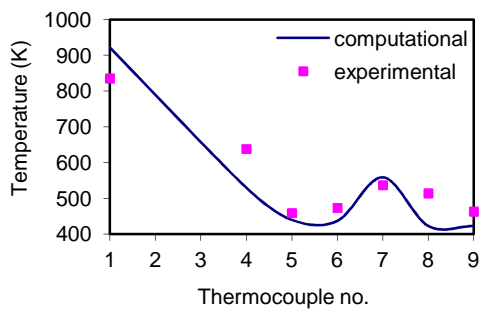
Case 5



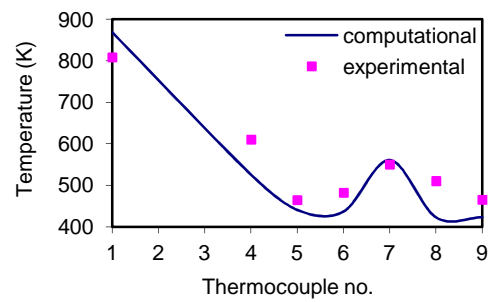
Case 6



Case 7

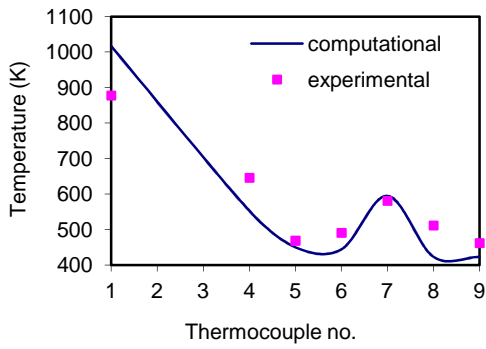


Case 8

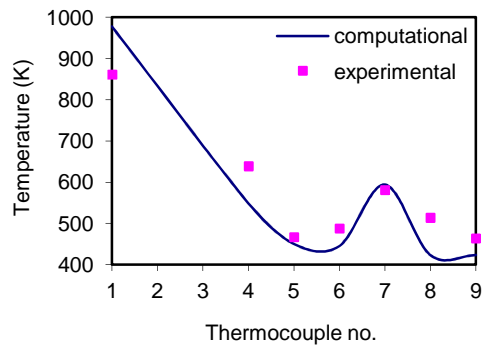


Case 9

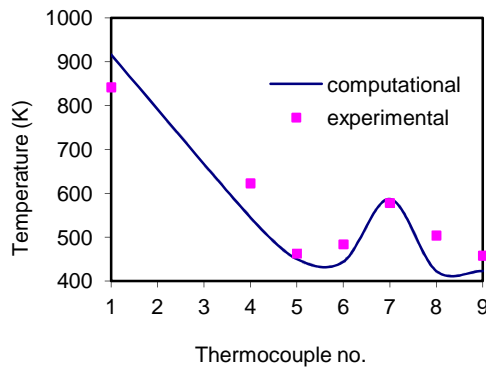
Figure 6.13 (a): Comparison between the simulated and the experimental reactor temperatures for cases 4 to 9



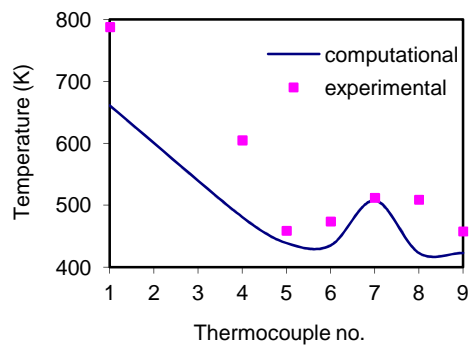
Case 10



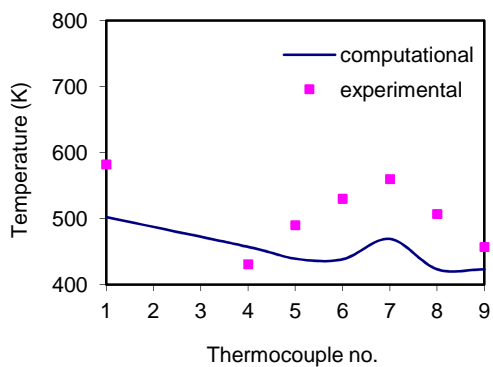
Case 11



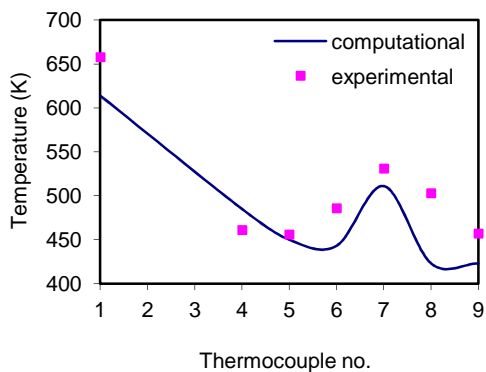
Case 12



Case 13

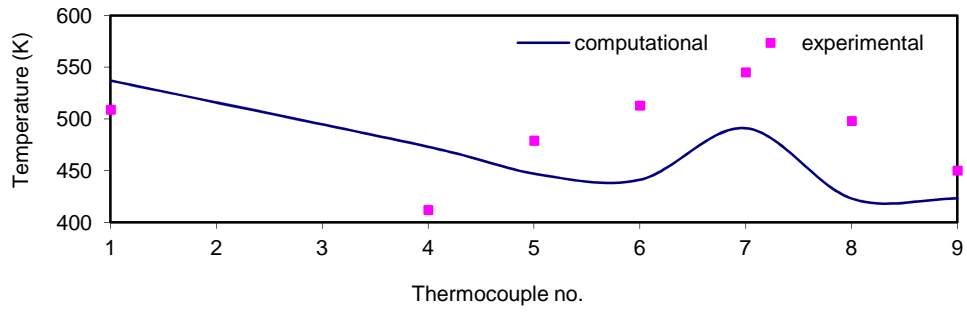


Case 14

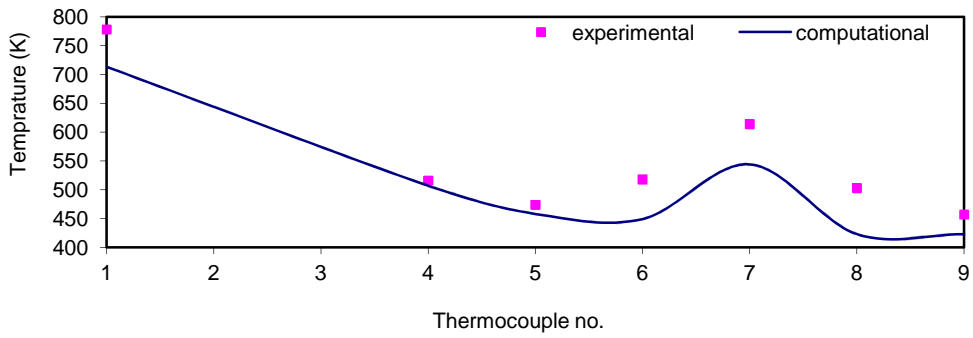


Case 15

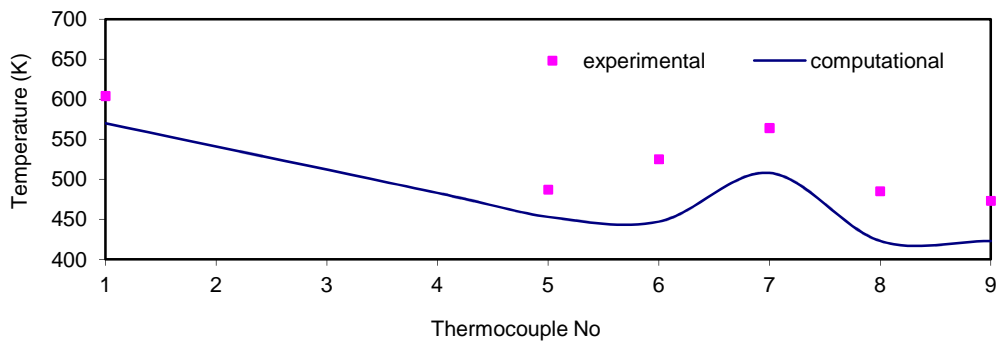
Figure 6.13 (b): Comparison between the simulated and the experimental reactor temperatures for cases 10 to 15



Case 16



Case 17



Case 18

Figure 6.13 (c): Comparison between the simulated and the experimental reactor temperatures for cases 16 to 18

experimental trials. This re-confirms the earlier prediction that the reaction takes place a little away from the feed nozzles. Figure 6.13 (a) to (c) show the comparison of the simulated and the experimental temperature readings recorded at different locations of the reactor. There is a good match between the experimentally observed and the computationally predicted temperature values. The computed data follows the experimental trend of increase and decrease in the temperatures when a particular parameter is changed. In the cases 4 to 12, T1, T4 reduce and T7 increases. The net change in these temperatures varies from 20 to 50 K. In the cases 13 to 18, the T1 and T4 values plunge to the extent of ~160 K. For all the cases, the average of the difference in the observed and the predicted data varies from 0.002 to 0.1 times the experimental temperature; whereas the standard deviation about the mean is between 0.07 and 0.16.

The validated numerical model was used to study the velocity and the concentration profiles in the reactor. Figure 6.14 shows the velocity contours for different cases. The velocity of the F_2+N_2 stream is more than that of the H_2 stream in all the cases. There is a surge in the fluid velocity in the reaction zone due to the rise in the temperature resulting from the release of heat of reaction between hydrogen and fluorine. For the cases 4, 6, 10 and 12, this velocity decreases with the increase in the percentage excess of hydrogen, perhaps due to enhanced cross mixing at the higher hydrogen flow rates. Figures 6.15 to 6.18 show the contour plots for mole fraction of different species present in the reactor. The mixture inside the reactor contains excess H_2 , un-reacted F_2 , product HF and inert N_2 . In Figure 6.15, for the cases 4 to 6, 7 to 9 and 10 to 12, the hydrogen concentration near the fluorine nozzle is seen to be rising with increase in its flow rate. The hydrogen concentration increase in this region helps in faster dissipation of reaction heat. As seen in Figure 6.16 and also observed in the Figure 6.7, the fluorine reaction does not set in over a very short distance near the exit of the fluorine nozzle where mixing is weaker. It gets completely exhausted by reacting rapidly

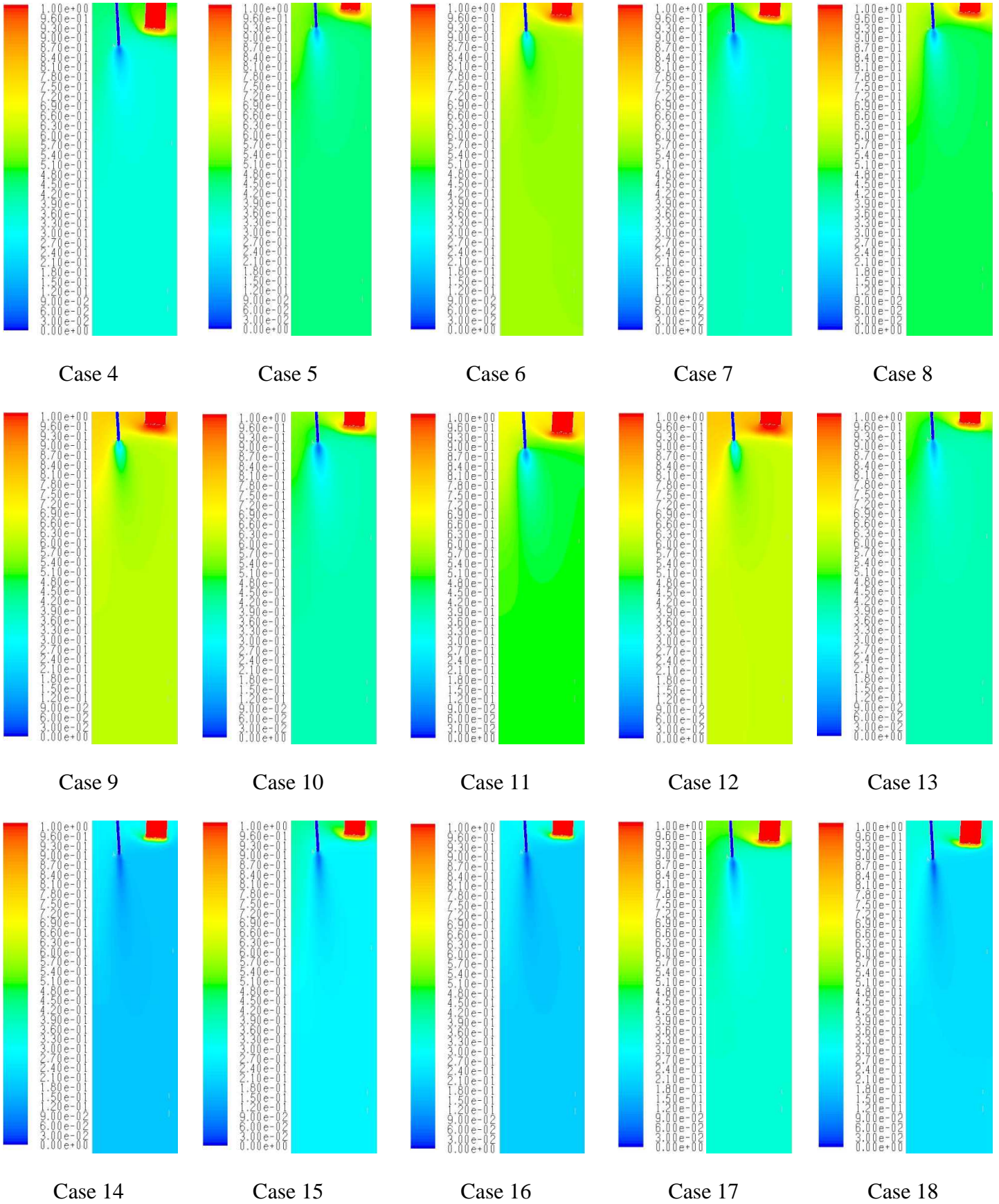


Figure 6.15: Contour plots of hydrogen mole fraction for cases 4 to 18

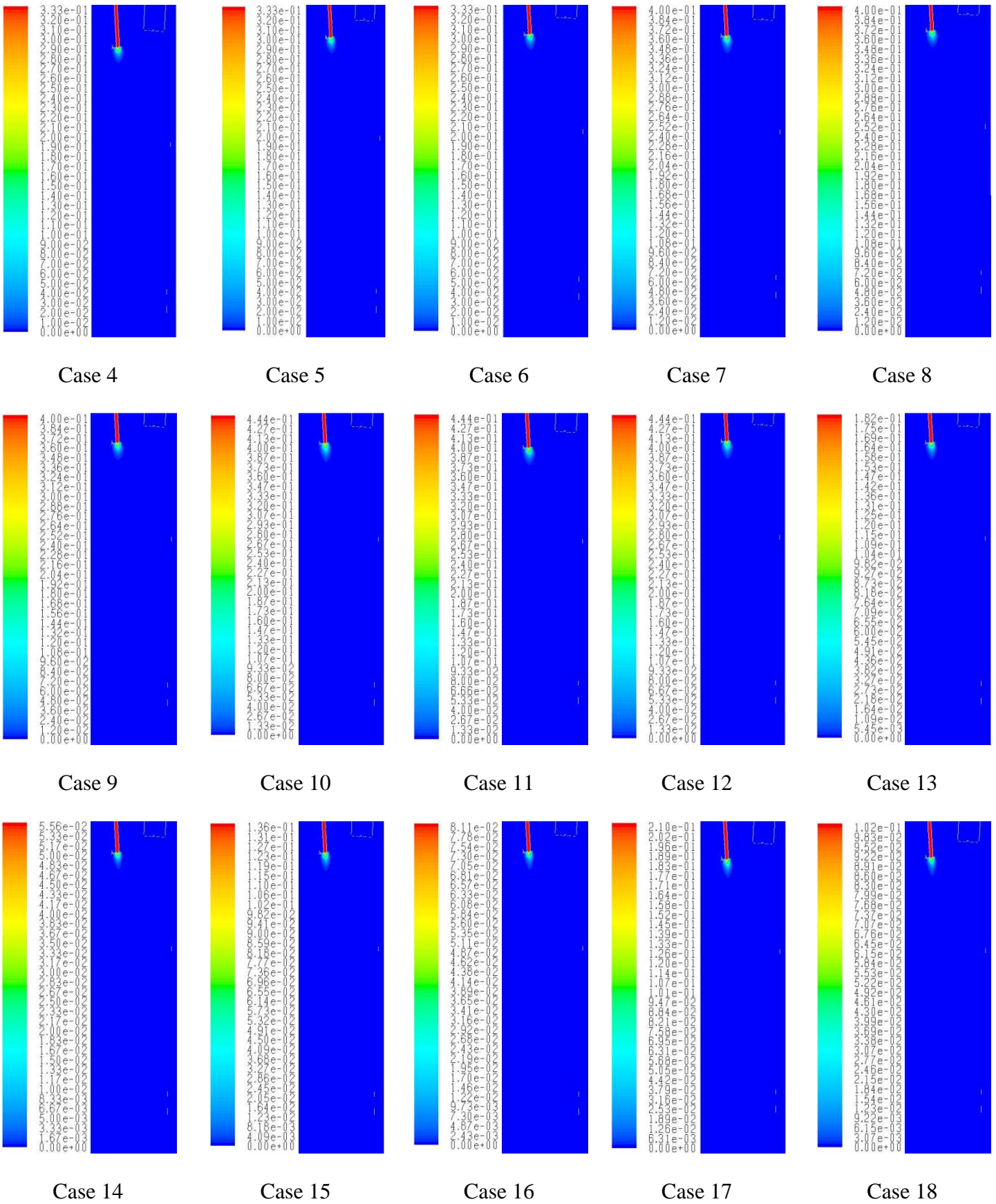


Figure 6.16: Contour plots of fluorine mole fraction for cases 4 to 18

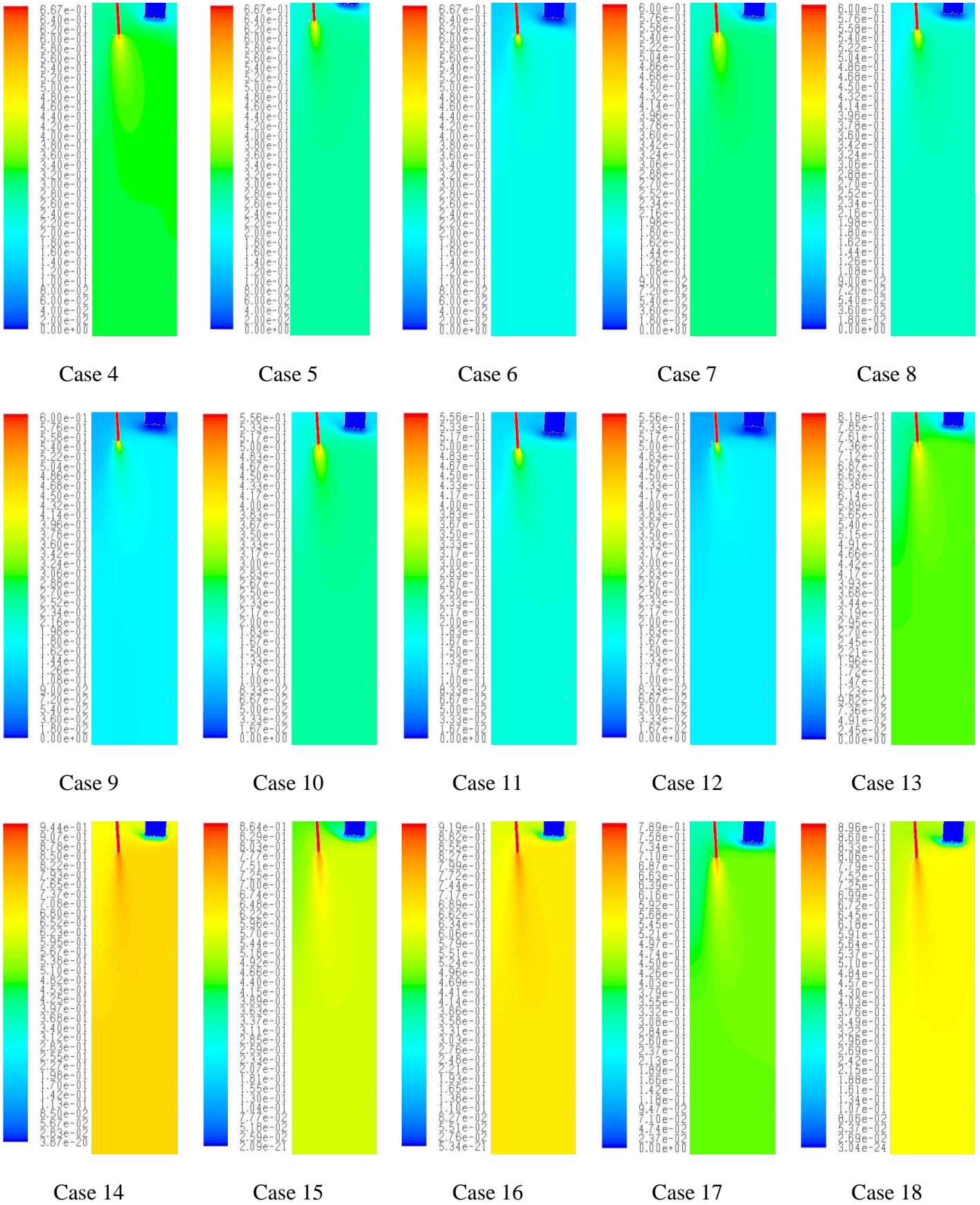


Figure 6.18: Contour plots of nitrogen mole fraction for cases 4 to 18

with the hydrogen in the reactor. Though the length of the un-reacted fluorine plume is a little longer when there is increase in the fluorine flow rate, it is almost unchanged with rise in the hydrogen excess. Figure 6.17 shows the contour plots for HF mole fraction in the reactor. The HF concentration near the fluorine nozzle drops immediately with increase in either hydrogen or nitrogen. Figure 6.18 shows the nitrogen concentration contours in the reactor. As expected, for the cases 13, 14, 15, 16, 17 and 18, the F_2+N_2 stream exiting from the fluorine nozzle travels longer with increasing nitrogen fraction. This is because of the extra momentum imparted to this stream due to the addition of nitrogen. Higher nitrogen flow rate thus results in the dilution of the reactants and their mixing length.

6.2.4 Summary of the results of influence of excess H_2 and N_2 in the H_2-F_2 flame reactor

The effect of excess of hydrogen and nitrogen flow rate on the H_2-F_2 reactor temperature has been studied experimentally. It has also been computationally simulated. The quantity of hydrogen has direct and immediate effect on the reactor temperatures, particularly nearer to the high temperature reaction zone. With increasing flow of hydrogen, the temperature near the nozzles drops while the reactor temperature away from the nozzles increases. The difference between them reduces leading to the uniformity of the temperature distribution, which is a desirable factor in many applications. The effect of excess hydrogen is limited to ~120 mm length of the reactor.

The effect of the nitrogen flow rate on the reactor temperatures has also been investigated extensively. The increase in the nitrogen content premixed with the fluorine stream delays the reactant access and hence the reaction zone expands outwards. The drop in the temperatures near the nozzle area is substantial with increasing nitrogen flow rate. The computational results also show similar behaviour. The good match between the experimental

results and the numerical predictions validate the computational model. This tool can be used to assist in the design of a scaled up H₂-F₂ reactor. The simulations shall be carried out with higher reactant flow rates to study the equipment safety aspects at higher reactor temperatures.

6.3 EFFECT OF PREHEATING OF THE REACTANT GASES AND THE REACTOR WALL ON THE REACTOR TEMPERATURE DISTRIBUTION

6.3.1 Introduction

The present investigation was planned to study how a change in the temperature boundary condition affects the flame reactor temperature profile. Many researchers have demonstrated the importance of preheating on the performance of a variety of combustors. Zhao et al. (2008) carried out investigations on the effect of air preheating on the combustion characteristics of corn straw and found that the average burning rate and the propagation velocity of the ignition front increased with the increasing preheating temperature of the air. The effect of preheating on the combustion temperature, the degree of conversion, and the product composition of a self-propagating, high-temperature synthesis (SHS) of tantalum nitride (TaN) was studied by Yeh et al. (2004). Their experimental results showed that preheating the sample prior to the ignition contributed to higher combustion temperatures, thus leading to an increase in the conversion percentage. With preheating temperatures between 423 and 573 K, the conversion increased by about 15% when compared with that without preheating. During experiments in a medical incinerator, Jangsawang et al. (2005) observed that the preheating of the primary chamber from 773 to 1073 K accelerated the rate of the volatile gas release causing a negative effect on the overall performance of the combustor. Mishra and Kumar (2008) observed that the length of the LPG-H₂ diffusion flame

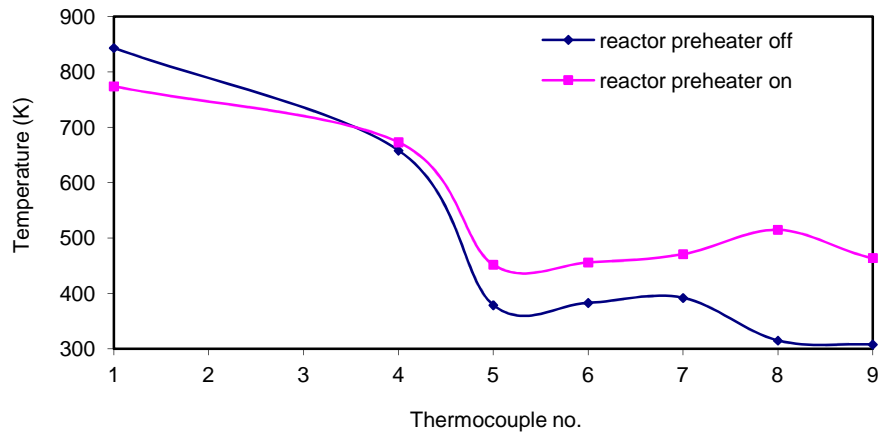
reduced due to the enhanced flame temperature caused by an increase in the temperature of the reactants. Stadler et al. (2009) carried out a few investigations by varying the wall temperature and the burner excess air ratio and noticed their appreciable impact on the char gasification reactions. The performance of several combustors were compared under the conditions of different preheating temperature of the fuel gas by Zhou et al. (2010). They suggest that proper preheating can increase the reaction temperatures inhibiting the thermal extinction.

Three base flow rates of fluorine namely, 0.2, 0.3 and 0.4 slpm, which were selected in the earlier study on influence of excess hydrogen and additional nitrogen (section 6.2), were chosen again to perform investigations on the change in the reactor temperatures when, (a) reactor wall temperature varies from ambient temperature (298 K) to 423 K and, (b) the feeding line temperature changes from ambient temperature (298 K) to 423 K. The experimental set up and the operation methodologies were similar to the ones discussed in the previous sections (sections 6.1 and 6.2). A few cases from the above set of trials were picked up for computational simulation to check the robustness of fine-tuned CFD model and the simulation tool. The experimental observations and the numerical simulations are discussed below.

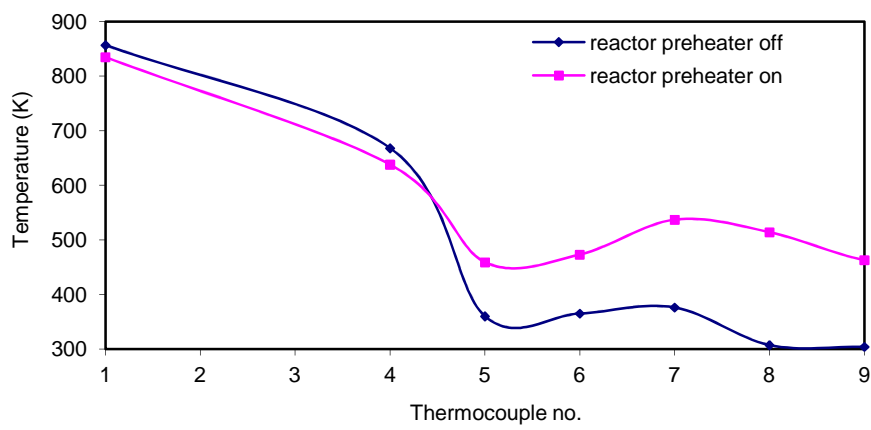
6.3.2 Experimental observations

The experimental trials for a total 9 cases (cases 31 to 39) were carried out as a part of the study on the effect of preheating. The reactor temperature profile when the reactor preheater was switched off is shown in Figures 6.19 (a) to (c). It is also compared with the data when the reactor wall was kept hot at 423 K. As seen in these figures, there is little effect of the wall temperature on the reactor temperatures in the reaction zone (reflected by temperature values of T1 and T4). However, the magnitude of change in the values of the

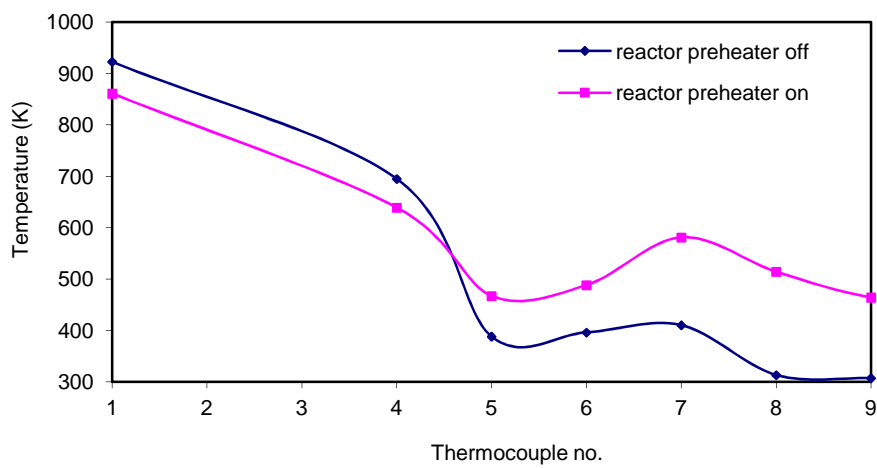
reactor temperatures in the downward direction is significant. The adiabatic temperature of a flame does not depend on the wall temperature of a reactor where it is produced. The increase in the wall temperature causes a decrease in the net temperature difference (the driving force for heat transfer) between the flame and the wall and hence a decrease in the quantum of heat transfer in the radial direction. Therefore, more heat is carried forward by the bulk gas in the direction of its motion and the thermocouples installed further downstream register higher temperatures. Figures 6.20 (a) to (c) show the reactor temperature profile demonstrating the influence of the preheating of the reactant gases. There is a marginal effect of the preheating of the feed gases on the reactor temperatures. The reaction between hydrogen and fluorine being exothermic, an increase in the temperature should drive the reaction in the backward direction. But, the reaction equilibrium constant being very high, there is almost no effect of the temperature on the equilibrium conversion and, therefore, the amount of energy liberated in the cases with and without preheating should be equal. The sensible enthalpy added to the system by preheating is merely 0.2% of the heat energy liberated from the reaction. The quantity of heat energy given to the gases is small compared to the dissociation energy of fluorine (158 kJ/gmol, <http://www.transtutors.com>) and hydrogen molecules, (436 kJ/gmol, http://en.wikipedia.org/wiki/Bond-dissociation_energy) and hence its effect on the reaction thermodynamics is negligible. This effect nevertheless may be noticeable if gases are heated to very high temperatures. The adiabatic temperature of the flame, however, will be higher when the initial temperature of the gases is more. At higher temperature, there is an increase in the volumetric flow rate of gases for the same mass flow. Consequently, the feeding velocities increase resulting in a longer flame.



(a)

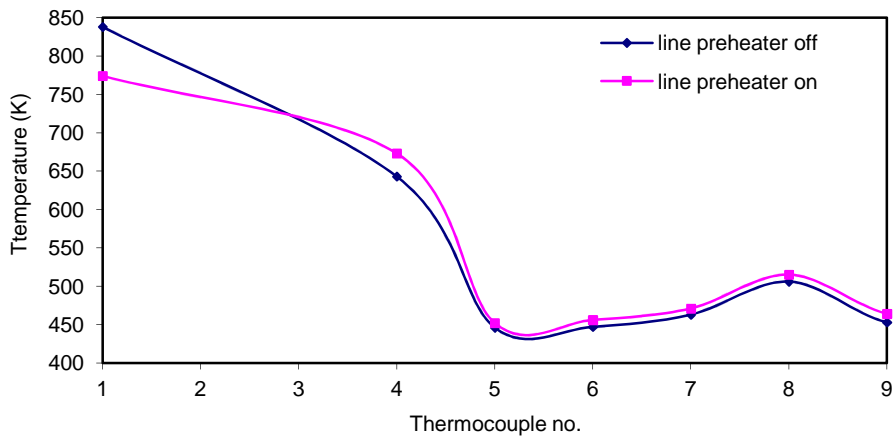


(b)

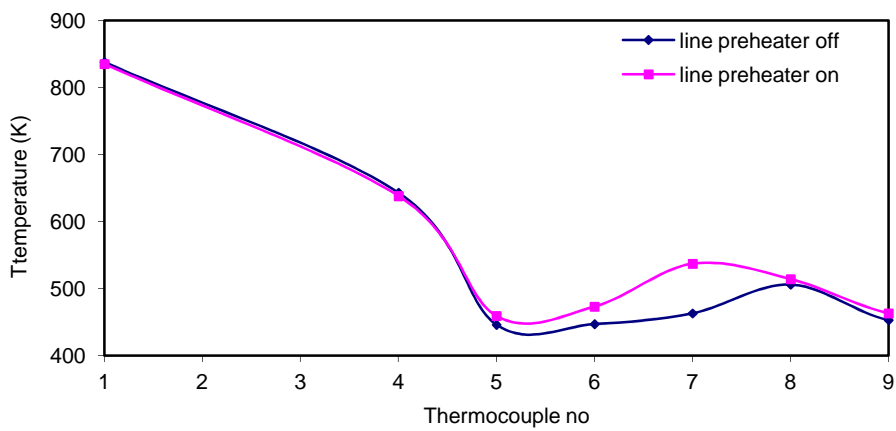


(c)

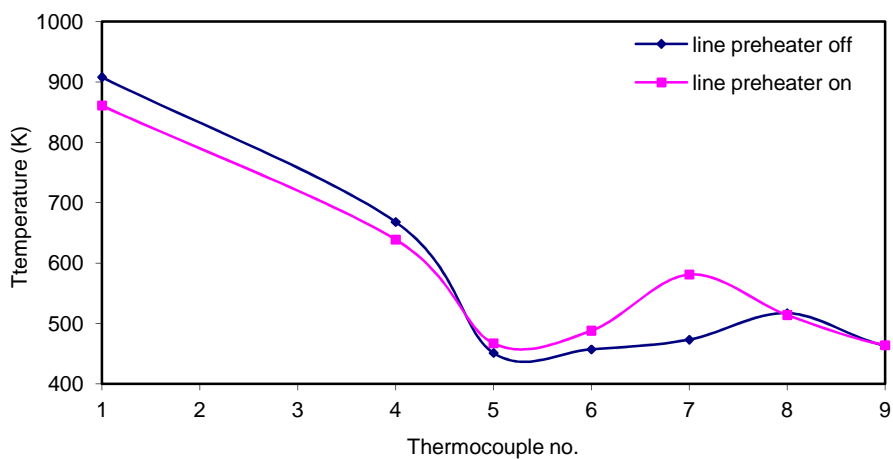
Figure 6.19: The reactor temperature profile for (a) case 31 (0.2 slpm F_2), (b) case 32 (0.3 slpm F_2), and (c) case 33 (0.4 slpm F_2)



(a)

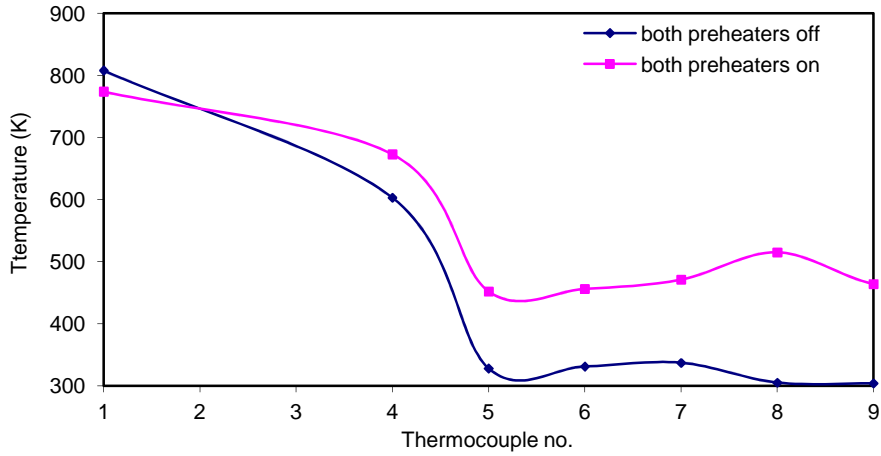


(b)

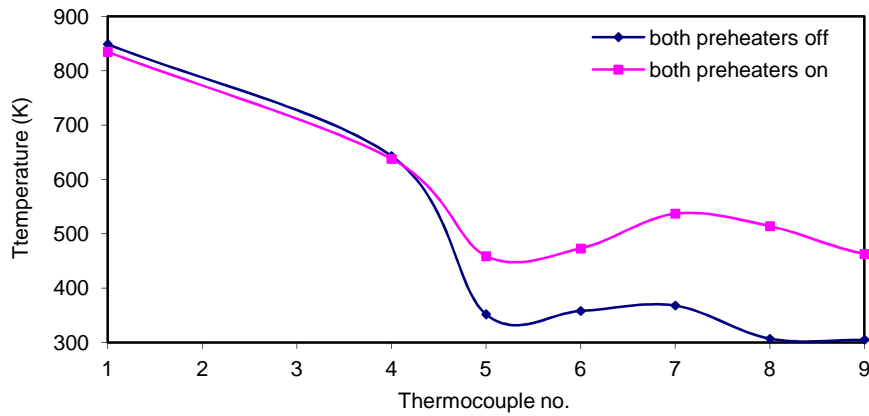


(c)

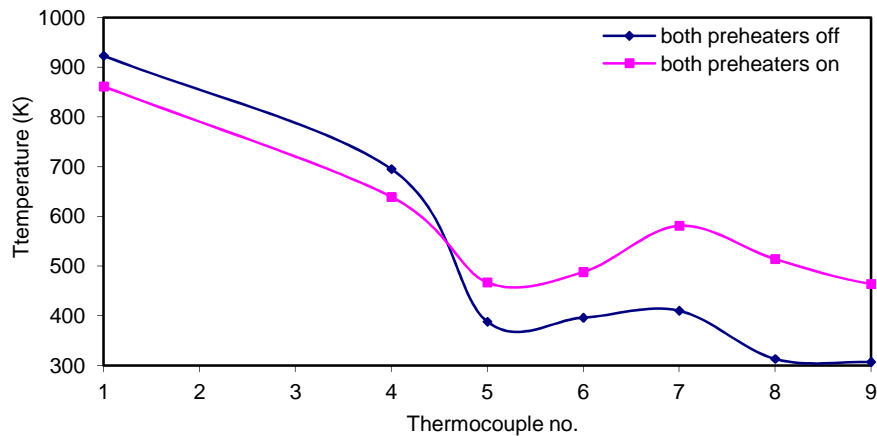
Figure 6.20: The reactor temperature profile for (a) case 34 (0.2 slpm F_2), (b) case 35 (0.3 slpm F_2), and (c) case 36 (0.4 slpm F_2)



(a)



(b)



(c)

Figure 6.21: The reactor temperature profile for (a) case 37 (0.2 slpm F_2), (b) case 38 (0.3 slpm F_2), and (c) case 39 (0.4 slpm F_2)

The change in the reactor temperatures when both the reactor as well as the line preheaters was not in use is shown in Figures 6.21 (a) to (c). The resultant temperature profile is visibly a superposition of the two individual effects. The variation in the temperatures away from the flame forming region is much more than in the ones which are located closer to the feeding nozzle outlets. The maximum difference in the values showed by K type thermocouples (located at the axial distance more than 120 mm from the fluorine nozzle) is to the extent of 200 K in comparison to ~60 K near the nozzle. As a consequence of preheating, there is a reduction in the temperature gradient in the axial direction, which may be useful in many applications.

6.3.3 Discussions of experimental and simulation results

Cases 31, 32 and 33, where the reactor preheater was not operated, were simulated to see whether it has any impact on the reactor temperatures. The temperature contours for these cases are presented in Figure 6.22. While comparing with the cases 5, 8 and 11 in Figure 6.12 (where the preheater was switched on), it is found that the flame temperature is more in the cases 31, 32 and 33, although the theoretical adiabatic flame temperature is the same (because, the gaseous flow rates and their temperatures are similar). The difference in the maximum temperature inside the reactor is nearly 380 K. One of the plausible reasons for the occurrence of this phenomenon could be the poor heat transfer coefficient due to the reduced intensity of the convection currents near the solid wall maintained at a lower temperature. Relatively flatter temperature profile obtained in the case where the wall is preheated, further confirms the assumption that, the heat transfer characteristics are different in both the situations. Comparing the two figures mentioned above, it is also observed that the flame structure remains more or less the same. It implies that there is no significant change in the fluid dynamic behaviour with change in the wall boundary conditions. But, this can be

important when the difference in the wall temperatures is huge; so much so that it affects the velocity pattern inside the reactor. The comparison between the predicted and the observed temperatures is made and shown in Figure 6.23. Though there is disparity in the temperature values near the nozzle (T1), the trend of change in the thermal behaviour of the reactor as a whole is correctly captured. When compared with the temperature values in the cases 5 and 8

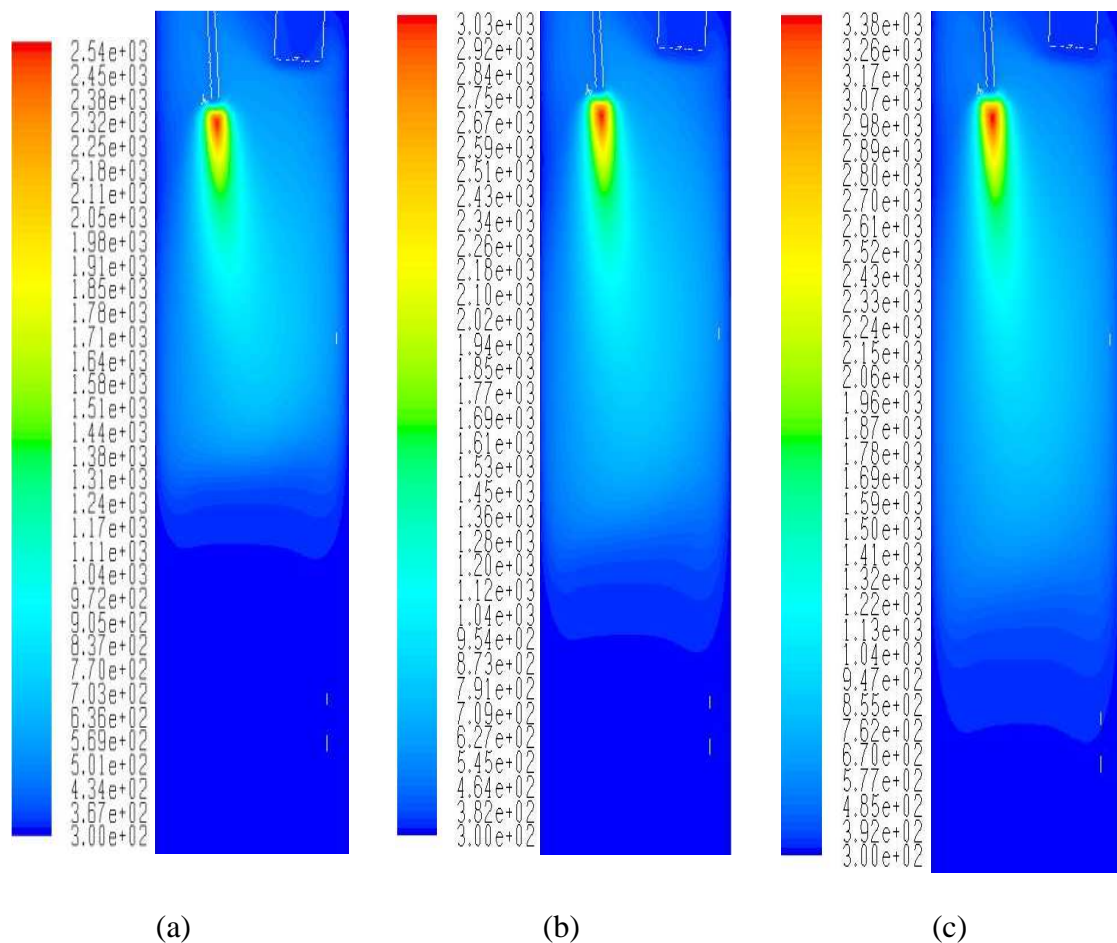
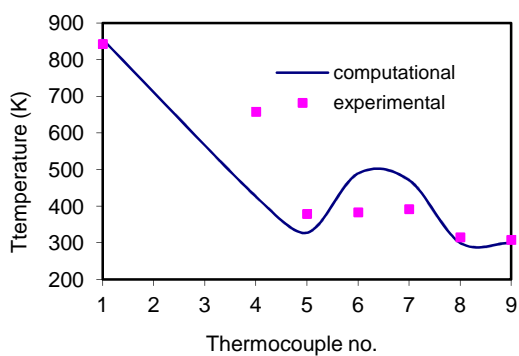
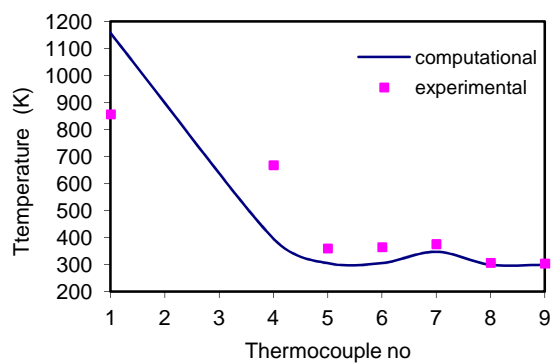


Figure 6.22: Temperature contours when reactor preheater is switched off for (a) case 31 (0.2 slpm F_2), (b) case 32 (0.3 slpm F_2), and (c) case 33 (0.4 slpm F_2)

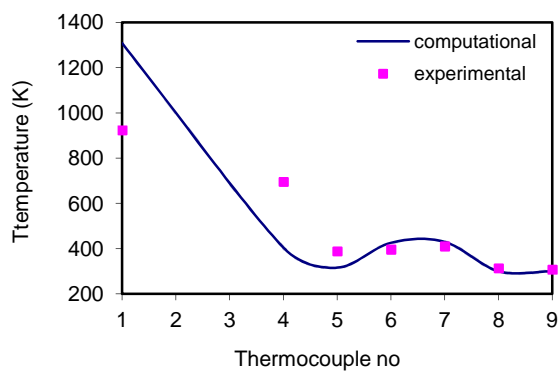
in the figure 6.13 (a) and case 11 in the figure 6.13 (b) (where the reactor preheater is kept on), there is an increase in the temperature registered by T1 when the wall is not preheated. Even the temperature gradients predicted in the present investigation are found to be much



(a)



(b)



(c)

Figure 6.23: Comparison between the experimental and the predicted temperature values when the reactor preheater is switched off for (a) case 31 (0.2 slpm F_2), (b) case 32 (0.3 slpm F_2), and (c) case 33 (0.4 slpm F_2)

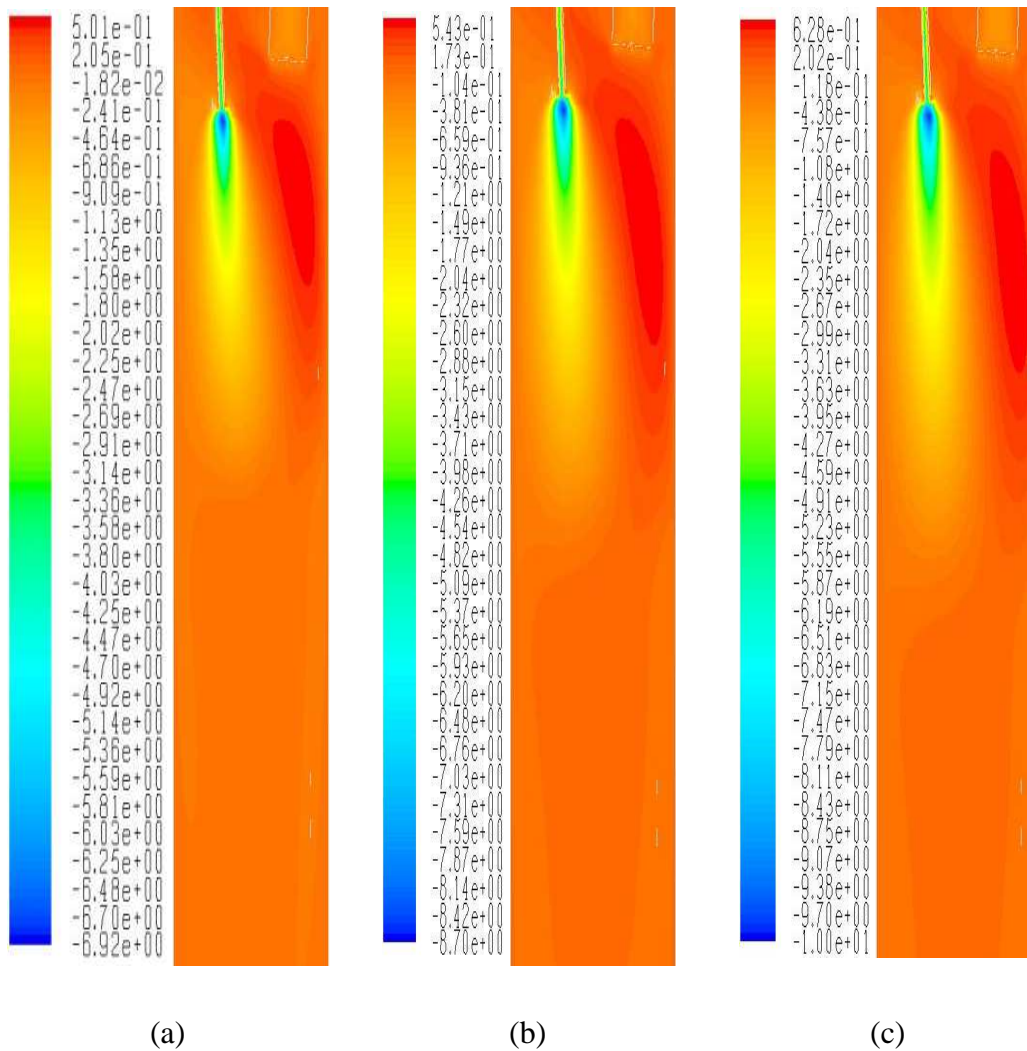


Figure 6.24: Velocity contours when reactor preheater is switched off for (a) case 31 (0.2 slpm F_2), (b) case 32 (0.3 slpm F_2), and (c) case 33 (0.4 slpm F_2)

more than the cases which were studied with the hot reactor wall. The velocity and the concentration contours were extracted from the simulation results and are presented in Figures 6.24 to 6.28. Since the difference in the wall temperature is only 125 K, there is no significant change in the pattern of these contours when they are compared to the figures 6.14 to 6.18, wherein, similar results are displayed for those cases which have higher wall temperature.

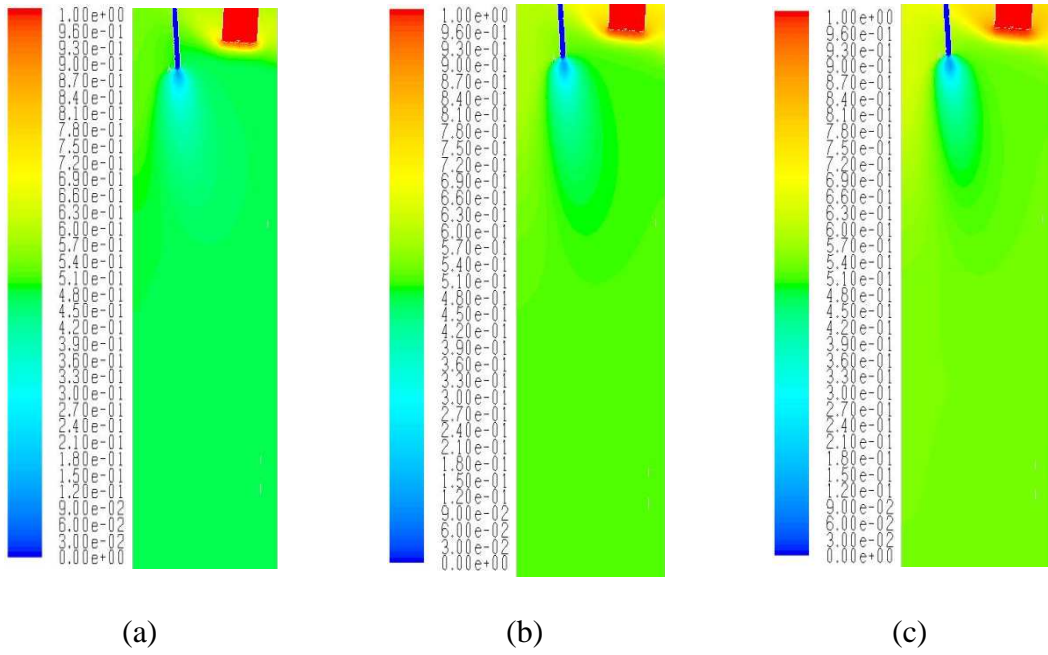


Figure 6.25: Contours of hydrogen mole fraction when reactor preheater is switched off for (a) case 31(0.2 slpm F_2), (b) case 32 (0.3 slpm F_2), and (c) case 33 (0.4 slpm F_2)

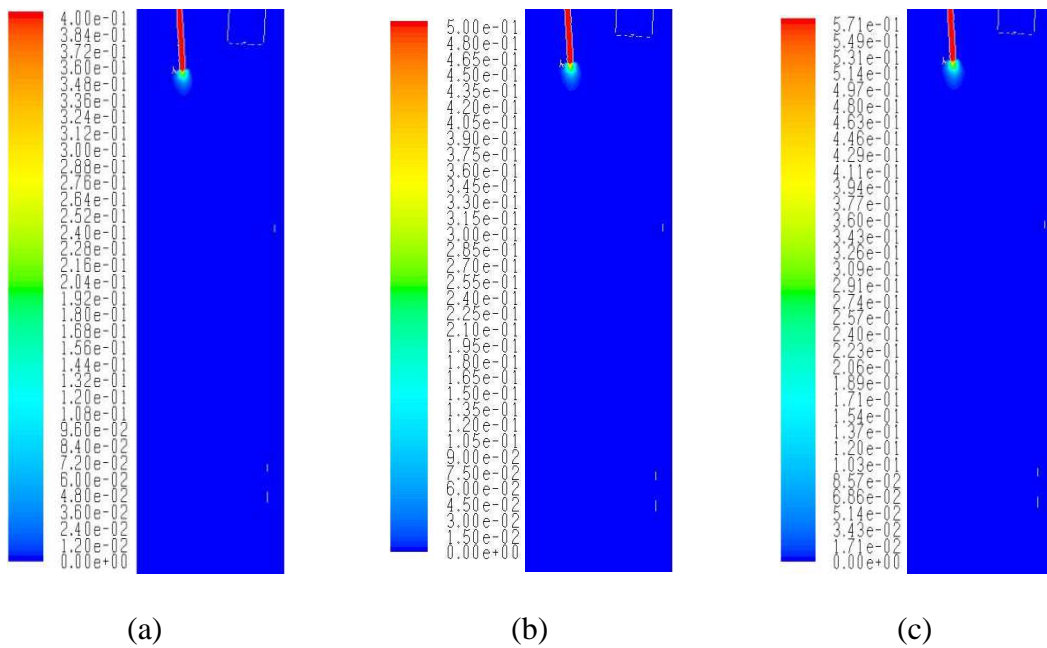


Figure 6.26: Contours of fluorine mole fraction when reactor preheater is switched off for (a) case 31(0.2 slpm F_2), (b) case 32 (0.3 slpm F_2), and (c) case 33 (0.4 slpm F_2)

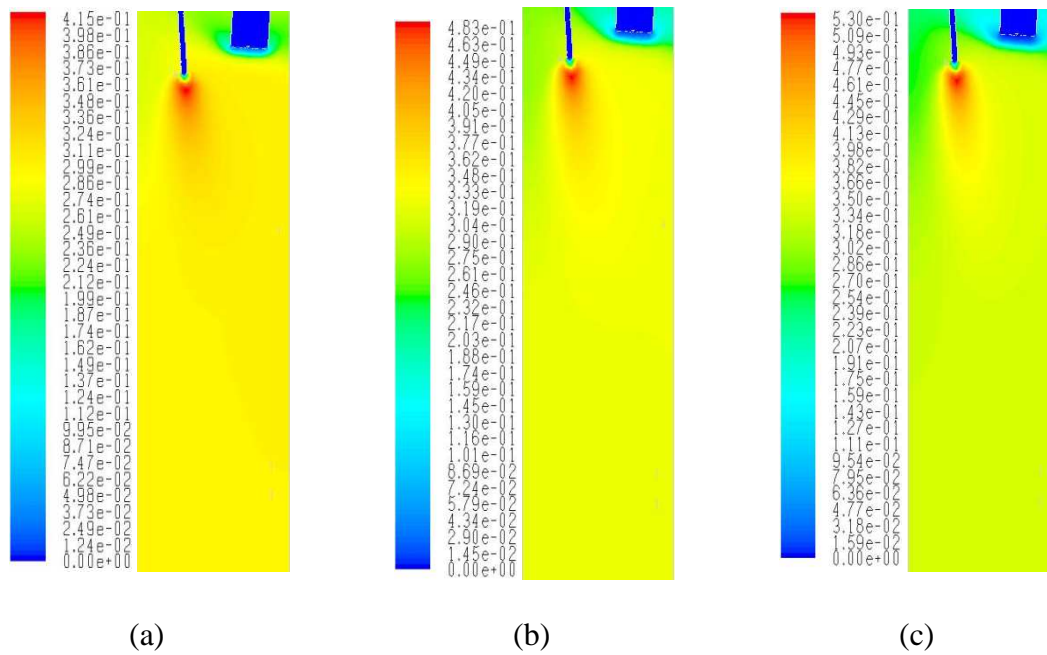


Figure 6.27: Contours of hydrogen fluoride mole fraction when reactor preheater is switched off for (a) case 31(0.2 slpm F_2), (b) case 32 (0.3 slpm F_2), and (c) case 33 (0.4 slpm F_2)

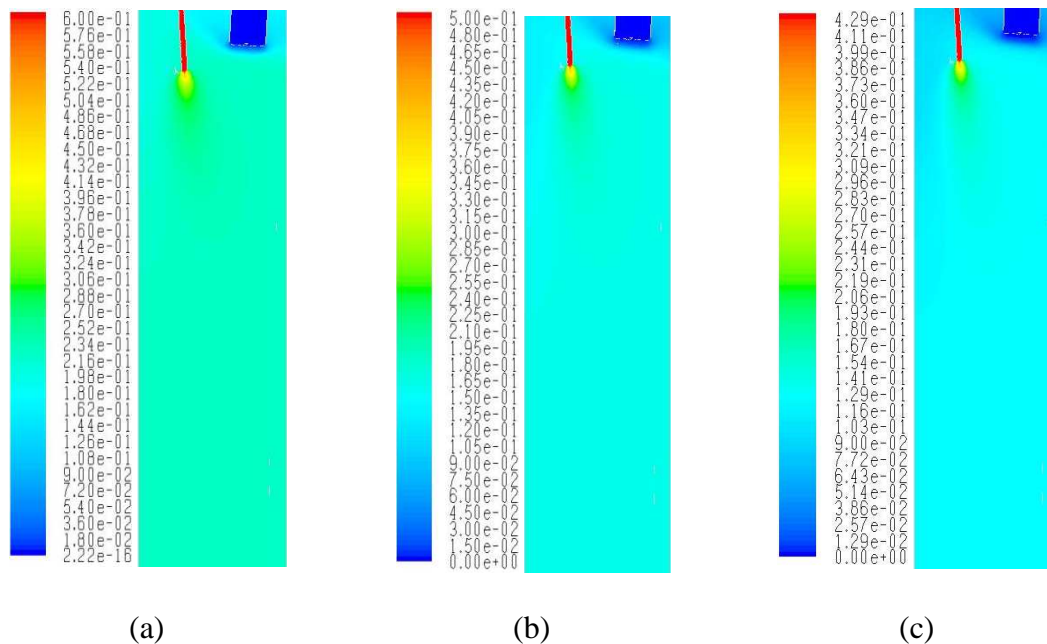


Figure 6.28: Contours of nitrogen mole fraction when reactor preheater is switched off for (a) case 31(0.2 slpm F_2), (b) case 32 (0.3 slpm F_2), and (c) case 33 (0.4 slpm F_2)

6.3.4 Summary of the results of the effect of preheating

Both the experimental and the computational studies on the behavioural change in a flame reactor have been carried out by varying initial temperatures of the feed gases and the reactor wall. Raising the temperature of the reacting gases by 125 K has almost no influence on the reactor temperatures as the heat given to the gases is small as compared to the reaction enthalpy. On the contrary, there is a noticeable effect in the distribution of the reactor temperatures when the wall temperature is varied. With a rise in the wall temperature, there is an appreciable change in the flame as well as the reactor temperatures. Higher wall temperature results in a relatively uniform reactor temperature profile. The change in the thermal behaviour when both the line and the reactor preheaters are either switched on or switched off is simply superposition of the two individual effects. The numerical simulations conducted for these studies predicted similar trend and there was good match with the experimental data. It would be meaningful to simulate a few more cases to see the change in the system behaviour when the wall and the feed gases are preheated to further higher temperatures. Nonetheless, the present data backed up by the validated simulation tool is helpful in optimizing the efficient utilization of chemical energy in a flame reactor.

6.4 BEHAVIOUR OF H₂-F₂ FLAME REACTOR AT HIGHER FLUORINE FLOW RATES

6.4.1 Introduction

Since a flame reactor is a cold wall type reactor, the only method by which the heat input can be increased is through increasing the reactant flow rates. A change in the flow rates will bring about a change in mutual mixing and therefore a change in the distribution pattern of the temperature, the velocity and the species distribution. Since the same nozzle

configuration is retained (refer the VCR in Chapter-4), an increase in the individual gas flow rate results in increase in the issuing velocity. As long as the flow ratio between the fuel and the oxidizer streams is maintained, the adiabatic flame temperature does not change because it is a function of their equivalence ratio. However, Feng et al. (2010), through their simulation results showed that the inlet velocity has a significant influence on the reaction zone. The reaction zone expands as the flame front shifts downstream with increase in velocity. In the present examination, the fluorine flow rate is increased from 0.4 to 0.8 slpm while maintaining a fixed molar ratio between hydrogen and fluorine. Before conducting the experiments, the computational simulations have been performed with the envisaged higher flow rates to ensure safety. The experimental set up comprising of the VCR as described in the Chapter-4 is used to conduct these experimental runs. Based on the experimental data, energy balance has been carried out for each case to quantify the heat loss to the surroundings. Reflection of increase in the amount of reactants on the reactor temperature and its distribution pattern has been evaluated, presented and discussed.

6.4.2 Discussion of simulation results

The cases 40, 41 and 42 dealing with the increasing fluorine flow rates were simulated basically to see the influence of higher flow rates on the flame structure and to ensure the equipment safety. The converged temperature contours as predicted by the computational simulations are presented in Figures 6.29 (a) to (c). As seen in these figures, the flame structure appears to be stable and the reactor temperatures adjoining the wall boundary are also seemingly low (near ambient temperature). The flame gets longer with the increase in the gas flow rate, albeit its diameter remains comparable. Although the calculated adiabatic flame temperature in all the three cases is identical, there is an increase in the simulated flame temperature as the fluorine flow rate is increased. While the flame temperature is affected by

the fluid dynamic conditions prevailing in the reactor, the increase in the flame length in the longitudinal direction is due to the momentum gained by the reacting fluids because of increased volumetric flow rates. Having established the safety through the CFD simulations, the experiments were carried out to study other factors as discussed below.

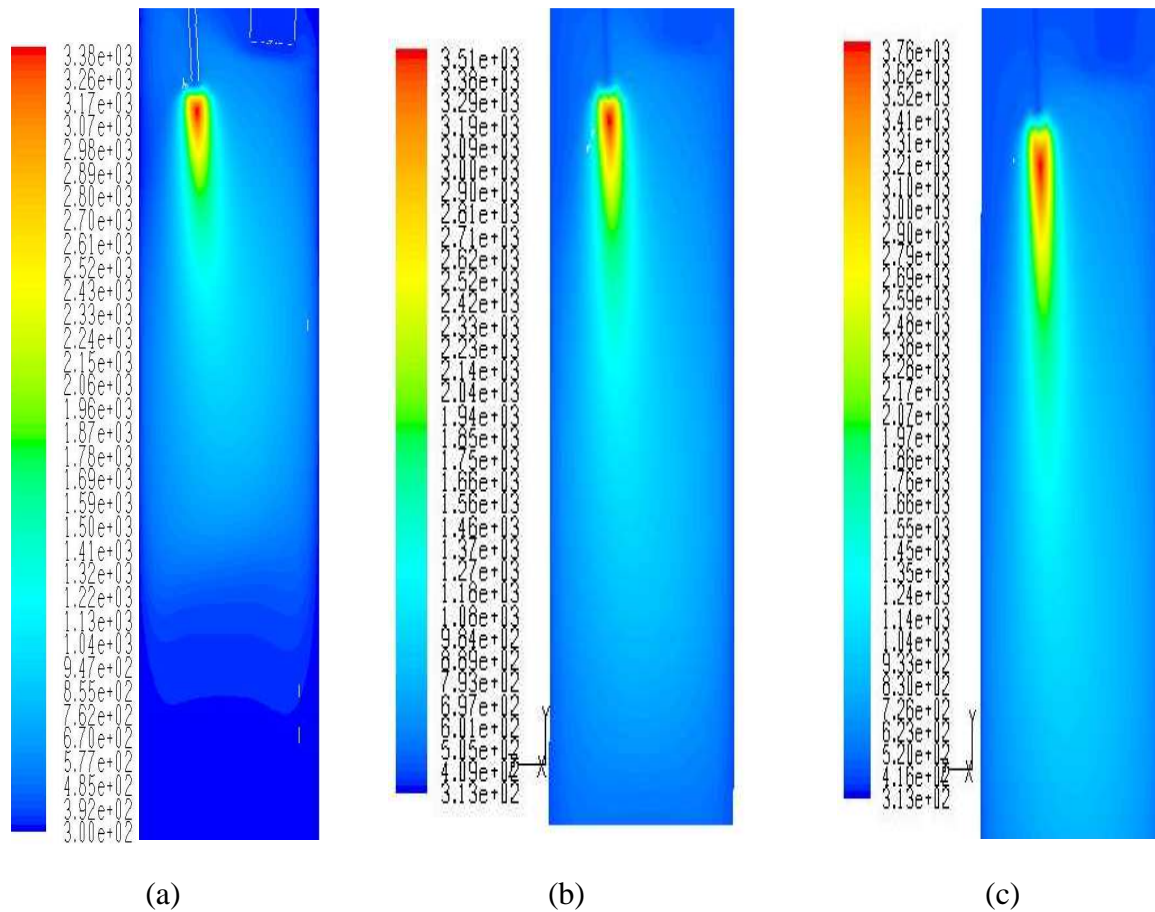
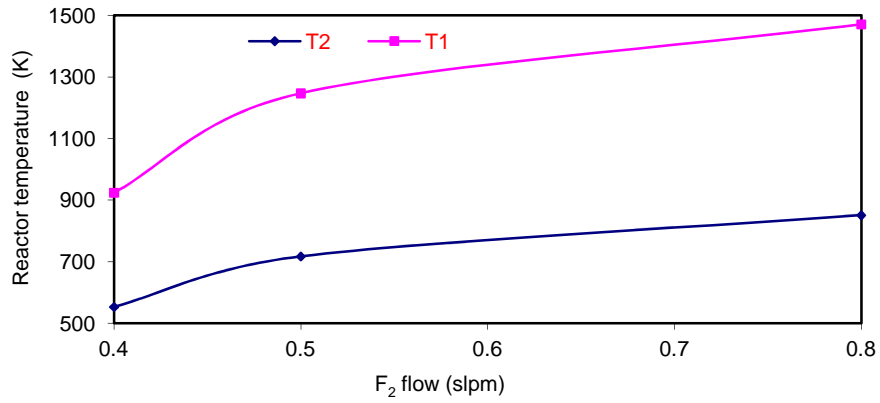


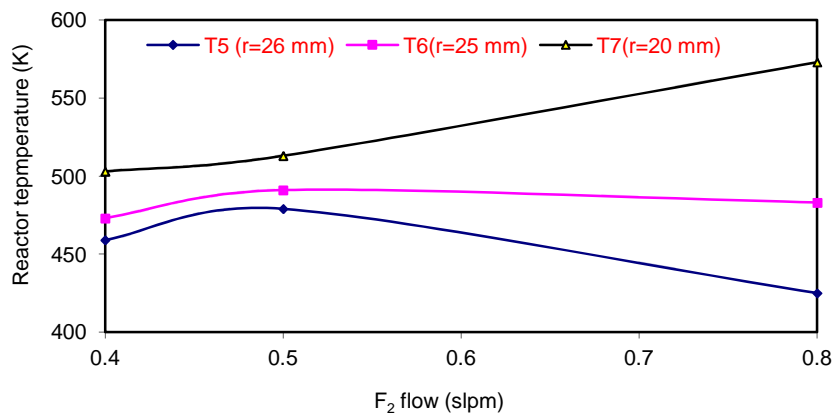
Figure 6.29: Contours of reactor temperature with higher fluorine flow rates for (a) case 40 (0.4 slpm F₂), (b) case 41 (0.5 slpm F₂) and, (c) case 42 (0.8 slpm F₂)

6.4.3 Experimental observations

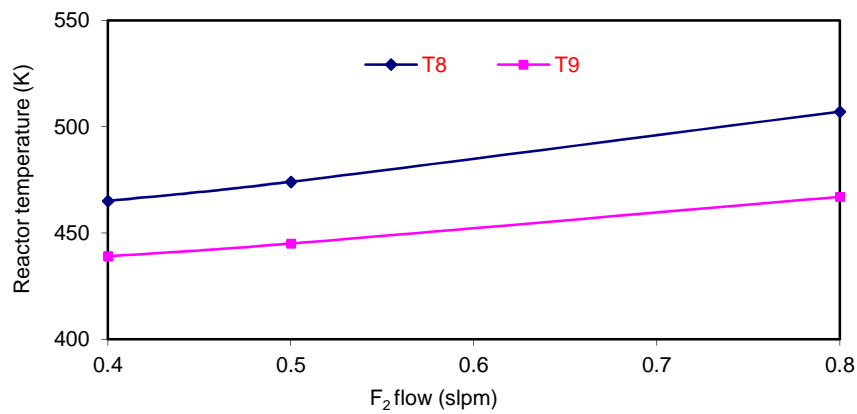
The effect of increasing fluorine flow rates reacting with hydrogen in a fixed molar ratio is displayed in Figure 6.30. During the experiments, it was observed that, there is an appreciable rise in the cooling fluid flow requirements to maintain a constant wall temperature, when the fluorine flow rate is increased from 0.4 to 0.8 slpm. While the use of



(a)



(b)



(c)

Figure 6.30: Change in the reactor temperatures with higher fluorine flow rates at (a) near the nozzle region, (b) 120 mm from the nozzle exit and (c) far nozzle region

air as the cooling medium in all the three reactor zones (Reactor zones are discussed in the Chapter-4, see Figure 4.1) was adequate up to a fluorine flow rate of 0.5 slpm, it had to be replaced by water in the 'Zone-1' when fluorine was fed @ 0.8 slpm into the reactor. In the other two zones however, the air was used as the cooling fluid. With respect to Figure 6.30 (a), though there is a continuous rise in the T1 and T2 (near nozzle thermocouples) values with increase in the fluorine quantity or heat input, the rate of the temperature increase with respect to fluorine flow declines gradually. The reason for occurrence of this phenomenon is explained through figures provided in Table 6.1. As the heat input to the reactor increases, there is a non-linear rise in the portion of energy carried away by the cooling fluid in order to maintain the reactor wall at the prescribed temperature. The higher flow rates cause enhancement in the heat transfer and hence the heat loss. In other words, with increasing heat content per unit of reactor volume, the energy utilization efficiency of reactor of this type (cold wall reactor) decreases drastically. The effect of the fluorine flow rate on the radial temperature profile at ~120 mm distance from the fluorine nozzle exit is shown in Figure 6.30 (b). It suggests that, while the bulk fluid temperature (T7) rises consistently, the variation in the reactor temperature along the radius, $\left(\frac{\partial T}{\partial r}\right)$, increases continuously with the quantity of the reacting species. Further down the reactor length, Figure 6.30 (c) shows a monotonous rise in the recorded reactor temperatures (though low) as the quantity of fluorine is increased. Since the radial and the angular positions of the thermocouples T8 and T9 are the same in the cylindrical reactor (VCR), the widening gap between T8 and T9 in this figure proposes that, it will take a longer distance to attain a fully developed thermal boundary layer when the content of heat introduced into the reactor is increased.

Table 6.1

Energy balance with increasing fluorine flow rate

Case no	Fluorine flow rate (slpm)	Energy utilization efficiency (fraction of heat absorbed by product gases as sensible heat), (%)
40	0.4	92.8
41	0.5	92.3
42	0.8	54

(Note: The uncertainty in the measurement of the flow rate is $\pm 1\%$ of the reading)

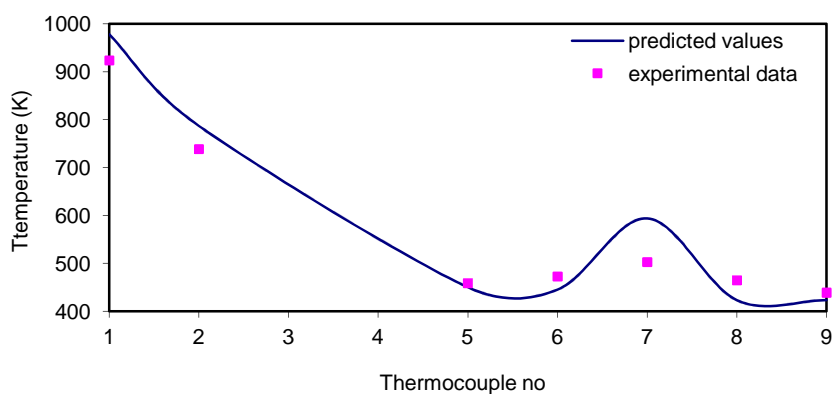


Figure 6.31 (a): Comparison between the recorded and the simulated reactor temperatures with higher fluorine flow rates for case 40 (0.4 slpm F_2)

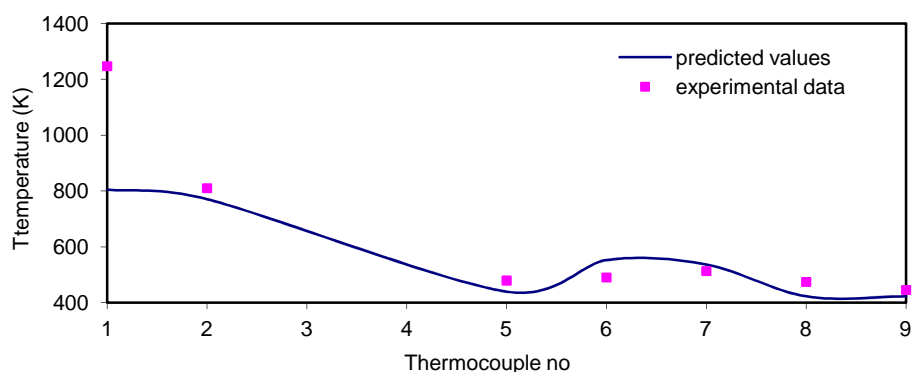
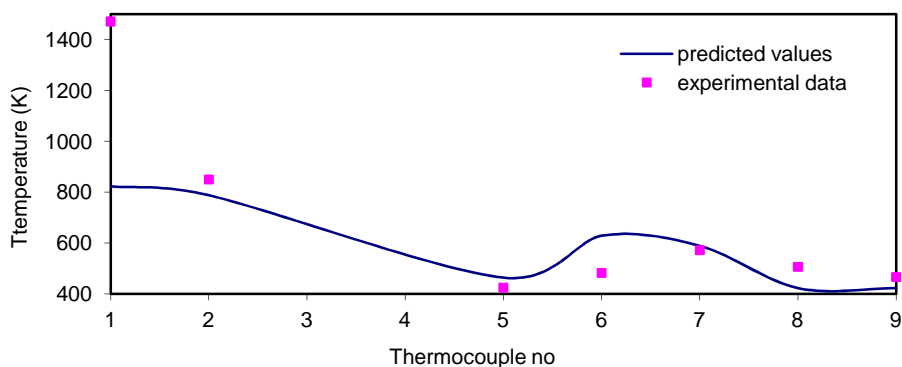


Figure 6.31 (b): Comparison between the recorded and the simulated reactor temperatures with higher fluorine flow rates for case 41 (0.5 slpm F_2)



(c)

Figure 6.31 (c): Comparison between the recorded and the simulated reactor temperatures with higher fluorine flow rates for case 42 (0.8 slpm F₂)

6.4.4 Comparison between the simulation and the experimental results

The predicted temperatures at various locations of the reactor are again compared with the recorded data and the results are plotted in Figures 6.31 (a) to (c). Satisfactory match between them reinforced the reliability of the CFD simulation tool to be used in future endeavours.

6.4.5 Summary of reactor behaviour at higher fluorine flow rates

Increase in the quantity of the reacting species results in rise in the reactor temperatures together with heat loss to the surroundings due to enhanced heat transfer at higher flow rates. The resultant flame is longer due to added momentum. Also, it takes a longer distance to achieve thermally uniform condition because of higher average fluid velocity. Proportional increase in the quantity of the reactants should not be adopted for acquiring higher reactor temperatures, as it leads to more heat losses and a sharper temperature gradient along the radius. Higher power density (reaction enthalpy per unit reactor volume) in the reactor leads to a drop in the energy utilization efficiency and may not be desirable in those cases where a flatter temperature profile is the requirement. Further, as a

consequence of higher velocity, the residence time of the fluids in the reactor decreases, which may affect the product quality in those flame reactors where nucleation, growth and agglomeration of a solid product take place.

6.5 STUDY OF EFFECTS OF TYPE AND QUANTITY OF DILUENTS ON H₂-F₂ REACTION IN A BATCH REACTOR

6.5.1 Introduction

This section addresses the change in the H₂-F₂ flame reactor behaviour when different types of diluents are premixed with hydrogen in varying proportions. In every experiment, the hydrogen used is nearly 100% above its stoichiometric requirement for fluorine, thus making the mixture rich in fuel. Further details on the type and the quantity of gases are given in Table 3.6 and Table 3.7 of Chapter-3. In many applications (pertaining to the flame reactors) dealing with the mixtures rich or lean with fuel, the reaction temperatures are not very high and hence the chances of molecular dissociations are less. Under such conditions, even though the ratio of the reactants may remain the same, the initial pressure prevailing in the reactor can turn out to be a significant factor dictating the reactor behaviour. Therefore, besides the type of diluent, the effect of pressure is also studied at two levels, namely, 800 and 100 mbar. 800 and 100 denote the chamber pressure containing pure hydrogen before a diluent is added. Although the experiments were carried out at two pressure levels, the ratio of hydrogen to fluorine was the same in all the conditions. The thermal response of the reactor at the two pressure levels is found to be different. They are further discussed in the following sections.

6.5.2 Experimental observations and discussions

The controlled reaction between fluorine and hydrogen premixed with the diluents was carried out in a batch mode. The HCR, whose details are explained in Chapter 4, was employed as the experimental system for this part of the investigations. The diluents chosen for the study in increasing order of molecular weight are helium, nitrogen and argon, which are easily available commercially. The reactor behaviour in terms of the temperature and the pressure change during the H₂-F₂ reaction is assessed in the presence of various types of diluents. The thermal conductivity, the dynamic viscosity, mass and thermal diffusivities of the gases are calculated using Lennard-Jones parameters given in Table 6.2. The correlations used to calculate these properties are adapted from Rosner (1986). The specific heat of gases is taken from Perry's (7th edition, 1999) hand book. The maximum temperature and pressure recorded during the experiments were 1243 K and 3054 mbar respectively. Therefore, to calculate the thermophysical properties, the temperature range chosen is from 301 to 1273 K, and the pressure range between 100 and 3200 mbar. The specific heat, the thermal conductivity and the dynamic viscosity are assumed to be function of the temperature only, while the mass diffusivity changes both with the temperature and the pressure. The properties

Table 6.2

Lennard-Jones (L-J) Potential parameters for gases

Gas	L-J size parameter, σ_{L-J} in m	L-J energy parameter, $(\epsilon/k_b)_{L-J}$ in K
H ₂	$2.827 \cdot 10^{-10}$	59.7
He	$2.551 \cdot 10^{-10}$	10.22
N ₂	$3.798 \cdot 10^{-10}$	71.4
Ar	$3.54 \cdot 10^{-10}$	93.3
F ₂	$3.357 \cdot 10^{-10}$	112.6
HF	$3.148 \cdot 10^{-10}$	330

of the gases thus evaluated are tabulated in Table 6.3 for reference.

Table 6.3

Thermal and transport properties of gases

Gas	Thermal conductivity, k in w/m-K Temperature range: 301-1273 K	Dynamic viscosity μ in 10^{-6} Pa-s Temperature range: 301-1273 K	Specific Heat, C_p in J/kg-K, T in K	Mass diffusivity of the gas in hydrogen in m^2/s (multiply the value by 10^{-4}). Temperature range: 301-1273 K		Thermal diffusivity, m^2/s (multiply the value by 10^{-4}) Temperature range: 301-1273 K.
				100 mbar	3200 mbar	
H ₂	0.17-0.48	8.7-22.5	$13835.8+1.7*T$	12.8-70.8	0.4-4.41	1.46-15.68
He	0.157-0.406	20-51.9	5193.65	14.2-78	0.44-4.86	1.87-20.41
N ₂	0.0244-0.0698	17.5-45.4	$970.36+0.15*T$	6.8-37.2	0.21-2.32	0.21-2.24
Ar	0.0181-0.0468	23.1-59.8	519.365	7-38.8	0.22-2.43	0.21-2.35
F ₂	0.025-0.0713	24.3-62.9	$715+0.11*T$	7.4-41.2	0.235-2.58	0.22-2.29
HF	0.033-0.104	16.9-43.7	$1311.02+0.418*T$	7.4-41.6	0.24-2.6	0.28-2.95

Several sets of H₂-F₂ reaction were carried out in the horizontal cylindrical reactor.

The thermocouples responded to rise in the temperatures the moment fluorine was admitted into the batch reactor. The thermocouple T21 recorded maximum temperature in all the runs.

Therefore, the reactor temperature referred hereafter is the temperature as indicated by T21.

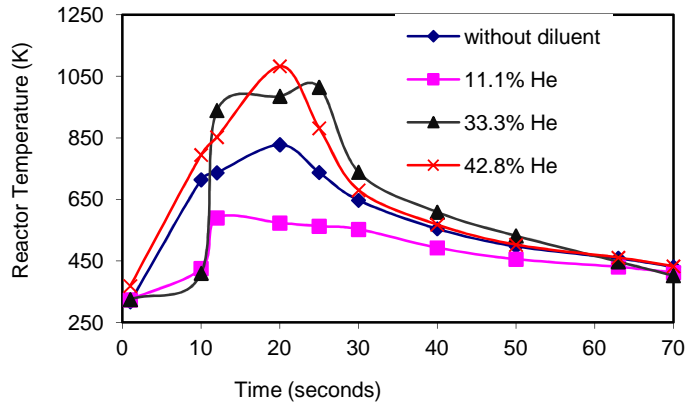
The various observations noticed during the experiments are as follows.

6.5.2.1 Reactor behaviour with diluents at higher initial pressure (800 mbar)

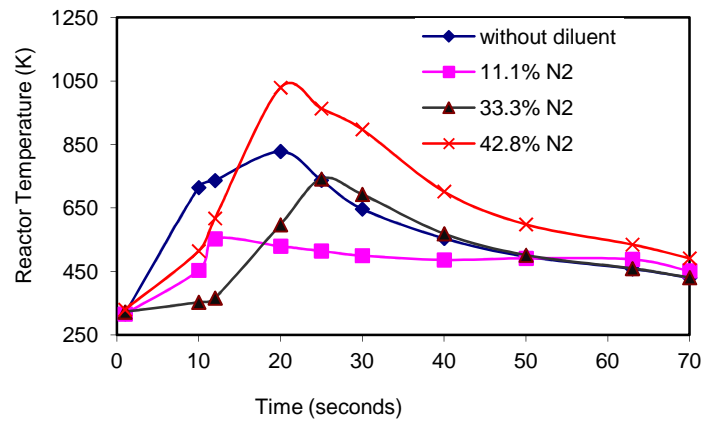
The ten cases, which were investigated for various compositions of the diluent gases, are given in Table 3.6 of Chapter-3. In all the trials, hydrogen was filled in the beginning up to 800 mbar and then the diluent was added. The composition of the diluents was varied with a fixed quantity of fluorine and hydrogen, so as to ensure that the equal amount of heat is released in every experiment. The base reaction is the one where no diluent was added. The composition of the diluents varied from 0 to ~43%. In each case, the pulsed jet of fluorine was injected into the reactor at a steady rate for about 250 ms time. The temperature and the pressure change observed during the experiments are discussed as below.

(a) Temperature change in the reactor with diluents

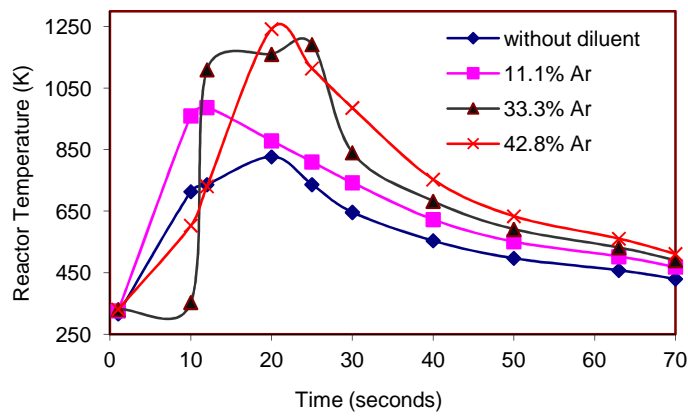
The temporal change in the reactor temperature is shown in Figures 6.32 (a) to (c). In all the cases, the time lapsed to reach the peak temperature value is between 12 and 30 seconds. The rate of rise in the temperature is steeper than its fall, which is also evident from the fact that, even after 70 seconds, the temperature reading is more than 430 K. The process of fall in temperature after reaching the maximum is slow because, a) the reactor is thermally insulated and b) the heat deposited on the thermowell is dissipated into an environment that has already attained a relatively higher temperature due to the energy release. Incidentally, the time taken to reach the peak temperature is the least (even less than the base case) at 11.11% concentration for all the three diluents. At higher concentrations, this time is slightly more than the time taken by the base reaction. If the peak temperature is directly related to the extent of reaction and the speed of reaching it is treated as an indication of the reaction rate then one can observe that the temperature value may decrease or increase depending on the nature of the inert, but the rate of reaction is augmented at lower diluent fractions. Enhanced collision in the presence of a third body can be a reason for this. When the diluent content is more, the mixture becomes lean with fluorine, the frequency of collision between



(a)



(b)



(c)

Figure 6.32: Temporal changes in the reactor temperature (T21)

the hydrogen and the fluorine molecules is reduced and hence the reaction rate is lower. But, the fact that the ultimate reactor temperature in a few cases is more than the base reaction, hints at possible participation of the diluent molecules in the chemical kinetics besides heat and momentum transfer. The recorded peak reactor temperature with diluent addition is shown in Figure 6.33.

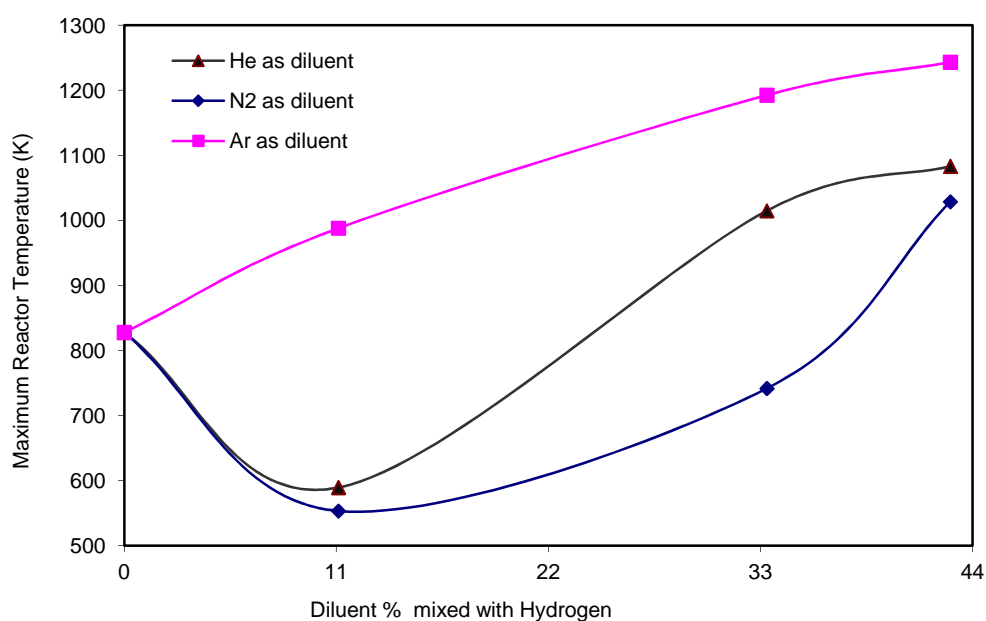
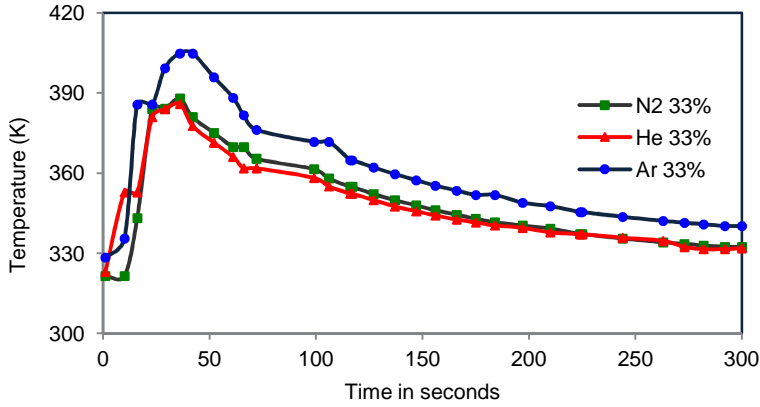
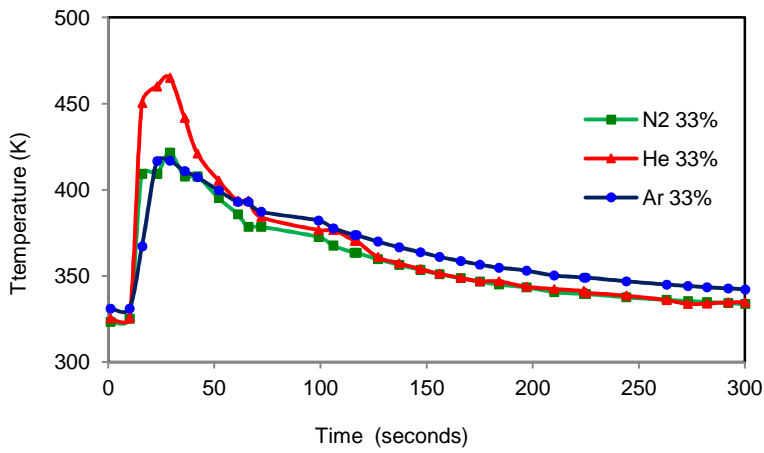


Figure 6.33: Maximum temperature recorded during H_2-F_2 reaction experiment in the HCR at higher pressure (Note: The uncertainty in the measured temperature is ± 2.2 K)

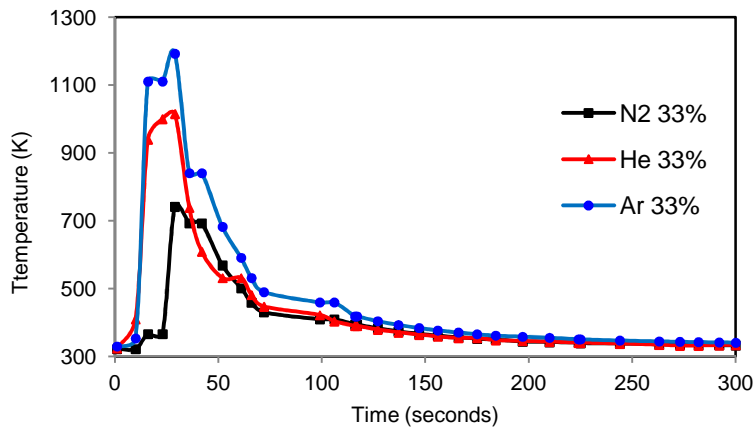
The experimental results obtained for the cases 45, 48 and 51 were selected for further investigations to see the effect of the type of diluent on mixing in the reactor. The dilution level in these cases was 33.33%. The behaviour shown by the three thermocouples, namely, T17, T20 and T21 are presented in Figures 6.34 (a) to (c). The pattern of variation in the temperature with time as recorded by the three thermocouples, did not alter with the type of diluent albeit, the values did change. The temperature readings of T17 and T20 are lower than that of T21 because of their distant location from the nozzle tip. The peak temperature of T20



(a)



(b)



(c)

Figure 6.34: Comparison of the responses of thermocouples (a) T17, (b) T20 and (c) T21

(Note: The uncertainty in the measured temperature is ± 2.2 K)

and T21, which are located in the upstream direction, were recorded after ~29 seconds while T17, which is behind the fluorine nozzle reached its maximum at ~36 seconds. It is thermal diffusion from the hot zone formed in front of the nozzle to the back side of the nozzle, which causes the delay. Since the time at which the peak temperature occurs does not differ with the type of diluent, one can conclude that the mixing is independent of the diluent. However, change in the species concentration, rate of chemical reaction and eventually temperature distribution in the region where flame is supposedly formed is strongly affected by them.

(b) Pressure change with diluents

There was a monotonous increase in the reactor pressure with inert composition. As seen in Figure 6.35, for a typical case involving helium, the pressure rise is recorded earlier than the corresponding temperature rise (Figure 6.32 (a)), because the response time of a pressure transmitter is faster than that of a thermocouple. For various concentration levels of helium, the time consumed to reach the maximum pressure is between 10 and 14 seconds against 12 to 30 seconds taken to register the peak temperature. The pressure starts decreasing slowly after reaching the ultimate value. Similar behaviour was noted with nitrogen and argon. The trend of the steeper rise and slower fall in the reactor pressure matches with the change in the reactor temperature with time. Though the stable pressure readings were comparable with the final reactor pressure calculated assuming an isothermal, non-reactive system; anomalous behaviour was observed in the recorded peak pressures which are shown in Figure 6.36. There is variation in the quantum of the pressure rise with respect to the type of diluent. It is the highest for argon followed by nitrogen and helium. The effects observed through pressure surge in the reactor do not exactly corroborate to the thermal behaviour. For example, at 11.11% dilution, the maximum temperatures recorded with helium, nitrogen and argon are 589.4, 553.3 and 988 K respectively, while the

corresponding peak pressures for them are 2508, 2600 and 2611 mbar. The rise in the pressure can take place not only because of evolution of heat in the given volume, but also by the extra species generated from collision between inert molecules and the reactants. Since there is no direct relation between the thermal change and the pressure escalation, the possibility of the chain avalanche is reinforced.

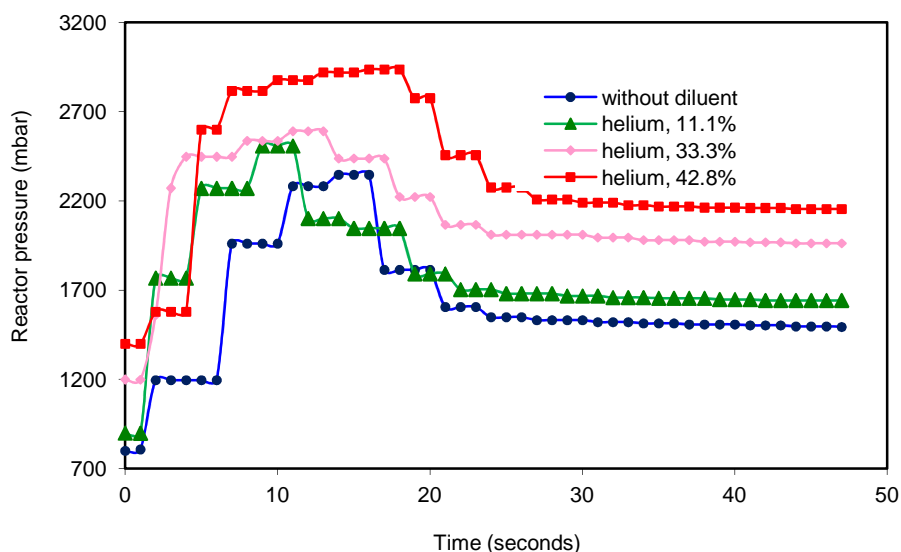


Figure 6.35: Temporal change in the reactor pressure with change in helium concentration

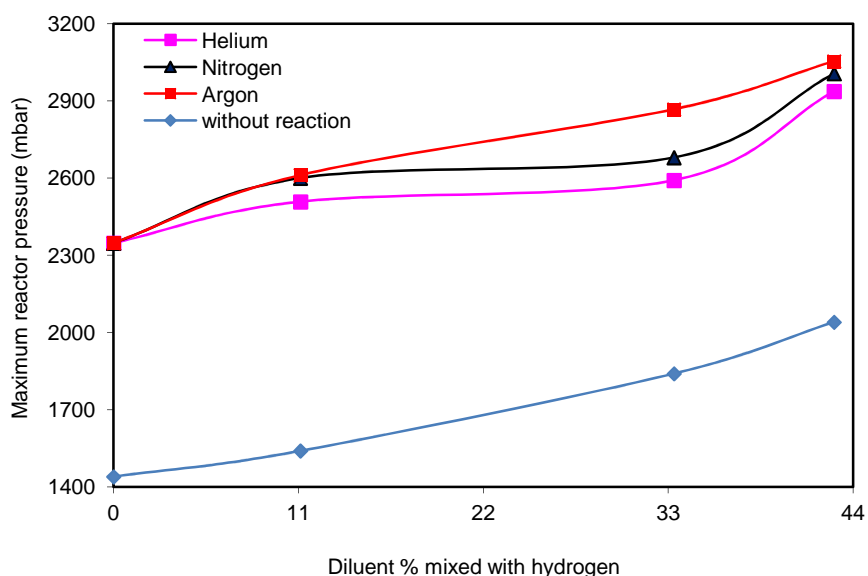


Figure 6.36: Maximum pressure recorded during H_2-F_2 reaction

(Note: The uncertainty in the measurement of pressure is within $\pm 0.1\%$ of the value)

(c) Thermal analysis of the reactor system

The reaction between hydrogen and fluorine being very fast, the longer time taken to register the peak temperature suggests the process to be governed by heat transfer through the barriers right from the flame surface to the temperature sensor. The following analytical cum empirical approach has been adopted to explain the observations in the selected cases 45, 48 and 51. In all the three cases, initially, the gas inside the chamber was in thermal equilibrium with the wall. Three hundred seconds after the reaction had started, all the thermocouples showed almost the same reading attaining equilibrium with the wall again. The net difference in the gas temperature was ~ 10 K in each case. Since the reaction time between hydrogen and fluorine is almost negligible and, fluorine introduction to the reactor is for a very small period (~ 250 ms), initially, the entire heat released from the chemical reaction is assumed to be deposited in the gases inside the reactor. Subsequently, the reactor temperature reduces continuously due to transfer of heat to the surrounding through radiation and convection. When energy balance was carried out, it was found that nearly 92% of the total energy liberated as heat of reaction was deposited on the wall, while the rise in enthalpy of gases accounted for $\sim 0.2\%$. This indicates that the heat picked by the gases is quickly dissipated to the wall. Since the reactor wall was insulated, nearly 8% energy loss to the atmosphere appears to be on the higher side. The error in the energy balance may be due to the estimation of the thermal capacity of the reactor wall. During the course of heat transfer, the variation in the wall temperature was very small as compared to the gas temperature because of the large difference in their heat capacity values. The rate of heat transfer is rapid in the beginning due to large thermal gradient between the source (hot reaction plume) and the sink (wall and the bulk gas). The thermowells did not receive significant radiated energy because of very low view factor (~ 0.02) and got heated by convection currents only. Hablani and Simmons (1967) reported the adiabatic flame temperature for the stoichiometric H_2-F_2 flame to be ~ 4220 K

through infrared spectroscopic study. At this temperature, the hot gaseous molecules emit thermal radiation in the far infra red region. Based on the information from Vinti (1932), Safary (1951) and Yoshino (1970), none of the gases from HF, He, N₂ and Ar absorb radiation in this region. Hydrogen too does not have any absorption spectrum in this wavelength (<http://csep10.phys.utk.edu/astr162/lect/light/absorption.html>). Therefore, the gaseous mixture does not gain energy from the radiative heat transfer and gets heated up by convection alone. Subsequently, the hot gases transfer the excess heat to comparatively cooler thermowell and the reactor wall. Since there is a finite heat source for a short time, a peak in the gas temperature is observed. After reaching a maximum, the hot gas starts cooling by losing its heat to the wall. Using simple equations and empirical correlations, the following steps are adopted to predict the wall and the gas temperature. Initially, the heat of reaction available to be dissipated (Q_d) in the reactor is given by

$$Q_d = Q_0 \quad \text{----- (6.1)}$$

The flame temperature ‘T_f’ is calculated through iterations on energy balance assuming adiabatic conditions. Agueda et al. (2010) suggest the dependence of the emissivity of the flame, ε_f on the flame diameter, d_f as,

$$\varepsilon_f = 1 - e^{-0.72 * d_f} \quad \text{----- (6.2)}$$

The radiative heat transfer from the flame surface to the chamber wall is obtained by

$$Q_r = \sigma \varepsilon_f A_f (T_f^4 - T_w^4) \quad \text{----- (6.3)}$$

To start with, initial values of d_f and l_f, which are required to calculate A_f are taken from the simulation results obtained in the previous section, 6.1. Having obtained Q_r, the radiative heat transfer coefficient h_r is calculated as

$$h_r = \frac{Q_r}{A_w(T_f - T_w)} \quad \text{----- (6.4)}$$

Due to the large temperature gradients existing inside the reactor, the heat transfer in the bulk fluid occurs by virtue of free convection. The reactor pressure comes down because of the

thermal change in the batch reactor. It can be assumed that the initially set up velocity circulations persist longer than required for dissipation of heat in the bulk. Under such condition, the heat transfer film coefficients are obtained with respect to the reactor wall. However, the relative order of change in this coefficient with type of diluent is maintained so that, the nature of the experimental trends can be explained. For Rayleigh no. (based on spacing between the two parallel surfaces) more than 1000, the correlation for the coefficient of heat transfer by free convection in a limited volume, as mentioned in the book by Isachenko (1977) is given by,

$$\frac{h_c \delta}{k_g} = 0.18 (\text{Gr Pr})^{0.25}, \left(\frac{h_c \delta}{k_g} = \text{Nusselt No.} \right). \quad \text{----- (6.5)}$$

' $h_c \delta$ ' is also called the effective thermal conductivity. Using properties of the gases as given in Table 6.3 and applying the mixture rule for ideal gases, the range of Rayleigh no calculated for the given geometry and fluid conditions is between 2400 (considering the bottom reactor wall) and 1878000 (considering the top reactor wall). Therefore, the above correlation (equation 6.5) is used to calculate the heat transfer coefficient. Since the convective heat transfer coefficient ' h_c ' changes with the physical and the thermal properties of the mixture, during modeling, the following ratio of heat transfer coefficients has been considered to account for the change in the diluent; $h_c (\text{N}_2/\text{He}) = 0.8175$ and $h_c (\text{Ar}/\text{He}) = 0.7769$. Having obtained h_c and h_r from the above equations, for a time step, the transient change in the reactor wall temperature is modeled by the following equation

$$m_w C_{pw} \frac{dT_w}{d\theta} = (h_r + h_c) A_w (T_f - T_w). \quad \text{----- (6.6)}$$

Similarly, variation in the chamber gas temperature is obtained by

$$m_g C_{pg} \frac{dT_g}{d\theta} = h_c A_w (T_f - T_g). \quad \text{----- (6.7)}$$

During the experiments, the perfect contact between thermocouple's hot junction and the thermowell wall was ensured. Therefore, it would not be erroneous if the temperature at the

tip of the thermowell, T_{tw} is assumed to represent the recorded gas temperature. Having obtained T_w and T_g by equations 6.6 and 6.7, and, the radiative component not being a part of the heat transfer, T_{tw} is calculated using the extended heat surface model equation [Bird, Stewart & Lightfoot (1994)] as,

$$\frac{T_{tw}-T_g}{T_w-T_g} = \frac{1}{\cosh \sqrt{\frac{h_c l^2}{k_{th} B}}} \quad \text{----- (6.8)}$$

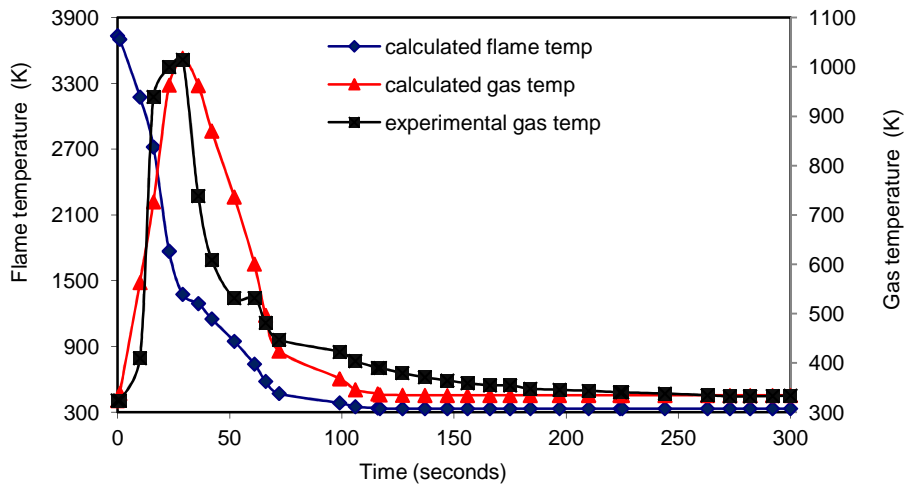
The appropriate changes are made in the lumped parameter $\epsilon_f A_f$ (as used in the equation 6.3) and the steps 6.3 to 6.8 are repeated till consistency between the calculated and the observed temperatures of the gas and the wall is achieved. The value of the lumped parameter is found to be different for different diluents. After iteration, the remaining energy available for further dissipation is

$$Q'_d = Q_0 - m_g C_{pg} \Delta T_g - m_w C_{pw} \Delta T_w \quad \text{----- (6.9)}$$

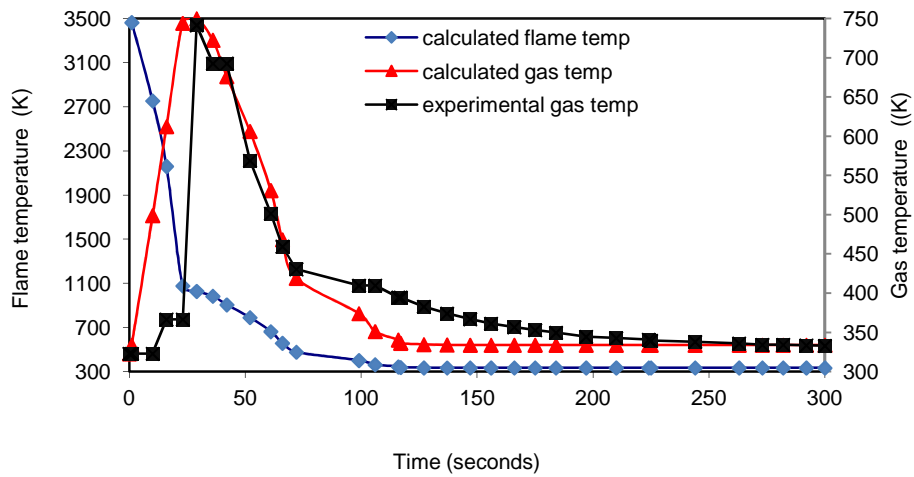
Q_d in equation 6.1 is replaced by Q'_d and equations 6.1 to 6.9 are solved again to get a new values of T_f , T_w , T_g and T_{tw} . These calculations continue till the remaining energy Q'_d is close to zero or steady state (no apparent change in T_g and T_w with time) is achieved. The results obtained by solving equations 6.6, 6.7 and 6.8 for various diluents are presented in Figures 6.37 (a) to (c). There is a fall in the flame temperature with time, while the wall gains temperature. The trend of first increase, reaching the peak value and then decrease in T_{tw} is well captured and compares well with the experimental data.

(d) Discussion of the experimental and modeling results

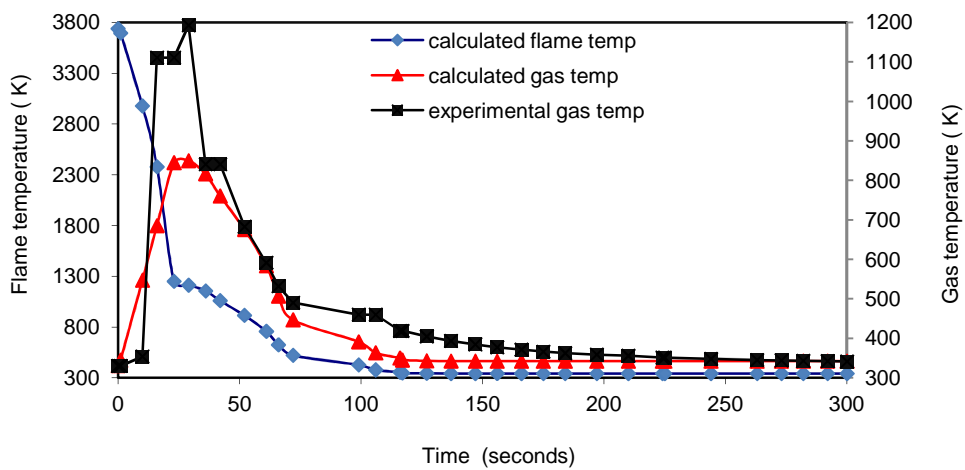
The gases being transparent to the thermal radiation at moderate temperatures (<5000 K), the heat energy picked up by the gases in a flame reactor is less if the mixture of the fuel and the oxidizer is close to their stoichiometric ratio (the calculated adiabatic flame temperature is maximum at the stoichiometric composition). Therefore, it is recommended to



(a)



(b)



(c)

Figure 6.37: Comparison between modeling and experimental reactor temperature for (a) helium (b) nitrogen and (c) argon as diluent

operate such reactors at higher/lower equivalence ratios where the flame temperatures would be lesser. Although lower flame temperatures can be achieved with mixtures either lean or rich with fuel, particularly for H₂-F₂ system, it is safer to have more hydrogen than fluorine for the reason that the latter gas is more toxic and difficult to handle. From Table 6.4, the peak reactor temperature increased with the concentration of argon whereas, it showed a decreasing and increasing trend with helium and nitrogen. The effectiveness of the diluents in

Table 6.4

Maximum temperature and pressure during reaction at higher pressure (800 mbar)

Case no	Maximum chamber temperature recorded in K	Maximum chamber pressure recorded during H ₂ -F ₂ reaction mbar(abs)	Calculated final pressure of the chamber due to addition of gases, without considering reaction. mbar (abs)
43	827.7	2347	1440
44	589.4	2508	1540
45	1014.9	2591	1840
46	1083	2937	2040
47	553.3	2600	1540
48	741.6	2680	1840
49	1028.7	3006	2040
50	988	2611	1540
51	1192.6	2867	1840
52	1243.1	3054	2040

(The uncertainty in the measurement of temperature is ± 2.2 K while the uncertainty in the measurement of pressure is within $\pm 0.1\%$ of the value)

reducing the reactor temperature is found to be in the order of $N_2 > He > Ar$. The adiabatic flame temperature with nitrogen is lower than argon and helium in the mixture. Therefore it is found to be most effective among all. The observed gas temperature is more when helium is present in the mixture in place of nitrogen because, apart from having a lower specific heat, the former gas is also a better heat carrier than the latter. It was interesting to see the contrasting behaviour shown by helium and argon, though both of them belong to the family of the noble gases and the mixtures have identical adiabatic flame temperatures. The observed temperatures with helium are lower than argon in the mixture. The density of the gaseous mixture containing argon is more than that of containing helium. Consequently, the jet spread is more in the presence of argon in the mixture, which leads to an increase in the heat transfer. Furthermore, from reaction $HF^* + M \rightarrow HF + M$ and $H_2^* + M \rightarrow H_2 + M$, helium is relatively more effective in de-energizing the excited HF and H_2 molecules, preventing further generation of the active species participating in the chemical reaction.

6.5.2.2 Reactor behaviour with diluents at lower initial pressure (100 mbar)

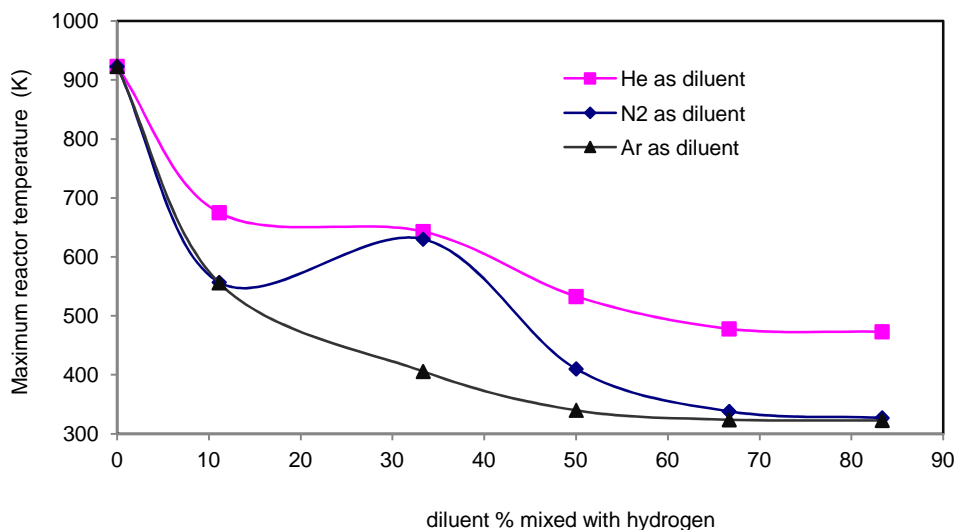
Having investigated the role of the diluents on H_2 - F_2 reaction in a flame at a relatively higher operating pressure, a few more studies were carried out to see the effect of the initial pressure on the reactor behaviour. A total of sixteen cases including the base case (diluent fraction is zero) were examined with an initial chamber pressure of 100 mbar instead of 800 mbar maintained earlier. The details of the runs are provided in Table 3.7 of Chapter-3. Since the operating pressure regime was on the lower side, the range of composition of the diluents admixture with the hydrogen was widened and it varied from 0 to ~ 83%. The peak temperature and pressure observed during these experiments are given in Table 6.5. They are also graphically presented in Figures 6.38 (a) and (b). From Figure 6.38 (a), it is seen that the response of the reactor temperature with different levels of dilution is different from the one

Table 6.5

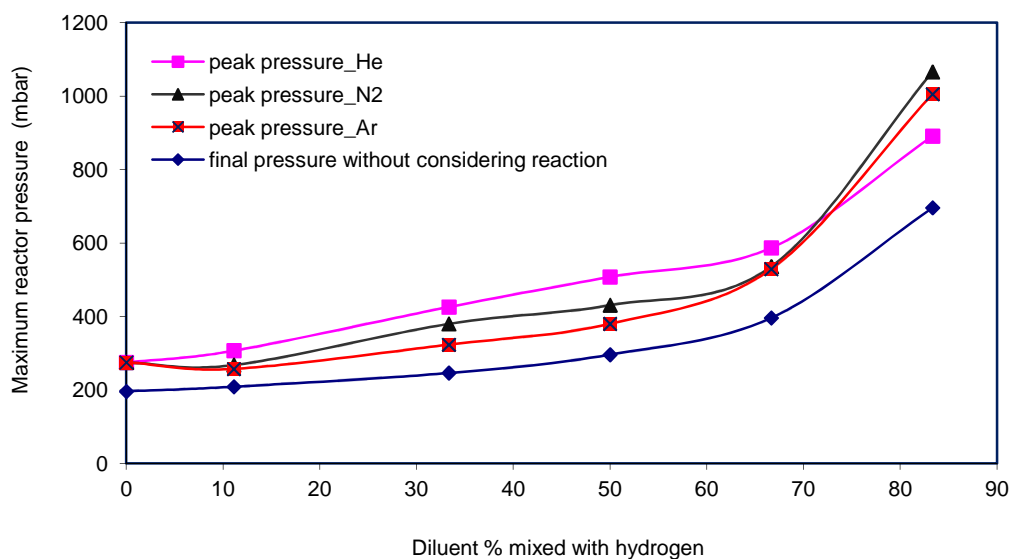
Maximum temperature and pressure during reaction at lower pressure (100 mbar)

Case no	Maximum chamber temperature recorded in K	Maximum chamber pressure recorded during H ₂ -F ₂ reaction mbar(abs)	Calculated final pressure of the chamber due to addition of gases, without considering reaction. mbar (abs)
53	923	275	196
54	675	307	208.5
55	643	426	246
56	533	508	296
57	478	587	396
58	473	891	696
59	557	268	208.5
60	630	380	246
61	410	431	296
62	338	536	396
63	327	1066	696
64	556	257	208.5
65	406	323	246
66	340	380	296
67	324	529	396
68	323	1005	696

(The uncertainty in the measurement of temperature is ± 2.2 K while the uncertainty in the measurement of pressure is within $\pm 0.1\%$ of the value)



(a)



(b)

Figure 6.38: (a) Maximum temperature and (b) peak pressure recorded during H_2-F_2 reaction experiment at initial pressure of 100 mbar

observed at higher pressure (800 mbar). Irrespective of the type of the inert, the temperature continuously decreases with increase in the quantity of the inerts. The temperature, when 33.33% nitrogen is added into the system, can be treated as an experimental outlier. The

effectiveness of the diluents in reducing the reactor temperature is found to be in the order of $\text{Ar} > \text{N}_2 > \text{He}$. Argon and nitrogen have comparable thermal diffusivities which is less than that of helium. The reactant gas molecules are less in number when the pressure is low and the heat released per unit volume is low. The experimental readings in this case suggest that the process is dominated by the heat transport characteristics of the gases rather than their possible role in the reaction kinetics. Figure 6.38(b) shows the peak pressures recorded during the experiments. The peak pressure values are always higher than what is expected from the change in the reactor temperature. This is a repetition of what was observed earlier at 800 mbar pressure.

6.5.3 Summary of the effects of type and quantity of diluents on $\text{H}_2\text{-F}_2$ reaction in a flame

The transient behaviour of a batch type $\text{H}_2\text{-F}_2$ flame reactor under various conditions has been experimentally investigated. The influence of the diluents such as helium, nitrogen and argon on the temperature and the pressure pattern of the $\text{H}_2\text{-F}_2$ flame reactor is studied at higher and lower initial pressure. Since gases like H_2 , He, HF, N_2 and Ar are transparent to thermal radiation at the reported $\text{H}_2\text{-F}_2$ flame temperatures, substantial part of the reaction heat is deposited on the reactor wall. At higher operating pressure, while the reactor temperature first decreased and then increased with increasing nitrogen and helium fractions, the addition of argon led to rise in the reactor temperatures at all compositions. This observation is different from the reported influence of diluents on HF chemical laser performance, $\text{H}_2\text{-Br}_2$ and $\text{H}_2\text{-O}_2$ reactions. The order of effectiveness of these molecules on the reactor temperature is found to be $\text{N}_2 > \text{He} > \text{Ar}$ instead of $\text{N}_2 > \text{Ar} > \text{He}$ for other systems. The reason for the higher reactor temperature with argon than helium is attributed to its effect on the flame geometry and the reaction kinetics. At lower operating pressure, there was

monotonous decrease in the reactor temperature with rising levels of diluent concentration. The order of effectiveness in causing the decrease in the reactor temperatures as $\text{Ar} \sim \text{N}_2 > \text{He}$, suggests that the thermophysical properties of the diluents dominate over their possible role in the kinetics at lower pressures. In either case, the pressure surges observed during the reaction does not follow the pattern expected on the basis of thermal or diffusion effect alone. This behaviour can be ascribed to the kinetic effects caused by the diluents leading to the phenomenon of the chain avalanche. Sophisticated analysis of the product gases such as by spectroscopy, may give more clues to the reaction kinetics. Suitable modeling incorporating the appropriate molecular theories can contribute to comprehensive understanding of such complex systems. Nonetheless, the results and the scientific data extracted from these studies will be useful in enhancing the scope of investigations in the field of combustion science and technology.

6.6 STUDY OF THE TEMPERATURE RESPONSE WITH VARIATION IN THE FLUORINE COMPOSITION FROM LEAN TO RICH

6.6.1 Introduction

The nature of the composition versus flame temperature curve of a fuel-oxidizer system depends upon the reaction equilibrium rate and the specific heat of the individual gases present in the product mixture. Though the percentage of hydrogen in the stoichiometric mixture with air is 29.6, Jones et al. (1931) found that the flame temperature is maximum in the region slightly rich with hydrogen (31.6% of H_2 fraction). The maximum flame temperature of $\text{H}_2\text{-O}_2$ mixture (~ 3080 K) was recorded to be more than $\text{H}_2\text{-Air}$ mixture (~ 2400 K) for obvious reason that, air also contains other gases such as nitrogen, which act as an inert. In order to produce the similar information on the $\text{H}_2\text{-F}_2$ system, several sets of

designed, unsteady state experiments as listed in Table 3.8 of Chapter-3 were conducted in the same reactor used for the dilution study discussed in the previous section, 6.5. The main objectives of these experiments were to study the behaviour of the hydrogen-fluorine flame reactor with respect to the change in temperature and pressure, when the fluorine composition in the mixture varies from lean (16%) to rich (90%). The preliminary calculations and discussions on the experimental results are as follows.

6.6.2 Preliminary calculations, experimental observations and discussions

The equilibrium conversions at temperatures ranging from 298 K to 5000 K were obtained using the thermochemical data of H_2 , F_2 and HF and are presented in the Figure 6.39. There is negligible dissociation of HF even when the temperature is as high as 5000 K. Therefore, the adiabatic flame temperatures shown in Table 6.6 were calculated assuming a

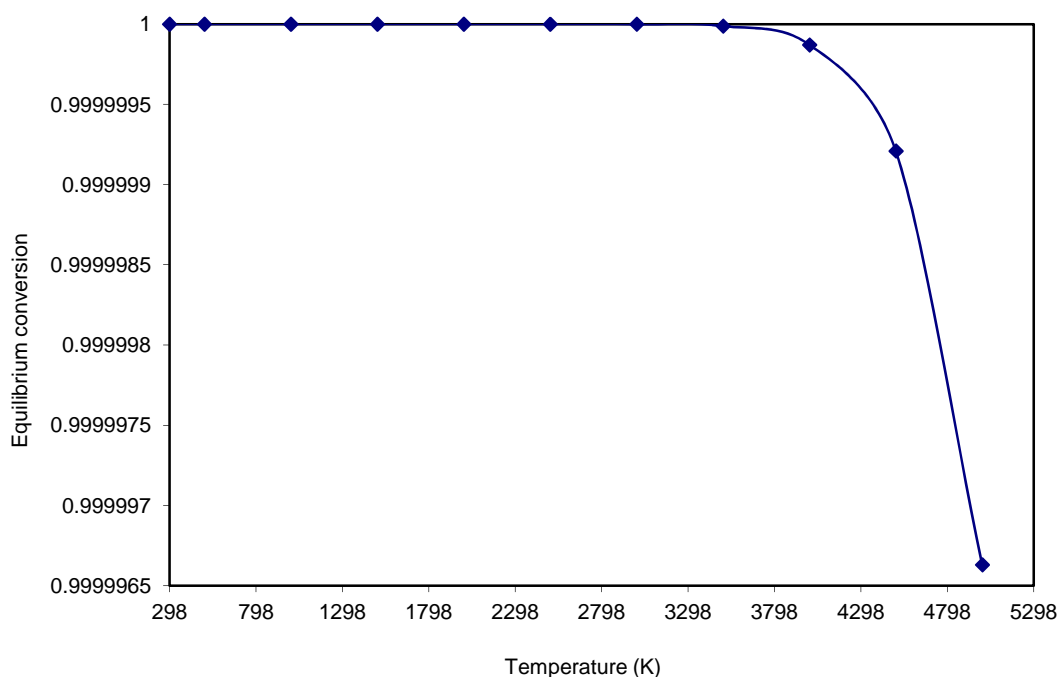


Figure 6.39: Equilibrium conversion of $H_2 + F_2 \rightleftharpoons 2HF$ reaction with temperature

complete conversion of the limiting reagent. During the experiments, thermocouples reflected rise in the temperatures almost immediately when fluorine was introduced into the batch reactor. Once again, the thermocouple T21 recorded the maximum temperature in all the trials and thereby, its values were considered to represent the reactor temperature. As soon as a short pulse of fluorine was fed into the chamber containing hydrogen, the reactor temperature started increasing, passed through a maximum at ~47 % F₂ and then began to decline. For further understanding, the resulting data in terms of the peak temperature and the pressure is tabulated in Table 6.6. It is graphically presented in Figure 6.40. As seen in this figure, the peak temperature is observed in the region rich with hydrogen, though theoretically, it should appear at 50% composition. The possible reason for the occurrence of this phenomenon could be as follows. The hydrogen molecules have got better mobility and hence increased probability of collision, which is not the case with fluorine. Moreover, since the rate of reaction is proportional to the reactant concentration near the stoichiometric ratio, a further increase in the hydrogen quantity enhances the rate of reaction before it reaches a limit when, the excess hydrogen starts acting as a heat sink. A polynomial equation as given below is obtained with an R² value of 0.9725 when the above data was regressed,

$$T_R = 4216.4 x_f^3 - 8924 x_f^2 + 5492.3 x_f - 96.307 \quad (6.10)$$

Here, T_R is the reactor temperature in Kelvin and x_f is the fluorine mole fraction. The value of T_R as calculated from this correlation at x_f equal to 0.5 is 945.88 K, which is less than the peak temperature of 953 K. There was pressure surge in the reactor as the reaction progressed. As seen from Figure 6.41, the highest pressure surge ratio (the ratio of the peak pressure to the stabilized pressure observed during a single experiment) of 1.57 occurs when the fluorine mole fraction is 0.375. This ratio at the fluorine fraction where reactor temperature is the highest is 1.5. There is not much of a difference in the peak temperature values at these two compositions (the values are 931 and 953 K respectively). Therefore, it

would not be erroneous to assume that the rise in the temperature of gases causes the pressure rise.

Table 6.6

Mole fractions of F₂ and corresponding peak temperature in the H₂-F₂ batch reactor (HCR)

Case no	Mole fraction of fluorine	Recorded peak reactor temperature in K	Adiabatic flame temperature in K
69	0.166667	585	2489
70	0.333333	914	3820
71	0.375	931	4083
72	0.473684	953	4626
73	0.545455	946	4548
74	0.565217	923	4476
75	0.583333	885	4415
76	0.6	869	4365
77	0.62963	863	4284
78	0.6875	843	4155
79	0.791667	794	3986
80	0.846154	707	3917
81	0.891304	681	3868

(The uncertainty in the measurement of temperature is ± 2.2 K)

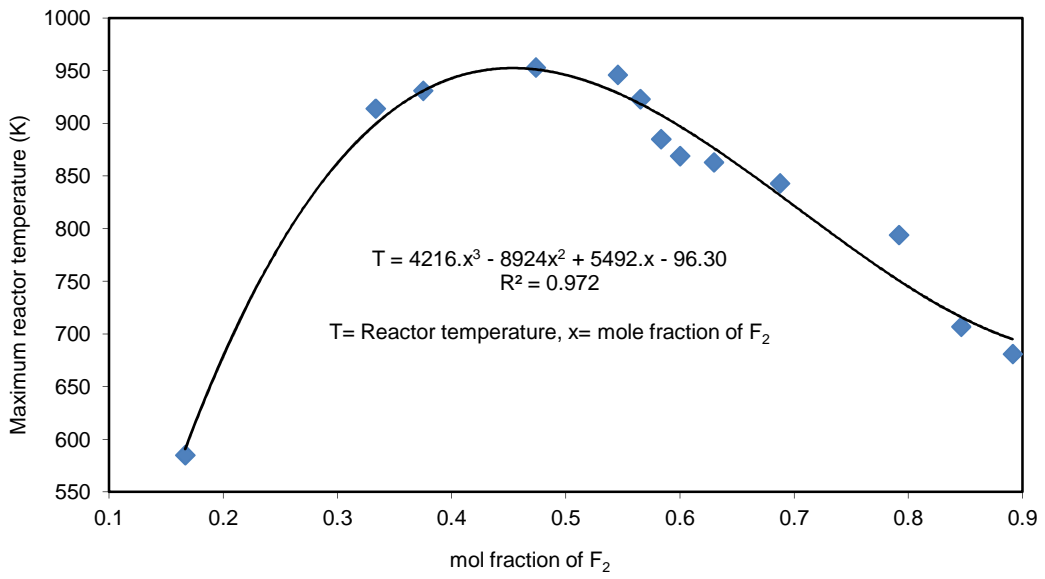


Figure 6.40: Variation in the maximum reactor temperature recorded with change in the fluorine mole fraction

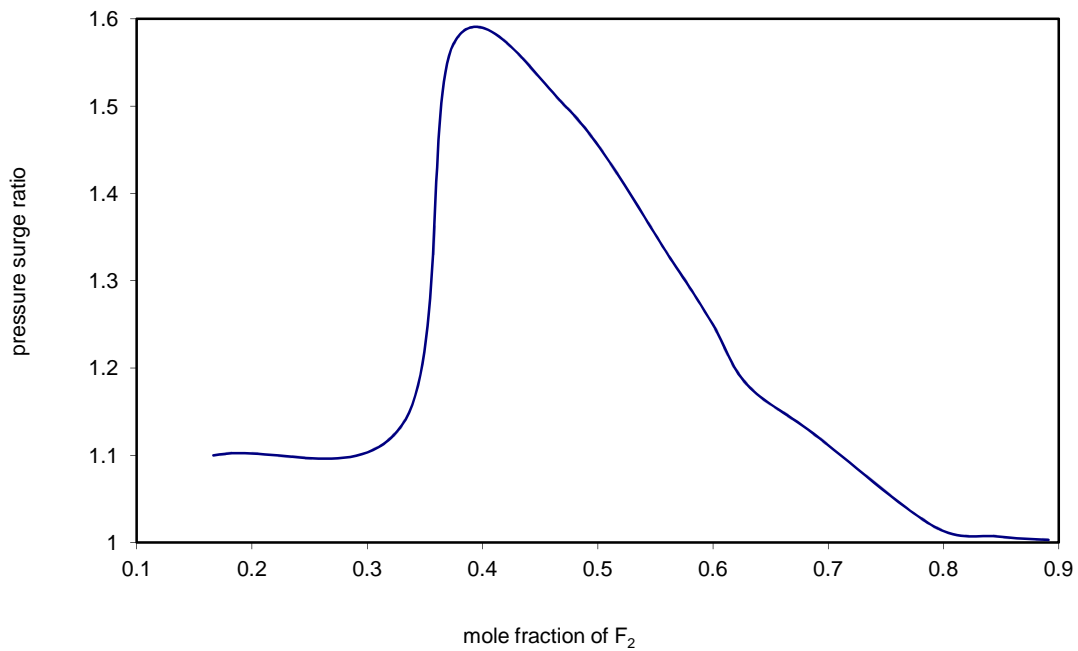


Figure 6.41: Pressure surge ratio recorded with change in fluorine mole fraction

6.6.3 Summary of the temperature response with variation in the fluorine composition from lean to rich

The equilibrium conversion of exothermic $\text{H}_2\text{-F}_2$ reaction is close to one even when the temperature is as high as 5000 K. Therefore, it can be safely assumed that the entire quantity of the limiting reagent is fully exhausted during the course of the reaction and the reaction mixture, at any point of time, contains only HF, the excess reactant and the inert. The composition-temperature curve for hydrogen-fluorine reaction has been experimentally generated which by and large emulates the pattern of variation in the adiabatic flame temperature. Similar behaviour has also been reported for other systems such as $\text{H}_2\text{-Air}$. Incidentally, the oxidizer in both the $\text{H}_2\text{-F}_2$ and the $\text{H}_2\text{-Air}$ systems contains nitrogen as the only impurity. As expected, the observed reactor temperature is found to be lower in the regions lean and rich with fluorine. But, counter to our intuition, the maximum temperature is not seen at the stoichiometric ratio. Similar to the $\text{H}_2\text{-Air}$ system, the maximum temperature in $\text{H}_2\text{-F}_2$ reaction is also recorded in the region slightly rich with hydrogen. While the reported value of the hydrogen concentration in air at which the reaction temperature is maximum is 31.6%, the corresponding value in the $\text{H}_2\text{-F}_2$ system, as found experimentally is close to 53%. It is a matter of coincidence that the peak temperature is registered when hydrogen in the mixture is ~6% above the respective stoichiometric composition, namely 29.6% for $\text{H}_2\text{-Air}$ and 50% $\text{H}_2\text{-F}_2$ system. Thus, the hydrogen concentration at the maximum temperature for $\text{H}_2\text{-Air}$ system is $29.6 \times 1.06 = 31.6\%$, whereas, it is $50 \times 1.06 = 53\%$ for $\text{H}_2\text{-F}_2$ system.

6.7 DILUTION EFFECT IN A FLOWING TYPE $\text{H}_2\text{-F}_2$ FLAME REACTOR

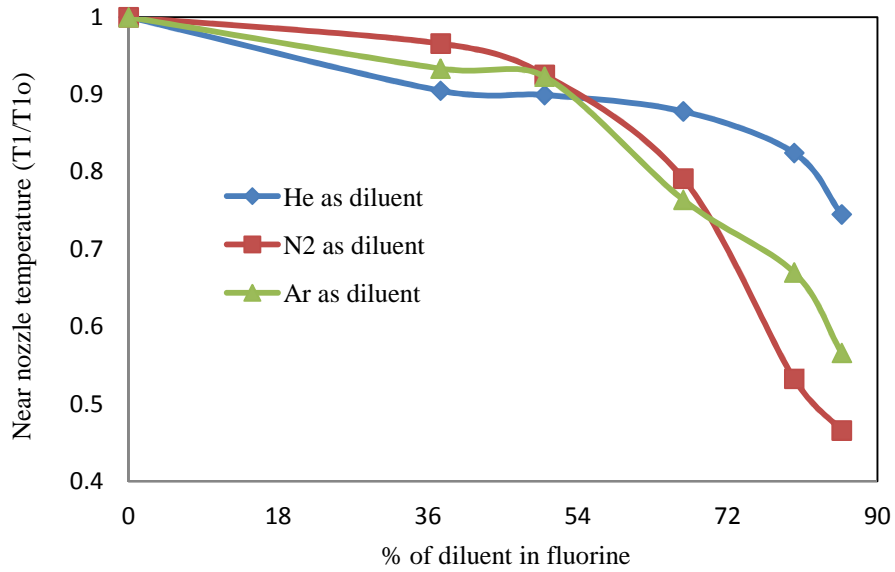
6.7.1 Introduction

The present part of the report focuses upon the behaviour of the H₂-F₂ flame reactor in the presence of the intended quantities of inert gases, such as, helium, nitrogen and argon in a continuous mode of operation. Fluorine and hydrogen in the ratio of 1:4 (F₂: 0.5 slpm and H₂: 2 slpm) are fed from separate nozzles into the VCR. A number of experiments, whose details are provided in Table 3.9 of Chapter-3, were carried out and the observations and the interpretations are discussed in the following sections. Selective cases are simulated and the predictions are compared with the experimental data. The velocity and the concentration profiles obtained from the validated simulations help in understanding the physics more comprehensively. A good match between the predicted and the observed data supports the diverse applicability of the simulation tool and eventually provides a handy method to optimize the temperature distribution pattern inside a flame reactor, by premixing the diluents with one of the reactants.

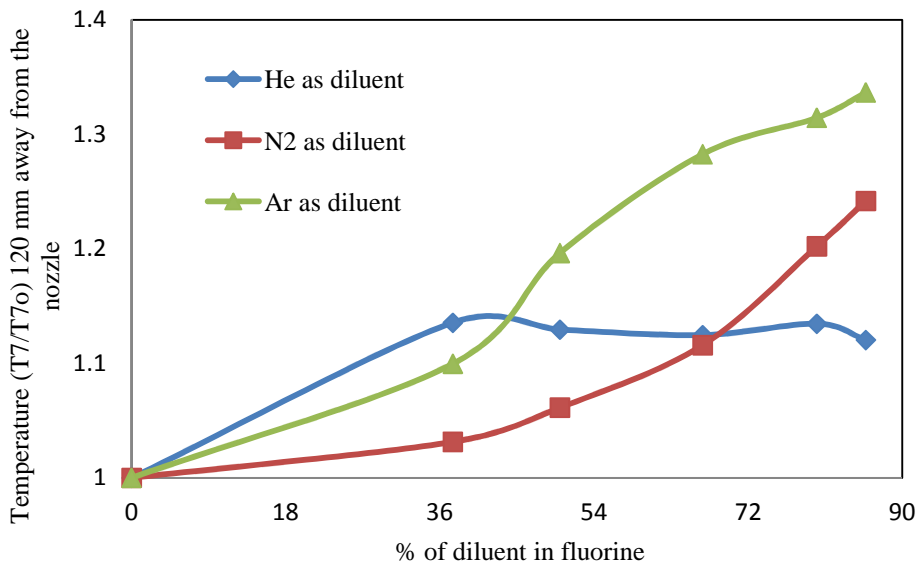
6.7.2 Experimental observations and discussions

In the present arrangement, since the feed nozzles are oriented almost parallel to each other, the mixing is relatively poor as compared to the batch reactor (HCR) studied earlier (section 6.5). The thermocouple, T1, located closer to the region where the reaction flame is supposedly formed, responded quickly to the onset of the reaction. Once the steady state was achieved with a given set of parameters, subsequent change in the reactor temperatures with change in the diluent flow rate was observed within a few seconds. From the energy balance based on the observed gas temperatures, the frequency of switching on/off of the reactor preheater and the cooling fluid flow rates, it is found that most of the heat is absorbed by the flowing gases in the form of sensible heat. Only a small fraction of heat is transferred to the reactor wall. This analysis is different from the previous study where the major portion of the heat energy was transferred to the reactor wall. The effect of the inerts on the reactor

temperatures is shown in Figures 6.42 (a) to (d). From these figures, it is observed that, all the diluents cause decline in the near nozzle temperature, T1 (Figure 6.42 (a)) and increase in the temperature recorded by T7 (Figure 6.42(b)). There is no significant change in the temperatures recorded by the thermocouples located farther, namely, T8 (Figure 6.42 (c)) and T9 (Figure 6.42(d)). The diluents not only act as a heat sink but also delay the mutual access of the reacting species, namely, hydrogen and fluorine. Furthermore, since the quantity of fluorine is fixed in every experiment, addition of a diluent leads to an increase in the jet momentum and hence the convective heat transfer. The inert species pick up heat near the feed nozzles and transport it a little away from them, resulting in a drop in T1 temperature and gain in T7 temperature. The effect of the diluents on the reactor temperatures further downstream is not appreciable because of the balance between the heat absorbed and transferred by the diluents. As is seen in Figure 6.42(a), the observed reactor behavioural pattern at diluent fraction below ~54% is different from when it is more than 54%. At lower concentrations, the dilution effect of bringing down the temperature (T1) is the maximum for helium, followed by argon and nitrogen. Thus the order of effectiveness in bringing down the reactor temperature is $\text{He} > \text{Ar} > \text{N}_2$. This observation is different from the ones noted in the batch reactor, which may be attributed to the difference in the mixing effects. Helium, with excellent thermophysical properties rapidly reduces the reactor temperatures by diffusive heat transfer. In case of argon and nitrogen, lesser reduction in the reactor temperature, perhaps, owes to their poor mixing and relatively poor heat transfer properties. At higher concentration levels however, mixing is comparatively aggressive (because of higher velocity ratios as seen in Table 3.9) and, the order of effectiveness changes to $\text{N}_2 > \text{Ar} > \text{He}$. Nitrogen and argon present in sizeable amount have greater impact on the reactor temperatures. Between nitrogen and argon, the effect is slightly more in the case of nitrogen because of its higher heat capacity value. The temperatures recorded with the higher concentrations of helium however

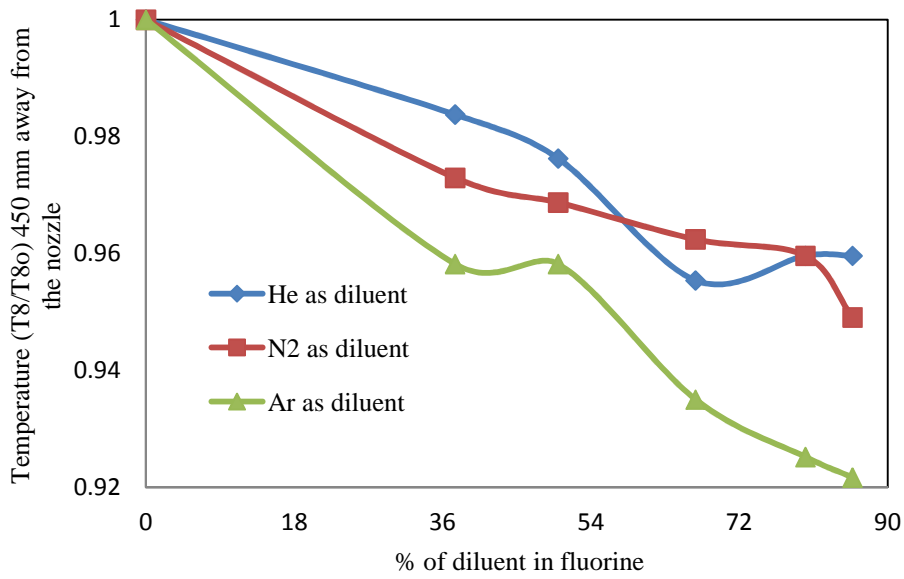


(a)

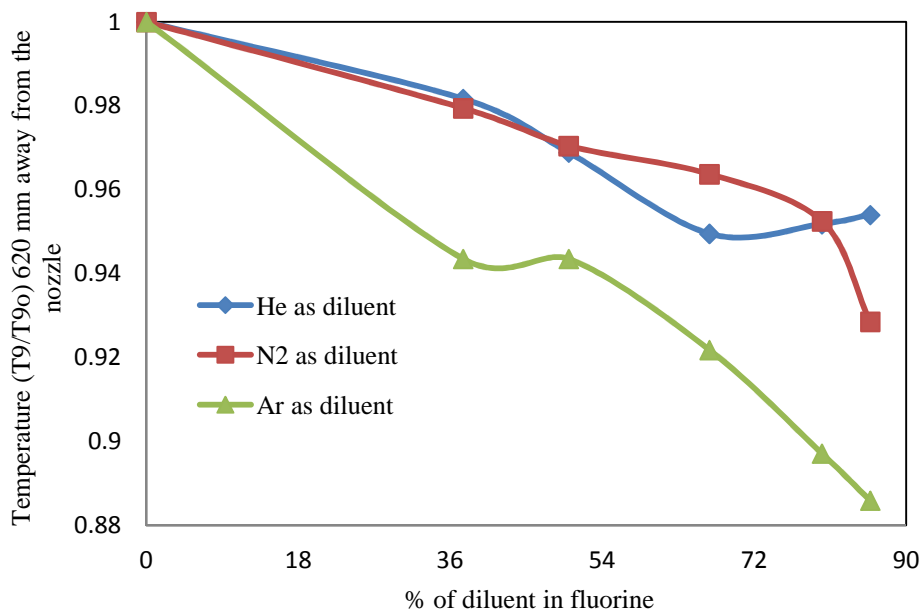


(b)

Figure 6.42: Effect of diluent content in fluorine on reactor temperatures in flowing condition: (a) Change in near nozzle temperature, T_1 and (b) Change in temperature, 120 mm away from nozzle (T_7). T_{1o} and T_{7o} are T_1 and T_7 temperatures at zero diluent concentration in fluorine.



(c)



(d)

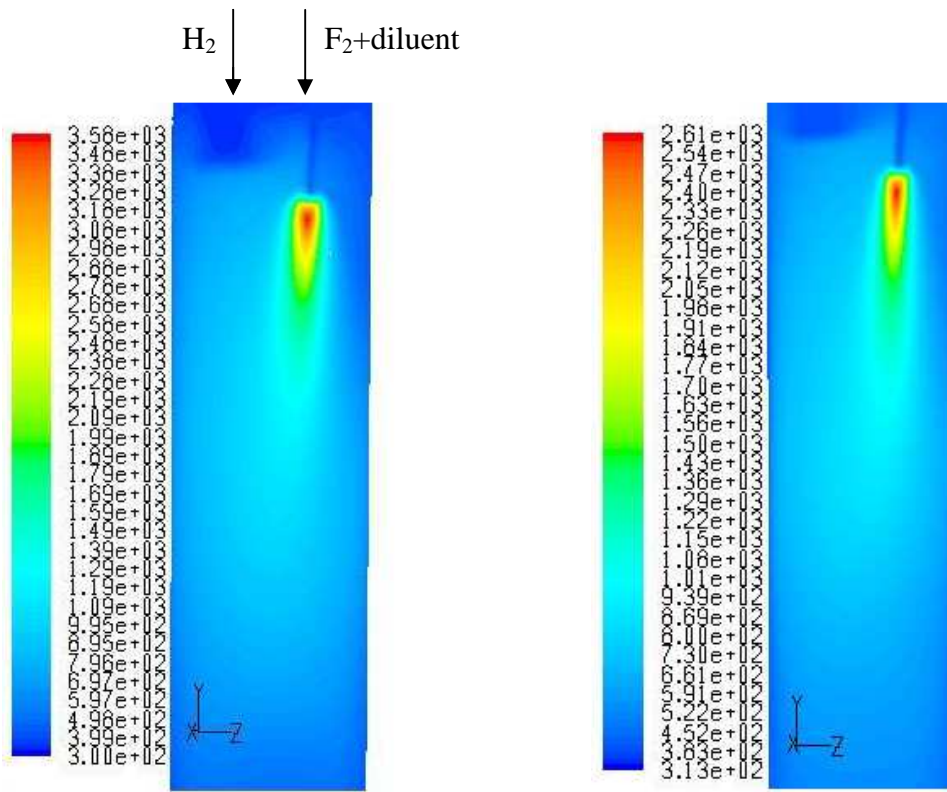
Figure 6.42: Effect of diluent content in fluorine on reactor temperatures in flowing condition: (c) Change in temperature, 450 mm away from nozzle (T8) and (d) Change in temperature, 620 mm away from nozzle (T9). T_{8_0} and T_{9_0} are T8 and T9 temperatures at zero diluent concentration in fluorine.

are asymptotically constant, because of its higher thermal diffusivity. The pattern of change in the reactor temperature as shown by T7 in Figure 6.42 (b) correlates well with the change in T1. The trends observed in the figures 6.42 (a) and (b) suggest that there will be much more effect on the reactor temperatures, when the reaction mixtures have higher levels of diluents. The nominal change in the values recorded by T8 and T9 in the figures 6.42 (c) and 6.42 (d), indicates that the dilution effect in the present system is limited to nearly 450 mm from the fluorine nozzle. This length is more than the reported length of 120 mm in the earlier studies with the excess of hydrogen and nitrogen (section 6.2), where, the flow rate of fluorine to the reactor was limited to 0.4 slpm. This is probably due to the higher jet momentum resulting from the increased gas flow rates.

6.7.3 Results from simulations, comparison with experiments and discussions

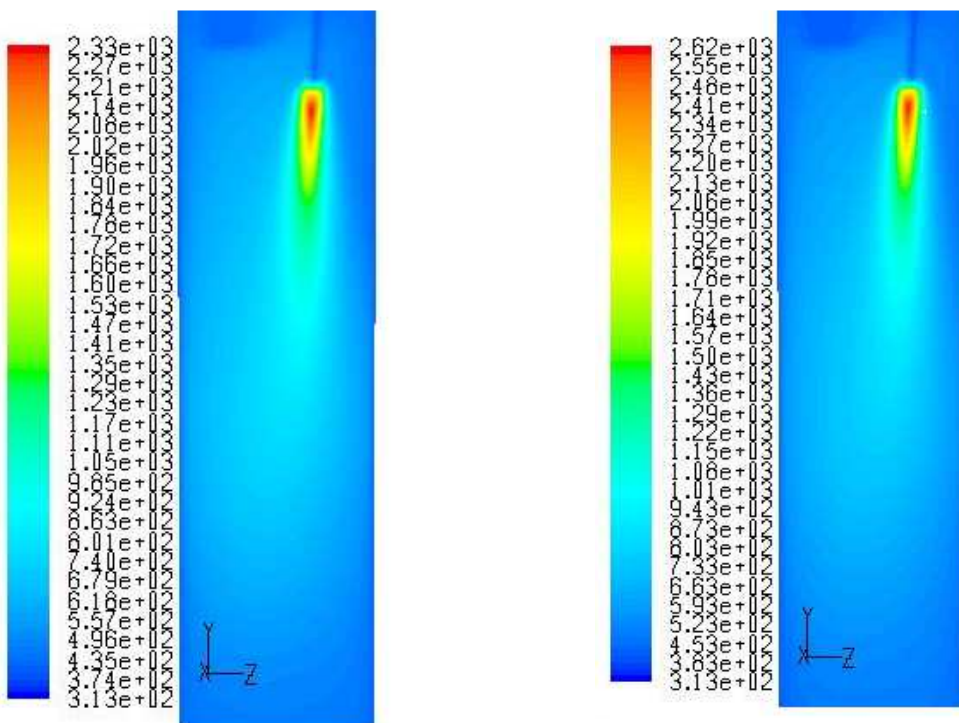
The same models and the software package as described in the Chapter-5 and used in the previous studies with the VCR, were used to simulate the four cases (case numbers 82, 85, 90 and 95). The diluent concentration in each case except the case 82 was 66.66% with respect to its mixture with fluorine.

The temperature contours obtained from the simulated cases are shown in Figure 6.43 where slight increase in the jet length with addition of diluent is apparent. The reduction in the central core temperature of the flame, as seen in this figure is in accordance to the specific heat value of the diluent. The predicted temperatures are compared with the experimental data in Figure 6.44. The T2, T3 and T4 temperatures could not be recorded as they became dysfunctional during the experiments. Except for T1, there is a good match between the predicted and the observed reactor temperatures. The large difference between the experimental and the simulated value of T1 is owing to the error involved in the experimental measurement, where high temperature gradient exists, for example, near the feed nozzles.



(a) Case 82 (no diluent)

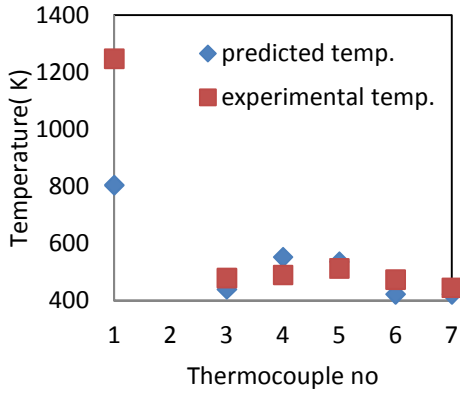
(b) Case 85 (66.6% He with F_2)



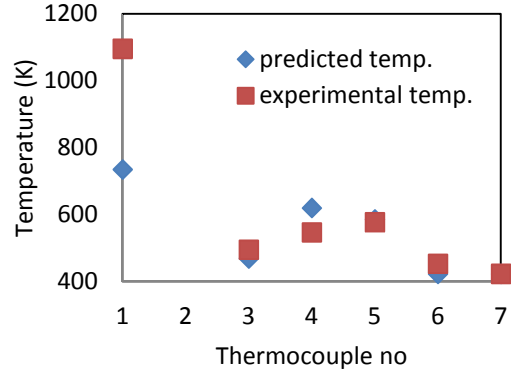
(c) Case 90 (66.6% N_2 with F_2)

(d) Case 95 (66.6% Ar with F_2)

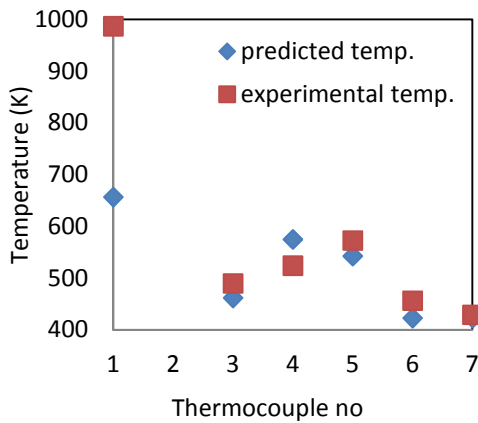
Figure 6.43: Temperature contours of different cases



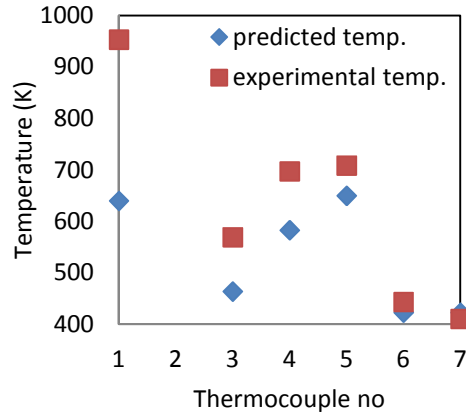
(a) Case 82 (no diluent)



(b) Case 85 (66.6% He with F₂)



(c) Case 90 (66.6% N₂ with F₂)



(d) Case 95 (66.6% Ar with F₂)

Figure 6.44: Comparison between the experimental and the simulated data

The simulations not only capture the trend of decrease in T1 and increase in T7 with dilution, but also the order of effectiveness of the inerts is the same in both the experimental and the computational investigations (Table 6.7). The plots for radial variation in the temperature, the velocity and the concentration of the product HF were obtained from the validated model at distances of 3, 5, 10, 20, 50, 120, 200 and 450 mm from the tip of the fluorine nozzle. Figures 6.45 (a)-(d) show the temperature plots for the four cases. As seen from these figures, the radial peak temperature at any of the axial distances is the lowest for nitrogen (case 90). The

Table 6.7

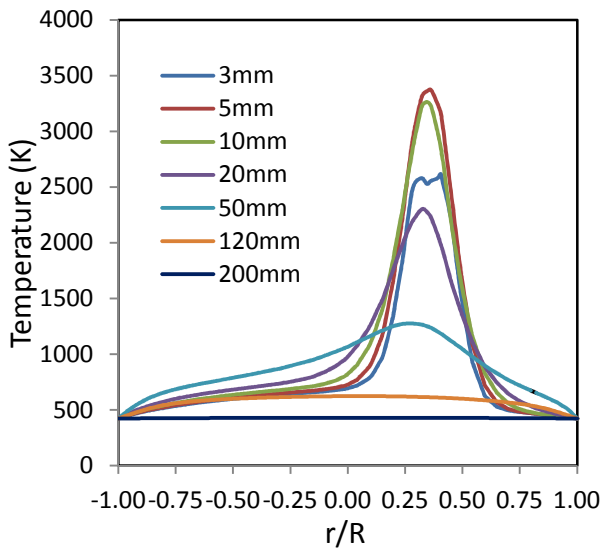
The experimental and the predicted temperature values of T7 when 66.66% diluent is added with the fluorine stream

Type of diluent	T7 temperature values	
	Experimentally observed temperature in K	Predicted temperature in K
No diluent (case 1)	513	537
Helium (case 4)	577	586
Nitrogen (case 9)	573	543
Argon (case 14)	659	650
Order of effect	Ar>He>N ₂	Ar>He>N ₂
	(Effectiveness of diluents in increasing the temperature shown by T7)	

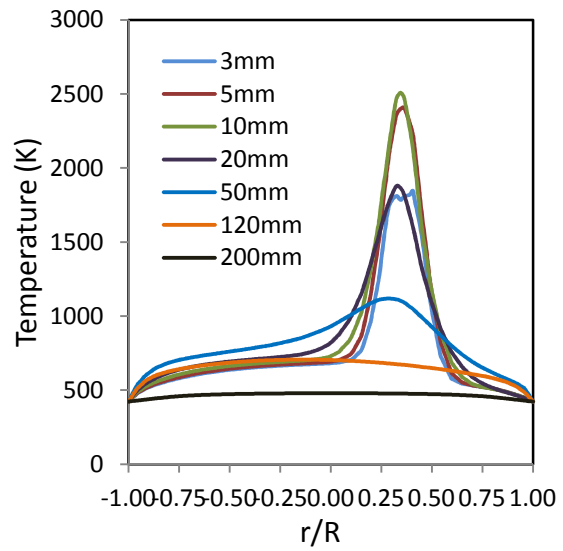
next higher peak is observed for helium (case 85) closely followed by argon (case 95). For an example, the predicted peak temperatures at 10 mm distance from the fluorine nozzle for nitrogen, helium and argon as the diluent, are around 2293, 2507 and 2554 K respectively. The location of the peak temperature in all the cases is observed asymmetrically below the fluorine nozzle. However, it gets shifted towards the central axis of the reactor downstream. This is because the temperature distribution follows the flow pattern which is tilted towards

the central axis due to the inclined nozzles. Inadequate mixing between the reactants in the proximity of the fluorine feed nozzle results in a lower temperature. Therefore, in none of the cases, the maximum temperature is observed at the nearest distance of 3 mm. In the case of reaction with no diluent (Figure 6.45 (a)), the peak temperature at 5 mm is more than at 3 mm. Beyond 5 mm, it decreases with distance and becomes almost asymptotically constant at 200 mm. As seen in Figure 6.45 (b), magnitude of the reactor temperatures came down when helium was added to fluorine. Moreover, the temperature at 10 mm distance is marginally higher than at 5 mm and 3 mm. The closeness of the temperature values between 5 and 10 mm distance may be attributed to the enhanced heat transfer characteristics due to the presence of helium in the gaseous mixture. On addition of nitrogen (Figure 6.45 (c)) and argon (Figure 6.45 (d)) to the fluorine stream, the difference between the temperatures at 5 mm and 10 mm distance increases. Unlike the trends observed in the figures 6.45(a) and 6.45(b), the radial temperature distribution computed at 10 mm and 20 mm distance have higher peak than at 3 mm distance. Poor movement of hydrogen and fluorine molecules through the diluent nitrogen or argon delays the chemical reaction between them, and consequently, the reaction volume increases causing increase in the temperatures away from the feed nozzle.

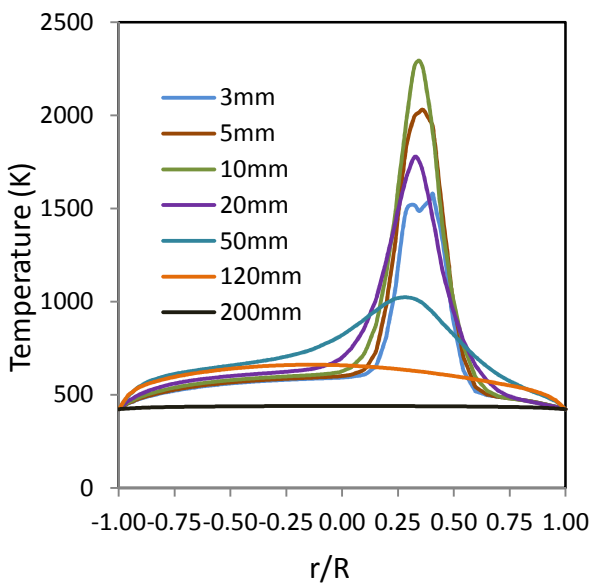
As seen from Figures 6.46 (a)-(d), the concentration of HF is more at the locations of the higher temperatures, following the temperature trend discussed above. Taking all the four cases into consideration, there is no appreciable change in the values of HF mole fraction beyond 120 mm distance. Therefore, it can be assumed that 120 mm of the reactor length is required to achieve thorough mixing of the reactant species. Further, the distribution of the product HF is seen to be asymmetric around the fluorine nozzle axis. The concentration of HF radially away from the fluorine nozzle (towards the reactor wall opposite to the hydrogen nozzle) is lean due to poor mixing in this region which is further illustrated by the vector



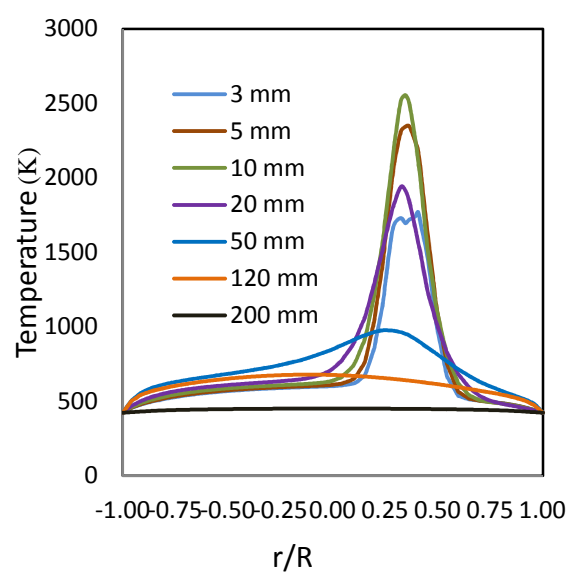
(a) Case 82 (no diluent)



(b) Case 85 (66.6% He with F₂)

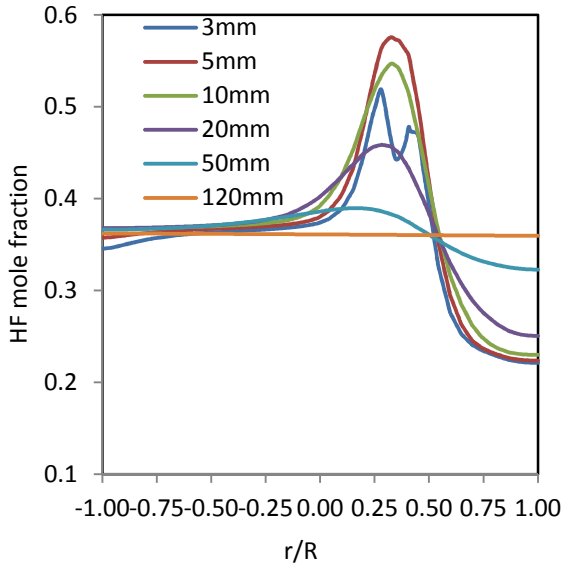


(c) Case 90 (66.6% N₂ with F₂)

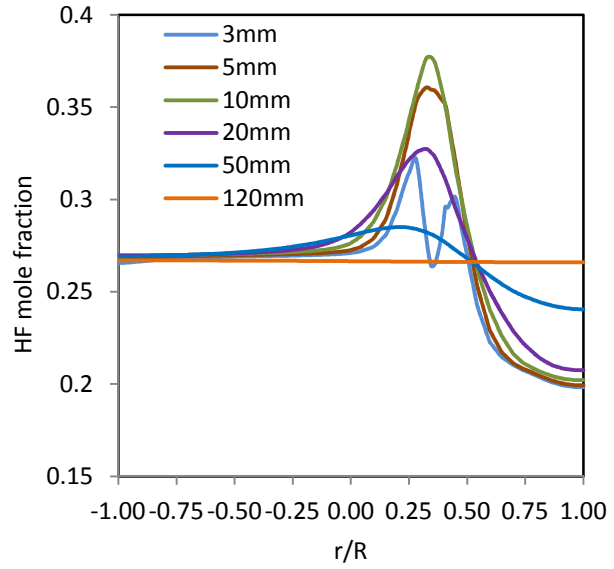


(d) Case 95 (66.6% Ar with F₂)

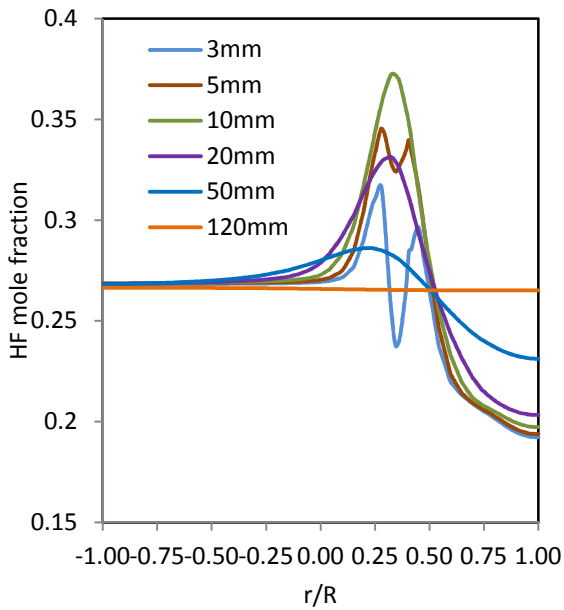
Figure 6.45: Radial temperature distribution in presence of diluents as predicted at various longitudinal distances. 'r' is any radial distance whereas 'R' is the reactor radius



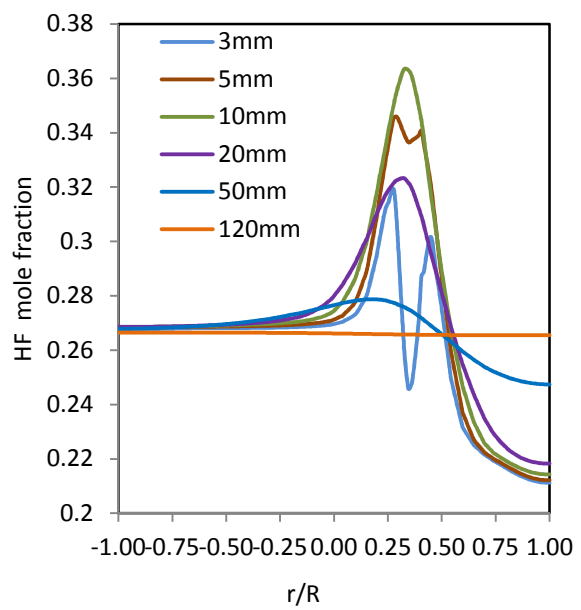
(a) Case 82(no diluent)



(b) Case 85 (66.6% He with F₂)



(c) Case 90 (66.6% N₂ with F₂)



(d) Case 95 (66.6% Ar with F₂)

Figure 6.46: Radial distribution of HF mole fraction in presence of diluents as predicted at various longitudinal distances. ‘r’ is any radial distance whereas ‘R’ is the reactor radius

plots shown in Figures 6.47 (a)-(d). They show more recirculation patterns present between the feed nozzles and towards the left of the hydrogen nozzle (towards the reactor wall opposite to the fluorine nozzle) due to buoyancy effects. On the other side of the fluorine nozzle, where the concentration of HF is lower, recirculatory flows are almost absent. The

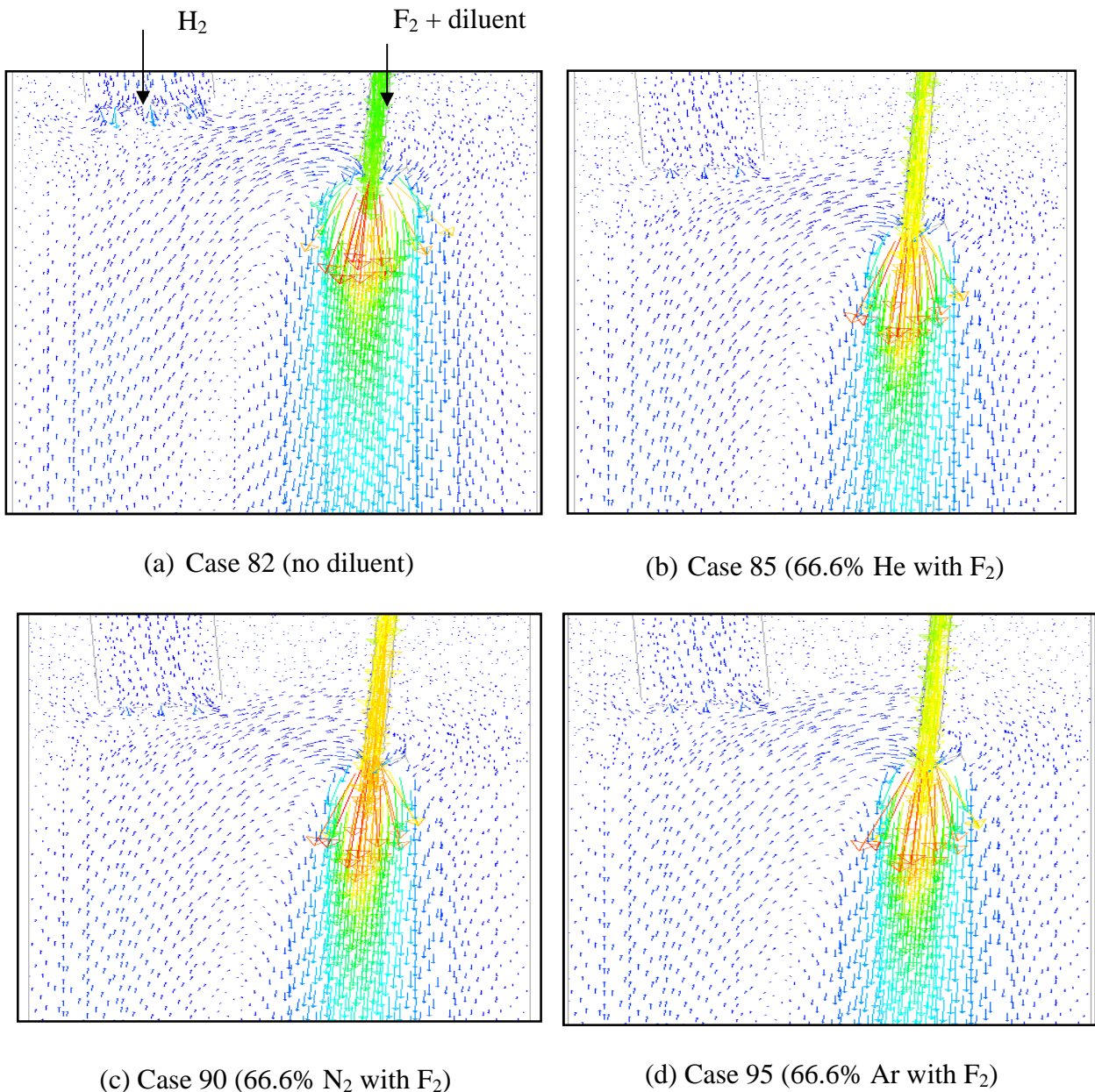
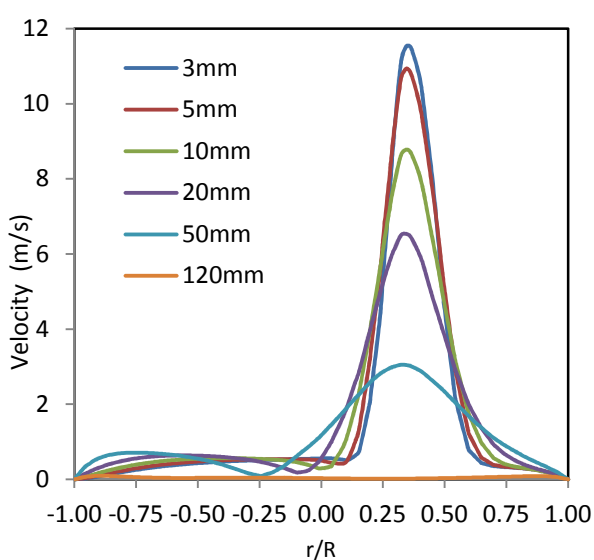
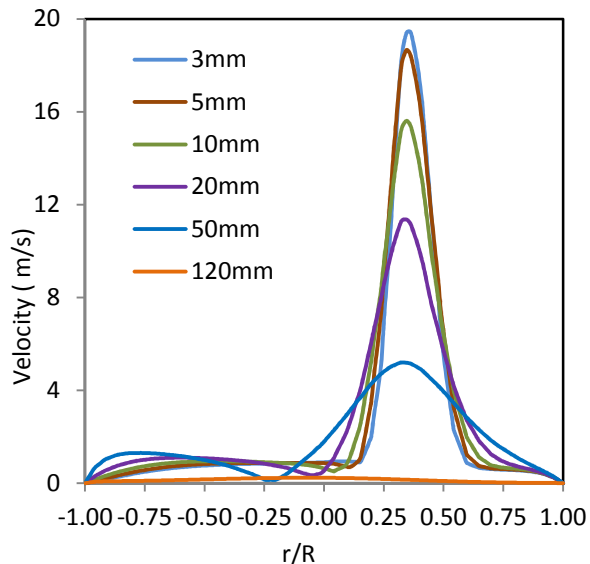


Figure 6.47: Velocity vectors near the nozzles as obtained from simulations

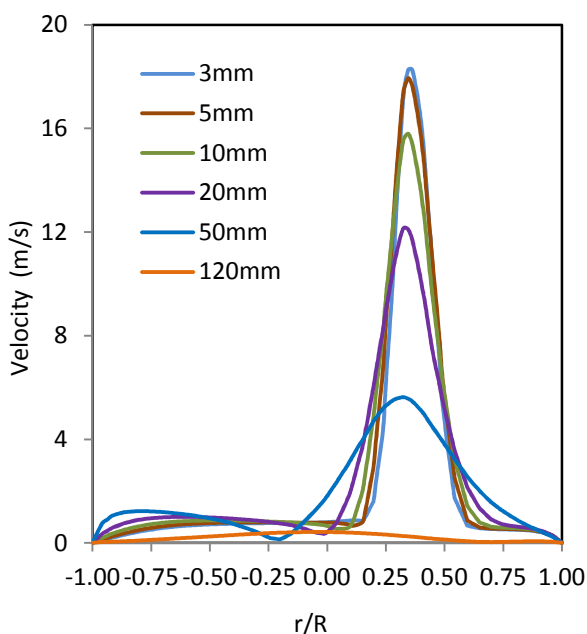
velocity plots for the above mentioned cases as obtained from the simulations are shown in Figures 6.48 (a)-(d). The nature of the velocity plots is similar to the temperature plots described earlier, in the sense that the reduction in the near nozzle temperature also leads to a



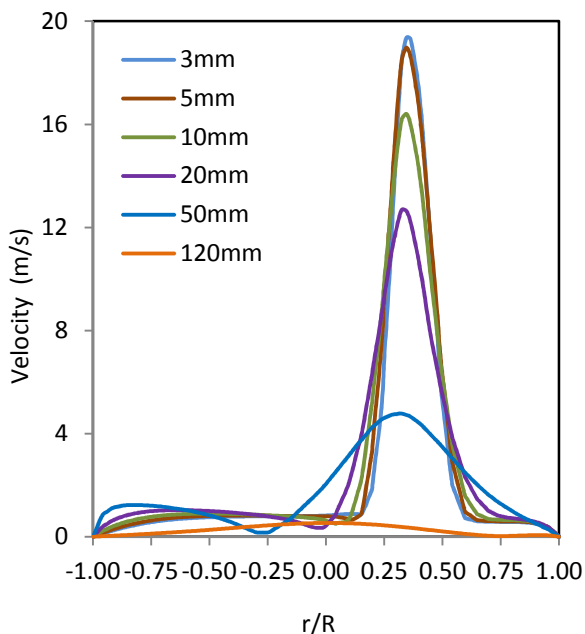
(a) Case 82 (no diluent)



(b) Case 85 (66.6% He with F₂)



(c) Case 90 (66.6% N₂ with F₂)



(d) Case 95 (66.6% Ar with F₂)

Figure 6.48: Radial variation in the velocity in presence of the diluents as predicted at various longitudinal distances. 'r' is any radial distance whereas 'R' is the reactor radius

drop in the velocities resulting from the release of the reaction heat. Once again, the velocity data after 120 mm length is ignored as it is almost a plug flow beyond this point. The average velocity of the fluorine stream without a diluent is 5.78 m/s and, it increases to 13.3 m/s with 66.66 mole % diluent addition. While the velocity increases by a factor of two (from 5.78 m/s to ~12 m/s) during the H₂-F₂ reaction in absence of a diluent, the presence of a diluent brings this factor down to around 1.5 (from 13.3 to ~20m/s). The region near the feed nozzles has higher velocity than the average nozzle exit velocity. Increase in the velocity due to the higher temperature generated from the chemical reaction is so high that it leads to local turbulence. This further justifies the assumption of choosing a turbulence model to simulate such problems.

6.7.4 Summary of the dilution effect in a flowing type H₂-F₂ flame reactor

The effect of the diluents on the behaviour of a flowing type, tubular H₂-F₂ flame reactor has been experimentally studied and numerically investigated. Higher jet momentum resulting from addition of the diluents increases the reaction zone in a flow type flame reactor. The diluents cause considerable decrease in the temperatures near the fluorine feed nozzle and in the thermally induced fluid velocities. The effect of helium as diluent is more visible than others at lower concentrations when the diffusive heat transport dominates over the mixing effects. At higher concentrations of diluents, argon and nitrogen are more effective in dispersing the reaction sites and changing the pattern of the temperature distribution in the reactor. In some of the applications, the latter property of the diluents may be desirable. The simulation results are able to capture the dilution effect on the reactor temperatures. A good match between the computed and the observed data validates the model, which can now be used to optimize the temperature distribution pattern inside a flame reactor, where the reactants are premixed with the diluents. Modification in the reaction

model with properly conceived kinetic schemes in the presence of the diluents may contribute to more comprehensive understanding of such intricate systems. The choice and the quantity of diluents however, would depend upon the kind of process requirements for a given application. The data from these trials will be useful in safety analysis and design optimization of the industrial scale flame reactors.

CHAPTER 7

STUDY OF SCALE-UP OF H₂-F₂ FLAME

REACTOR

The present chapter discusses the scale-up issues of a flame reactor. The criteria for scale-up are split into two parts; one for the feeding nozzles and the other for the reactor. While the only basis of similar reactor power density (the energy liberated in reactor per unit time, per unit volume) is adopted for calculating the reactor dimensions, several scale-up models for the design of the feeding nozzles are proposed. Different cases are simulated with the validated CFD tool and the results are discussed.

7.1 Introduction

Flame reactors have been successfully used in industry for several decades to manufacture more than 90% in volume and value of nanoscale commodities, for example, carbon black, silica, alumina, and titania. Unfortunately, the flame reactors have been developed through evolutionary research to make typically a single product, such as a ceramic powder with tight specifications [Pratsinis (1998)]. As a result, there is not much information regarding the process design for new products and the scale-up. Sadakata et al. (1996) reported that the reactor temperature and pressure, the initial reactant gas concentration and the ratio of nozzle diameter to nozzle outlet velocity must be kept constant during the scale-up of a coaxial jet flow aerosol reactor producing SiC. Smart (1998) derived the correlations for constant velocity and constant residence time scaling of turbulent jet flames, but pointed out that it was impossible to scale a burner to achieve the basic thermochemical structural features using either criterion. Jang (1999) observed that the product particle size decreases in a flame aerosol reactor when the burner tube diameter increases at a constant reactant flow rate. For a fast reaction kinetics, Chen and Driscoll (1990) and Villermaux and Rehab (2000) suggested that the correlations describing the reactant mixing in diffusion flame aerosol reactors might facilitate scale-up. The mixing of the reactant gases plays a key role in controlling the particle size since it affects the temperature profile, the residence time, the length of the flame, the volume of the reaction zone and the initial particle concentration in the flame. The mixing in turn is affected by several parameters such as flow rates, relative velocity, reactant concentration, reactor geometry, etc. However, linking process parameters measurably to the product characteristics requires a good understanding of the physico-chemical fundamentals of the synthesis process. Wegner and Pratsinis (2003) investigated the design and scale-up of co-flow diffusion flame reactors producing silica nanoparticles from hexamethyldisiloxane. They showed that the

velocity difference across the shear layer between the precursor/fuel jet and the annular oxidant jet is a key parameter determining the reactant mixing and the flame quenching. For a given fuel flow rate, the size of the product particle decreased with increase in the flow rate of the oxidizer gas and it (the particle size) was almost the same in three different types of reactor configurations. Also, for each relative velocity between the fuel and the oxidizer, they suggested that increase in the particle diameter with an increase in the production rate follows a power law. Later, they [Wegner and Pratsinis (2005)] also showed that the operation of a flame reactor with different fuel compositions, but with the same combustion enthalpy content, still results in the same size nano particles.

A brief review of the various approaches used in the flame reactor design scale-up is given below. The simulations are carried out on the proposed schemes and the results are discussed in this chapter. The effort has been to evolve a combination of the nozzle and the reactor design for a prescribed scale up ratio, which offers a favourable reactor temperature profile and simultaneously assures the equipment safety.

7.2 Scale-up Criteria

For acquiring design information for an envisaged scale-up, one of the cases, namely, case 82 (details in Chapter-3) is taken up as the ‘benchmark case’ for carrying out the simulation studies. While scaling up, selection of the design parameters such as nozzle size, individual stream velocity, velocity ratio and the reactor dimensions should be such that the resultant temperature profile and the residence time in the reactor are similar to the smaller reactor, the VCR, where the benchmark case was studied. The earlier simulation results have shown that the H_2-F_2 flame has a definite boundary. Dissipation of heat in the flame takes place in a manner such that there is a low temperature region near the reactor wall. The flame does not touch the solid wall on any occasion and the radial variation in the reactor

temperature gradually reduces as the gases approach the wall. Further, there is no effect of the reactor wall on the flame structure. Therefore, the flames resulting from the nozzle assemblies would not interfere with each other in case the scale-up is based on the concept of multiple nozzle modules. Based on this approach, the simplest scale-up design can be to multiply the existing module in a single large reactor having length equal to the VCR and place as many nozzle assemblies as required. The sketch of the scale-up of reactor by a factor of five is shown in Figure 7.1. A total of five nozzle assemblies are placed in a large reactor made of a 200 NB pipe. Each assembly consists of two nozzles, one for hydrogen and the other for fluorine. The clear distance between the two nozzle assemblies is kept equal to the internal diameter of the VCR. Though good results are expected from this concept, the disadvantages associated with this approach are a higher capital cost and an increased maintenance due to presence of multiple nozzle units. Hence, other contingent scale-up methodologies are also conceived and evaluated. The reaction between H_2 and F_2 is driven by mixing in the reactor. The size and the orientation of the feeding nozzles affect the mixing between the reactant gases and therefore they are important for the scale-up. Distribution of the temperature inside the reactor would also depend upon the reactor volume in which the gases are fed. With this objective in mind, the design approach has been divided into two parts; the first part being the selection of the feed nozzles. In the benchmark case as discussed earlier (Chapter-4), fluorine is issued from a single, diffuser type nozzle while hydrogen is fed through a perforated disc. While keeping the orientation of the feed nozzles the same as in the benchmark case, the following criteria are adopted to choose the nozzle sizes.

1. Calculate the Reynolds no. at the exit of each feeding nozzle of the benchmark case, and size the nozzles to maintain the same Reynolds no. in the scaled up version.

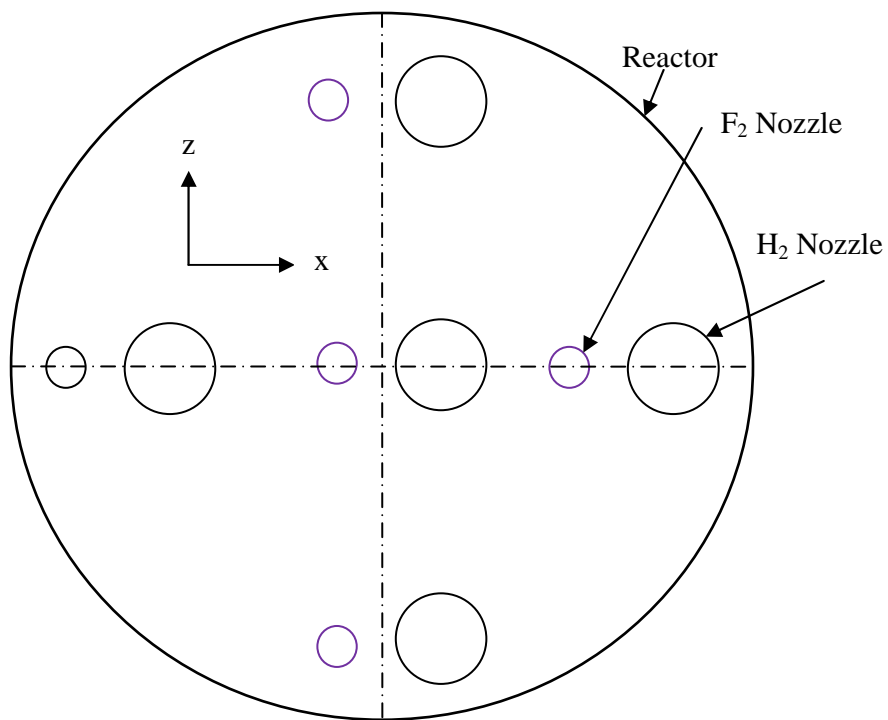
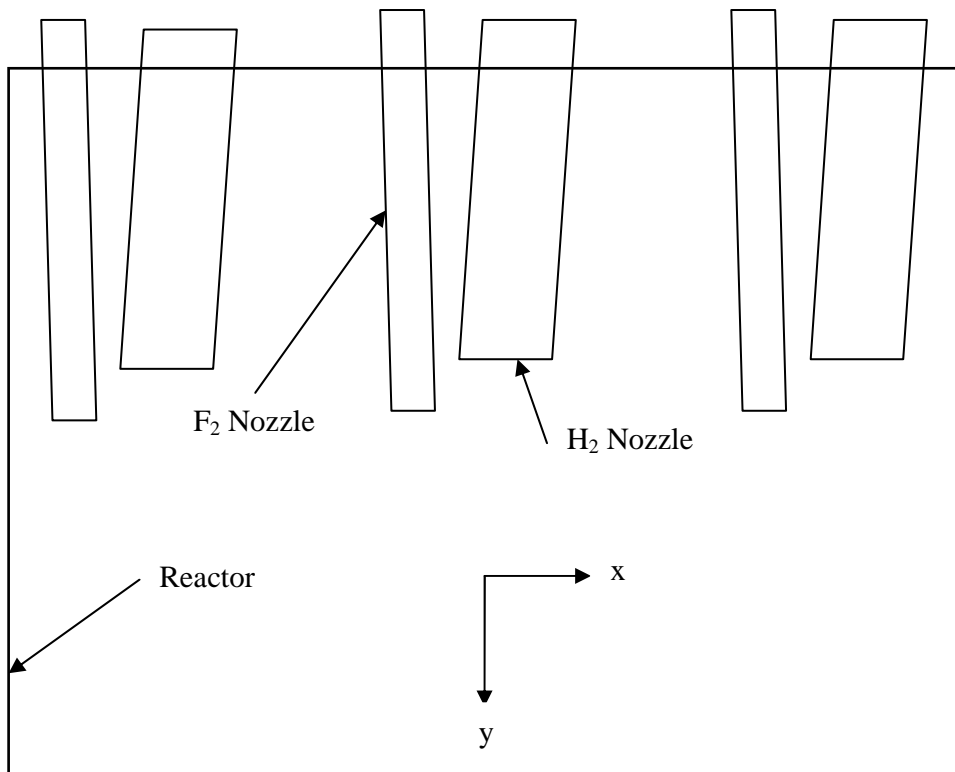


Figure 7.1: Sketch of scale-up reactor (multiple feed nozzles)

2. Calculate the nozzle diameters for the scale-up reactor such that, the exit velocities and thereby, the ratio between the velocities of the reacting gases is similar to that of the selected case.

After finalization of the nozzle sizes, the second part of the design is the sizing of the reactor. For a reactor of cylindrical shape, its dimensions are decided based on i) energy density (reaction enthalpy per unit reactor volume in watts/m^3) as in the benchmark case, ii) commercial availability of the pipe required for the reactor and, iii) the feasibility to accommodate the feed nozzles in the reactor. The first criterion of equal energy density, incidentally, also ensures that the residence time in both the reactors (the scale-up and the benchmark reactor) will be the same. Thus, the steps involved in the reactor sizing, after the feed nozzles have been chosen, are as follows:

1. Calculate i) the enthalpy per unit volume for the benchmark case and, ii) the quantum of heat liberated consequent to chemical reaction in the scale-up reactor. Divide (ii) by (i) to obtain the volume of the scale-up reactor.
2. Having obtained the volume, select an L/D ratio which not only can accommodate the feed nozzles but also is convenient to procure, fabricate and install.

The designs of the reactor and the nozzles thus evolved are shown in Figures 7.2 (a) and (b) respectively. Though a 100 NB, Sch-40 pipe is chosen for the reactor in both the cases, the feeding nozzles are different in them. The line passing through the centre of the hydrogen feed nozzle has been considered as the reference for all the radial distances in later sections. The axial distances however are taken from the tip of the fluorine nozzle in the discussions to follow. The simulations described below for the three kinds of scale-up reactors have been carried out using the CFD model and the software package used earlier (Chapter-5).

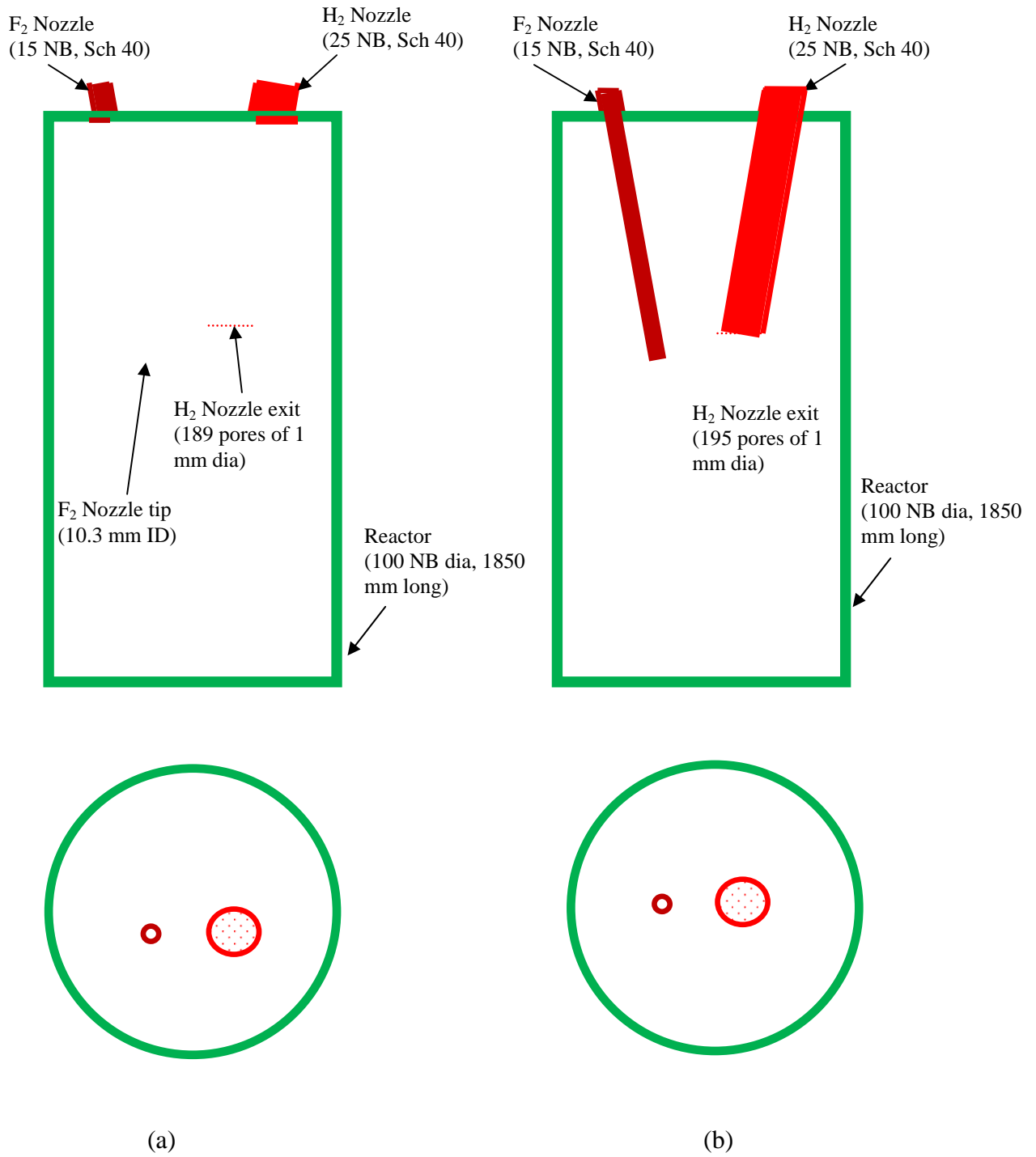


Figure 7.2: Sketch of the scale-up geometry, (a) based on the same Reynolds number at the nozzle exits and (b) based on the same velocity at the nozzle exits

7.3 Simulation results and discussion

The methodologies of simulation are the same as discussed in the Chapter-5. A fixed reactor wall temperature, inlet mass flow rates for the fluorine and the hydrogen streams, and ‘outflow’ as the exit condition have been assigned as the boundary conditions during the simulations. Figure 7.3 shows the temperature contours as predicted for the scale-up reactor based on the ‘multiple module’ concept. While the x-y plane shown in Figure 7.3 (a) bisects the feeding nozzles, the y-z plane in Figure 7.3 (b) passes through the space between the two nozzles (hydrogen and fluorine). That is why, the predicted temperatures shown in Figure 7.3 (a) appear higher than that in Figure 7.3 (b). Further, as follows from these figures, there is a difference in the shapes of the reaction flames emanating from different nozzle assemblies, indicating mutual interference between the neighbouring flames. In absence of a solid body like the wall, the fluid particles do not get decelerated and the fluid carries over its momentum to interact with the adjoining layers. Consequently, the flames tend to bend towards the reactor wall. It is further confirmed by the vector plot shown in Figure 7.4 (a) where the streamlines are seen bending towards the wall. Figure 7.4 (b) also suggests the presence of the recirculation in the plenum space (The reactor space above the feeding nozzles). The temperature and the velocity plots at various axial distances in both the x-y and the y-z planes are displayed in Figure 7.5 and 7.6 respectively. As observed earlier (sections 6.3, 6.4 and 6.7 in the Chapter-6), in this case too, the temperature near the fluorine nozzle exit is low. The temperature profile gets flattened at almost 140 mm distance from the F₂ nozzle tip. The velocity profile is similar to the one discussed under the sub-section 6.7.3 of Chapter-6. As seen from these results, the temperature gradient near the wall is relatively higher, which is not desirable. Further, the reaction flame bending towards the reactor wall may pose safety concerns and therefore this model should not be adopted for the planned scale-up.

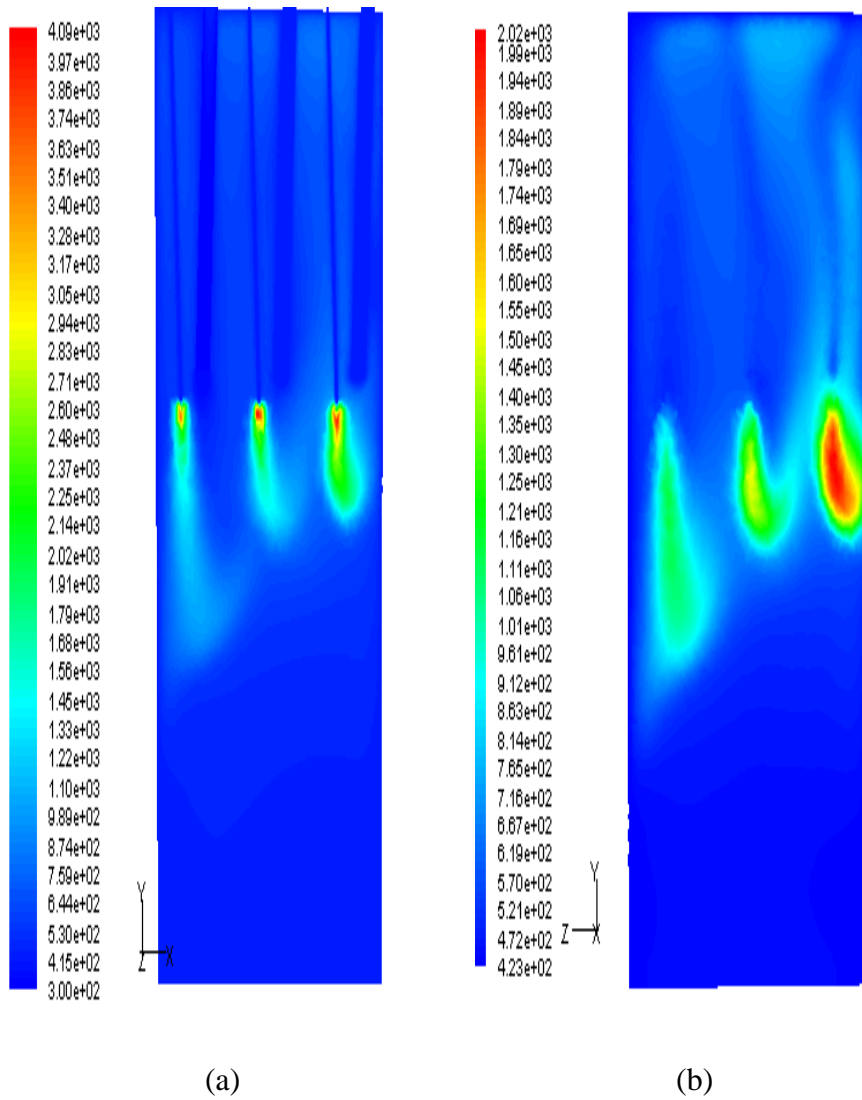
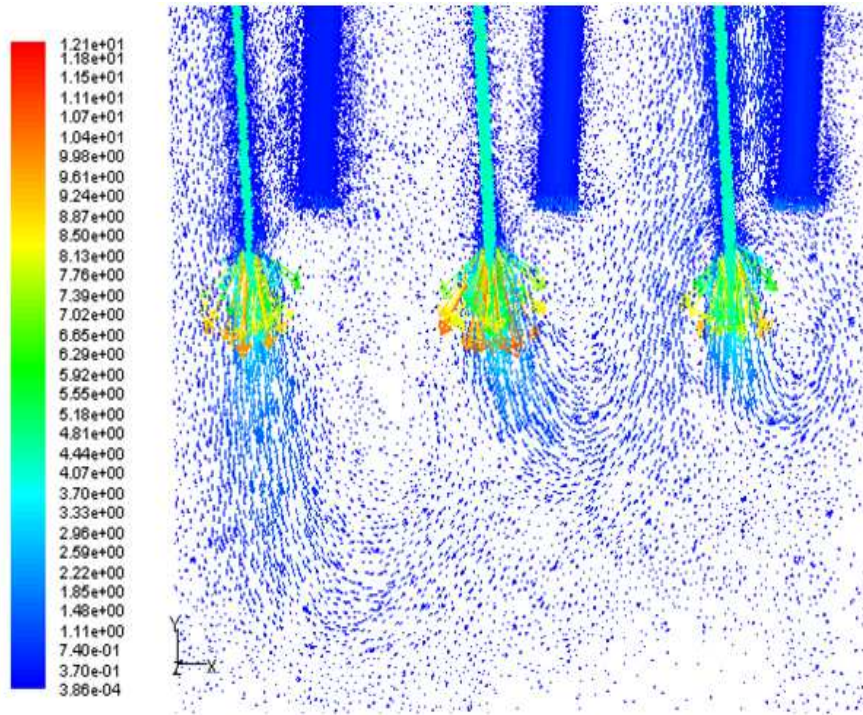
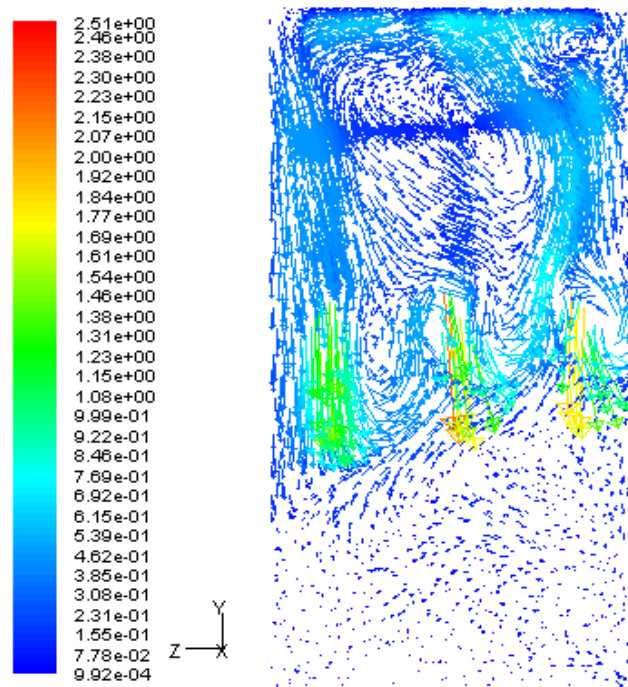


Figure 7.3: Temperature contours of the multiple nozzle scale-up reactor (a) section at $z=0$ on $x-y$ plane and (b) section at $x=0$ on $y-z$ plane

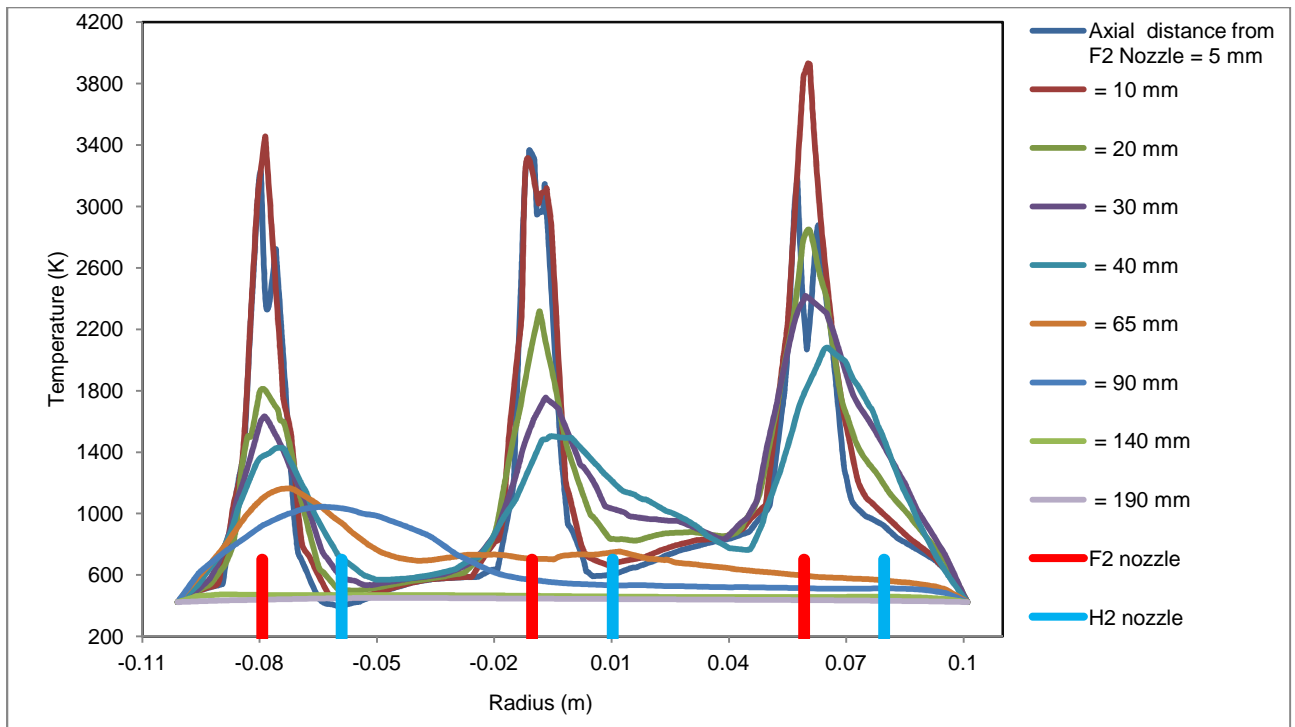


(a)

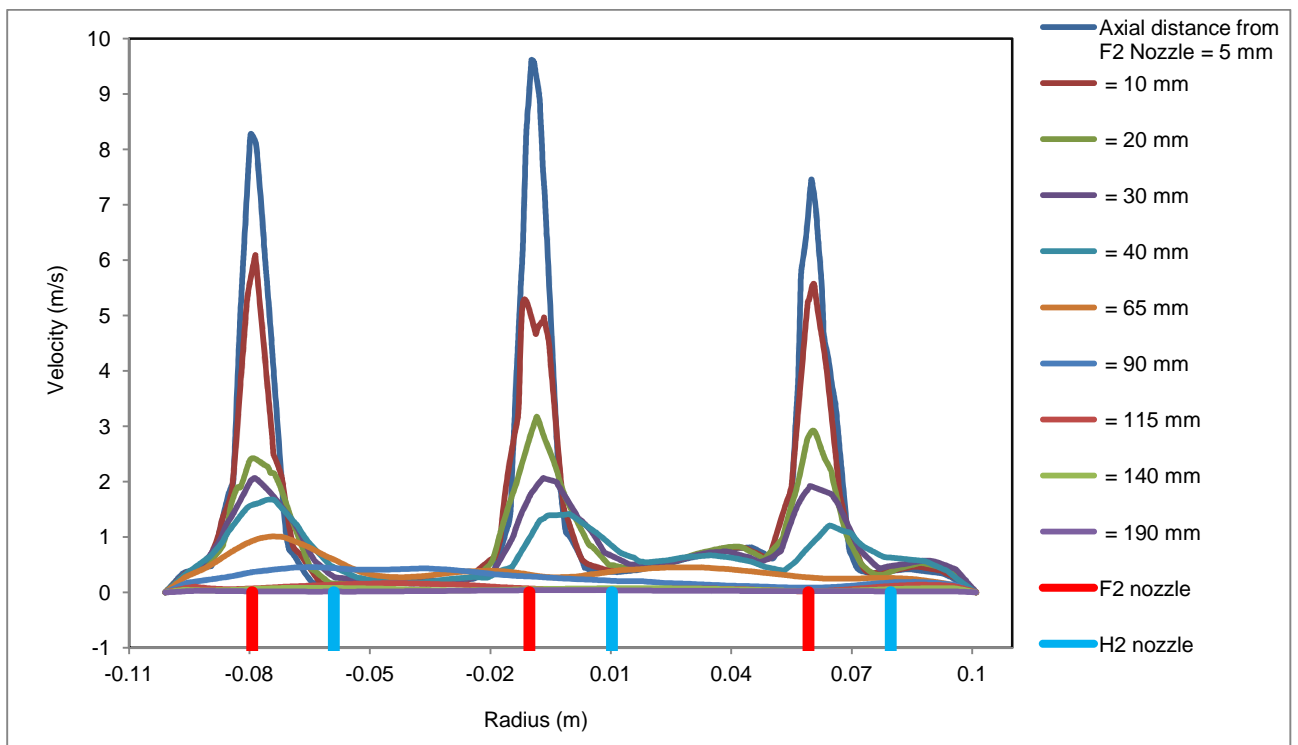


(b)

Figure 7.4: Vector plot of the multiple nozzle scale-up reactor (a) section at $z=0$ on $x-y$ plane and (b) section at $x=0$ on $y-z$ plane

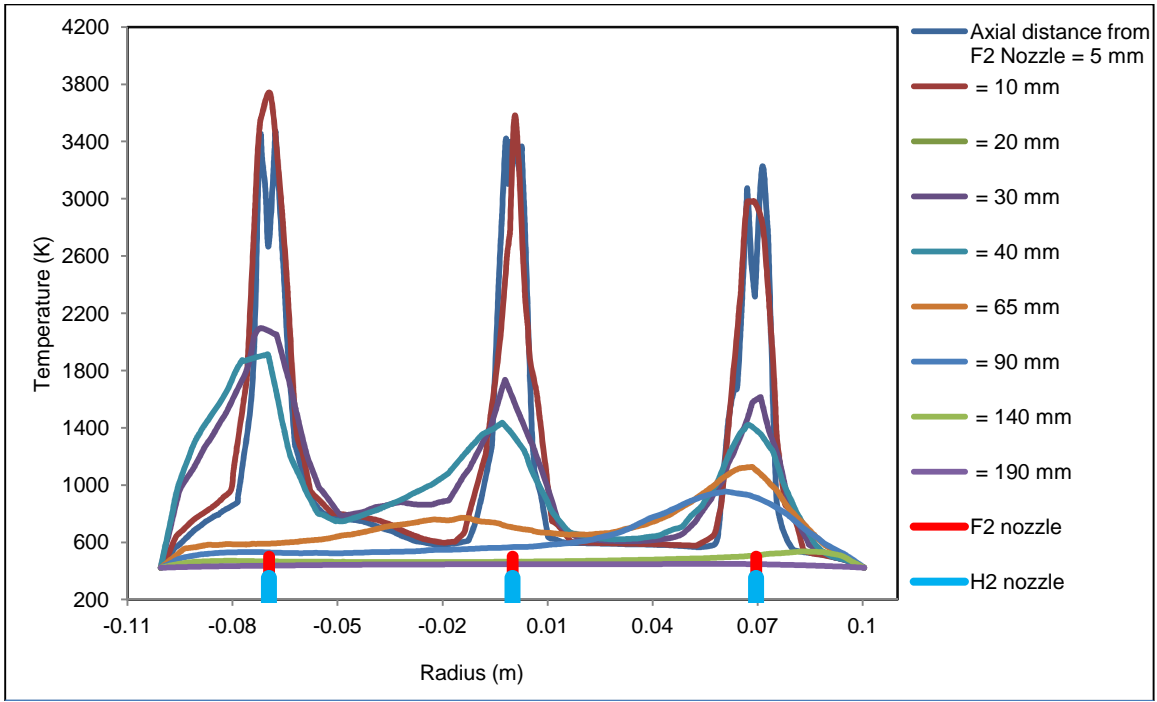


(a)

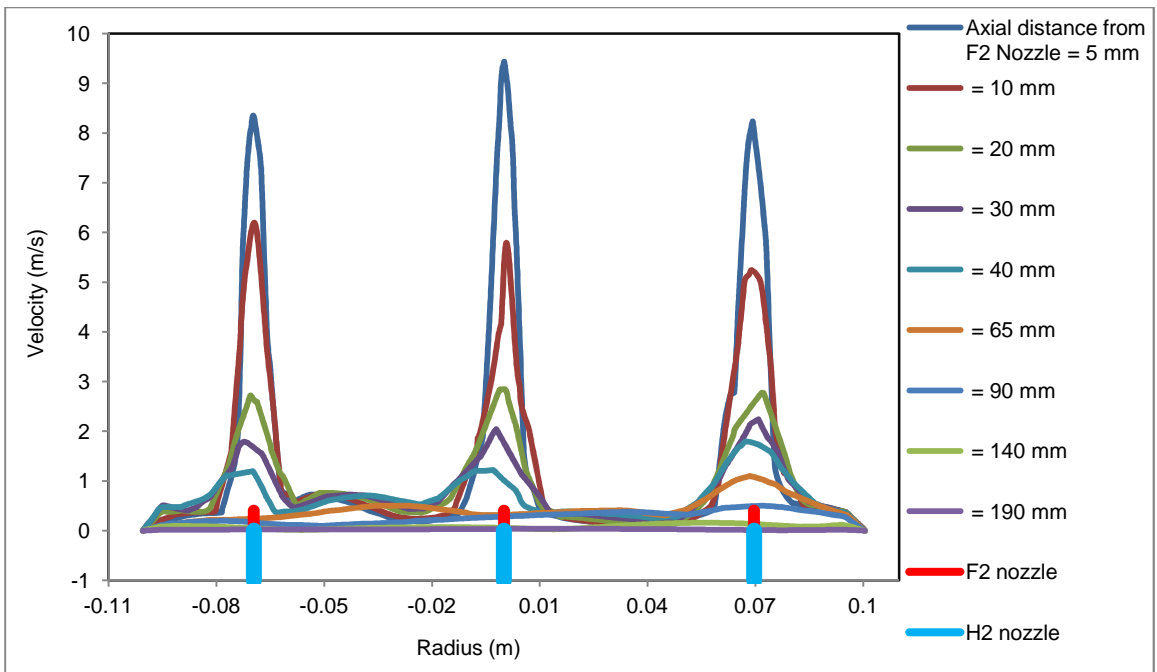


(b)

Figure 7.5: (a) Temperature and (b) velocity plots for the multiple nozzle scale-up reactor
(section at $z=0$ on x - y plane)



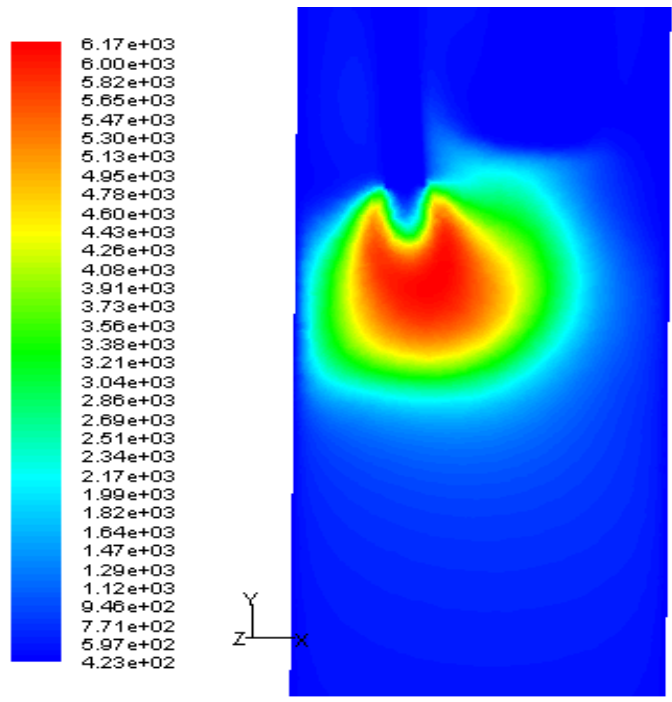
(a)



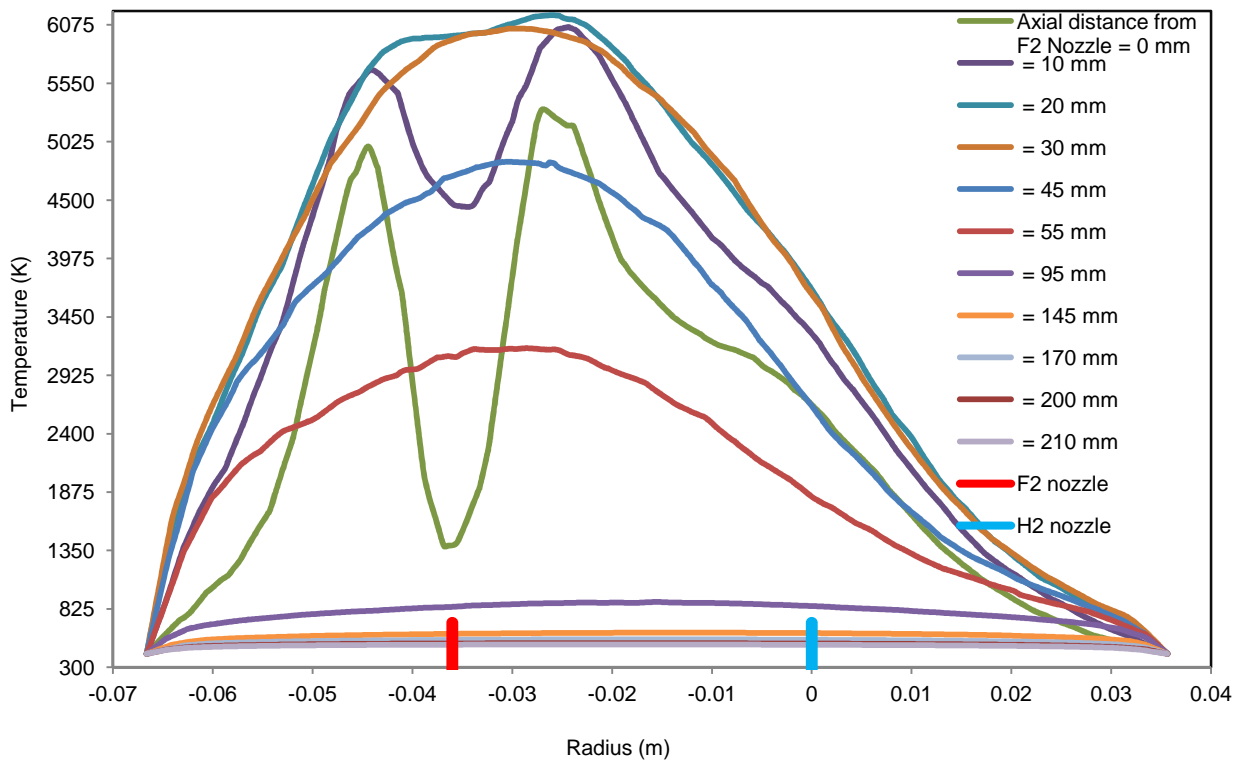
(b)

Figure 7.6: (a) Temperature and (b) velocity plots for the multiple nozzle scale-up reactor (section at $x=0$ on $y-z$ plane)

The other scale-up of the flame reactor is based on an equal Reynolds number at the feeding nozzle exit. The corresponding simulations have produced results as displayed in Figures 7.7 and 7.8. While maintaining the same Reynolds number with the higher gas flow rates in the scale up design, the fluorine stream velocity decreases by ~ 20% whereas the hydrogen velocity is reduced to ~90% of the original velocity in the VCR. The difference between the velocities of the two streams is also reduced. As a consequence, the observed flame is wider and small. The flame length is seen to be nearly 100 mm in comparison to ~150 mm seen in the benchmark case. The predicted flame temperature as shown in Figure 7.7 (a) is as high as 6170 K. This is far too more than the temperatures predicted in the multiple nozzle scale-up reactor (The maximum temperature predicted in the multiple nozzle reactor is ~4090 K). Figure 7.7 (b) suggests a significant fall in the reactor temperatures in the axial direction. The observed peak temperatures at a longitudinal distance of 30, 55 and 95 mm are 6040 K, 3160 K and 820 K respectively. There is almost a flat temperature profile at ~170 mm where the average reactor temperature is close to 550 K. Besides this, the figure also shows a higher temperature gradient near the reactor wall. This feature of the temperature distribution pattern is also not acceptable as it poses equipment safety concerns. The reduction in the peak velocity with axial distance can be seen from the velocity contour and the velocity plots in Figures 7.8 (a) and (b) respectively. The wavy nature of the velocity distribution pattern near the nozzle exit indicates the unstable region arising from inadequate mixing. The velocity pattern is not stabilized even up to a distance of 210 mm due to poor mixing at a lower velocity difference. The pattern beyond 210 mm could not be obtained because of the limitation on the computing machine.

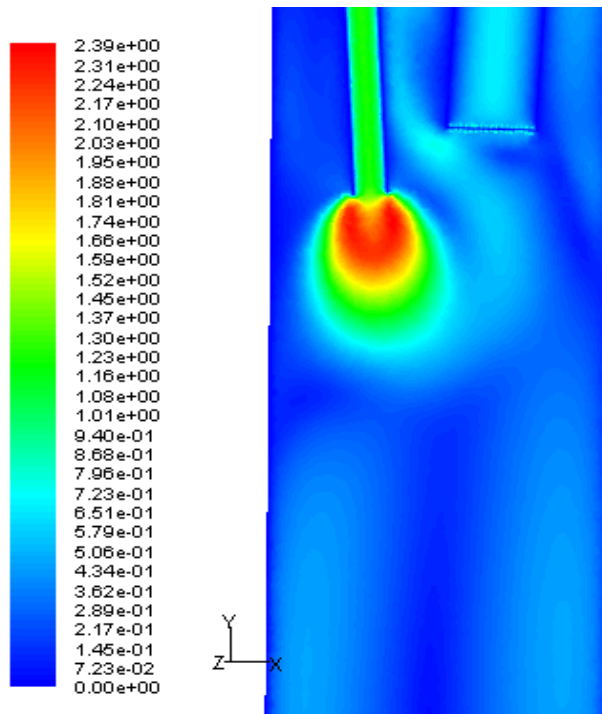


(a)

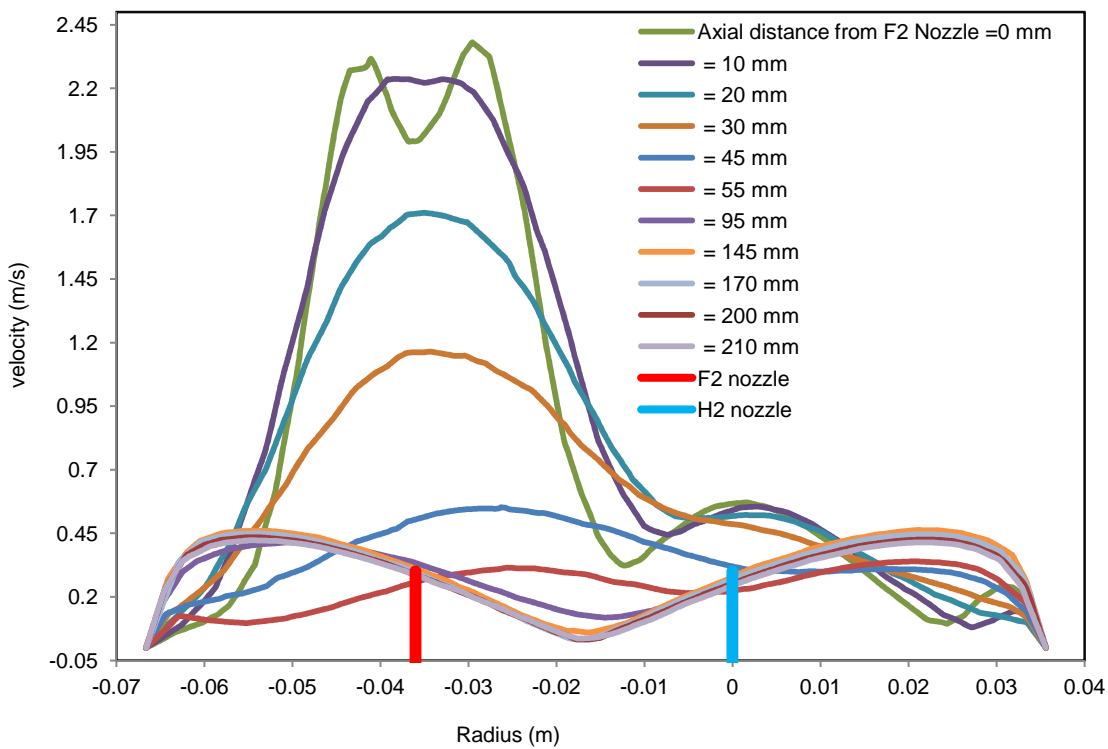


(b)

Figure 7.7: (a) Temperature contour and (b) Temperature plot for the scale-up reactor based on similar Reynolds no. at the nozzle exits



(a)

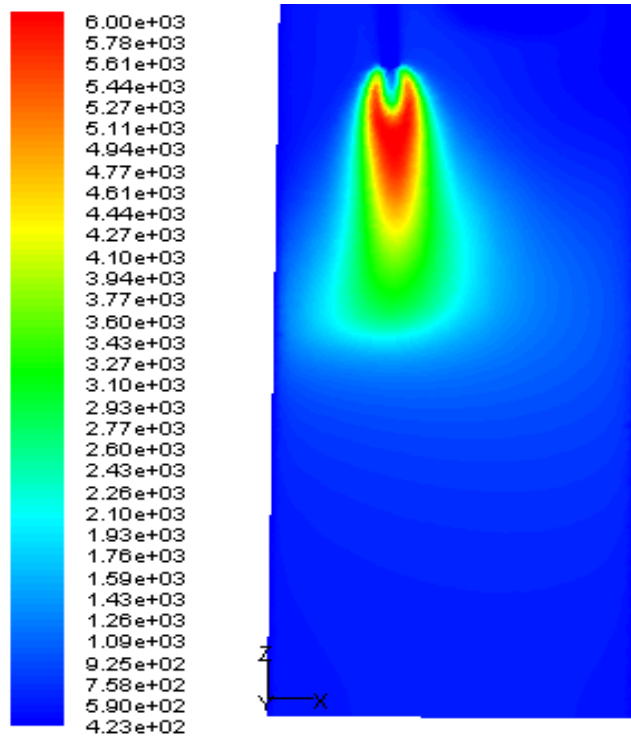


(b)

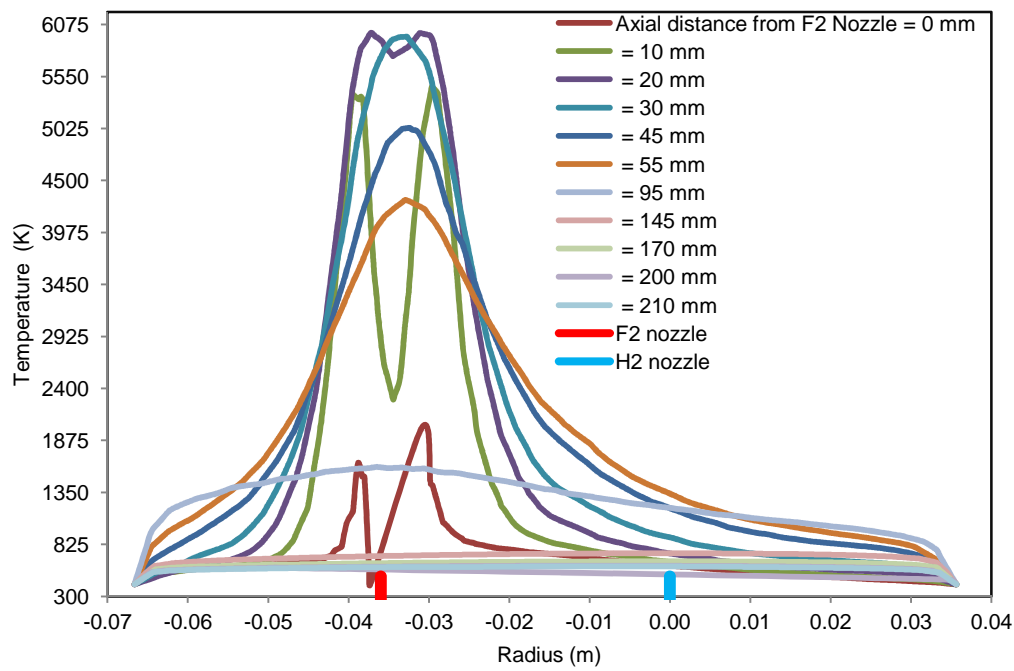
Figure 7.8: (a) Velocity contour and (b) Velocity plot for the scale-up reactor based on similar Reynolds no. at the nozzle exits

The next set of scale-up model considered for the simulations is based on maintaining similar velocities of the reactant gases at the nozzle exits. For the same reactant gas flow rates, the individual velocities as well as the difference between the velocities of the two streams in this case is higher as compared to the one based on the equal Reynolds number. Therefore, the temperature distribution pattern inside the reactor is expected to be different. The simulation results as obtained for this case are shown in Figures 7.9 and 7.10. While the maximum predicted reactor temperature is close to 6000 K (Figure 7.9 (a)), the temperature distribution pattern shown in Figure 7.9 (b) is different from the one shown earlier in the Figure 7.7 (b). The corresponding peak temperatures at a distance of 30, 55 and 95 mm in this case are 5935, 4300 and 1600 K respectively. The length of the flame increases due to the higher momentum carried by the gases and the heat is dissipated further downstream. That is why even at a distance of 180 mm from the fluorine nozzle the average reactor temperature is as high as 625 K. The longer and the narrower flame leads to a temperature distribution where the variation in the temperature near the wall is less sharp in comparison to the Figure 7.7 (b). The temperature plots, the velocity contour shown in Figure 7.10 (a) and the velocity plots shown in Figure 7.10 (b) also suggest a stretched out flame. As it follows from these figures, the range of the fluid velocities inside the reactor is higher than the previous case (Figure 7.8 (a) and (b)).

Furthermore, to meet the objective of dissipation of the reaction heat in a larger reactor volume so that a larger portion of the flame reactor has a higher temperature, nitrogen is added as a diluent in the fluorine stream. Nitrogen is effective in bringing down the higher reactor temperatures closer to the feed nozzles where formation of the flame takes place (section 6.7 of Chapter-6). The temperature predictions, when the fluorine stream is diluted with nitrogen to the extent of 50 % by volume, are seen in Figures 7.11 (a) and 7.11 (b). As expected, there is further increase in the length of the flame without any significant change in

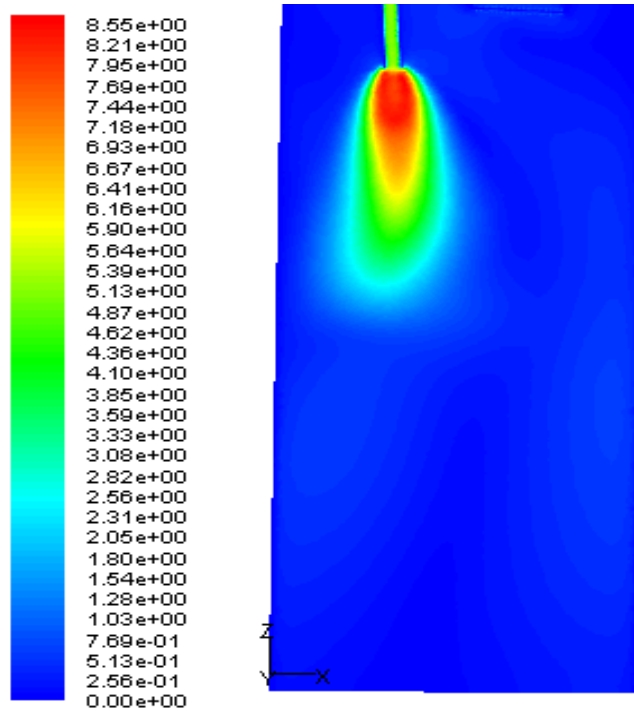


(a)

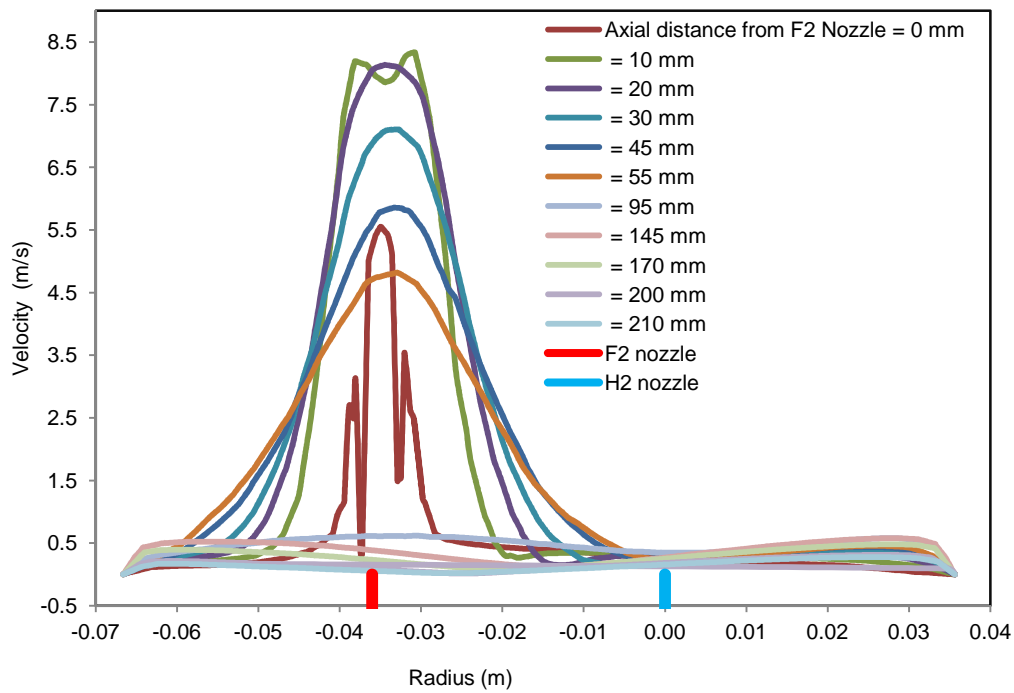


(b)

Figure 7.9: (a) Temperature contour and (b) Temperature plot for the scale-up reactor based on similar velocity at the nozzle exits

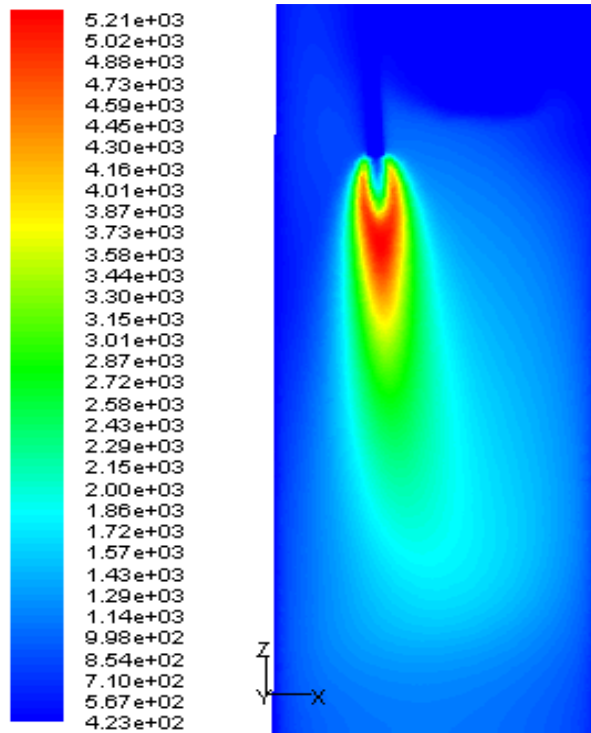


(a)

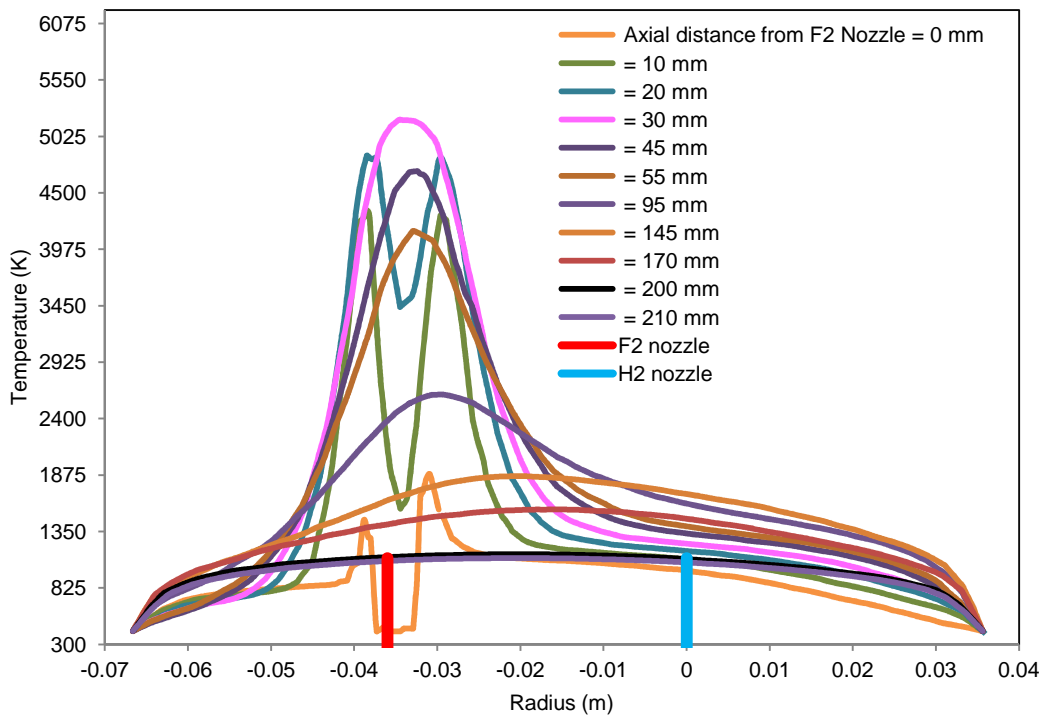


(b)

Figure 7.10: (a) Velocity contour and (b) velocity plots for the scale-up reactor based on similar velocity at the nozzle exit

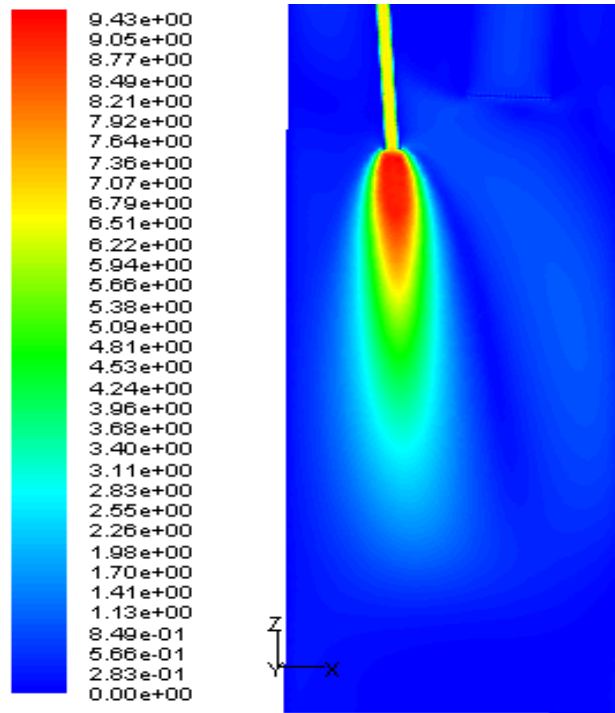


(a)

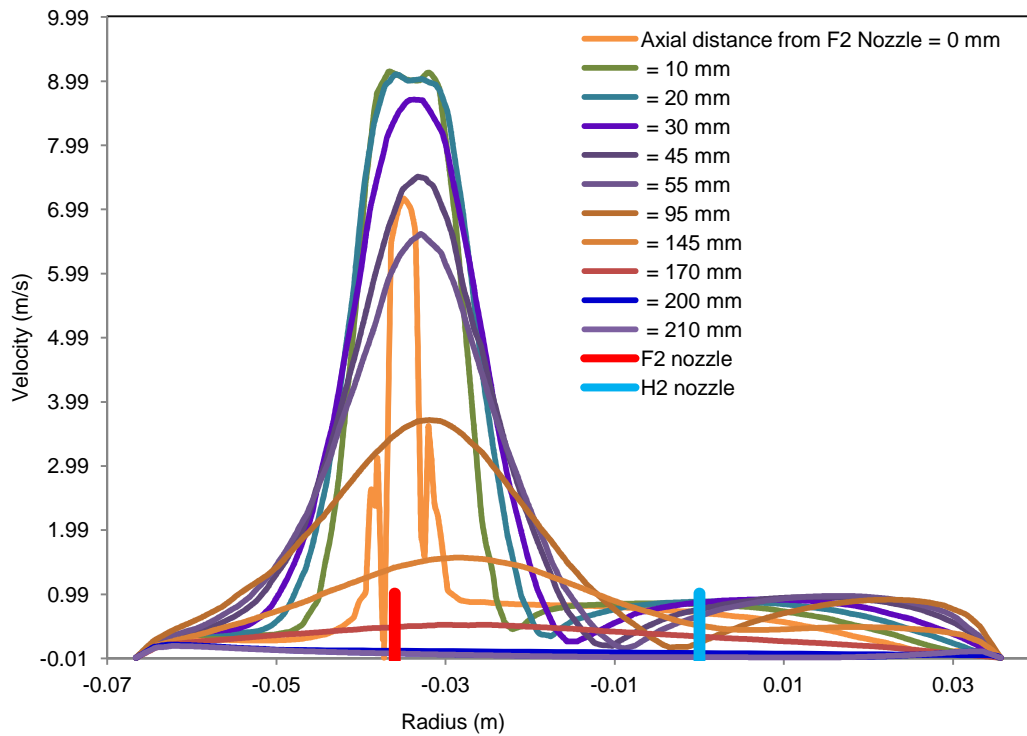


(b)

Figure 7.11: (a) Temperature contour and (b) Temperature plots for the scale-up reactor based on fluorine mixed with nitrogen as the diluent



(a)



(b)

Figure 7.12: (a) Velocity contour and (b) Velocity plots for the scale-up reactor based on fluorine mixed with nitrogen as the diluent

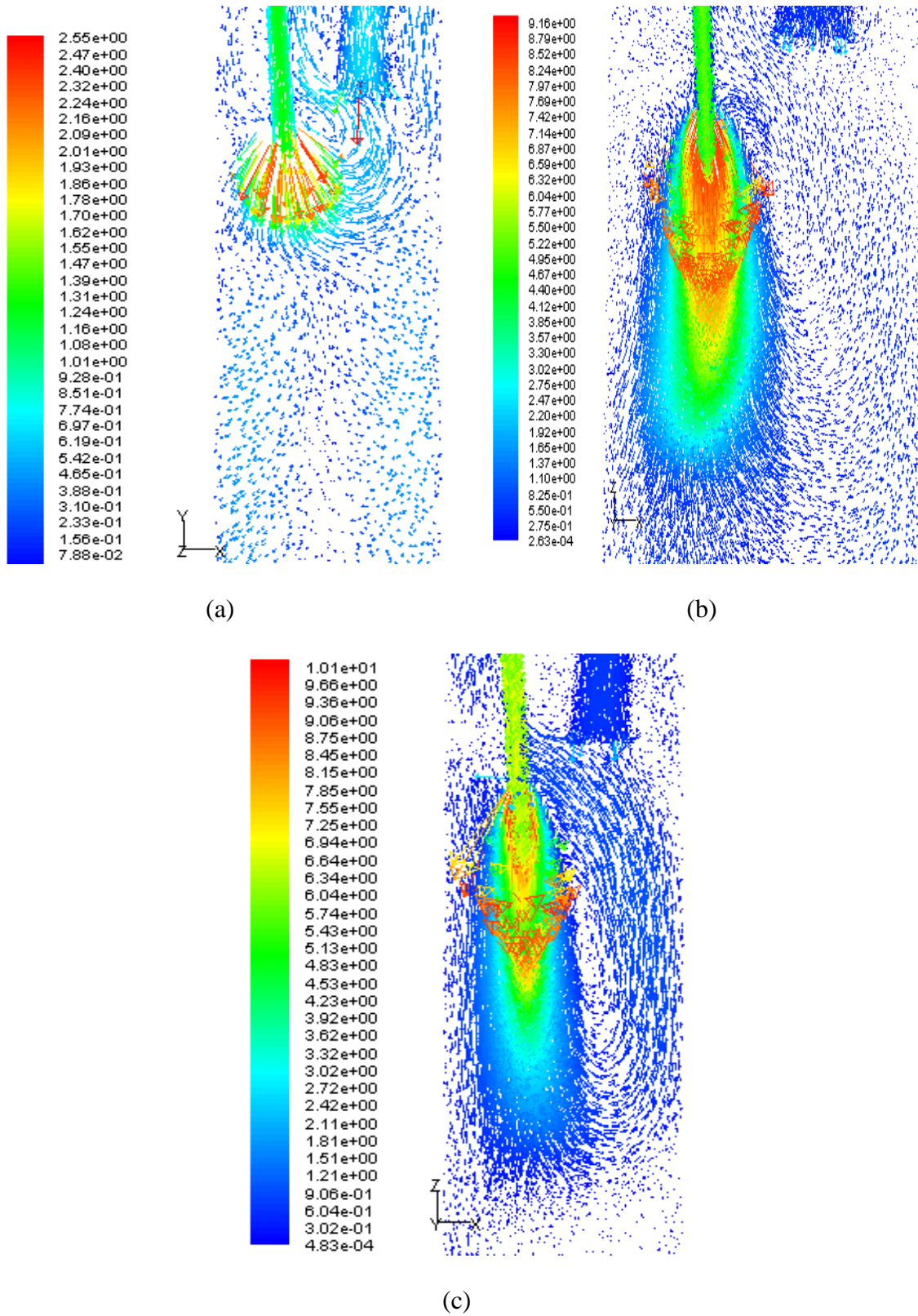


Figure 7.13: Vector plots for (a) Reynolds no. based, (b) Velocity based and (c) fluorine mixed with nitrogen as diluent based scale-up designs

its shape. While the reactor peak temperature decreases to ~ 5200 K from ~ 6000 K in the earlier case, a reactor temperature as high as 1100 K can be seen even at 210 mm from the feed nozzle (Figure 7.11 (b)). The temperatures near the reactor wall are also seen having values lower than the earlier cases. The unchanged shape of the flame and the increase in its length is further confirmed by the velocity contour shown in Figure 7.12 (a). The increase in the velocity as observed in Figure 7.12 (b) is evident because of an increase in the flow rate of the fluorine stream due to addition of nitrogen. Figure 7.13 shows the different recirculation patterns observed in the last three simulation cases, because of the lower velocities.

7.4 Conclusions

Three scale-up designs of the H₂-F₂ flame reactor have been simulated and the results are reported. While different criteria may be adopted for the feed nozzle design, similar enthalpy per unit reactor volume is the only basis considered for the reactor sizing. The length to diameter ratio of the reactor however, is decided based on the availability of the standard pipe size and the feasibility of the placement of the nozzle assemblies in the reactor. In the 'multiple nozzle assembly' model, overlapping of the flame boundaries and tilting of the flame towards the reactor wall can lead to a safety hazard. The reactor design based on the equal Reynolds no. at the nozzle exit leads to the formation of a wider and shorter flame, as a result of which there is a quick fall in the reactor temperatures along the length. The scale-up based on the similar velocities at the feeding nozzle exits yielded better results but needed some improvisation in order to extend the higher temperature regime in the reactor. This to some extent is achieved by addition of nitrogen in the fluorine stream.

During simulations, the length of the reactor has been limited to 210 mm due to the constraints on the computational machine. In principle, computational investigations with a

larger reactor length and different nozzle orientation (change in angle between the nozzles) can be carried out to see their effect on the reactor behaviour. During the simulation of the scale-up cases, the reactor wall temperature was fixed and therefore, the effect of ratio of inner surface area to volume of the reactor on the wall temperature is not seen. However, to maintain a constant wall temperature in flame reactors of different sizes, the amount of heat to be added or to be removed would depend on the flame geometry, the quantum of heat transferred from the flame to the wall and the reactor size. Validation of the simulation predictions with the experimental data in future will generate more confidence in the computational tool to verify new designs.

CHAPTER 8

SUMMARY AND CONCLUSIONS

A summary of the work carried out highlighting the major conclusions and the achievements is presented in this part of the thesis. The future studies as an extension to this work are also proposed in the end.

In the present thesis, an attempt has been made to assess the behaviour of a $\text{H}_2\text{-F}_2$ flame reactor by conducting experiments under various conditions. A CFD model of the flame reactor has been validated by the experimentally generated data. The CFD model is subsequently deployed to study the performance of the planned scale-up designs. A brief summary of the work followed by important conclusions and achievements is presented below.

8.1 Flame reactor: $\text{H}_2\text{-F}_2$ and $\text{H}_2\text{-O}_2$ systems

A flame reactor is a chemical reactor which provides heat energy in-situ to drive the chemical processes which require high temperatures. Some of the well known examples of chemical reactions which are used in a flame reactor include $\text{H}_2\text{-O}_2$ and $\text{H}_2\text{-F}_2$. In this work, the $\text{H}_2\text{-F}_2$ system has been chosen as the source of flame because i) the reaction is instantaneous and can take place even at ambient conditions, ii) it has higher enthalpy of reaction and iii) there is no oxide contamination of the final product. Besides $\text{H}_2\text{-F}_2$, a few other examples of exothermic reactions which can be used as source of heat in a chemical reactor are $\text{H}_2\text{-O}_2$, $\text{H}_2\text{-Br}_2$, $\text{H}_2\text{-Cl}_2$, methane-air, propane-air, etc. One similarity which exists between all of these systems is that the reaction is of chain type and the free radicals and/or active atoms produced by the initiation process become the chain carriers. The $\text{H}_2\text{-O}_2$ reaction in particular resembles the $\text{H}_2\text{-F}_2$ more, in the sense that both are highly exothermic and can lead to an explosion if not handled in a controlled way. The literature information on the reaction mechanism, the flammability limits, the detonation limits, the burning velocity, effect of excess oxygen, effect of dilution etc. has been summarized for the $\text{H}_2\text{-O}_2$ system. The reaction mechanisms of the $\text{H}_2\text{-F}_2$ reaction are proposed only by a few researchers. Since not much information is available on the $\text{H}_2\text{-F}_2$ reaction, a comparison between the two

systems has been useful to understand and plan the research work. Some distinct differences between the two systems are as follows.

- (1) The $\text{H}_2\text{-O}_2$ reaction requires ignition to start at ambient condition, whereas hydrogen reacts readily with fluorine.
- (2) Water vapour, the product of combustion of hydrogen in oxygen acts as a flame quencher as it absorbs a significant amount of heat energy liberated from the reaction flame. On the other hand, the product HF from the $\text{H}_2\text{-F}_2$ reaction, promotes the chain propagation by releasing energy during the process of de-excitation. This energy has also been used in producing lasing action in the HF chemical laser.
- (3) The thermodynamic equilibrium constant for $\text{H}_2\text{-F}_2$ reaction as computed is many orders higher than that of $\text{H}_2\text{-O}_2$ reaction. For example, the equilibrium constants for $\text{H}_2\text{-O}_2$ and $\text{H}_2\text{-F}_2$ reactions at 4500 K are 2.63 and 1.96×10^6 respectively.
- (4) The influence of oxygen as a diluent has been reported to be different in both the reaction schemes. While an increase in the oxygen content speeds up the rate of $\text{H}_2\text{-O}_2$ reaction, the rate of formation of HF reduces by addition of O_2 . This is due to the formation of stable radicals such as HO_2 and FO_2 which terminate the chain propagating steps.

Furthermore, the effect of different types of diluents has been studied on various systems such as methane-air, acetylene-oxygen and hydrogen-bromine. It is reported that the diluents not only affect the reaction system by virtue of their thermophysical properties but they may also cause production of more and more active species by participating in the breakdown of the reactant molecules into respective atoms. The diluents may also lead to the termination of the chain process by relaxation or recombination. In view of the contrasting

characteristics shown by the diluents, the dilution effect on the H_2-F_2 system was included as a part of study. The important conclusions are also listed later in this chapter.

8.2 Plan for safe conduct of experiments and range of experimental studies

The reaction between hydrogen and fluorine has been attempted at this scale (flow rate of fluorine up to 0.8 slpm) with almost no information in the literature, except that it is a chain reaction and could be dangerous if the excess heat is not removed from the reactor system. Theoretically, in a fuel-oxidizer system, the flame temperature is the maximum at the stoichiometric ratio. Since fluorine is more toxic and difficult to handle than hydrogen, the gas mixture was kept lean in fluorine in all the experiments. Initially, the experiments were carried out with a very high excess of hydrogen in the mixture to gain confidence in safe and smooth handling of toxic chemicals and conducting controlled experiments. Subsequently, the designed experiments for the parametric investigation of H_2-F_2 reaction were taken up. The experimental trials were carried out in two kinds of reactor, one being a flowing type vertical tubular reactor while the other one a horizontal cylindrical batch reactor. While the effects of excess flow of hydrogen, the flow rate of fluorine, the feed gas temperature, the reactor wall temperature and the dilution were studied in the flowing type reactor, the transient studies were carried out to see the influence of hydrogen to fluorine ratio and the type of diluent on the behaviour of H_2-F_2 reaction in a batch reactor. The diluents chosen for the study of effect of dilution were helium, nitrogen and argon. In the batch reactor, the studies with these inerts were carried out at two different initial pressures while maintaining a similar molar ratio of the gases. Table 8.1 shows the summary of the range of parameters for which the experimental investigations were conducted in the two types of reactors.

Table 8.1

Summary of experimental investigations

Type of reactor	Type of study	Range of parameter
Flowing type reactor, VCR*	Effect of excess of hydrogen	Flow rate of F ₂ : 0.2 to 0.4 slpm Flow rate of H ₂ : 0.63 to 2.54 slpm
	Effect of addition of nitrogen	Flow rate of F ₂ : 0.2 to 0.4 slpm Flow rate of H ₂ : 0.85 to 1.7 slpm Flow rate of N ₂ : 0.4 to 3.4 slpm
	Effect of preheating	Flow rate of F ₂ : 0.2 to 0.4 slpm Flow rate of H ₂ : 0.85 to 1.7 slpm Feed gas temperature: from 298 K to 423 K Reactor wall temperature: from 298 K to 423 K
	Effect of flow rate of fluorine	Flow rate of F ₂ : 0.4 to 0.8 slpm Flow rate of H ₂ : 1.6 to 3.2 slpm
	Effect of addition of a diluent (He, N ₂ and Ar) in a flowing type reactor	Flow rate of F ₂ : 0.5 slpm Flow rate of H ₂ : 2 slpm Flow rate of diluents (He, N ₂ , Ar): 0 to 3 slpm
Batch reactor, HCR**	Generation of temperature curve	Fluorine composition in the mixture of hydrogen and fluorine: 16.7% to 89.1% (v/v)
	Effect of type and quantity of diluents (He, N ₂ and Ar) on H ₂ -F ₂ reaction in a	Higher initial pressure Diluent % (mole basis): 0 to 42.86 Lower initial pressure Diluent % (mole basis): 0 to 83.33

	flame in a batch reactor	
--	--------------------------	--

*VCR: Vertical Cylindrical Reactor (flow reactor)

**HCR: Horizontal Cylindrical Reactor (batch reactor)

Adequate safety precautions had been taken at the design stage and during operation. The integrity of the set up components such as piping, valves and instruments had been checked thoroughly during the installation. The leak tightness and the control adequacy had been ensured each time before taking up an experimental trial. Further, engineered safety features such as adequate ventilation, installation of the gas detectors and periodic surveillance have been adopted to ensure the personnel safety during operation. The process instruments such as thermosensors, pressure transmitters, pressure switches and flowmeters used in the facility are of superior quality and are calibrated at periodic intervals. The selection of the thermosensors and the pressure transmitters has been such that they are quick to response and are compatible with the fluoride gases. The thermocouples have been placed inside the reactor in different directions such that, a broad picture of the reaction flame can be inferred during the experiments. The flow rates of gases and the reactor wall temperature were controlled by tuned PID controllers. Sufficient process interlocks and the safety trips had been implemented to provide inherent safety in the system. Since the reaction between the two gases is potentially explosive, the manpower has been adequately trained and a thoroughly planned sequence of operation has been followed. The manual operation/control using indicators and manual controllers has been avoided and instead a programmable logic based control has been incorporated in the system. The experiments have been conducted from a remote location (control room) using the SCADA mimic and the data has been stored in the operating console. The experimental results and the important conclusions are discussed in the later section.

8.3 CFD modeling of the flame reactor

In order to comprehensively model the behaviour of the H₂-F₂ flame reactor under the influence of several parameters discussed above, a CFD tool has been adapted. Instead of developing a numerical model ab initio from the governing equations of mass, momentum, energy and species balance, it has been decided to deploy the commercially available 'FLUENT' as the CFD tool. The segregated solver approach had been used to solve the discretized conservation equations. The selection of the grid size and the computational models has been based on the physics of the problem, available resources of the computing machines and the time required to run the simulations.

The CFD simulations have been carried out on a variety of parameters to study the effect of flow ratio, preheating of gases, inclusion of diluents etc., to check the diversity of the application of the software tool. The in-situ release of large amount of heat energy and a huge difference in the temperatures within the reactor during hydrogen-fluorine reaction creates turbulence inside the reactor. Therefore, though individual stream flow before the start of the reaction was in laminar regime, the turbulence model had been considered in the reactor domain during simulations. As the kinetics of the hydrogen-fluorine reaction is fast, the eddy dissipation model instead of the finite kinetic model had been chosen for the species distribution. The enthalpy of the reaction had been included as the source term in the energy balance equation. The grid independence test had also been carried out to rule out any effect of the grid size on the simulation results.

The temperature data from the experiments have been used to validate the computational model and fine-tune the commercially available CFD tool to emulate the practical observations. The assumption made for the simulation, that is, the reaction between hydrogen and fluorine is instantaneous and the flow field is turbulent has produced results

which match well with the experimental observations. The major parameters of the CFD modeling adopted in the report work are as given in Table 8.2.

Table 8.2
Details of CFD modeling

Title	Details
Type of mesh	<ul style="list-style-type: none"> • Unstructured meshing using GAMBIT 2.2.30. • Near the feed nozzles: tetrahedral meshes (1 mm size) • Away from the feed nozzles: hexahedral meshes (1.5 mm size)
No. of cells	$\sim 2.3 \times 10^6$
Type of solver	3D, Segregated, Implicit, Steady State (FLUENT 6.3)
Type of flows	Incompressible and Turbulent
Type of turbulent model	k- ϵ (standard) model
Viscous heating	Not considered
Buoyancy effects	Considered
Heat transfer	Convective diffusion
Species transport	Eddy dissipation model
Fluid properties	Standard database
Inlet boundary condition	Mass flow inlet at both the feed nozzles, temperature of the feed gases

Wall boundary condition	Constant temperature, no-slip condition at the wall
Exit boundary condition	Outflow
Operating conditions	
Pressure	101325 Pa
Acceleration due to gravity	9.81 m/s ²
Solution controls	
Under relaxation factors	
Pressure	0.3
Momentum	0.7
Turbulent kinetic energy, k	0.8
Turbulent dissipation rate, ϵ	0.8
Density, Body forces	1
Discretization	
Pressure	Standard
Pressure-velocity coupling	SIMPLE
Momentum, k, ϵ	First order upwind

The salient conclusions from the computational simulations are summarized later in this chapter.

8.4 Performance analysis of scale-up designs

In an attempt to evolve a combination of the nozzle and the reactor design for a prescribed scale up ratio which offers a favourable reactor temperature profile and simultaneously assures the equipment safety, simulations have been carried out on three

different design approaches and the results have been analyzed. One of the cases, case 82 (details as given in the Table 3.9 of Chapter 3), investigated earlier has been chosen as the benchmark case for scaling up to a factor of five. The simulations have been carried out by the validated CFD model of earlier studies. Overlapping of the flame boundaries and bending of the flame towards the reactor wall has been seen in the ‘multiple nozzle assembly’ model where the scale up is achieved by having as many feeding nozzle assemblies as required for the desired scale-up. The flame reaching the reactor wall may result in damage of the equipment and pose safety hazards. The reactor design based on similar Reynolds no. at the nozzle exit leads to the formation of a wider and shorter flame, as a consequence of which there is a rapid fall in the reactor temperatures in the longitudinal direction. The scale-up based on the equal feeding velocities has given better results. The higher temperature region inside the reactor has been further extended by addition of nitrogen in the fluorine stream.

8.5 Important conclusions

8.5.1 Experimental investigations

The important conclusions drawn from the experimental component of this work are as follows:

- (1) The reaction between hydrogen and fluorine takes place even at room temperature forming a reaction flame.
- (2) The flame is formed in front of the nozzle feeding fluorine but a little away from its tip. There is a relatively lower temperature zone at the nozzle exit due to insufficient concentration of hydrogen present there. The fact that the feeding nozzles have been clean and intact even after a number of trials further confirms this observation.

- (3) For a given flow rate of fluorine, an increase in the quantity of hydrogen reduces the near nozzle reactor temperatures by virtue of its excellent heat transfer characteristics. Simultaneously, there is a rise in the reactor temperatures little away from the feed nozzles due to improved heat dissipation. This effect however is not visible at higher ratios ($> 400\%$ stoichiometric excess of hydrogen) when hydrogen acts more as a heat sink than a heat dissipater.
- (4) For a given ratio of fluorine to hydrogen, the reactor temperatures increase with increase in the fluorine flow rate. However, a larger fraction of the reaction heat is lost through the reactor walls at higher flow rates of the fluorine stream. This is because of the enhanced convective heat transfer at higher flow rates of the reacting species.
- (5) The preheating of the reactant gases, namely, hydrogen and fluorine has a marginal effect on the H_2-F_2 reaction because i) the activation energy required for the reaction is low and ii) the heat given to the gases is small as compared to the reaction enthalpy. Conversely, a change in the wall temperature has a pronounced effect on the distribution of the reactor temperatures. A higher wall temperature reduces the radial heat transfer by reducing the driving force between the source of heat (reaction flame) and the heat sink (reactor wall) resulting in a relatively uniform reactor temperature profile.
- (6) The reaction between hydrogen and fluorine, for all practical reasons, can be considered as an irreversible reaction because the equilibrium conversion at 5000 K is nearly one.
- (7) The composition-temperature curve for hydrogen-fluorine reaction has been experimentally generated, and as expected, it is found to be lower in the regions of lean and rich concentrations of fluorine in the mixture. The maximum temperature

however has been seen at 53% hydrogen in the mixture and not at the stoichiometric ratio. This observation is similar to the behaviour shown by the H₂-Air system where the maximum temperature is reported at 31.6% hydrogen in the mixture instead of 29.6%, the stoichiometric composition.

- (8) In a batch reactor, at higher operating pressure, the order of effectiveness of diluents in reducing the reactor temperature has been found to be N₂>He>Ar instead of N₂>Ar>He for other systems. The reason for the higher reactor temperature observed with argon than helium is attributed to its effect on the flame geometry and the reaction kinetics.
- (9) At lower operating pressure however, the order of effectiveness changes to Ar>N₂>He, which suggests that the thermophysical properties of the diluents dominate over their possible role in the kinetics at lower pressures.
- (10) In the case of a flowing type reactor, the diluents cause a significant decrease in the temperatures near the fluorine feed nozzle consequently reducing the thermally induced fluid velocities. At lower concentrations, helium has been more effective as a diluent when the diffusive heat transport dominates over the mixing effects. At higher concentrations however, argon and nitrogen have been more effective in dispersing the reaction sites and changing the pattern of the temperature distribution in the reactor.

8.5.2 Computational investigations

Some of the important features of the developed simulation tool and the important conclusions from the computational investigations are as given below.

- (1) The k-ε model for turbulence and eddy dissipation model for species transport work well to simulate those chemical reactions which are fast and highly exothermic.

- (2) In the given reactor geometry, a grid size of 1 mm near the feed nozzles and 1.5 mm away from them has given satisfactory results saving computation time significantly.
- (3) The effect of radiation on the energy balance modeling has not been found to be crucial and can be safely ignored to reduce the expense on simulations. A narrow flame having low emissivity value contributes poorly towards the radiative heat transfer in the system.
- (4) The simulated flame is seen to be narrow and is formed in front of the fluorine nozzle. The region near the feed nozzles has velocity higher than the average nozzle exit velocity due to higher temperatures.
- (5) For the flow rates of F_2 and the reactor geometry selected in this work, only a small proportion of the flame heat reaches the reactor wall. This is largely due to poor radiative heat transfer from the reaction flame to the reactor boundary.
- (6) The computational results have been able to capture the pattern of effect of various parameters on the reactor temperatures. The utility of the CFD tool and the chosen CFD models has been proven by validating the simulation results with the practical data under varying scenarios.

8.6 Major contributions

The major achievements of the present work are listed as follows:

- (1) The H_2 - F_2 experiments in a relatively large scale have been carried out in a safe and controlled manner. The flow rate of the fluorine stream has been varied from 0.2 slpm to 0.8 slpm in a tubular reactor of 52.5 mm internal diameter.
- (2) The reactor temperatures as high as 1800 K have been measured inside the reactor. The temperatures mapped inside the reactor are used to validate a CFD tool and the computational models chosen in it.

- (3) The effect of parameters such as the excess of hydrogen, the fluorine flow rates, the reactant preheating and the temperature of the reactor wall on the behaviour of the H₂-F₂ flame reactor are experimentally studied and computationally predicted with a good match between the two.
- (4) That the maximum temperature would occur when the mixture of hydrogen and fluorine is slightly rich with hydrogen (with respect to the stoichiometric ratio) has been found experimentally.
- (5) It is established that the behaviour of a H₂-F₂ flame reactor under the influence of diluents is affected by the level of operating pressure. It has been found that the probability of diluents affecting the reaction kinetics is more at higher pressure and the concentration of a diluent is also one of the important factors which affects the temperature distribution inside a flame reactor.
- (6) A CFD tool is fine-tuned and the simulations are carried out which predict temperatures that are very close to the experimental values. The tool thus developed can be used for any future endeavour.
- (7) Three different scale-up reactor designs have been simulated giving out important clues for a future action.

8.7 Future work

Although many unattended areas hitherto have been investigated, the followings may be suggested as an extension to the reported work.

- (1) With safety concerns in mind, the reactor wall preheating has been limited to 423 K during the experiments. As wall heating has shown a significant effect on the reactor temperature distribution, it will be meaningful to simulate a few more cases to assess the reactor behaviour when the wall is heated to still higher temperatures.

- (2) Due to severe corrosion problems in the presence of gases such as fluorine and hydrogen fluoride and a very high temperature region within the reaction zone, it has not been possible to portray a complete picture of the H₂-F₂ reaction flame. A few advanced techniques may be explored to map the temperature profile of the flame under the hostile atmosphere in the reactor.
- (3) In combustion, the effect of pressure at higher and lower equivalence ratios is more, as there is less dissociation at these ratios. Having carried out the investigations related to the effect of diluents at two pressure levels, namely, 800 and 100 mbar, and getting different results in both of them, it is worthwhile to conduct a few more studies covering a wider range of operating pressure.
- (4) The diluents affect the thermal behavior of H₂-F₂ flame reactor not only because of their thermophysical properties but also take part in the reaction kinetics through the process of collision, relaxation and recombination. Comprehensive analysis of the product gases such as by spectroscopy may provide useful hints on the participating reaction steps and their kinetics in the hydrogen-fluorine reaction scheme.
- (5) Computational simulation of the batch reactor has not been attempted in this work. The CFD modeling of a fuel-oxidizer reaction in a static system can contribute to an all inclusive understanding of such complex systems.
- (6) The CFD simulation on a few more scale-up cases with different feed nozzle orientation may be carried out to see its effect on the reactor behaviour. It would be better if the results from these simulations are verified by the experimental data from the large scale set-up.

The results and the data extracted from these efforts will be useful in enhancing the scope of scientific developments in the field of combustion science and technology.

REFERENCES

1. Agueda, A.; Pastor, E; Perez, Y. and Planas, E. (2010) Experimental study of the emissivity of flames resulting from the combustion of forest fuels. *International Journal of Thermal Sciences*, 49, 543-554.
2. Babushok, V.; Noto, T.; Burges, D.R.F.; Hamins, A. and Tsang, W. (1996) Influence of CF_3I , CF_3Br , and CF_3H on the high-temperature combustion of methane. *Combustion and Flame*, 107 (4) 351-367.
3. Basov, N.G.; Kulakov, L.V.; Markin, E.P.; Nikitin, A.I. and Oreavskii, A.N. (1969) Emission spectrum of a chemical laser using $\text{H}_2\text{-F}_2$ mixture. *ZhETF Pisva Red*, 9, 613.
4. Bergthorson, J.M.; Johnson, M.B.; Bonanos, A.M.; Slessor, M.; Wei-Jen Su and Dimotakis, P.E. (2009) Molecular mixing and flowfield measurements in a recirculating shear flow. Part I: Subsonic flow. *Flow Turbulence Combust*, 83:269–292.
5. Bird, R.B.; Stewart, W.E. and Lightfoot, E.N. (1994) *Transport Phenomena*. John Wiley and Sons, Singapore.
6. Brokaw R. S. (1965_a) A suggested mechanism for the hydrogen-fluorine reaction. *The Journal of Physical Chemistry*, 69, 2488-2489.
7. Brokaw R. S. (1965_b) A suggested mechanism for the hydrogen-fluorine reaction. II. The oxygen – inhibited reaction. *The Journal of Physical Chemistry*, 69, 2808-2809.

8. Chen, Hao-Lin; Daugherty, J. D.; and Fyfe, W. (1975) TA5-H₂/F₂ flame propagation and repetitively pulsed hydrogen fluoride (HF) chain-reaction chemical laser, *IEEE Journal of Quantum Electronics*, QE-11 (8), 648-653.
9. Chen, R. H. and Driscoll, J. F. (1990) Nitric oxide levels of jet diffusion flames: Effects of coaxial air and other mixing parameters. *Twenty-third Symposium (International) on Combustion*, pp. 281–288.
10. Cheng, R.K. and Oppenheim, A.K. (1984) Autoignition in methane-hydrogen mixtures. *Combustion and Flame*, 58, 125-139.
11. Clingman, W.H.; Brokaw, R.S. and Pease, R.N. (1953) Burning velocities of methane with nitrogen-oxygen, argon-oxygen and helium-oxygen mixtures. 4th *Symposium on Combustion*, Williams and Wilkins Co., Baltimore, 310-313.
12. Cummings, J.C.; Broadwell, J.E.; Shackelford, W.L.; Witte, A.B.; Trost, J.E. and Emanuel G. (1977) H₂-F₂ chain rate investigation. *J. Quant. Spectrosc. Radiat. Transfer*, 17, 97-116.
13. Das, L.M. (1996) Hydrogen-oxygen reaction mechanism and its implication to hydrogen engine combustion. *International J, Hydrogen Energy*, 21 (8), 703-715.
14. David, W.T. and Mann, J. (1942) Influence of water vapour on flame gas temperature. *Nature*, 150 (3809), 521.
15. Dimotakis, P.E. and Hall, J.L. (1987) A simple model for finite chemical kinetics analysis of supersonic turbulent shear layer combustion. *AIAA/SAE/ASME/ASEE, 23rd joint propulsion meeting*, paper 87-1879.
16. Drell I.L.; Belles, F.E. (1957) Survey of hydrogen combustion properties. Report 1383-National Advisory Committee for Aeronautics.

17. Egolfopoulos, F.N.; Dimotakis, P.E.; Bond, C.L. (1996) On strained flames with hypergolic reactants: the $\text{H}_2/\text{NO}/\text{F}_2$ system in high-speed, supersonic and subsonic mixing-layer combustion. *Proc. Combust. Inst.* 26, 2885–2893.
18. Eyring, H. and Kassel, L. (1933) The homogeneous reaction between hydrogen and Fluorine. *J. American Chemical Society*, 55, 2796.
19. Fackler, K. B.; Karalus, M.F.; Novosselov, I.V.; Kramlich, J.C. and Malte, P.C. (2011) Experimental and Numerical Study of NO_x Formation From the Lean Premixed Combustion of CH_4 Mixed With CO_2 and N_2 . *J. Eng. Gas Turbines Power*, 133 (12).
20. Feng, Liang; Liu, Z.; Li, Y. (2010) Numerical study of methane and air combustion inside a small tube with an axial temperature gradient at the wall. *Applied Thermal Engineering*, 30, 2804-2807
21. Fluent Inc. user guide, (2003) Using the solver. Chapter 24.
22. Foon, R; Kaufman, M. (1975) A review report. *Progress in Reaction Kinetics*, 8 (2), 81-160.
23. Frank, K. Truby (1978) Spontaneous explosions in multi atmosphere $\text{H}_2\text{-F}_2\text{-O}_2$ mixtures. *Journal of Applied Physics*, 49, 3481.
24. Galkin, N.P.; Sudarikov, B.N. (edited) (1964) *Technology of uranium*, Atomizdat.
25. Galkin, N. P.; Sudarikov, N. and Zaitsev, V. A. (1961) Methods of reducing uranium hexafluoride. Translated from *Atomnaya Energiya*, Vol. 10, No. 2, pp. 149-155.
26. Glassman, I. (1986) *Combustion*. Academic Press Inc.

27. Grosse, A.V. and Kirshenbaum, A.D. (1955) The premixed H_2-F_2 flame and its burning velocity. *J. of American Chemical Society*, 77, 5012-5013.
28. Hablani, H.B. and Simmons, F. S. (1967) "Infrared spectroscopic study of hydrogen- fluorine flames." *AIAA Journal*, Vol. 5, No. 4, pp. 778-786.
29. Hahn, D.W.; Bui-Pham, M.N. and Meeks, E. (1997) Modeling analysis for the optimization of diamond deposition in a stagnation-flow flame reactor. *Combustion Science and Technology*, 126 (1-6), 175-199.
30. Hanser, A. D.; Wolden, C. A.; Perry, W. G.; Zheleva, T.; Carlson, E. P.; Banks, A. D.; Therrien, R. J. and Davis, R. F. (2007) Analysis of reactor geometry and diluent gas flow effects on the metalorganic vapor phase epitaxy of AlN and GaN thin films on $\alpha(6H)$ -SiC substrates. *J. of Electronic Materials*, 27 (4), 238-245.
31. Harrison. (1960) *Handbook of chemistry and physics*, p.1882-1915, p.1919-1921, 42nd ed.
32. Henkes, R. A. W. M.; Van der Flugt, F. F. and Hoogendoorn, C. J. (1991) Natural convection flow in a square cavity calculated with low Reynolds number turbulence models. *Int. J. of Heat and Mass Transfer*, 34, 1543-1557.
33. Hermanson, J.C.; Dimotakis, P.E. (1989) Effects of heat release in a turbulent, reacting shear layer. *J. Fluid Mechanics*, 199, 333-375.
34. Hess, L.D. (1972) HF chemical laser studies: Use of MOF_6 to increase reaction rates in H_2-F_2 mixtures. *Journal of Applied Physics*, 43 (3), 1157.
35. Hinze, J.O. (1975) *Turbulence*. McGraw-Hill Publishing Co., New York.

36. Huffstutler, M.C.; Rode, J.A.; Anderson R.C. (1955) Effect of diluents on burning velocities in hydrogen-bromine mixtures. *Journal of the American Chemical Society*, 77 (3), 809-810.
37. IAEA-TECDOC-1115 (1999) Minimization of waste from uranium purification, enrichment and fuel fabrication. International Atomic Energy Agency, ISSN 1011-4289 (Total 48 pages)
38. Isachenko, V.P.; Osipova, V.A. and Sukomel A.S. (1977) Heat Transfer. Mir Publishers Moscow, third edition.
39. Jang, H. D. (1999) Generation of silica nanoparticles from tetraethylorthosilicate (TEOS) vapor in a diffusion flame. *Aerosol Science and Technology*, 30, 477-488.
40. Jangsawang, W.; Fungtammasan, B.; Kerdsuwan, S.(2005) Effects of operating parameters on the combustion of medical waste in a controlled air incinerator. *Energy Conversion and Management*, 46, 3137-3149.
41. Jones, G.W.; Lewis, Bernard and Seaman, Henry (1931) The flame temperatures of mixtures of methane oxygen and methane acetylene with air. *Journal of the American Chemical Society*, 53 (11), 3992-4001.
42. Kapralova, G. A.; Trofimova, E .M.; Chaikin, A.M. (1976) Chain branching in the fluorine-hydrogen reaction. *Reaction Kinetics and Catalysis Letters*, 4(3), 381-387.
43. Kani, Y.; Sasahira, A.; Kuniyoshi, H. and Kawamura F. (2009) New reprocessing system for spent nuclear reactor fuel using fluoride volatility method. *Journal of Fluorine Chemistry*, 130, 74-82.

44. Kaye, S. (1961) Flat Flame Burner for Burning Undiluted Premixed Hydrogen and Fluorine. *Review of Scientific Instruments*, 32(8), 965.
45. Kim, Sung-Ho; Cho, Ung-In. (1994) Theoretical investigation on the effects of additive oxygen in HF chemical laser performance. *Bull. Korean Chem. Soc.*, 15(9), 724-729.
46. Kobayashi, H.; Amano, O.; Kawamura, F; Aoi, M; Hoshino, K; Sasahira, A and Kani Y. (2005) Fluorex Reprocessing System for the Thermal Reactors Cycle and Future Thermal/Fast Reactors (Coexistence) Cycle. *Progress in Nuclear Energy*, 47 (1-4), 380-388.
47. Koroll; G.W., Mulpuru; S.R. (1986) The effect of dilution with steam on the burning velocity and structure of premixed hydrogen flames. Twenty first symposium (International) on combustion/ The combustion institute, 1811-1819.
48. Kuehl, D.K. (1962) Effects of water on the burning velocity of hydrogen-air flames. *Am. Rock. Soc. J.*, 32, 1724.
49. Langan, J.G.; Beck, S.E.; Felker, B.S. and Rynders, S.W. (1996) The role of diluents in electronegative fluorinated gas discharge. *Journal of Applied Physics*, 79 (8), 3886-3894.
50. Launder, B.E. and Spalding, D. B. (1972) *Lectures in Mathematical Models of Turbulence*. Academic Press, London, England.
51. Lavroskii et al. (1959) *Transactions of the Second International Conference on the Peaceful Uses of Atomic Energy (Geneva, 1958)*. Atomic Energy Press (Moscow). *Selected Reports of non-Soviet Scientists*. Vol. 7, p. 615.

52. Levy J. B.; Copeland B. K. W. (1963) The kinetics of the hydrogen-fluorine reaction-I. Magnesium reactor. *J. Phys. Chem.*, 67, 2156.
53. Levy J. B.; Copeland B. K. W. (1965) The kinetics of the hydrogen-fluorine reaction-II. The oxygen inhibited reaction. *J. Phys. Chem.*, 69, 408.
54. Levy J. B.; Copeland B. K. W. (1968) The kinetics of the hydrogen-fluorine reaction-III. The photochemical reaction. *J. Phys. Chem.*, 72(9), 3168-3177.
55. Lewis B.; Elbe G.V. (1961) *Combustion, flames and explosions of gases*, second edition. Academic Press Inc. New York.
56. Liu Y. and Most Jean-Michel. (2009) Effects of diluents on the behaviour of the diluted combustion regime. European Combustion Meeting, VUT, Vienna, Austria, 14-17 April.
57. Magnussen, B. F. (1981) On the structure of turbulence and a generalized eddy dissipation concept for chemical reaction in turbulent Flow. 19th AIAA Meeting, St. Louis.
58. Magnussen, B. F. and Hjertager, B. H. (1976) On mathematical models of turbulent combustion with special emphasis on soot formation and combustion. 16th International Symposium on Combustion, The Combustion Institute.
59. Mellish, C. E. and J. W. Linnett. (1953) The influence of inert gases on some flame phenomena." Proceedings of the 4th Symposium (International) Combustion, Baltimore, MD: pp. 407-420.
60. Millikan, R.C. and White, D.R.. (1963) Systematics of vibrational relaxation. *Journal of Chemical Physics*, 39, 3209.

61. Mishra, D.P.; Kumar, P. (2008) Experimental investigations of laminar LPG-H₂ jet diffusion flame with preheated reactants. *Fuel*, 87 (13-14), 3091-3095.
62. Muller-Dethlefs, K and Schlader, A.F. (1976) The effect of steam on flame temperature, burning velocity and carbon formation in hydrocarbon flames. *Combustion and Flame*, 27, 205.
63. Mungal, M.G. and Dimotakis, P.E. (1984) Mixing and combustion with low heat release in a turbulent shear layer. *J Fluid Mechanics*, 148, 349-382.
64. Nedoseev, G.L.; Rusanov, V. D.; Smol'skii, V. N.; Spektor, A. M.; Shiryayevskii, V. L. and Sholin, G.V. (1989) Influence of diluents on the pulse characteristics of an F₂-H₂ laser under conditions of high-power initiation by a relativistic electron beam, *Sov. J. Quantum Electron.* 19 (8), 1100-1101.
65. Okada, M. and Makuuchi, K. (1969) Direct fluorination of polyethylene powder. *Ind. Eng. Chemistry Product Research and Development*, 8(3), 334-335.
66. Park, J.; Kim, Seung-Gon; Lee, Kee-Man; Kim T.K. (2002) Chemical effect of diluents on flame structure and NO emission characteristics in methane-air counterflow diffusion flame. *International J of Energy Research*, 26(13), 1141-1160.
67. Perry, R.H.; Green D.W. (1999) *Chemical Engineers' Handbook*, seventh edition (Chapter 6). McGraw Hill publishers, New York.
68. Potter, Jr. A.E. and Berlad, A.L. (1956) The quenching of flames of propane-oxygen-argon and propane-oxygen-helium mixtures. *Journal of Phy. Chem.*, 60, 97.

69. Pratsinis, S. E. (1998) Flame aerosol synthesis of ceramic powders. *Progress in Energy and Combustion Science*, 24, 197–219.
70. Rabideau, S.W., Hecht, H.G. and Burton, L.W. (1972) A study of the Kinetics of the reaction between H_2-F_2 by EPR Methods. *J. of Magnetic Resonance*, 6, 384-395.
71. Rabinowitch, E. (1937) The recombination-velocity of free atoms. *Trans. of the Faraday Soc.*, 33, 283-293.
72. Rakov, E.G.; Fomina, E.V. and Grunskii, A.V. (2001) Computer calculation of flame processes in uranium technology. *Atomic Energy*, 91 (1), 555-559.
73. Rittner, M.N. (2002) Market analysis of nanostructured materials, *American Ceram. Soc. Bull.* 81 (2002) 33– 36.
74. Rodi, W. (1993) *Turbulence Models and Their Application in Hydraulics, A state of the art Review*. A.ABalkema/Rotterdam/Brookfield, 29.
75. Rosner, D.E. (1986) *Transport processes in chemically reacting flow systems*. Butterworth publishers, Boston, MA.
76. Sadakata, M.; Xu, Y. B.; & Harano, A. (1996) A systematic approach for the design of aerosol reactors. *Powder Technology*, 88, 261–266.
77. Safary, E.; Romand, J. and Vodar, B. (1951) Ultraviolet absorption spectrum of gaseous hydrogen fluoride. *Journal of Chemical Physics*, 19, 379-380.
78. Sakurai, T. (1974) Comparison of the fluorinations of uranium dioxide by bromine trifluoride and elemental fluorine. *The Journal of Physical Chemistry*, 78 (12), 1140-1144.

79. Sandri, R. (1956) On flame propagation in explosive mixtures of gases III. Flame propagation in mixtures of methane and nitrogen air, helium air and argon air. Canadian journal of chemistry, 34, 331-337.
80. Schroeder, V., Holtapples, K. (2005) Explosion characteristics of hydrogen-air and hydrogen-oxygen mixtures at elevated pressures. International Conference on Hydrogen Safety, Pisa, Italy, September 8-10, 2005.
81. Seeger, C.; Rotzoll, G.; Lubbert, A. and Schugerl, K. (1981) A Study of the reactions of fluorine with hydrogen and methane in the initiation phase using a miniature tubular reactor. International Journal of chemical kinetics, XIII, 39-58.
82. Shebeko, Yu.N.; Tsarichenko, S.G.; Trunev, A.V.; Korol'chenko, A.Ya.; Kaplin, A.Yu. (1994) The influence of inert retardants on the combustion of hydrogen-oxygen mixtures under elevated temperatures and pressures. Combustion, Explosion and Shock Waves, 30 (2), 183-188.
83. Shrestha, Bade S.O.; Karim, G.A. (2001) Predicting the effects of the presence of diluents with methane on spark ignition engine performance. Applied Thermal Engineering, 21, 331-342.
84. Siegel, R. and Howell, J. R. (1992) Thermal Radiation Heat Transfer. Hemisphere Publishing Corporation, Washington D.C.
85. Smart, J. P. (1998) Some simple considerations on the turbulent mixing process in relation to flame scaling. Journal of the Institute of Energy, 71, 152-155.
86. Smiley and Brater. (1959) Transactions of the Second International Conference on the Peaceful Uses of Atomic Energy (Geneva, 1958). Atomic Energy Press (Moscow). Selected Reports of non-Soviet Scientists. Vol. 7, p. 587.

87. Spencer, D.J.; Mirels H. and Durran, D.A. (1972) Performance of cw HF laser with nitrogen or helium diluent. *Journal of Applied Physics*, 43 (3), 1151.
88. Stadler, H.; Toporov, D.; Forster, M.; Kneer, R. (2009) On the influence of the char gasification reactions on NO formation in flameless coal combustion. *Combustion and Flame*, 156 (9), 1755-1763.
89. Streblow, R.A. (1984) *Combustion fundamentals*. McGraw Hill Book Company.
90. Suchand, S.N.; Sutton, D.G. (1973) *IEEE Journal of Quantum Electronics*, QE-9, 83.
91. Sullivan, J.H., (1975) Dependence of the second explosion limit of hydrogen-fluorine-oxygen-hydrogen fluoride on a hot atom effect. *The Journal of Physical Chemistry*, 79 (11), 1045-1050.
92. Sullivan, J.H.; Feber, R.C. and Starner, J.W. (1975) Mechanism and types of explosives behavior in hydrogen-fluorine systems. *The Journal of Chemical Physics*, 62(5), 1714-1725.
93. Tieszen S.R. (1986) Detonation cell size measurements in hydrogen-air-steam mixtures. *Prog. Astronaut. Aeronaut.*, 106, 205-219.
94. Tressaud A.; Durand E.; Labrugere C.; Kharitonov A.P.; Kharitonova L.N. (2007) Modifications of surface properties of carbon based and polymeric materials through fluorination routes: From fundamental research to industrial application. *J. of fluorine chemistry*, 128, 378-391.
95. Tuve, G.L. (1953) Air velocities in ventilating jets. *Heating, Piping and Air Conditioning*, **25**(1), 181–191.

96. Villermaux, E. and Rehab, H. (2000) Mixing in coaxial jets. *Journal of Fluid Mechanics*, 425, 161-185.
97. Vinti, J.P. (1932) The dispersion and absorption of helium. *Physical Review*, 42, 632-640.
98. Wegner, K. and Pratsinis, S.E. (2003) Scale up of nanoparticle synthesis in diffusion flame reactors. *Chemical Engineering Science*, 58, 4581-4589.
99. Wegner, K. and Pratsinis, S.E. (2005) Gas-phase synthesis of nanoparticles: scale-up and design of flame reactors. *Powder Technology*, 150, 117-122.
100. Wheatly, P.J. and Linnett, J.W. (1952) Burning velocity determinations. Part 8- Some acetylene+oxygen+inert gas mixtures. *Trans. of the Faraday Soc.*, 48, 338-345.
101. Wilcox, D. C. (1998) *Turbulence Modeling for CFD*. DCW Industries, Inc., La Canada, California.
102. Willbourn, A. H. and Hinshelwood C. N. (1946) The Mechanism of the Hydrogen-Oxygen Reaction. I. The Third Explosion Limit. *Proceedings of the Royal Society of London. Series A, Mathematical and Physical Sciences*, 185 (1003), 353-369
103. Wilson, R.H., Conway, J.B., Engelbrecht, A., and Grosse, A.V. (1951) The temperature of hydrogen-fluorine flame. *J. of American Chemical Society*, 73, 5514.
104. Yeh, C.L.; Liu, E.W.; Chang, Y.C. (2004) Effect of preheating on synthesis of tantalum nitride by self-propagating combustion. *Journal of the European Ceramic Society*, 24, 3807–3815

105. Yoshino, K. (1970) Absorption spectrum of the Argon atom in the vacuum-ultraviolet region. *Journal of the Optical Society of America*, 60 (9), 1220-1229.
106. Zabetakis, M.G.. (1967) *Safety with cryogenic fluids*. Plenum Press, New York, USA.
107. Zebib, A., Williams, F.A. and Kassoy, D.R. (1975) Effects of kinetic mechanism on diffusion-controlled structure of hydrogen-halogen reaction zones. *Combustion Science and Technology*, 10(1-2), 37-44.
108. Zhao, Wei; Li, Zhengqi; Zhao, Guangbo; Zhang, Fangshi; Zhu, Qunyi. (2008) Effect of air preheating and fuel moisture on combustion characteristics of corn straw in a fixed bed. *Energy Conversion and Management*, 49, 3560–3565.
109. Zhou, J.; Wang, Y.; Yang, W.; Liu, J.; Wang, Z.; Cen, K. (2010) Effects of preheating fuel gas to micro-scale flame. *Transactions of the Chinese Society of Agricultural Machinery*, 41(8), pp.90.
110. <http://csep10.phys.utk.edu/astr162/lect/light/absorption.html>, Department of Physics and Astronomy, University of Tennessee. Accessed on 19.8.11.
111. <http://www.azonano.com/ads/abmc.aspx?b=376>. Accessed on 30.11.11
112. <http://www.cfd-online.com/Wiki/Combustion>. Accessed on 19.1.2012.
113. http://en.wikipedia.org/wiki/Autoignition_temperature. Accessed on 10.3.12.
114. http://en.wikipedia.org/wiki/Hydrogen_safety. Accessed on 10.3.12.
115. http://www1.eere.energy.gov/hydrogenandfuelcells/pdfs/h2_safety_fsheets.pdf. Accessed on 11.3.12.
116. http://www.hysafe.org/download/1042/BRHS_Chap3_hydrogen%20ignition%20version_0_9_0.pdf. Accessed on 11.3.12.

117. http://www.hysafe.org/download/997/BRHS_Ch1_Fundamentals-version%201_0_1.pdf. Accessed on 11.3.12
118. http://en.wikipedia.org/wiki/Adiabatic_flame_temperature. Accessed on 11.3.12
119. http://www.engineeringtoolbox.com/fuels-higher-calorific-values-d_169.html. Accessed on 9.4.12
120. <http://www.world-nuclear.org>. Accessed on 9.4.12
121. <http://www.nist.gov/data/nsrds/NSRDS-NBS31.pdf>. Accessed on 10.4.12
122. <http://fire.nist.gov/bfrlpubs/fire96/PDF/f96102.pdf>. Accessed on 10.4.12
123. <http://www.transtutors.com/chemistry-homework-help/s-and-p-block-elements-bond-dissociation-energy-bond-length-halogens.aspx>. Accessed on 10.4.12
124. http://en.wikipedia.org/wiki/Bond-dissociation_energy. Accessed on 10.4.12.

List of publications

i) Published in peer reviewed international journals: **04**

- a. **Tiwari, A.K.;** Patkar, V.C.; Yadav, C.; Ahamed, R.; Patwardhan, A.W.; Fani, H.Z.; Prasad, C S R; Singhal, A.K. and Gantayet, L M. (2011) Experimental and Numerical Investigation of Sub-atmospheric H₂-F₂ reaction. Combustion Science and Technology, 183 (4), 303-320.
- b. **Tiwari, A.K.;** Prasad, C.S.R.; Patkar, V.C.; Patwardhan, A.W. and Gantayet, L.M. (2011) Influence of excess hydrogen and nitrogen on temperature distribution of a hydrogen-fluorine flame reactor". Combustion Science and Technology, 183 (9), 883-896.
- c. **Tiwari, A.K.;** Prasad, C.S.R.; Patwardhan, A.W. and Gantayet, L.M. (2013) Dilution effect in a tubular H₂-F₂ flame reactor. Combustion Science and Technology, 185 (8), 1169-1183.
- d. **Tiwari, A.K.;** Patwardhan, A.W.; Sanyal, A. and Gantayet, L M. (2014) Study of effects of type and quantity of diluents on H₂-F₂ reaction in a batch reactor. Combustion Science and Technology, 186 (9), 1166-1190.

ii) International conferences: **01**

- a. **Tiwari, A.K.;** Prasad, C.S.R.; Patwardhan, A.W. and Gantayet, L.M. (2011) Effect of preheating and reactant flow rate on temperature distribution in a H₂-F₂ flame reactor. International Conference on Numerical Combustion (ICNC-2011) held at National Technological University, Corfu, Greece, April 26-29, 2011.

iii) BARC newsletter: **01**

- a. **Tiwari, A.K.;** Prasad, C.S.R.; Patwardhan, A.W. and Gantayet, L.M. (2011) H₂-F₂ reaction in a tubular reactor. Founder's Day special issue of BARC news letter, Oct. 2011.
